

ระบบของไฟลจุลภาคสำหรับการคัดแยกเม็ดเลือดแดงที่ติดเชื้อมาลาเรียโดยใช้แควลำดับแม่เหล็ก



บทคัดย่อและแฟ้มข้อมูลฉบับเต็มของวิทยานิพนธ์ตั้งแต่ปีการศึกษา 2554 ที่ให้บริการในคลังปัญญาจุฬาฯ (CUIR)  
เป็นแฟ้มข้อมูลของนิสิตเจ้าของวิทยานิพนธ์ ที่ส่งผ่านทางบันทึกวิทยาลัย

The abstract and full text of theses from the academic year 2011 in Chulalongkorn University Intellectual Repository (CUIR)  
are the thesis authors' files submitted through the University Graduate School.

วิทยานิพนธ์นี้เป็นส่วนหนึ่งของการศึกษาตามหลักสูตรปริญญาวิศวกรรมศาสตรมหาบัณฑิต  
สาขาวิชาวิศวกรรมเครื่องกล ภาควิชาวิศวกรรมเครื่องกล  
คณะวิศวกรรมศาสตร์ จุฬาลงกรณ์มหาวิทยาลัย  
ปีการศึกษา 2558  
ลิขสิทธิ์ของจุฬาลงกรณ์มหาวิทยาลัย

A MICROFLUIDIC SYSTEM FOR SEPARATING MALARIA-INFECTED RED  
BLOOD CELLS USING A MAGNET ARRAY



A Thesis Submitted in Partial Fulfillment of the Requirements  
for the Degree of Master of Engineering Program in Mechanical Engineering  
Department of Mechanical Engineering  
Faculty of Engineering  
Chulalongkorn University  
Academic Year 2015  
Copyright of Chulalongkorn University

Accepted by the Faculty of Engineering, Chulalongkorn University in Partial  
Fulfillment of the Requirements for the Master's Degree

Dean of the Faculty of Engineering

(Associate Professor Supot Teachavorasinskun, D.Eng.)

## THESIS COMMITTEE

Chairman

(Associate Professor Boonchai Lertnuwat, Ph.D.)

### Thesis Advisor

(Assistant Professor Alongkorn Pimpin, Ph.D.)

Thesis Co-Advisor

(Praprudddee Piyaviriyakul, Ph.D.)

**Examiner**

(Assistant Professor Werayut Srituravanich, Ph.D.)

External Examiner

(Mayuree Chanasakulniyom, Ph.D.)

**สุรศักดิ์ เกษตรศิริกุล :** ระบบของไอลจุลภาคสำหรับการคัดแยกเม็ดเลือดแดงที่ติดเชื้อมาลาเรียโดยใช้แควร์ลัมบ์แม่เหล็ก (A MICROFLUIDIC SYSTEM FOR SEPARATING MALARIA-INFECTED RED BLOOD CELLS USING A MAGNET ARRAY) อ.ที่ปรึกษา วิทยานิพนธ์หลัก: ผศ. ดร.อลองกรณ พิมพ์พิณ, อ.ที่ปรึกษาวิทยานิพนธ์ร่วม: อ. น. สพ. ดร. ประพุตติ ปิยะวิริยะกุล, 158 หน้า.

วิทยานิพนธ์นี้ได้พัฒนาเทคโนโลยีและแบบชิพที่จะลดเวลาวินิจฉัยและปรับปรุงให้ง่ายต่อการใช้งานสำหรับการคัดแยกเม็ดเลือดแดงที่ติดเชื้อมาลาเรีย โดยอาศัยคุณสมบัติแม่เหล็กที่มีความแตกต่างกันระหว่างเม็ดเลือดแดงปกติและที่ติดเชื้อ การศึกษานี้ได้พัฒนาแบบจำลองเพื่อใช้ในการทำนายการเคลื่อนที่ของเซลล์ โดยใช้รัฐเบียบริการไฟโนต์อิลิเมนต์ด้วยโปรแกรมคอมโวตในการหารูปแบบของสนามแม่เหล็ก ในการศึกษาพบว่าแควร์ลัมบ์แม่เหล็กช่วยเพิ่มเกรดเดียนของสนามแม่เหล็ก รวมทั้งขนาดของแรงที่ช่วยในการแยกเม็ดเลือดแดงด้วย และเขียนโปรแกรมแมทแลป ด้วยวิธีไฟโนต์ดิฟเพื่อเรนซ์เพื่อหาเส้นทางการเคลื่อนที่ของวัตถุเซลล์และนำมาเทียบกับผลการทดลองขนาดของระบบของไอลที่สร้างได้มีความกว้างของช่องทางการไอลหลัก 500 ไมโครเมตร และมีความสูง 100 ไมโครเมตร มีทางเข้า 3 ทางและ ทางออก 2 ทางและมีแควร์ลัมบ์แม่เหล็กกว้างอยู่ด้านข้างของช่องทางการไอล โดยในการทดลองอนุภาคแม่เหล็กขนาด 5 และ 10 ไมโครเมตร พบร้าแบบจำลองที่ใช้ทำนายเส้นทางการเคลื่อนที่มีเปอร์เซ็นต์ความผิดพลาดเฉลี่ย 18.61% และ 17.61% ตามลำดับ ซึ่งความผิดพลาดน่าจะมาจากระยะห่างที่ไม่สม่ำเสมอระหว่างแนวทางการไอลของเม็ดเลือดและแควร์ลัมบ์แม่เหล็กเนื่องมาจากความแม่นยำของกระบวนการสร้าง และความไม่แน่นอนของการระบุระบบของอนุภาคเพราะภาพที่ได้จากการกล้องจุลทรรศน์จะจับอนุภาคแม่เหล็กที่ระยะในแนวตั้งๆ ในส่วนของการทดลองกับเม็ดเลือดแดงที่ติดเชื้อในเลือดหนูด้วยสายพันธุ์พลาสโนมเดียมเบอกลิอย แบบจำลองแสดงให้เห็นว่าเม็ดเลือดที่ติดเชื้อสามารถเคลื่อนที่เข้าหาแควร์ลัมบ์แม่เหล็กได้ประมาณ 36.44 ไมโครเมตรภายในระยะเวลาสามทิศทางการไอล 3 เซนติเมตร หากเม็ดเลือดอยู่ห่างจากแควร์ลัมบ์แม่เหล็ก 600 ไมโครเมตรและมีอัตราการไอล 0.2 ไมโครลิตรต่อนาที และในการทดลองพบว่าการสังเกตด้วยกล้องจุลทรรศน์นั้นทำได้ยาก เนื่องจากอัตราการไอลต่ำทำให้เม็ดเลือดฟุ้งกระจายด้วยผลของการแพร์

# # 5770340921 : MAJOR MECHANICAL ENGINEERING

KEYWORDS: MALARIA, SEPARATION, MICROFLUIDICS, MAGNETOPHORESIS

SURASAK KASETSIRIKUL: A MICROFLUIDIC SYSTEM FOR SEPARATING MALARIA-INFECTED RED BLOOD CELLS USING A MAGNET ARRAY. ADVISOR: ASST. PROF. ALONGKORN PIMPIN, Ph.D., CO-ADVISOR: PRAPRUDDEE PIYAVIRIYAKUL, Ph.D., 158 pp.

This thesis aims to develop a lab-on-a-chip technology which could reduce diagnostic time and eases of use for malarial-infected erythrocytes separation. The principle relies on their magnetic properties which distinguish from common erythrocytes. The mathematical model of infected erythrocytes is developed to predict the trajectory influenced by the magnetic field. The methodology of the study is to use Finite Element software, COMSOL Multiphysics, for clarifying the magnetic field distribution from a magnet array. With the array, the high gradient of magnetic field as well as the magnitude of the force exerting on the erythrocytes could be enhanced. After that, the trajectory of the erythrocytes due to the exerting force is computed using Finite Difference with Matlab programming. To validate the model, experiments with magnetic beads have been performed. The device used in the study consists of 500 micrometer in width, 100 micrometer in height, three inlets and two outlets, and magnet array placing beside the channel. In experiments for 5 and 10 micrometers of magnetic beads, the model to predict the trajectory has an error about 18.61% and 17.61% respectively. The error stems from the non-uniform distance between the magnet array and bead-focusing stream due to the poor precision of the fabrication and a difficulty to identify a plane of motion of particles due to relatively long focal-depth of examined images in the experiments. In the case of blood experiment, this study has used P.Berghei-infected mouse blood. The model suggests that infected cells should move laterally about 36.44 micrometers under flow rate of 0.2 microliter per minute within the downstream of 3 cm when the cells are far from the magnet of 600 micrometers at the beginning. In the experiment, due to cell diffusion at low flow rate, it is hard to observe the motion within this short distance clearly under the microscope.

Department:	Mechanical Engineering	Student's Signature .....
Field of Study:	Mechanical Engineering	Advisor's Signature .....
Academic Year:	2015	Co-Advisor's Signature .....

## ACKNOWLEDGEMENTS

I would like to express my profoundly appreciation to Asst. Prof. Alongkorn Pimpin, my thesis advisor, who kindly advises me not only research knowledge but also real life experience and supports me unequivocally to finish this thesis, and Asst. Prof. Werayut Srituravanich, who always advises and helps comment on my research thesis during laboratory meeting.

I would like to express my deeply gratification to all committee, Assoc. Prof. Boonchai Lertnuwat and Dr. Mayuree Chanasakulniyom, who make attentive comments on my thesis and helpful recommendation to my reserach during the examination

I would like express my gratification to the graduate school, Chulalongkorn University for financially supporting me to present my research in 8th Asia-Pacific Conference of Transducers and Micro-Nano Technology in Japan. Moreover, this thesis is financially supported by Chulalongkorn University through the Chulalongkorn Academic Advancement into its 2nd Century Project (Smart Medical Device)

I would like to express my deeply appreciation to all professors in CSC research group from Faculty of Veterinary Medicine, Chulalongkorn University, named Assoc. Prof. Achariya Sailasuta, and Dr. Prapruddee Piyaviriyakul who is my thesis co-advisor, who give me a lot of knowledge especially on biological aspects which I definitely do not get familiar with. Particularly Asst. Prof. Morakot Kaewthamasorn helps me prepare for blood sample for the experiment.

I would like to express my thanks to Prof. Sung Yang for giving me another view of research aspects and valuable research experience for six weeks at BioMEMS laboratory, Department of Medical System Engineering, Gwangju Institute of Science and Technology, Korea Republic. In addition, I would like to express my appreciation to Prof. Barry Lutz and Dr.Pahnit Seriburi for giving me valuable research experiences in the world-class working environment and inspiring me to pursue my advance study in the biomedical field for three months at Lutz lab, Department of Bioengineering, University of Washington, The United States.

Finally, I would like to express my cordial thanks to all of labmates always supporting not only research idea but also life experience including my family, friends and others who are a part of my life and always support me to finish this thesis.

## CONTENTS

	Page
THAI ABSTRACT .....	iv
ENGLISH ABSTRACT .....	v
ACKNOWLEDGEMENTS .....	vi
CONTENTS .....	vii
LISTS OF TABLES .....	1
LISTS OF FIGURES .....	1
NOMENCLATURE .....	1
Chapter 1 Introduction .....	1
1.1 Background and Motivation .....	1
1.2 Malaria life cycle .....	2
1.3 Overview of Malaria Diagnosis .....	3
1.4 Laboratory method.....	4
1.4.1. Giemsa Staining method.....	4
1.4.2. Flow cytometry method .....	5
1.4.3. Immunological diagnosis .....	6
1.5 Rapid Diagnostic Tests (RDTs) .....	10
1.6 Lab-on-a-chip technology .....	11
1.6.1 Technology used LOC for detecting Malaria.....	11
1.6.2 LOC used magnetophoresis for Malaria detection .....	14
1.7 Objectives of the thesis .....	20
1.8 Scopes of the thesis .....	20
1.9 Thesis methodology .....	21

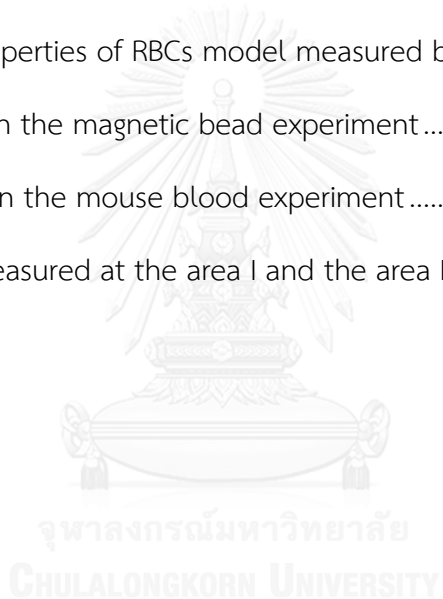
	Page
1.10 Expected outcomes.....	21
1.11 Summary.....	22
Chapter 2 Magnetism and Computational Model .....	23
2.1 Magnetophoretic principles.....	23
2.2 Magnetic field sources.....	24
2.2.1 Permanent magnet.....	24
2.2.2 Electromagnetic .....	24
2.2.3 Magnetic field induced by ferromagnetic materials .....	24
2.3 Proposed configuration and necessary data used in the study .....	25
2.4 Magnetic field distribution (Analytical and computational solutions) .....	27
2.5 Trajectory of blood cell by influence of an array of magnets .....	34
2.6 Summary .....	40
Chapter 3 Fabrication process and Experimentation.....	41
3.1 Microfluidic conventional fabrication process.....	41
3.2 Equipment and fabrication process.....	43
3.2.1 List of equipment .....	43
3.2.1.1. Instruments .....	43
3.2.1.2. Materials and reagents .....	43
3.2.2 Fabrication process.....	44
3.2.2.1. Preparation of acrylic mold.....	44
3.2.2.2. PDMS casting .....	44
3.2.2.3. Glass preparation.....	44
3.2.2.4. Bonding PDMS with glass slide .....	45

	Page
3.2.2.5. Connect inlet and outlet tubes and inspection .....	45
3.3 Summary.....	46
Chapter 4 Magnetic bead experiment.....	47
4.1 Trajectory of magnetic beads by influence of an array of magnets .....	47
4.2 Preparation of magnetic bead experiment.....	48
4.2.1 List of equipment .....	48
4.2.1.1. Instruments .....	48
4.2.1.2. Materials and reagents .....	49
4.2.2 Sample preparation.....	49
4.2.3 Experiment condition and installation .....	50
4.3 Experiment result of magnetic beads .....	52
4.3.1 Magnetic beads in DI water medium.....	52
4.3.2 Magnetic beads in PBS medium .....	54
4.4 Discussion.....	55
4.5 Summary .....	57
Chapter 5 Mouse blood experiment.....	58
5.1 Mice blood experiment .....	58
5.1.1 List of equipment .....	58
5.1.1.1. Instruments .....	58
5.1.1.2. Materials and reagents .....	58
5.1.2 Sample preparation.....	59
5.1.2.1. Culture infected erythrocytes.....	59
5.1.2.2. Nycodenz preparation .....	60

	Page
5.1.3 Experiment condition and setup .....	62
5.1.3.1 Flowing fluid .....	62
5.1.3.2 Stagnant fluid .....	65
5.2 Experiment result of mouse blood cells and discussion .....	65
5.3 Summary .....	67
Chapter 6 Conclusion .....	68
REFERENCES .....	71
APPENDIX.....	72
Appendix A. Numerical calculation and Code MATLAB.....	73
Appendix B. COMSOL Multiphysics .....	98
Appendix C. Computational methodology.....	123
Appendix D. Raw data of trajectory computation .....	135
Appendix E. Comparison percent difference between model and experiment ...	143
Appendix F. Equipment, materials and reagents .....	152
Appendix G. Nycodenz stock solution preparation .....	157
VITA.....	158

## LISTS OF TABLES

Table 2.1 Magnetic susceptibility of the blood components .....	26
Table 2.2 Constant properties used in the study .....	26
Table 2.3 Magnetic properties of magnetic beads .....	27
Table 2.4 Relative magnetic susceptibilities of each type of erythrocytes to water [22].....	27
Table 2.5 Physical Properties of blood.....	38
Table 2.6 Physical Properties of RBCs model measured by COMSOL .....	38
Table 4.1 conditions in the magnetic bead experiment.....	51
Table 5.1 Conditions in the mouse blood experiment.....	63
Table 5.2 Distance measured at the area I and the area II .....	64



## LISTS OF FIGURES

Figure 1.1 Malaria's life cycle from the mosquito to the human [4] .....	2
Figure 1.2 Example of thick film and thin film method [5] .....	4
Figure 1.3 Schematic diagram of flow cytometry by combining with fluorescence [6].....	5
Figure 1.4 Schematic diagram of IHA test.....	6
Figure 1.5 Schematic diagram of IFAT .....	8
Figure 1.6 Schematic diagram of ELISA .....	8
Figure 1.7 Schematic diagram of ICT .....	9
Figure 1.8 Polymerase Chain reaction principles .....	10
Figure 1.9 Example of commercially available LOC representing the various parts of tasks on the limited space device[10] .....	11
Figure 1.10 Schematic diagram showed the force diagram acting on both types of blood cells, which hRBCs will be equilibrated at the different height from iRBCs. [9].....	12
Figure 1.11 Integration diagram of wide range of tasks in their devices [9] .....	12
Figure 1.12 Schematic of device by illustrating iRBCs are going to move laterally to the wall of the channel [12] .....	13
Figure 1.13 Schematic diagram of the overall picture of crystal structure Hemozoin [16].....	13
Figure 1.14 Schematic diagram of magnetophoresis principle (a) Paul et al. (1981) (b) Zimmerman et al. (2006) (c) Bhakdi et al (2010) [17-19] .....	15
Figure 1.15 The domain combines the array of ferromagnetic wires with permanent magnet beneath the flowing micro channel [20].....	17

Figure 1.16 Computational result of trajectories under flow rate <i>left</i> 1 mL/min <i>right</i> 5 mL/min [20].....	17
Figure 1.17 Schematic and working principle of the study by having sheath flow controlled by flow rate to focus the sample streamline at the certain distance from the wall where the wire was placed [21].....	18
Figure 1.18 (a) Kong T.F. et al (2015) took advantage of rigidity of iRBCs to separate the target sample out and (b) used the Magnetic resonance relaxometry detection principle is used to detect the existence of iRBCs [22] .....	19
Figure 2.1 Magnetic force acting on the particle exposed to the area having gradient magnetic field.....	23
Figure 2.2 Effect of magnetic field distribution after adding the ferromagnetic wire commonly made from nickel .....	25
Figure 2.3 Configuration proposed by this study for separating infected erythrocytes.....	26
Figure 2.4 Domain and defined parameters used in the equation .....	28
Figure 2.5 Magnetic field distribution in x-axis at $y = b/2$ (a) the result computed by COMSOL (b) the result calculated by analytical solution by having average uncertainty 4.76%.....	30
Figure 2.6 Magnetic field distribution in y-axis at $x = a/2$ (a) the result computed by COMSOL (b) the result calculated by analytical solution by having average uncertainty 4.10%.....	30
Figure 2.7 Magnetic field distribution in z-axis at $x = y/2$ (a) the result computed by COMSOL (b) the result calculated by analytical solution by having average uncertainty 4.63%.....	30
Figure 2.8 the domain defined in COMSOL (a) with the gap 100 $\mu\text{m}$ between magnets (b) with the gap 500 $\mu\text{m}$ between magnets.....	31

Figure 2.9 Magnitude of magnetic force acting on 5- $\mu\text{m}$ magnetic beads by varying the distance from the magnets from 300 to 1000 $\mu\text{m}$ .....	31
Figure 2.10 Schematic diagram of the designed microfluidic device including dimensions.....	32
Figure 2.11 Domain used in the study including the boundary of infinite magnets ....	33
Figure 2.12 Magnetic field distributions A/m in illustrated by using color range .....	33
Figure 2.13 Magnetic field distribution at $d = 100$ and $d = 350 \mu\text{m}$ .....	34
Figure 2.14 (a) Schematic diagram of study domain (b) Force diagram acting on two types of erythrocytes exposed to the non-uniform magnetic force .....	35
Figure 2.15 Comparison of projected area between stokes' law modeling on spherical object and our RBCs model.....	37
Figure 2.16 Calculated result with various flow rates in the case 200 $\mu\text{m}$ from the magnet array.....	39
Figure 2.17 Calculated result with various flow rates in the case 300 $\mu\text{m}$ from the magnet array.....	40
Figure 3.1 Process flow of Soft lithography process .....	42
Figure 3.2 A microfluidic device used in the study .....	46
Figure 4.1 (a) Schematic diagram of study domain (b) Force diagram acting on two types of particles in the experiment under exposed to non-uniform magnetic force. ....	47
Figure 4.2 Schematic diagram of the experiment for both sizes of magnetic beads... ..	51
Figure 4.3 Calculation of uncertainty between the model and experiment (a) taken by a microscope (b) the conceptual principle of calculating error compared to experimental result.....	52
Figure 4.4 Example of experiment result of 5- $\mu\text{m}$ diameter magnetic beads in DI water medium plotted for comparing to the calculated result.....	52

Figure 4.5 Example of experiment result of 10- $\mu\text{m}$ diameter magnetic beads in DI water medium plotted for comparing to the calculated result.....	53
Figure 4.6 Average deviation including the error bar from 5.31% to 34.16% for 5- $\mu\text{m}$ diameter magnetic beads (three replicates) at 2 $\mu\text{L}/\text{min}$ .....	53
Figure 4.7 Average deviation including the error bar from 11.14% to 26.19% for 10- $\mu\text{m}$ diameter magnetic beads (three replicates) at 20 $\mu\text{L}/\text{min}$ .....	54
Figure 4.8 Average deviation including the error bar from 5.31% to 34.16% for 5- $\mu\text{m}$ diameter magnetic beads (three flow rates) at 2, 10 and 20 $\mu\text{L}/\text{min}$ and for 10- $\mu\text{m}$ diameter magnetic beads (one flow rate) at 20 $\mu\text{L}/\text{min}$ .....	55
Figure 4.9 Non-uniform thickness of wall channel .....	56
Figure 4.10 Percentage of error of different y-coordinate calculation .....	56
Figure 5.1 Giemsa staining of the infected mouse <b>left</b> 2 <sup>nd</sup> day <b>right</b> 5 <sup>th</sup> day .....	61
Figure 5.2 Schematic procedure of separation with Nycodenz gradient .....	61
Figure 5.3 Giemsa staining after passing Nycodenz gradient centrifugation .....	62
Figure 5.4 Investigation window for examining the lateral displacement .....	62
Figure 5.5 Example of the distance measurement in the (a) area I (b) area II under total flow rate 0.5 $\mu\text{L}/\text{min}$ .....	63
Figure 5.6 Plotted data from the Table 5.2 to illustrate the result under various flow rates.....	64
Figure 5.7 Example of force distribution in various distance from the streamline to the surface of a magnet array.....	66
Figure 5.8 Computational trajectory of infected cells under various distances from the surface of a magnet array at flow rate 0.2 $\mu\text{L}/\text{min}$ .....	66

## NOMENCLATURE

$a$	Radius of particle
$a_f$	Radius of ferromagnetic wire
$A_s$	Surface area
$B$	Magnetic field
$B_x$	Magnetic field in x-component
$B_y$	Magnetic field in y-component
$B_z$	Magnetic field in z-component
$C_L$	Lift coefficient
$D$	Diameter of particles
$D_h$	Hydraulic diameter
$F_B$	Buoyancy force
$F_D$	Drag force
$F_{D,x}$	Drag force in x-axis
$F_{D,y}$	Drag force in y-axis
$F_{D,z}$	Drag force in z-axis
$F_L$	Lift force
$F_m$	Magnetic force
$F_{m,x}$	Magnetic force in x-axis
$F_{m,z}$	Magnetic force in z-axis
$g$	Gravitational acceleration
$H$	Magnetic field norm
$h$	Height of magnet
$h_m$	Height of magnet
$I$	Current
$dl$	Unit vector of current
$J$	Current density
$l_m$	Length of magnet
$M_s$	Magnetization

$\mathbf{r}$	Position vector
$Re$	Reynolds number
$U_{max}$	Maximum velocity
$V_{BC}$	Volume of blood cells
$v_p$	Particle velocity
$v_{p,x}$	Particle velocity in x-axis
$v_{p,z}$	Particle velocity in z-axis
$\dot{v}_p$	Particle acceleration
$V_{rel}$	Relative velocity
$w$	Width of channel
$w_m$	Width of magnet
$x$	Local point in x-axis
$x_0$	Initial point in x-axis
$y$	Local point in y-axis
$y_0$	Initial point in y-axis
$z$	Local point in z-axis
$z_0$	Initial point in z-axis
$\kappa$	Magnetic constant
$\mu_0$	Permeability of free space ( $4\pi \times 10^{-7}$ )
$\mu_f$	Fluid dynamic viscosity
$\mu_{medium}$	Permeability of medium
$\mu_{particle}$	Permeability of particle
$\rho_p$	Particle density
$\rho_f$	Fluid density
$\rho_{cell}$	Targeted cell density
$\rho_{RBC}$	Red blood cell density
$\nu_f$	Fluid dynamic viscosity
$\chi_{buffer}$	Magnetic susceptibility of buffer
$\chi_{RBC}$	Magnetic susceptibility of healthy red blood cells
$\Delta\chi$	Relative magnetic susceptibility
$\nabla$	Volume of targeted cell

## **Chapter 1**

### **Introduction**

#### **1.1 Background and Motivation**

Malaria, a disease having an Anopheles mosquito as a carrier, becomes a severe medical issue to many countries in the tropical climate zone which has a high risk of a disease outbreak. According to the medical record all over the world, there have been patients about 300 – 500 million people a year. In that number, approximately 1 – 3 million patients have died of Malaria in each year due to a lack of medication that treats merely symptomatically. Thailand is among the countries that have a high rate of a seasonal disease outbreak particularly in the border of the country.[1, 2]

Moreover, global warming also plays an important role in spreading Malaria nowadays. Since warm climate is appropriate for the Anopheles mosquito to grow. Recently, WHO advises the novel method to treat Malaria so called Artimesinin along with other methods in order to help treatment work effectively. Artimesinin can eliminate the entire parasite in human body. However, the patients who are not treated incessantly enough cause the parasite to have drug resistance and also to enlarge the risk of disease outbreak. From the study of E.A. Ashlet et al (2014), they addressed that Malaria in the tropical climate zone such as Africa, South Asia and South East Asia has a tendency to have more resistance to Artimesinin more severely. Additionally, the area in the North Eastern and Western of Thailand especially the remote area close to a border has more risk of drug-resisting Malaria [3]. Due to its limitation of resources in those areas, they cause the difficulty and delay in patient separation, which leads to quickly spread out the disease due to its life cycles and increase the rate of demise.

## 1.2 Malaria life cycle

At the moment, Malaria has more than 100 species in mammals, poultry and reptile. There have been 22 species found in primates. In human, Malaria originating from five types of Plasmodium namely *P.falciparum*, *P.vivax*, *P.ovale*, *P.malariae* and recently found *P.knowlesi* has begun in the Anopheles' salivary glands called sporozite. When the mosquito bites the human, sporozite will enter blood circulating of a human body and go to hide inside a liver of the host within an hour. sporozite will proliferate itself in order to have enough amount to develop into merozoite stage. merozoite will come into blood circulation again and invade red blood cells to consume hemoglobin which is an indispensable chemical substance for carrying oxygen to all cells of the body. The life cycle of Malaria in erythrocytes can be divided into four phases called ring form, trophozoite, schizont and merozoite, which causes the red blood cells to be destroyed and merozoite will invade other blood cells repeatedly. The cycle shown in Figure 1.1 takes about 36 hours and a number of malaria parasites will increase exponentially.

Furthermore, some of the merozoite can develop into gametocyte which is asexual. If the mosquito bites infected patients already having gametocyte in their bodies, the mosquito will take the gametocyte from humans and spread the disease from one to another.

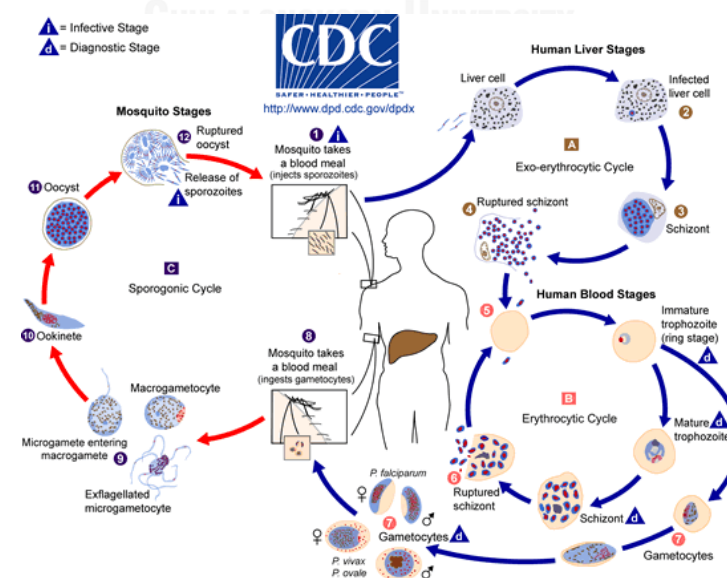


Figure 1.1 Malaria's life cycle from the mosquito to the human [4]

The important symptoms of the disease are high fever and quiver. These symptoms take short or long duration depending on the rest time of Malaria, type of Malaria, the amount of sporozite and immunity system of each person. The symptoms are categorized into three main stages of the symptoms as following

- Shivering period will take approximately 15-60 minutes. The infected patient shivers and becomes pale. These symptoms are matched the stage when the erythrocytes are destroyed.
- Fever period will take about 2-6 hours. The infected patient has a high fever and also feels nausea.
- Sweating period. In this phase, the infected patient loses water by being soaked with their perspiration, feels exhausted and has no fever following the stage in the life cycle mentioned above. Shivering will occur differently relying on the amount of infected pathogen, various stages of disease. After infected, the patient will have dark urine due to hemolysis. Moreover, some of them show symptoms of jaundice, splenomegaly or hepatomegaly [1].

### 1.3 Overview of Malaria Diagnosis

Regarding the infection between humans, it is necessity to filter and separate an infected patient out from the community by using rapid and accurate diagnostic methods. Nowadays there are three conventional diagnostic methods that are laboratory method, known as a gold standard, Rapid Diagnostic Tests (RDTs), and LOC (lab-on-a-chip) technology. The first two methods are general ways to diagnose in a hospital or medical center. The third one interests some groups of researchers to develop this technology and has a possibility to replace conventional methods, which is shown in a number of research papers in the recent 20 years. It is an alternative method that might be suitable in low-resource setting situation. Each particular method will be described later.

## 1.4 Laboratory method

This method is required specific laboratory instruments and done in the laboratory. The most common method is to use an optical microscope to indicate the blood sample from the patient. However, it needs an expert or well-trained laboratory technician to diagnose. The laboratory method can be separated into four methods described as follows.

### 1.4.1. Giemsa Staining method

This method needs an optical microscope to inspect the stained blood samples dropped on the glass slide. This method is divided into two types which are thin film and thick film.

- Thick Film method

This method starts by bringing the blood sample to drop on a glass slide, and then use a needle or spreader to the sample to have around 1 centimeter. There is a little trick whether the thick film is thicker than it should be or not by placing the newspaper to be under the glass slide and checking whether the reader can still read the newspaper or not. If the reader can read, it is ready to read under the condition of thick film method. After that, the reader stains the blood sample with Giemsa or Wright-Giemsa (WG). In the case using Wright-giemsa, the examiner needs to bring the sample to wash in clean water 2-3 times in order to lyse red blood cells and dilute the intensity of hemoglobin. Then, the examiner stains the sample with Wright-Giemsa. This method has several advantages that it does not take too long time and easily specifies the type of Malaria, but requires a specialist to analyze a result whether the patient is infected or not. The example of the thick film method is shown in Figure 1.2.

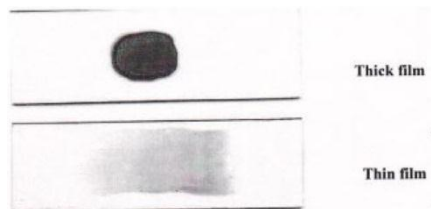


Figure 1.2 Example of thick film and thin film method [5]

- Thin Film method

The method begins by bringing the blood sample to drop on a glass slide, and then use a needle or spreader to spread the sample to get thin film. After getting the thin film, stain the sample with Wright-Giemsa then fix blood cells in the sample by using absolute methanol or ethanol for 1 – 2 minutes. This method also has many benefits that it is clearer to specify the type of the Malaria than the thick film, but it takes time to prepare the sample particularly staining step. The example of the thin film method is also shown in Figure 1.2.

#### 1.4.2. Flow cytometry method

This method needs a specific instrument by using the sensor mostly used the optical sensor such as a laser to define the physical and biological properties. In some cases, it requires fluorescence substances to tag the sample in order to be easily observed as a marker of diagnosis. The working principle is that it needs a targeted sample to set up the instrument by providing the information of the targeted cell physically and biologically. For malarial diagnosis, the blood sample is driven into the system and allows the sensor to define its characteristic. This method gives a quite high accuracy and specificity. The example of the flow cytometry is shown in Figure 1.3.

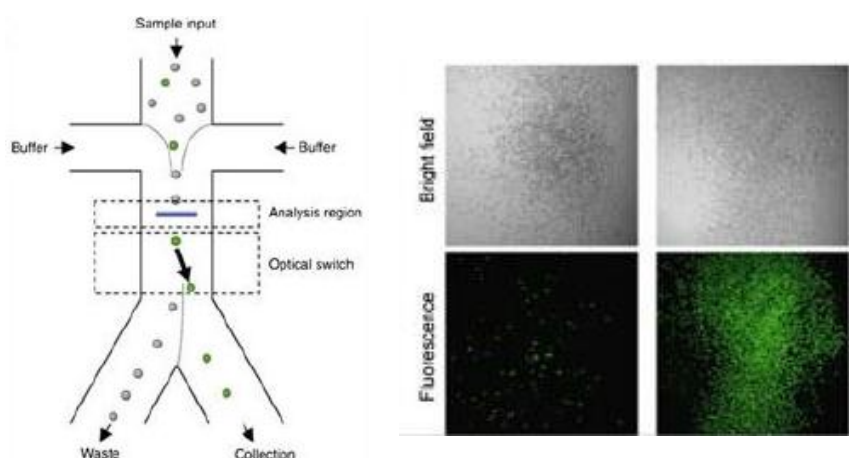


Figure 1.3 Schematic diagram of flow cytometry by combining with fluorescence [6]

### 1.4.3. Immunological diagnosis

This method takes advantages of antigen-antibody binding characteristic for a diagnosis which gives high specificity. The parasite releases some chemical substances such as antigen and protein in the blood circulation of an infected patient. Typical methods are divided into two major ways by detecting antibody and antigen of Malaria.

- Detecting antibody of Malaria
  - IHA (Indirect hemagglutination test)

This method observes the reaction between the blood and antigen of Malaria which coming from the patient, animals or cultured in vitro. Tannic acid and glutaraldehyde is used as catalyst for the reaction. The given antigen will catch the antibody in the blood sample and show the sedimentation product after reaction obviously. The schematic diagram of the method is shown in Figure 1.4. If the blood sample has Malaria parasites, supposed to have antibody of Malaria, it will react to given antigen and can be perceived easily with the intense sedimentation of the blood resulting from bondage between antigen and antibody. On the contrary, if the blood sample does not have Malaria parasites, the sedimentation of blood still happens according to its nature.

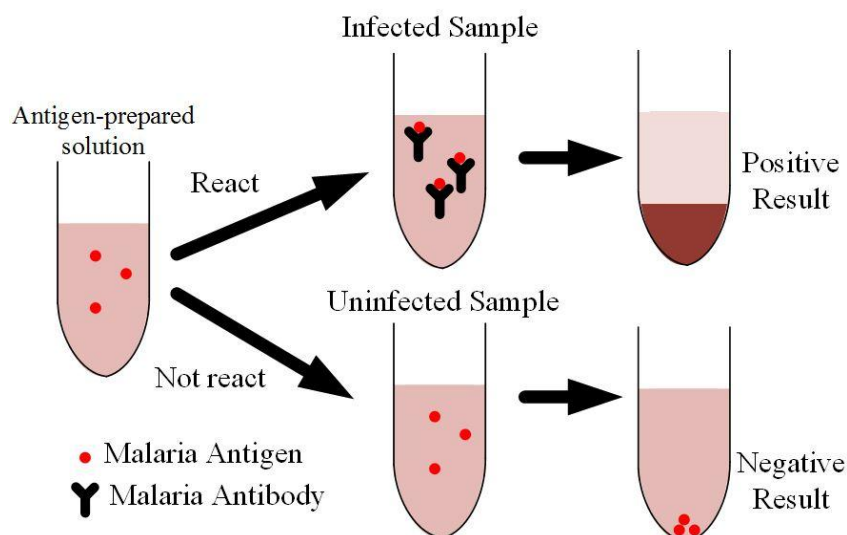


Figure 1.4 Schematic diagram of IHA test

- IFAT (Indirect immunofluorescent antibody test)

The principle of this method is to observe the fluorescence signal from the reaction. The blood sample is serially diluted and added the prepared Malaria antigen to react with the sample by centrifuging with PBS and fixing the sample with acetone for removing serum. After that, anti-human immunoglobulin already tagged fluorescence into the prepared sample and let the binding reaction work. When the bondage happens, the fluorescence will transmit its signal out. The working principle of the method is shown in Figure 1.5.

- ELISA (Enzyme-linked immunosorbent assay)

The working principle of the method is to take advantage of color-reacting enzyme such as horseradish peroxidase (HRP). This method will prepare the assay by coating the Malaria antigen which may be processed by genetic modification or ultrasonic on the microliter plate for the test. When the blood sample which may be done with serial dilution is added to the plate, the Malaria antibody in the sample will be bound by the fixed antigen. After binding reaction between the antigen and the antibody is completed, the color-reacting protein, such as enzyme in this case, captures the binding reaction and provides color difference depending on the concentration of the antibody in the blood sample. The examiner can analyze the result by using a plate reader to read the intensity of color inducing from the reaction. The working principle of the method is shown in Figure 1.6. If the Malaria antigen exists in the sample, the anti-antibody will detect the antibody of the Malaria. Then after adding the color substrate, the color will change and can be quantified by the plate reader.

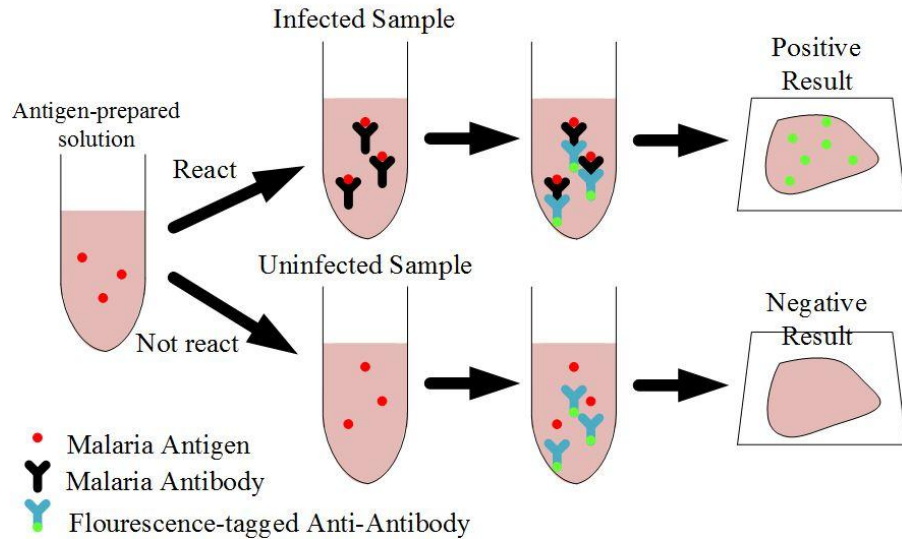


Figure 1.5 Schematic diagram of IFAT

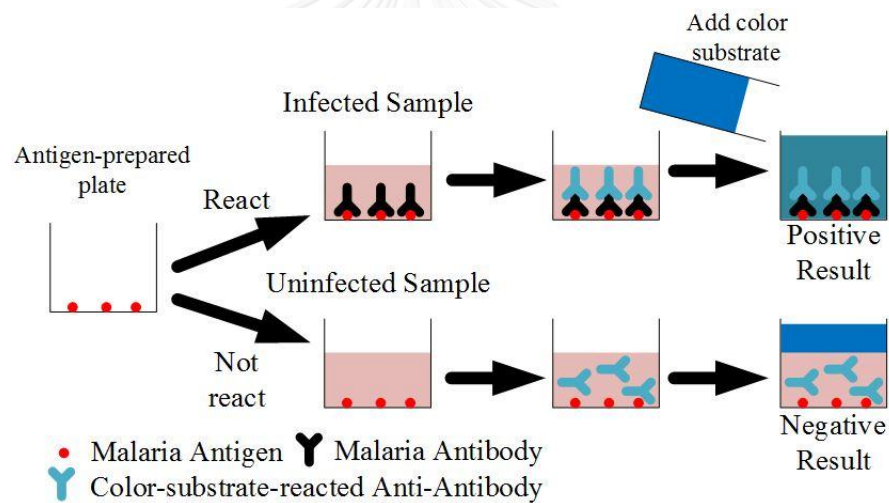


Figure 1.6 Schematic diagram of ELISA

- Detecting antigen of Malaria with ICT (ImmunoChromatography)

The principle of the method is to make use of lateral flow assay, usually used nitrocellulose as an assay. The assay at the certain distance is coated the antibody which can react with Malaria antigen from the dropped sample point, which is called test area. This method is required to prepare sample by lysing the red blood cells before doing the test. The assay is submersed into the prepared sample and then the sample driven by capillary force flows pass over the test area. The antigen in the

blood sample takes the antibodies-conjugated microspheres such as gold colloidal or latex particle passing over the test area. If the sample has the Malaria antigen, it will react to the antibody sensitive to Ag-Ab-conjugated microspheres and changing in color which is easily observed by naked eyes. The rest of the Ag-Ab-conjugated microspheres continue flowing to the control line which is supposed to change its color in every test for indicating the device to give the correct result. One of the benefits is taking 5-10 minutes to finish each test and can be used outside the laboratory. The working principle of the ICT test is shown in Figure 1.7.

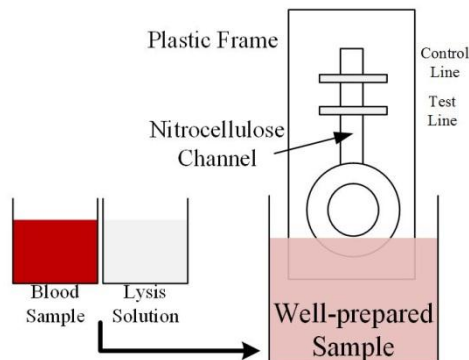


Figure 1.7 Schematic diagram of ICT

- Genetic code analysis

Genetic analysis can indicate species of Malaria thanks to its own genetic code. This technique gives us a specific and precise result, but the cost is expensive per a test. The most common genetic diagnosis method is polymerase chain reaction (PCR). PCR needs DNA probe, which many studies could define DNA sequence of Malaria in each species, to hybridize with the DNA of Malaria and can amplify the number of targeted DNA by using a thermal cycler [7]. Some of the methods use real-time PCR which can observe the intensity of fluorescence tagged in DNA probe immediately when the chain reaction occurs. By this mean, the advantage of this technique is to use small volume of the sample, but needs to prepare the sample carefully and requires sterile equipment to avoid contamination. The principle of this technique is shown in Figure 1.8.

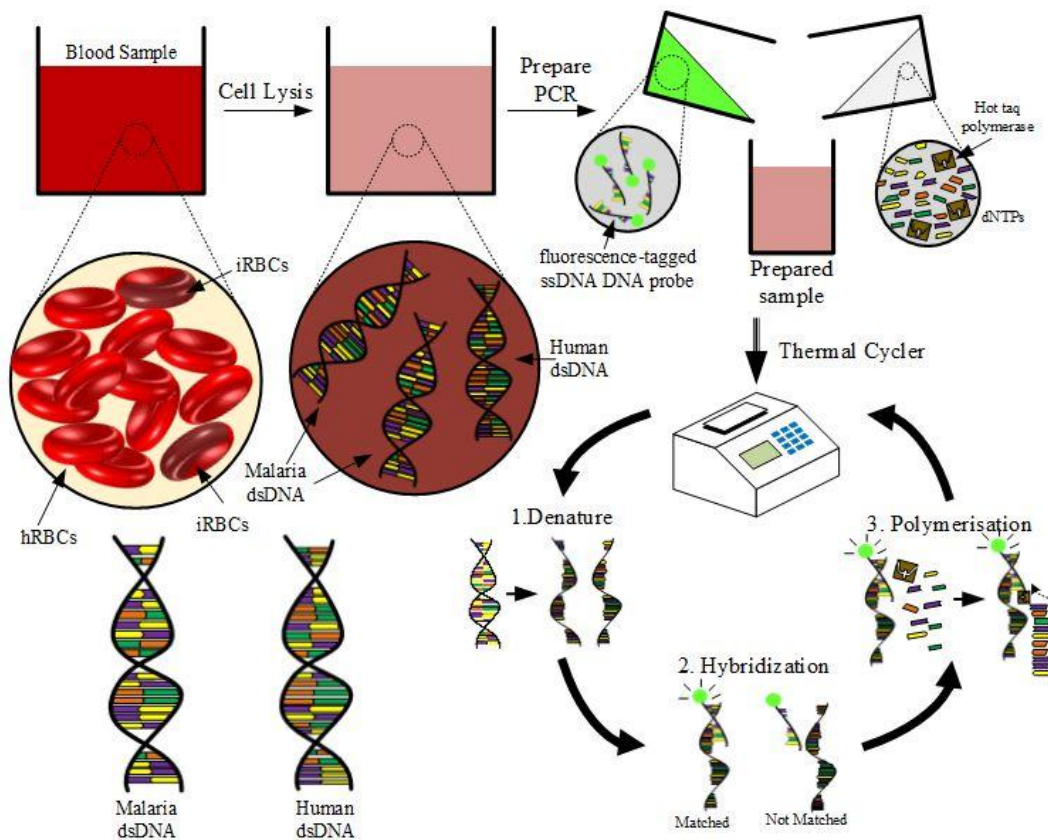


Figure 1.8 Polymerase Chain reaction principles

### 1.5 Rapid Diagnostic Tests (RDTs)

The method which is similar to ICT technique mentioned on the previous topic detects Malaria antigen by letting the sample flow through the porous membrane. Then, the antigen binds with coated antibodies in the given distance. Moreover, the test is different from each other depending on types of coated antibody. The antibody will be used as follows [8].

- Histidtine-rich protein 2 (HRP-2) is used to detect merely *P. falciparum*.
- Plasmodium lactate dehydrogenase (pLDH) is used to detect all species by using antibody bondage.
- Aldorase (Pan-specific) is used to detect all species by using enzyme.

The benefit of the method is the test can be used and analyzed without specialists by only perceiving the color line will appear on the test set.

## 1.6 Lab-on-a-chip technology

In the past two decades, lab-on-a-chip technology (LOC) has begun to be interesting among researchers because the technology can minimize the whole process in laboratory such as sample preparation or reaction to operate within the boundary of a glass slide. The type of LOC substrate has been not only on a glass slide depending on applications. The example of LOC shown in Figure 1.9 is applied to diagnose various tests. This topic will focus primarily on Malaria detection application, which is discussed as follows.

### 1.6.1 Technology used LOC for detecting Malaria

According to P. Gascogne et al. (2004), they took advantage of fluid flowing in microchannel or called Microfluidics. The working principle of their work used dielectrophoresis (DEP) by using high gradient electric field for separating Malaria-infected red blood cells (iRBCs). Thanks to distinctive electrical properties of iRBCs and making use of field-flow fractionation (FFF), the equilibrium position between electric force and gravitational force of iRBCs is higher than that of healthy red blood cells (hRBCs) comparing to the floor of the channel as shown in Figure 1.10. Furthermore, they integrated these two principles into one device shown in Figure 1.11.[9]

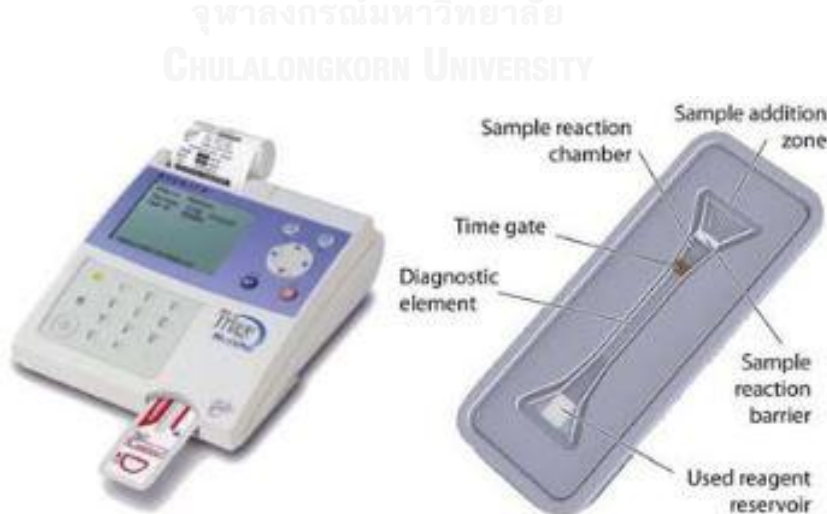


Figure 1.9 Example of commercially available LOC representing the various parts of tasks on the limited space device[10]

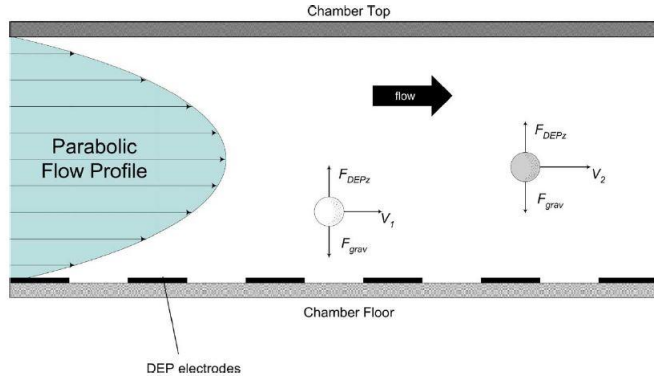


Figure 1.10 Schematic diagram showed the force diagram acting on both types of blood cells, which hRBCs will be equilibrated at the different height from iRBCs. [9]

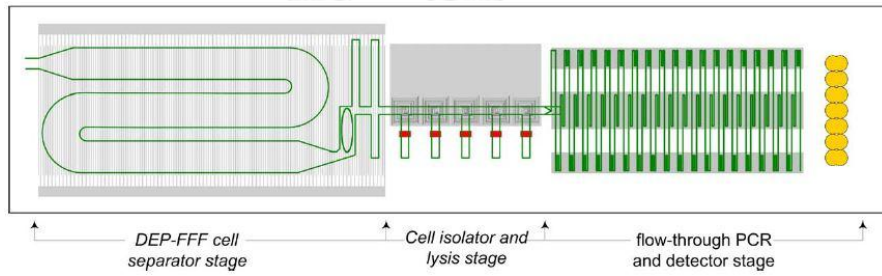


Figure 1.11 Integration diagram of wide range of tasks in their devices [9]

There have been diverse studies by many research groups about investigating physical, chemical and biological properties in order to take these characteristics to design their work for Malaria diagnosis. Moreover, they took advantage of lock-and-key mechanism of protein binding. For example, Stemple et al. (2012) combined Malaria antigen coated into a microfluidic device. Juul et al (2012) used restricted enzyme to detect Malaria. Handayani et al. (2009) found that iRBCs are smaller than hRBCs and they used this advantage to filter the iRBCs out by letting iRBCs flow through the designed area. Hsiang Hsu et al. (2011) designed the detection area for iRBCs by its changed surface of erythrocytes. Han et al (2010) designed their device to get iRBCs in ring stage and trophozoites as well as schizonts achieving 75% and 90% respectively by using the rigidity properties of iRBCs as shown in Figure 1.12 [11-15].

In addition, another example of taking an advantage of mechanical properties is that *P.falciparum* decreases the elasticity of erythrocytes as the parasite becomes mature, but it still has the same surface area. Nevertheless, in the case of *P.vivax*, it differentiates the mechanical properties of the erythrocytes by getting larger and more elastic. Under these conditions, many research groups have taken advantage of physical features and created various kinds of devices. Besides, many studies reported that when the Malaria parasite invades into erythrocytes. When it becomes larger and turns hemoglobin, which is a necessary component for human to carry oxygen through the whole body, into the magnetic crystal called hemozoin shown in Figure 1.13 [16]. It has an influence under non-uniform magnetic field. Some researchers have made use of magnetic properties, discussed in more detail in the next topic.

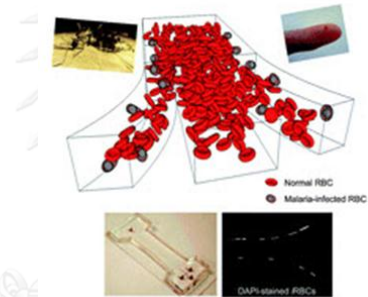


Figure 1.12 Schematic of device by illustrating iRBCs are going to move laterally to the wall of the channel [12]

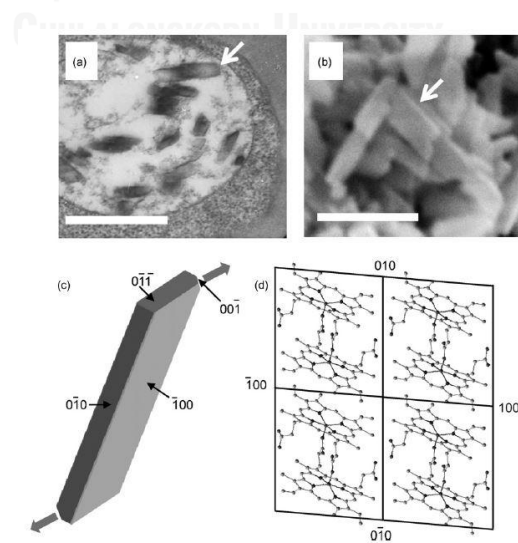


Figure 1.13 Schematic diagram of the overall picture of crystal structure Hemozoin [16]

### 1.6.2 LOC used magnetophoresis for Malaria detection

Firstly, Malaria detection research, F. Paul et al (1981) used permanent magnets with two chambers containing stainless wires 25  $\mu\text{m}$  in diameter. They reported that iRBCs, trophozoite and schizont stage, were stuck in the chamber approximately 75% under operating flow velocity of 0.19 mm/s. The illustration of their device is shown in Figure 1.14a. [17]

Malaria detection in Zimmerman et al. (2006) used the ferrite permanent magnets. Two magnets were placed with the opposite pole and there is an inter-polar gap between them 1.27 millimeters. They measured magnetic field at the line between two magnets and gradient of magnetic field 1.426 T and 804 T/m respectively. Both types of erythrocytes were attracted by magnetic force in perpendicular direction to the surface of the channel between the gap of two magnets. However, the magnetic properties of iRBCs are more concentrated than that of hRBCs. Therefore, the magnitude of magnetic force acting on iRBCs is significantly higher than that of hRBCs.

The other issue was that the longer distance RBCs are far from the surface, the lower the magnitude of magnetic force acts on RBCs. The purpose of the design was to get the highest magnetic force for acting on iRBCs by varying many parameters. Then they proposed the dimension of the device which was 6.4 millimeters in width, 0.25 millimeters in height and operated with flow rate 11.67  $\mu\text{L}/\text{min}$ , which had flowing velocity at the capturing area was 1.2 mm/s.

In the experiment, they flowed the sample into the device with the direction shown in Figure 1.14b, taking the sample approximately 2 seconds to flow through the detecting area, and discarded what came out from the device. In this step, the device had already captured iRBCs in detection area as shown in Figure 1.14b. Thus, they removed the magnet and flowed another buffer to bring and collect the captured sample out from the device and finally inspected it with Giemsa staining.

This method was reported that the device can separate iRBCs almost 100% of *P.falciparum*, 25% of *P.vivax*, almost 100% of *P.malariae* and 75% of *P.ovale*, comparing to the thin film method generally being capable of detecting with 2.7% *P.falciparum*, 0.1% of *P.vivax*, 0.4% of *P.malariae* and 0.2% of *P.ovale* concentration. [18]

In addition, another method for Malaria detection is done by Bhakdi et al. (2010). The working diagram is shown in Figure 1.14c. They concentrated the iRBCs by using permanent magnet in U shape, which has magnetic field around 0.7 Tesla and ferromagnetic stainless wire. They found that their device was able to separate iRBCs up to 94.8 – 98.4%. [19]

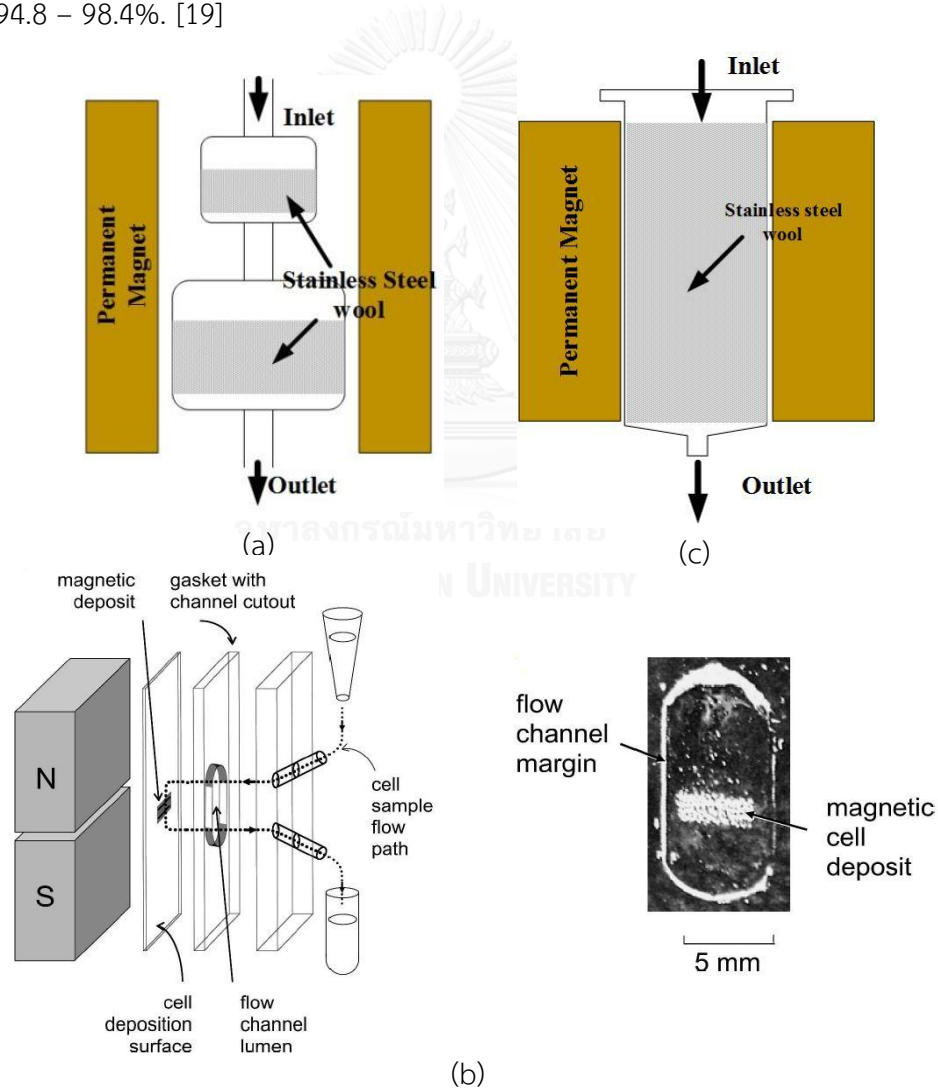


Figure 1.14 Schematic diagram of magnetophoresis principle (a) Paul et al. (1981) (b) Zimmerman et al. (2006) (c) Bhakdi et al (2010) [17-19]

Additionally, the study of J. Kim et al. (2012) was developing the mathematical model for separation by computing the trajectory of iRBCs. They proposed governing equations of iRBCs flowing in a microfluidic device by considering many parameters involved with iRBCs motion. The domain of their studies and the position of magnetic elements are shown in Figure 1.15 and the calculation equation is [20]

$$\frac{4}{3}\pi a^3 \rho_p \dot{v}_p = -\frac{2}{3}\pi a^3 \rho_f \dot{v}_p - 6\pi \mu_f a v_p - 6\pi \mu_f a \frac{a}{\sqrt{\pi v_f}} \int_{-\infty}^t \frac{\dot{v}_p(t_1)}{\sqrt{t-t_1}} dt_1 - \frac{4}{3}\pi a^3 g(\rho_p - \rho_f) \quad (1.1)$$

In this study, they derived from the original motion equation to the most proper form for calculation in order to find out numerically the trajectories of iRBCs moving through their system. The computational result is in Figure 1.16. They modeled ferromagnetic particle and iRBCs shown in Figure 1.16a and Figure 1.16b respectively. Both conditions are in the presence of magnetic flux intensity 0.3 Tesla. They defined their study domain with the distance between each wire 200  $\mu\text{m}$  and diameter of each wire 100  $\mu\text{m}$ , as well as the height of the channel 200  $\mu\text{m}$ . They attempted to compare the result by varying many parameters under given assumptions such as no interaction between each particle. Therefore, on condition that the given sample has too dense of particles, this model may still be used to compute accurately enough.

Not only did this study neglect the term of pressure gradient and added mass as well as Basset force effect but also many studies did not consider those effects because these parameters are not predominant to the motion of infected blood cells. Besides, there is an observation that the pressure gradient may be included in the fluid inertial effect already.

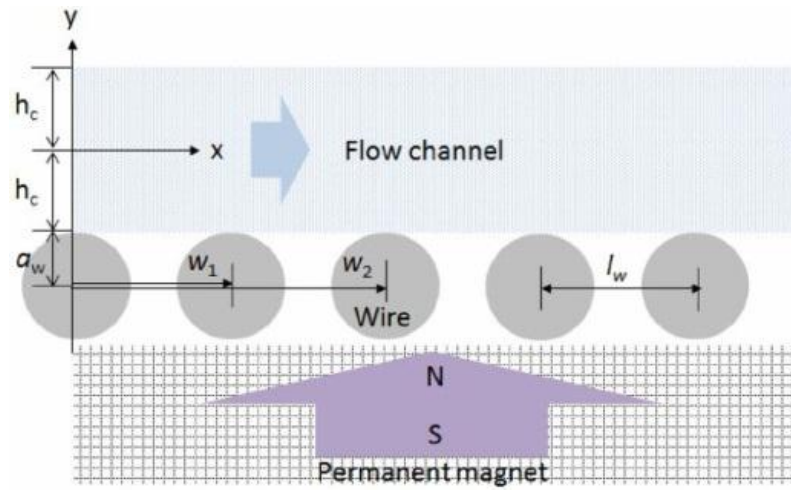


Figure 1.15 The domain combines the array of ferromagnetic wires with permanent magnet beneath the flowing micro channel [20]

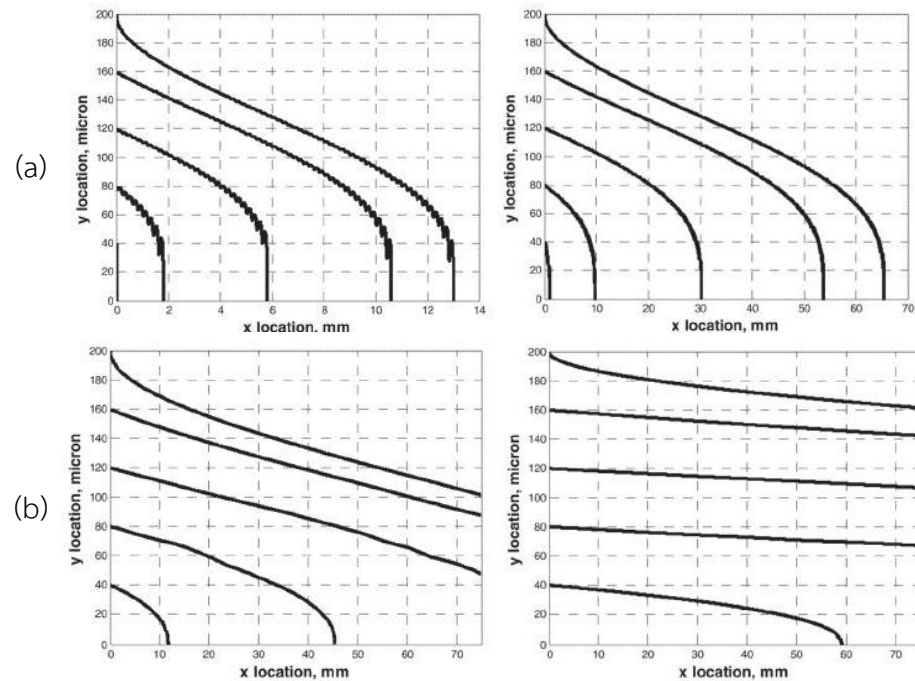


Figure 1.16 Computational result of trajectories under flow rate *left* 1 mL/min *right* 5 mL/min [20]

Moreover, according to J. Nam et al (2013), they demonstrated that the combination of the permanent magnet which had magnitude of magnetic field 0.6 Tesla and ferromagnetic wires which were made from nickel was successfully performed to separate various stages of infected erythrocytes. Their device and working principle are shown in Figure 1.17. The dimension of their device was 50  $\mu\text{m}$  high and 100  $\mu\text{m}$  wide. They also placed the nickel wire parallel along the channel in order to increase the gradient magnetic field at the local point as represented in Figure 2.2.

One of the crucial factors in the experiment is flow rate. Providing they use too high flow rate, the time exposure which the magnetic force acting on iRBCs for separation by attracting iRBCs out from the main streamline is too short.

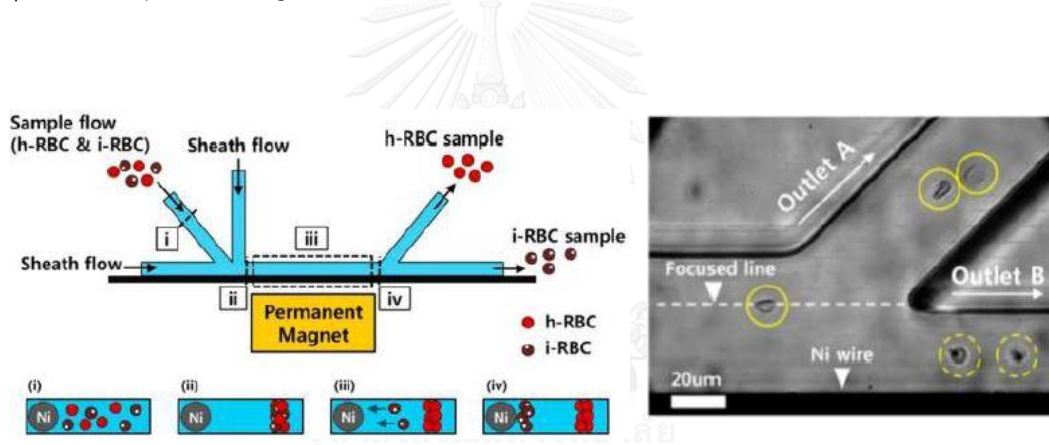


Figure 1.17 Schematic and working principle of the study by having sheath flow controlled by flow rate to focus the sample streamline at the certain distance from the wall where the wire was placed [21]

Furthermore, before they did the experiment with actual iRBCs, they performed modified hRBCs which were treated with sodium nitrite solution oxidizing the chemical compound in red blood cells from  $\text{Fe}^{2+}$  to  $\text{Fe}^{3+}$  which is the same compound produced by the parasite. They mixed the blood sample into the solution with 50 mM concentration and ratio of 1:40. The experiment result found that iRBCs are filtered in ring state 73% and in trophozoite and schizont stage 99.2% under the flow rate 0.8  $\mu\text{L}/\text{min}$ . Not affected by the magnetic force in the system, hRBCs were flowing out to the other outlet 100%.

Recently, pertaining to Kong T. F. et al (2015), their device was composed of two parts, separation and detection. In the separation procedure, they integrated another eminent characteristic of infected erythrocytes which have higher rigidity than healthy erythrocytes and also took advantage of the same principle as the research of Han et al (2010) mentioned previously. Besides, for the diagnosis principle, they used the concept of Magnetic resonance relaxometry (MRR). From their protocol of the experiment, they kept the sample from the streamline near the wall and took it into the diagnostic phase. In this phase, the sample flowed through the device having the area where radio frequency detect coil were placed. If there are iRBCs existing in the sample, the sensor will emit the signal due to their magnetic properties. The device of this study is shown in Figure 1.18. [22]

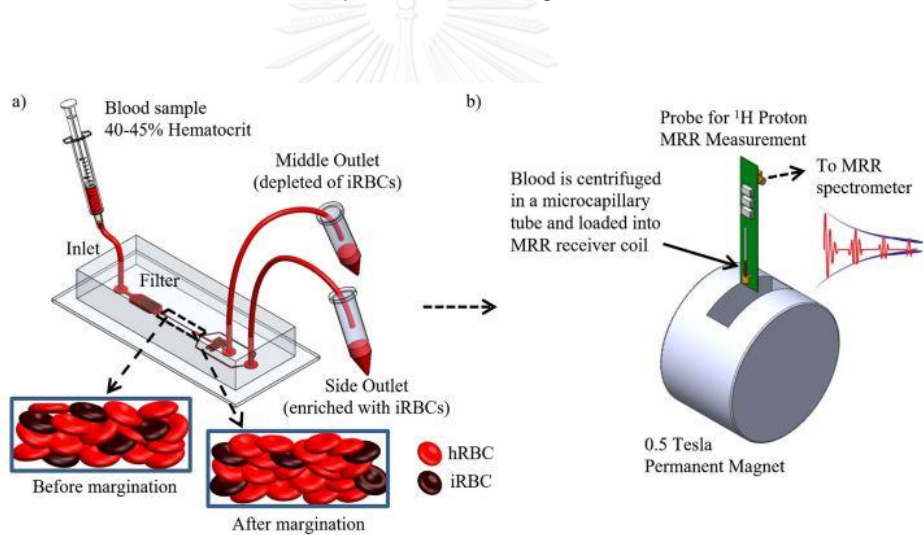


Figure 1.18 (a) Kong T.F. et al (2015) took advantage of rigidity of iRBCs to separate the target sample out and (b) used the Magnetic resonance relaxometry detection principle is used to detect the existence of iRBCs [22]

In conclusion, Lab-on-a-chip technology can combine many functions into only one device in the scale of micro- or nanometer. Additionally, there are predominantly physical characteristics of the Malaria, which have the magnetic-induced product as a biomarker without adding more steps for sample preparation, being useful for designing the system. There is the significant difference between the

magnetic properties of healthy and malaria-infected erythrocytes. Therefore, this thesis employed the magnetophoresis principle in order to separate the infected erythrocytes for separation or detection aspect, attempt to develop the mathematical model for predicting the trajectory of the infected erythrocytes and design as well as fabricate the microfluidic device for separation. However, one of the important issues using magnetophoresis principle is that the magnitude of magnetic force might be insufficient to control the motion of the infected erythrocytes because the common source of magnetic field can generate low gradient of magnetic field. Thus, the thesis also proposes the method to get high gradient of magnetic field by using a magnet array. The array can generate higher gradient of magnetic field comparing to a standalone magnet and be easier to fabricate than combining the ferromagnetic wire into the device, which makes the fabrication process difficult.

### **1.7 Objectives of the thesis**

- 1.7.1. Propose a novel method and design methodology for separating Malaria-infected erythrocytes under an array of magnets by using Finite Element method
- 1.7.2. Develop the fabrication processes, examine the performance of the designed microfluidic device by comparing between the computational and the experimental result.

### **1.8 Scopes of the thesis**

- 1.8.1. Use the Finite Element method and numerical method to analyze the trajectories of blood cells for designing the device
- 1.8.2. Fabricate and inspect the device with a magnet array
- 1.8.3. Perform experiment with 5 and 10  $\mu\text{m}$  magnetic beads and compare the results between the computational model and experiment

1.8.4. Perform experiment with Malaria-infected red blood cells and compare the results between the computational model and experiment

### **1.9 Thesis methodology**

1.9.1. Search for the general information of the Malaria disease such as the life cycle, the infection, and the physical and biological properties of Malaria-infected red blood cells

1.9.2. Review international and national journal papers about separating Malaria-infected in the presence of non-uniform magnetic field for supporting the proposed design

1.9.3. Use magnetophoresis principle by using Finite Element software and numerical method for designing a device.

1.9.4. Develop the mathematical model for predicting the trajectories of magnetic beads

1.9.5. Fabricate a microfluidic device from a proposed design and do the experiment with 5 and 10  $\mu\text{m}$  diameter of magnetic beads

1.9.6. Compare the trajectories resulting from the computational model to the experiment result.

1.9.7. Perform the experiment with mouse blood cultured and supported by Department of Parasitology, Faculty of Veterinary Medicine, Chulalongkorn University.

1.9.8. Summarize and analyze the result and write the thesis

### **1.10 Expected outcomes**

This research is to study and propose a novel method in diagnosing Malaria disease by using a microfluidic device. The microchannel is made from biocompatible polymer, PDMS, using CNC-processed acrylic mold. The separation system contains the array of magnet along one side of the channel. The study concentrates on using software, Finite Element method and numerical method for

calculating the trajectories which help design the microfluidic system. Hopefully, the study can enhance the system in diagnosing Malaria disease in order to filter more effectively the infected patient out in time from the community, which helps prevent spreading of the disease.

### 1.11 Summary

In this chapter, the background and motivation as well as what we have reviewed the literature are summarized. The content consists of Malaria health issues, conventional methods, alternative methods and the role of magnetophoresis in diagnosing Malaria so that the reader can perceive the overall picture of where we are and also the importance of the study. The expectation of the study is to propose a novel method to separate the Malaria-infected erythrocytes by using a microfluidic device and the principle of magnetophoresis, which are already discussed in many studies. In the next chapter, this thesis is about to provide the fundamental information about magnetophoresis principle, the computational model by using COMSOL Multiphysics for simulating the complex model and problem which we cannot solve analytically, and the definition of the mathematical model used to predict the trajectories of both magnetic beads and infected erythrocytes.

## Chapter 2

### Magnetism and Computational Model

This chapter provides the information about magnetism necessary to study such as magnetophoresis principle and the source of magnetic field, computation used by COMSOL Multiphysics, Finite Element calculation software, and the model calculated for predicting the trajectory of the targeted objects which are magnetic beads and malaria-infected erythrocytes so that we can design the device properly.

#### 2.1 Magnetophoretic principles

Magnetophoretic force or magnetic force will be acting on the particle, having magnetic properties. When it get exposed to non-uniform magnetic field as shown in Figure 2.1, the magnitude of magnetic force is calculated as follows [23].

$$F_m = 2\pi\mu_{medium}D^3 \left( \frac{\mu_{particle}-\mu_{medium}}{\mu_{particle}+2\mu_{medium}} \right) \nabla |\vec{H}|^2 \quad (2.1)$$

From Equation (2.1), the magnitude of magnetic force depends on the size of the particle in the third order, the permeability difference between the medium and the particle, and the magnitude of the gradient magnetic field. Thus, controlling the targeted particle can be done by designing the system to create high gradient magnetic field. The equation can be derived into the easier form as describes.

$$F_m = \frac{2}{3}\pi\mu_0\Delta\chi a^3 \nabla |\vec{H}|^2 \quad (2.2)$$

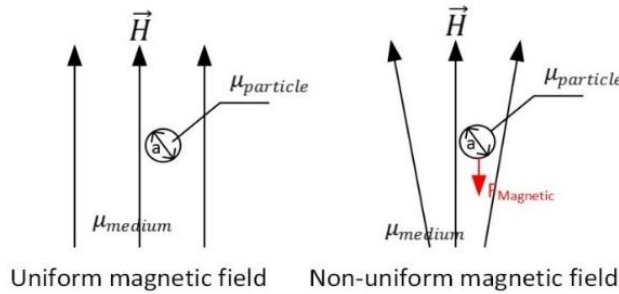


Figure 2.1 Magnetic force acting on the particle exposed to the area having gradient magnetic field

## 2.2 Magnetic field sources

### 2.2.1 Permanent magnet

The stability and strength of the permanent magnet relies on electricity of the material properties. The magnet can be distinguished into two major types that are the permanent magnet, not easily losing magnet stability, and temporary magnet, required to be excited by current. The standalone magnet cannot generate high gradient magnetic field, but if they are placed near to another as an array of magnets, they can create gradient of magnetic field.

### 2.2.2 Electromagnetic

In this source, the magnetic field is induced by the current. The more current density is, the more induced magnetic field intensity will be. Besides, the number of wires rounded around a metal core also affects the magnitude of the induced magnetic field. However, in the microfluidic applications, the tiny device cannot work properly owing to excessive heat accumulated by its structure. For this reason, the limitation of wire materials should be considered in the application of microfluidic devices.

### 2.2.3 Magnetic field induced by ferromagnetic materials

Ferromagnetic material changes the distribution of magnetic field around itself. It not only increases or decreases the intensity of magnetic field but only distort the line of magnetic field, which increases the gradient of magnetic field in a specific area. The influence of ferromagnetic material placed next to the permanent magnet is shown in Figure 2.2. Referring to J. Nam et al (2013), the study also proposed the magnetic force equation with adding the ferromagnetic material as follows [21].

$$F_m = -\Delta\chi V_{BC} \mu_0 M_s a_f^2 \frac{x(H_0 x^2 + \frac{M_s}{2} a_f^2 - 3H_0 y^2)}{(x^2 + y^2)^3} \quad (2.3)$$

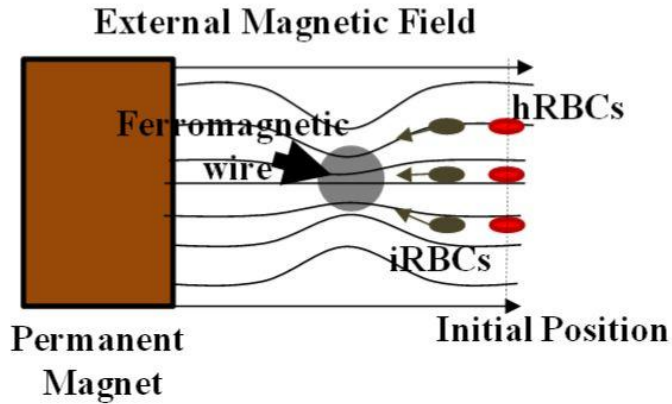


Figure 2.2 Effect of magnetic field distribution after adding the ferromagnetic wire commonly made from nickel

### 2.3 Proposed configuration and necessary data used in the study

From the literature, many studies have developed their devices by using magnetophoresis principle. One of the issues causing low efficiency of separation is low magnitude of magnetic force to control the targeted objects resulting from low gradient magnetic field. A magnet array is one of the solutions to the problem because the appropriate arrangement of the magnet array can produce high-gradient magnetic field. Therefore, we have proposed the configuration in this study as shown in Figure 2.3. One side of the microfluidic device will place a magnet array along the channel. The sample is pumped into the device by one inlet and two sheath flows to control the streamline of the sample by adjusting flow rates. The working concept of the device proposed by the study is that iRBCs will be attracted laterally toward the side of the channel in the presence of magnets. Hence, a calculation of iRBCs trajectory plays an important role in design. This study therefore develops the mathematical model to predict the trajectory of iRBCs for designing an effective microfluidic system to separate iRBCs.

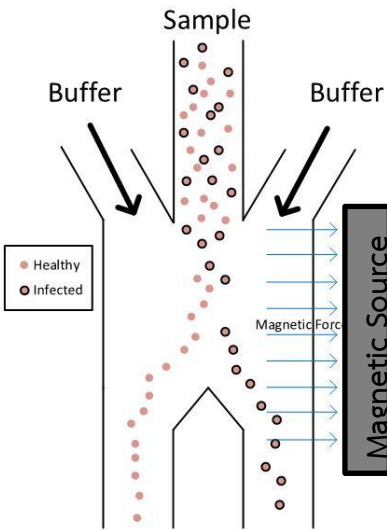


Figure 2.3 Configuration proposed by this study for separating infected erythrocytes

Table 2.1 Magnetic susceptibility of the blood components

Parameter	Healthy red blood cells (hRBCs)	Infected red blood cells (iRBC)	White blood cells (WBC)
Relative magnetic susceptibility	$0.01 \times 10^{-6}$ [11]	$1.80 \times 10^{-6}$ [11]	$-2.57 \times 10^{-6}$ [11]
Magnitude of magnetic force (pN)	0.0000556 0.000556 0.00556	0.01 0.1 1	0.014 0.14 1.4

Table 2.2 Constant properties used in the study

Parameter	Value
Viscosity of water at temperature $25^{\circ}\text{C}$	$8.93 \times 10^{-4} \text{ Ns/m}^2$ [24]
Density of water at temperature $25^{\circ}\text{C}$	$997 \text{ kg/m}^3$ [24]
Density of blood cells	$1100 \text{ kg/m}^3$ [15]
Lift Coefficient ( $C_L$ )	$0.5^{[12]}$
Density of polystyrene	$1050 \text{ kg/m}^3$

Table 2.3 Magnetic properties of magnetic beads

Parameter	Value
Magnetic Susceptibility	0.26 <sup>[25]</sup>
Relative Susceptibility	0.261 <sup>[25]</sup>
Adjusted diameter of magnetic beads size 10 $\mu\text{m}$	9.642
Adjusted diameter of magnetic beads size 5 $\mu\text{m}$	4.821

Table 2.4 Relative magnetic susceptibilities of each type of erythrocytes to water [22]

Type of RBCs	Relative Magnetic susceptibilities ( $\Delta\chi$ ) $10^{-6}$
Healthy	0.01
Early ring form	0.82
Late trophozite stage	0.91
Schizont stage	1.80

## 2.4 Magnetic field distribution (Analytical and computational solutions)

According to G.Xiao-Fan et al (2004), they proposed the analytical solution for magnetic field distribution of standalone rectangular permanent magnet under defined conditions at a local point as shown in Figure 2.4.

Define magnetic field at an arbitrary point

$$\mathbf{B} = B_x \mathbf{i} + B_y \mathbf{j} + B_z \mathbf{k} = \int_0^{h_m} dB_x \mathbf{i} + dB_y \mathbf{j} + dB_z \mathbf{k} \quad (2.4)$$

Magnetic field is directly derived from Biot-Savart law

$$dB = \frac{\mu_0 I dl \times r}{4\pi r^2} \quad (2.5)$$

Consider magnetic field at the side of A'B' in each axis as defines

$$dB_x = \frac{\mu_0 J dz_0}{4\pi} \int_0^{w_m} \frac{(z-z_0) dy_0}{[(x-l_m)^2 + (y-y_0)^2 + (z-z_0)^2]^{3/2}} \quad (2.6)$$

$$dB_y = 0 \quad (2.7)$$

$$dB_z = \frac{\mu_0 J dz_0}{4\pi} \int_0^{w_m} \frac{(l_m-x) dy_0}{[(x-a)^2 + (y-y_0)^2 + (z-z_0)^2]^{3/2}} \quad (2.8)$$

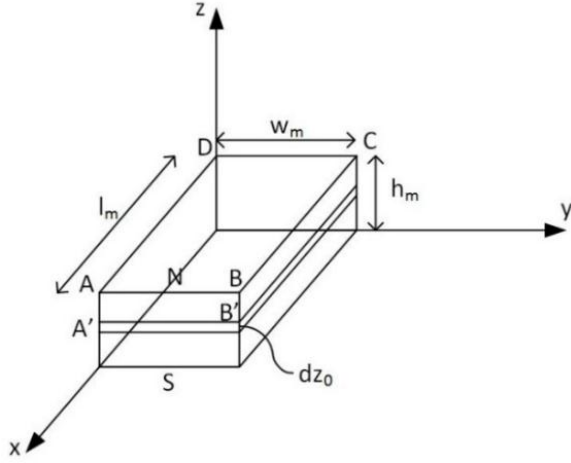


Figure 2.4 Domain and defined parameters used in the equation

Denote the related conditions as follows

$$K = \frac{\mu_0 J}{4\pi} \quad (2.9)$$

$$\Psi_i(\psi_1, \psi_2, \psi_3) = \frac{\psi_i}{(\psi_1^2 + \psi_2^2 + \psi_3^2)^{3/2}} \quad (i = 1, 2, 3) \quad (2.10)$$

$$\Gamma(\gamma_1, \gamma_2, \gamma_3) = \ln \frac{\sqrt{\gamma_1^2 + \gamma_2^2 + (\gamma_3 - z_0)^2} - \gamma_2}{\sqrt{\gamma_1^2 + \gamma_2^2 + (\gamma_3 - z_0)^2} + \gamma_2} \quad (2.11)$$

$$\phi(\varphi_1, \varphi_2, \varphi_3) = \begin{cases} \arctan \left[ \frac{\varphi_1}{\varphi_2} \frac{\varphi_3 - z_0}{\sqrt{\varphi_1^2 + \varphi_2^2 + (\varphi_3 - z_0)^2}} \right] & , \text{if } y \neq 0 \\ 0 & , \text{if } y = 0 \end{cases} \quad (2.12)$$

Derive the same way in other remaining sides, and find the summation of each set of equations then get total magnetic field equation in each axis.

$$B_x = \int_0^{h_m} dB_x = -\frac{K}{2} [\Gamma(l_m - x, y, z) + \Gamma(l_m - x, w_m - y, z) - \Gamma(x, y, z) - \Gamma(x, w_m - y, z)]|_0^{h_m} \quad (2.13)$$

$$B_y = \int_0^{h_m} dB_y = -\frac{K}{2} [\Gamma(w_m - y, x, z) + \Gamma(w_m - y, l_m - x, z) - \Gamma(y, x, z) - \Gamma(y, l_m - x, z)]|_0^{h_m} \quad (2.14)$$

$$B_z = \int_0^{h_m} dB_z = -K[\phi(y, l_m - x, z) + \phi(w_m - y, l_m - x, z) + \phi(l_m - x, y, z) \\ + \phi(l_m - x, w_m - y, z) + \phi(x, y, z) + \phi(x, w_m - y, z) \\ + \phi(w_m - y, x, z) + \phi(y, x, z)]|_0^{h_m} \quad (2.15)$$

In order to get the system having high gradient of magnetic field as much as possible, this study proposes to use an array of magnets instead of standalone magnet. This study therefore chooses the computational method to calculate the complicated model by using COMSOL Multiphysics. Before using the software for getting magnetic field distribution, the study also validates the model with the analytical result coming from Equations (2.13) – (2.15), giving the exact result to the problem. Domain and condition are given in Appendix B.2. From the validation, both computational and analytical results are shown in Figures 2.5 – 2.7. The average deviations between the results do not exceed over 5% which is considered that the conditions given to the model can be acceptable. Thus, the study is to use COMSOL Multiphysics for more sophisticated models in order to help design the system.

From the study of Zimmerman et al. (2006), the magnets in their system had an inter-polar gap causing the gradient of magnetic field to increase. After using COMSOL Multiphysics to validate analytical solution, we can define another model in the software to calculate the magnitude of the magnetic force acting on magnetic beads. We therefore investigate the correlation between the gap of two magnets and the magnitude of magnetic force. Defining the domain in COMSOL Multiphysics shown in Figure 2.8 is performed by varying the gap between two opposite pole magnets from 0 to 500  $\mu\text{m}$ , which increases 50  $\mu\text{m}$  in each case. Then, the magnetic field at the certain points which are far away from the surface of magnets with various distances from 300 to 1000  $\mu\text{m}$  is gathered.

From the result shown in Figure 2.9, the case which its distance measured from the surface of a magnet array less than 600  $\mu\text{m}$  showed the deviation of the magnitude of magnetic force. The more size of gap is, the less force will be. However, when the distance is increased, in the case the gap larger than 600  $\mu\text{m}$ ,

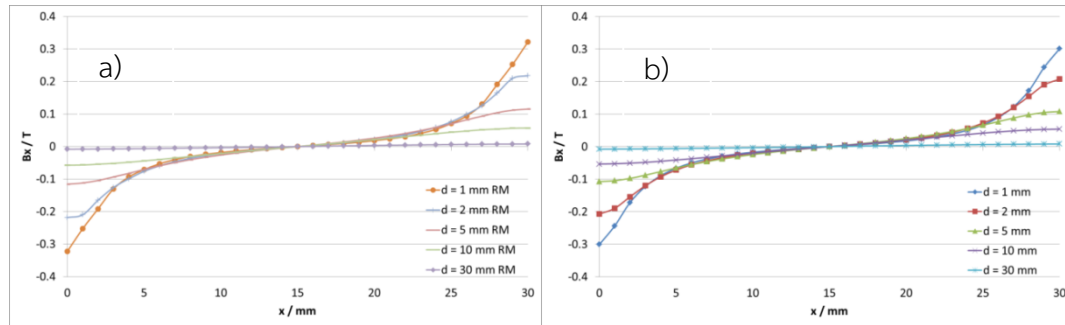


Figure 2.5 Magnetic field distribution in x-axis at  $y = b/2$  (a) the result computed by COMSOL (b) the result calculated by analytical solution by having average uncertainty 4.76%

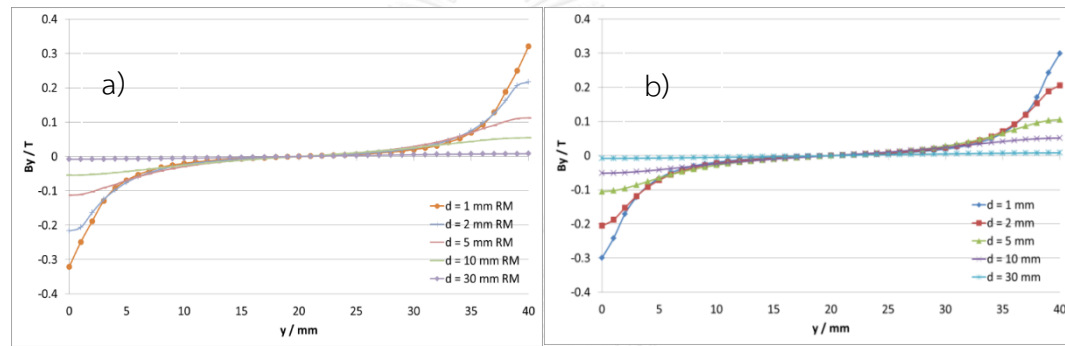


Figure 2.6 Magnetic field distribution in y-axis at  $x = a/2$  (a) the result computed by COMSOL (b) the result calculated by analytical solution by having average uncertainty 4.10%

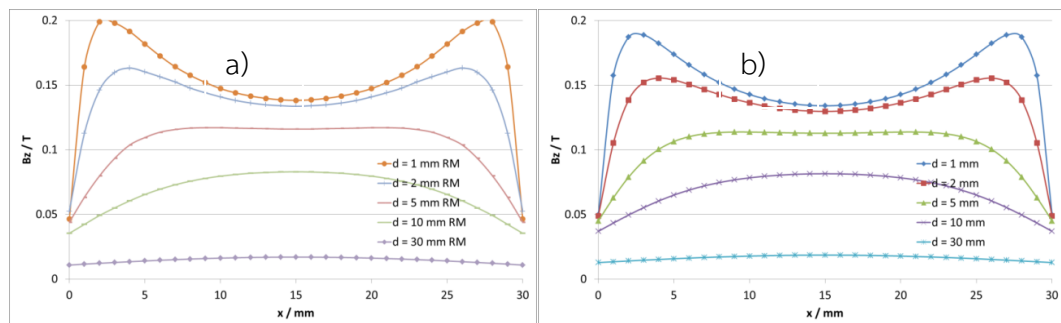


Figure 2.7 Magnetic field distribution in z-axis at  $x = y/2$  (a) the result computed by COMSOL (b) the result calculated by analytical solution by having average uncertainty 4.63%

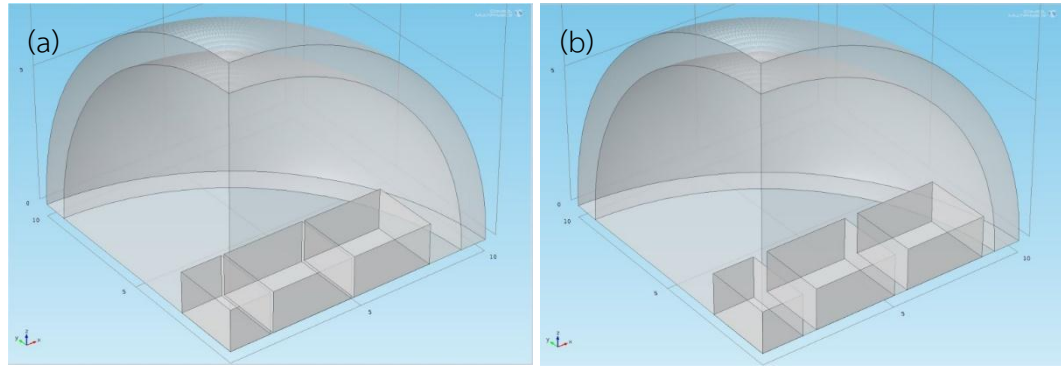


Figure 2.8 the domain defined in COMSOL (a) with the gap 100  $\mu\text{m}$  between magnets (b) with the gap 500  $\mu\text{m}$  between magnets

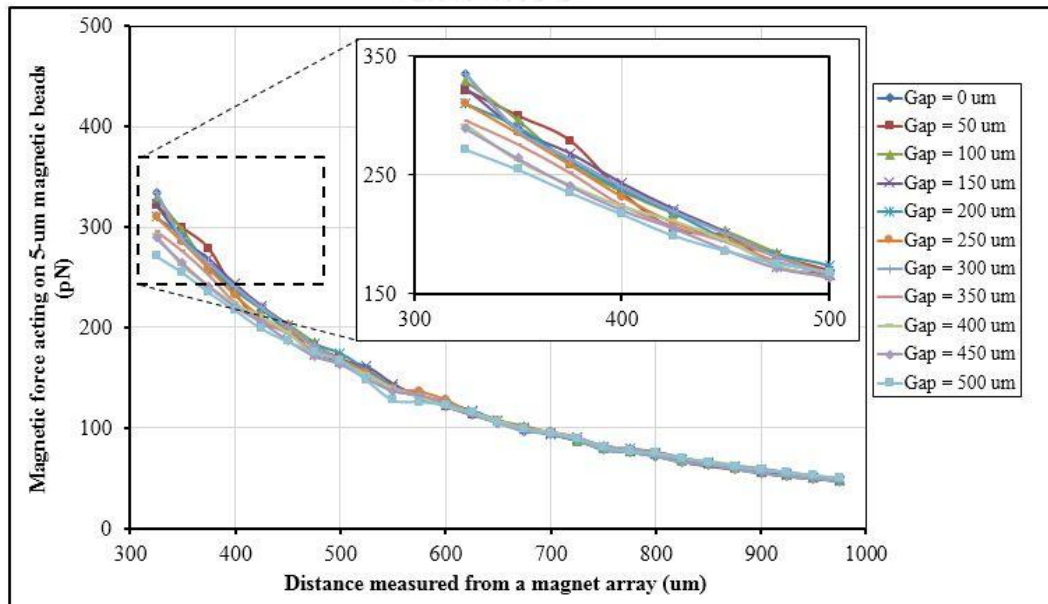


Figure 2.9 Magnitude of magnetic force acting on 5- $\mu\text{m}$  magnetic beads by varying the distance from the magnets from 300 to 1000  $\mu\text{m}$

there is no significant difference in each varied gap. Therefore, this result determines that the gap between two magnets is not predominant if the point we observe larger than the optimum gap which is 600  $\mu\text{m}$ , but the gap is significantly dominant on the condition that the distance is smaller than optimum value.

Furthermore, because of the limitation of fabrication process in the step of making a mold for casting PDMS, this study has proposed the designed schematic diagram of device shown in Figure 2.10. The microfluidic device is composed of 3 inlets, 2 outlets, 500  $\mu\text{m}$  wide and 3 cm long for main channel, as well as 100  $\mu\text{m}$  high for the whole channel. An array of magnets also lies at the one side of the channel.

In order to reduce the domain of the model and simplify the computation, this study has used COMSOL to simulate an array of magnets by being given infinite magnets. The domain as a rectangular domain shown in Figure 2.11 is given and the mesh size of elements is varied from 1 to 70  $\mu\text{m}$ . The magnetic field distribution is computed and shown as shown in Figure 2.12. After that COMSOL can provide the magnetic field at arbitrary point, shown the distribution in Figure 2.13, and the data is to calculate the magnetic force acting on targeted particles such as, in this study, magnetic beads or infected erythrocytes. The magnetic force distributions in z- and x-axis are calculated and fit curve for the equations which are used to calculate the trajectory in each model, discussed in the next section.

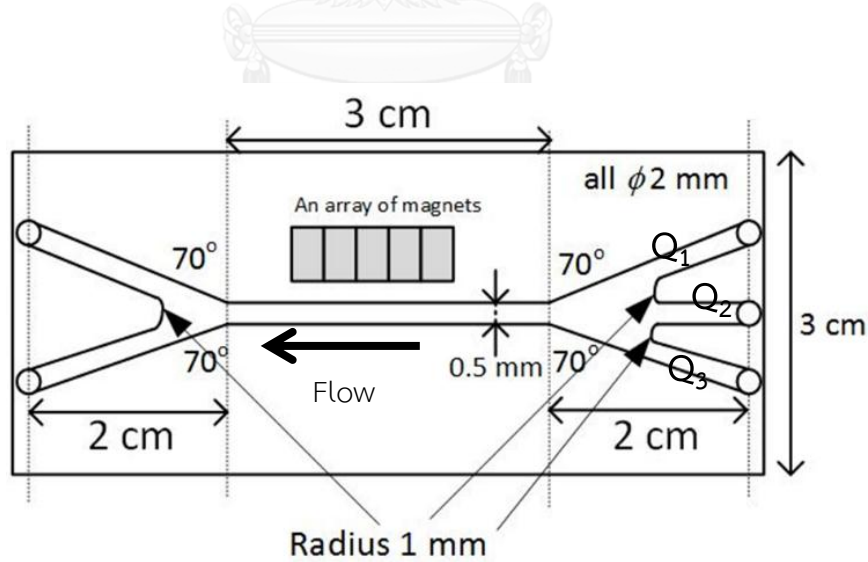


Figure 2.10 Schematic diagram of the designed microfluidic device including dimensions

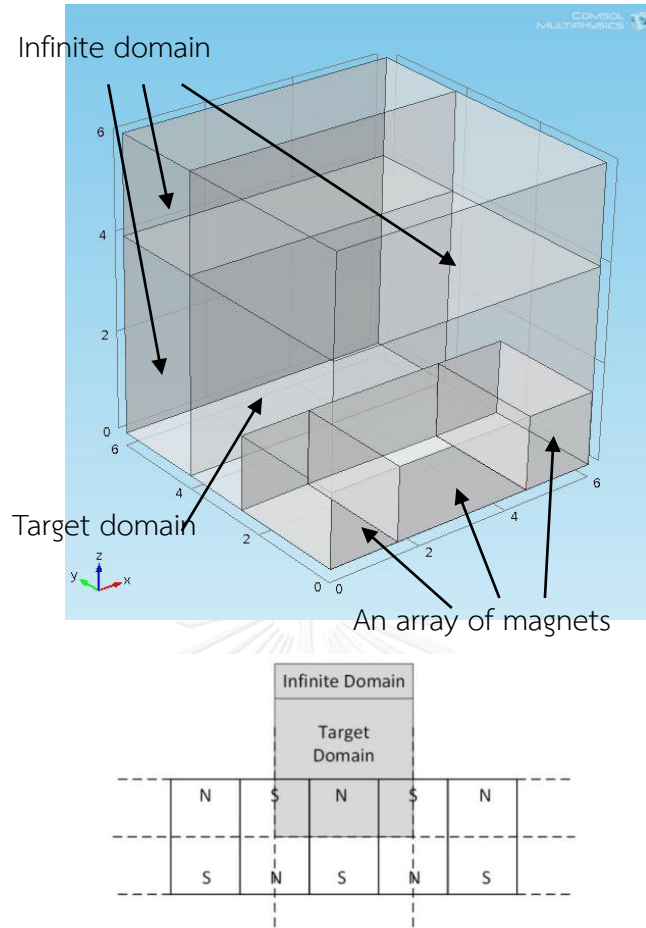


Figure 2.11 Domain used in the study including the boundary of infinite magnets

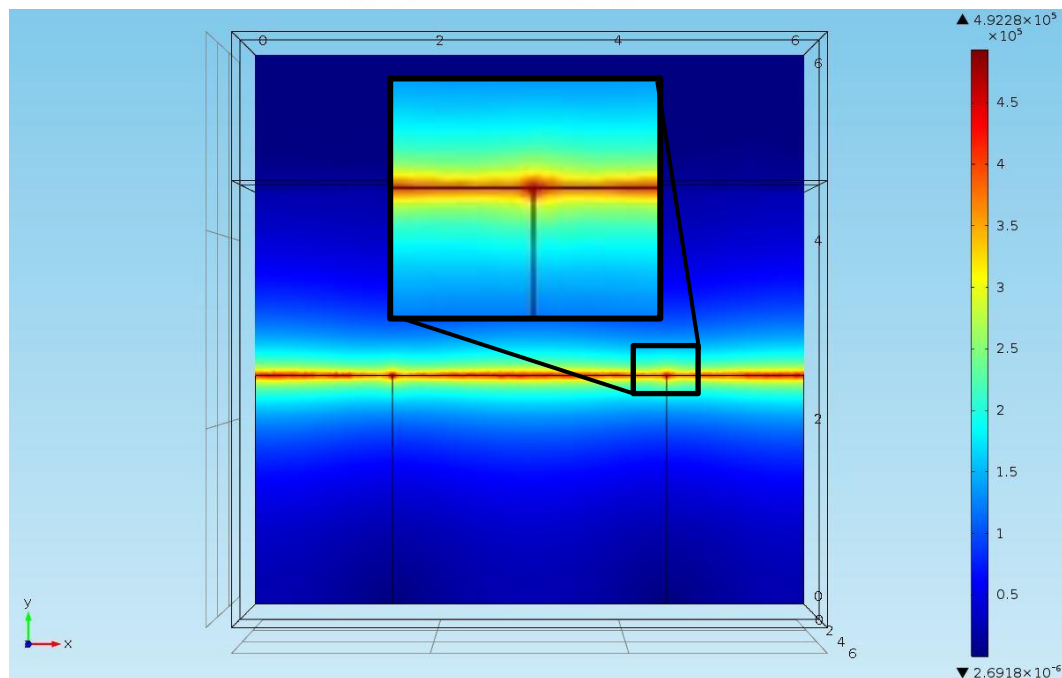


Figure 2.12 Magnetic field distributions A/m in illustrated by using color range

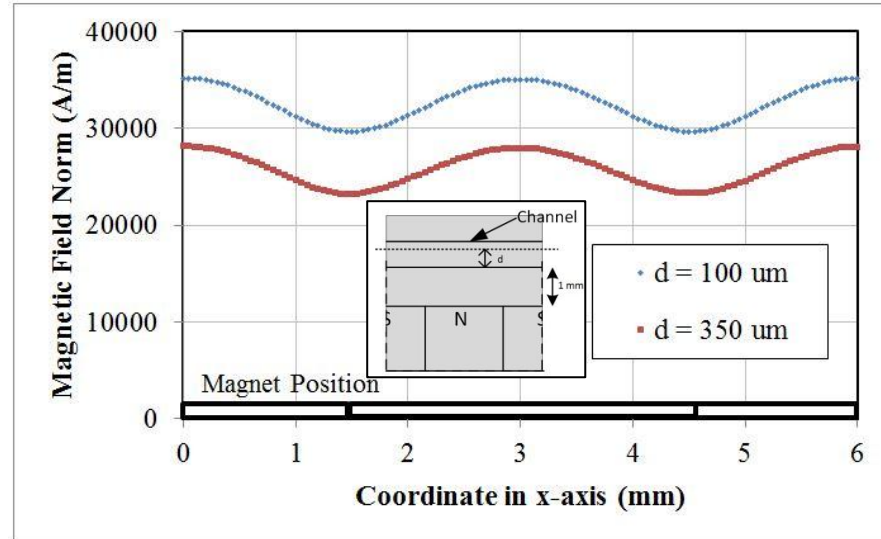


Figure 2.13 Magnetic field distribution at  $d = 100$  and  $d = 350 \mu\text{m}$

## 2.5 Trajectory of blood cell by influence of an array of magnets

The study has given the coordinate shown in Figure 2.14a by giving x-axis as flow direction, y-axis as the vertical direction comparing to the height of the channel and z-axis as the lateral direction. According to Basset-Bousinesq-Oseen equation (BBO), the force acting on blood cells consists of drag force, pressure gradient force, Basset, and added-mass-effect force as well as external force. In this study, the proposed model neglected the influence of added mass and Basset force because the magnitude of these forces acting on blood cells is relatively low. In terms of pressure gradient effect, there is some arguments about considering this effect to compute in the motion equation. Soo et al. (1975) indicated that this effect was already included in the effect of fluid inertial force. Therefore, its effect to the trajectory is also neglected. The detail of calculating the order of magnitude is shown in Appendix C.1.

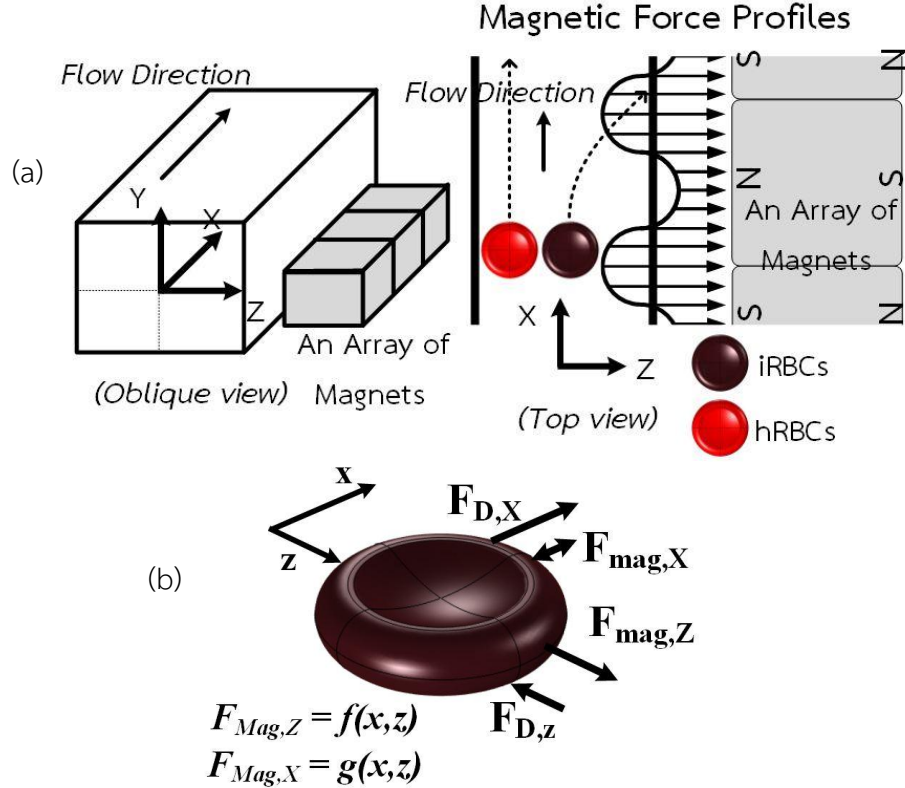


Figure 2.14 (a) Schematic diagram of study domain (b) Force diagram acting on two types of erythrocytes exposed to the non-uniform magnetic force

Therefore, the force considered in the model comprises merely drag force and magnetic force which is external force in this case. The force diagram is represented in Figure 2.14b. Similarly, trajectory of the model has been computed by using the Newton's law of motion. Besides, the equations used in the study are in the form of differential equations as follows

$$F_{D,x} = \rho_{RBC} V_{BC} \frac{d^2x}{dt^2} \quad (2.17)$$

$$F_{m,z} - F_{D,z} = \rho_{RBC} V_{BC} \frac{d^2z}{dt^2} \quad (2.18)$$

In this model, after getting the data extracted from COMSOL Multiphysics, the magnitude of magnetic force acting on infected erythrocytes is extremely low comparing to the order of drag force. In order to decrease computation time, we decide to deduct the magnetic force term in x-axis. One of factors involved in this model is the term of drag force because the shape of model is not simple. All

previous models has considered objects as spherical shape bringing about using stoke's law for drag force acting on the model. However, in this case, we consider the model as the biconcave shape which is simulated from the actual red blood cells drawn by COMSOL Multiphysics. Therefore, the drag force equation can be derived as

$$F_D = C_D \left( \frac{1}{2} \rho_f v_{rel}^2 A \right) \quad (2.19)$$

In this study, the flow in microchannel is considered as laminar flow.  $C_D$  can be defined as

$$C_D = \frac{24}{Re} \quad (2.20)$$

Substitute Equation (2.19) into Equation (2.20), the drag force of general shape can be described as

$$F_D = \frac{12 \mu_f v_{rel} A_s}{D_h} \quad (2.21)$$

From Equation (2.21), we consider the parameter  $A_s$  which is the projected area of object exposed to the fluid by mimicking the concept of Stokes' law. Figure 2.15 shows the exposure area between both models that affect the magnitude of drag force acting on the models. The characteristic of the model drawn by COMSOL Multiphysics is also shown in Tables 2.5 – 2.6 and Figure 2.14b.

The magnetic force term is fit from the results simulated by COMSOL Multiphysics, which uses the necessary constant properties in Tables 2.2 – 2.3. From the magnetic force distribution, the magnetic field at each point relies on position in the domain. Consequently, the force equation at the distance of 100, 200 and 300  $\mu\text{m}$  away from the array is in function of x and z coordinate as follows

$$\begin{aligned}
f_{m,z,100\mu m} = & \\
(1.383 \times 10^{-15} + 2.734 \times 10^{-17} \cos(2094x) - 1.17 \times 10^{-20} \sin(2094x) + & \\
2.913 \times 10^{-17} \cos(2 \times 2094x) + 1.933 \times 10^{-19} \sin(2 \times 2094x) - 2.014 \times & \\
10^{-17} \cos(3 \times 2094x) + 2.212 \times 10^{-19} \sin(3 \times 2094x) + 9.52 \times 10^{-18} \cos(4 \times & \\
2094x) - 6.058 \times 10^{-20} \sin(4 \times 2094x)) \cdot (4.723 \times 10^{17} \exp(1.52 \times 10^4 z) + & \\
(1.593 \times 10^4 \exp(-3344z))) & (2.22)
\end{aligned}$$

$$\begin{aligned}
f_{m,z,200\mu m} = & \\
(9.688 \times 10^{-16} + 3.976 \times 10^{-17} \cos(2094x) - 1.999 \times & \\
10^{-19} \sin(2094x) + 8.639 \times 10^{-18} \cos(2 \times 2094x) - 1.056 \times 10^{-19} \sin(2 \times & \\
2094x) - 6.43 \times 10^{-18} \cos(3 \times 2094x) + 5.17 \times 10^{-19} \sin(3 \times 2094x) + & \\
2.925 \times 10^{-18} \cos(4 \times 2094x) - 1.534 \times 10^{-19} \sin(4 \times 2094x)) \cdot (7.274 \times & \\
10^{11} \exp(-9906z) + (2369 \exp(-2623z))) & (2.23)
\end{aligned}$$

$$\begin{aligned}
f_{m,z,300\mu m} = & \\
(7.063 \times 10^{-16} + 4.373 \times 10^{-17} \cos(2094x) - 1.357 \times & \\
10^{-19} \sin(2094x)) \cdot (1.487 \times 10^{10} \exp(-8350z)) & (2.24)
\end{aligned}$$

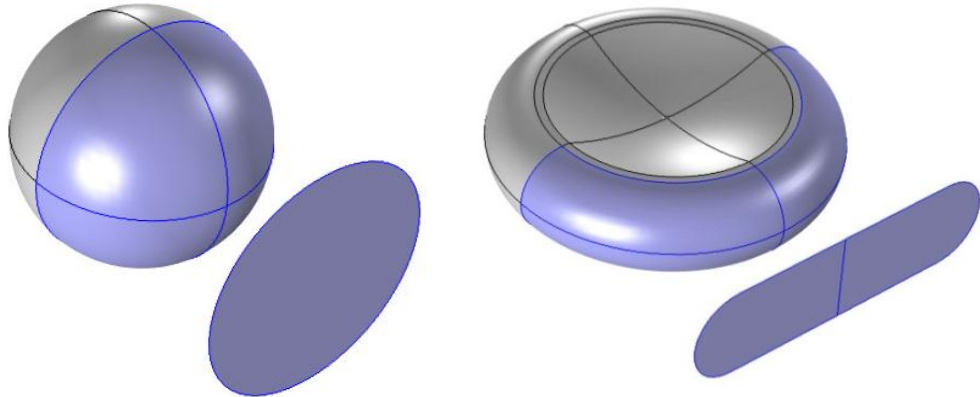


Figure 2.15 Comparison of projected area between stokes' law modeling on spherical object and our RBCs model.

Table 2.5 Physical Properties of blood

Parameter	Reference	Value	The study's selection
Size	B. Angelov et al. (2000) [26]	Diameter 6.9 – 9.3 $\mu\text{m}$ Thickness 2.4 – 3.7 $\mu\text{m}$ Surface area 104.7-193.3 $\mu\text{m}^2$ Volume 73 – 200 fL	
	M. Diez-Silva et al. (2010) [27]	Diameter 7.5 – 8.7 $\mu\text{m}$ Thickness 1.7 – 2.2 $\mu\text{m}$ Volume 94 fL	Diameter 8 $\mu\text{m}$ Thickness 2 $\mu\text{m}$
	I Udroiu et al. (2014) [28]	Diameter 7.2 $\mu\text{m}$ Thickness 2.25 $\mu\text{m}$ Surface area 136.55 $\mu\text{m}^2$ Volume 91.31 fL	
Viscosity	A. Zhanov et al. (2011) [29]	4 cP (Normal hematocrit) 2.5 – 4 cP	3 cP
Density	M.Takayasu et al. (1999) [30]	1125 $\text{kg}/\text{m}^3$	1125 $\text{kg}/\text{m}^3$

Table 2.6 Physical Properties of RBCs model measured by COMSOL

Parameter	Value
Surface area	139.12 $\mu\text{m}^2$
Volume	88.68 fL
Surface area, projection in x and z axis	17 $\mu\text{m}^2$

To improve the set of equations to be more accurate, the study decides to split the case for fitting force equations shown above in Equations (2.22) – (2.24). In each case is given by the initial position far away from the magnet 100, 200 and 300  $\mu\text{m}$  respectively. In addition, the force distribution is too complex to fit with 1<sup>st</sup> order fourier series function. We make a decision to use 4<sup>th</sup> order fourier series function which is more precise ( $R^2$  is nearly 1). Furthermore, the study selects the numerical method which is similar to the previous model shown in Appendix C.2 and C.3. The

whole trajectory will be calculated by finite difference method by defining small time step, 5  $\mu$ s in this model.

The defined conditions used in the study are no interaction between cells, neglect all secondary flow effects such as pressure gradient and dean effect etc. The magnetic force in x-axis is also neglected because its magnitude is not significant comparing to the order of drag force, and the another assumption is the object will move on the floor plane resulting from the result in Appendix C.2.

After that, we have designed the program to compute for the final position and turn it to be the next initial position as well as calculate reiterately until the program reaches the given numbers of iteration. The MATLAB code is in Appendix A.4 and also the detail about computational data and equations are shown in Appendix B.3 – B.6. The computational trajectory in the case far away from the magnet 200  $\mu$ m and 300  $\mu$ m shown in Figure 2.16 and Figure 2.17 respectively. They determine that the infected cells can move laterally from 29.14 to 100  $\mu$ m within 3 cm of the device.

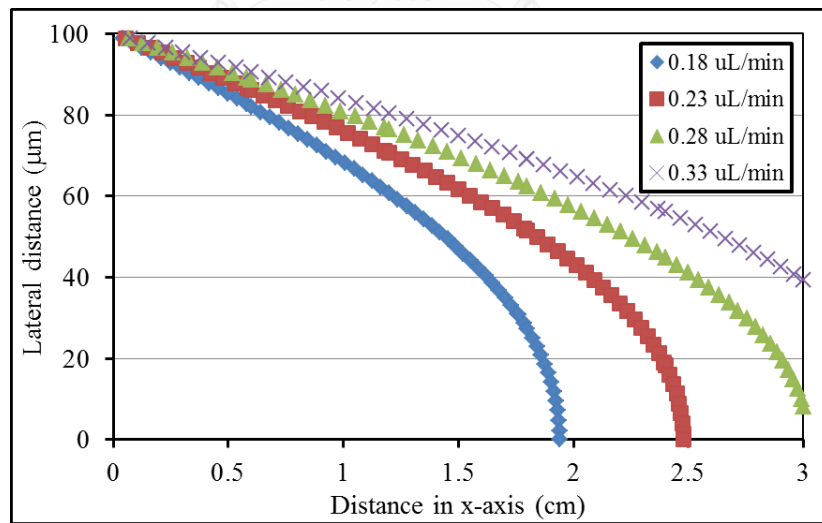


Figure 2.16 Calculated result with various flow rates in the case 200  $\mu$ m from the magnet array

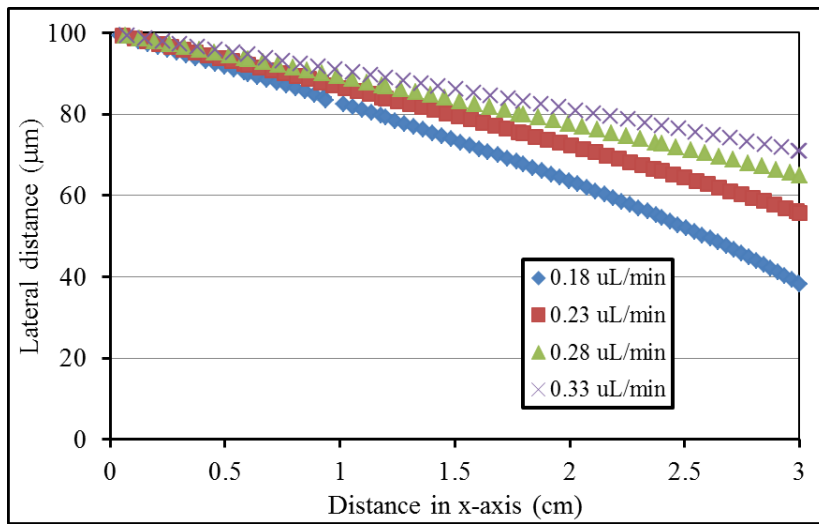


Figure 2.17 Calculated result with various flow rates in the case 300  $\mu\text{m}$  from the magnet array

## 2.6 Summary

In this chapter, we summarize the fundamental of magnetism particularly the magnetophoresis principle which plays an important role in controlling Hemozoin, magnetic crystal produced the parasite. The significant factors affect the magnitude of magnetic force that are its magnetic properties of the target, size and the magnitude of gradient magnetic field. One of these factors providing the highest magnitude of magnetic force as much as possible is the gradient magnetic field. As a consequence, we study which pattern or source can generate high gradient of magnetic field. In order to tackle this issue, COMSOL Multiphysics is used to simulate magnetic field distribution of the complex model, in this case a magnet array. The analytical solution is also used to validate to study how well the conditions properly defined in the domain of study. Then, the model is developed in order to predict the trajectory of infected erythrocytes by using the Newton's law of motion. Finally, all of the model will be validated by the result of the experiment, which is discussed later. The next chapter provides the information about the fabrication process and necessary preparation of the experiment.

## Chapter 3

### Fabrication process and Experimentation

This chapter recounts the fabrication process included the detail of each process and also explains about the experiment detail from the list of equipment to the conditions of each case. Besides, this study goes more detail about a biological preparation of blood culture and solutions etc.

#### **3.1 Microfluidic conventional fabrication process**

Conventional fabrication process creating a microfluidic device is known as Soft lithography process shown the detail in Figure 3.1. The photoresist SU-8, common used in the fabrication, is coated on a silicon substrate by a spinner for uniform distribution. After that, the substrate will be exposed to the ultraviolet (UV) light called photolithography. UV light is penetrating through transparent area of the designed mask. UV light changes chemical properties of the negative type of photoresist to become hardened. Then, the substrate is developed by SU-8 developer, which removes the unexposed part of the photoresist and the hardened part will be as a mold. In the process of casting, liquid polymer, PDMS (Polydimethylsiloxane) is mixed and poured onto the SU-8 mold. Then, liquid polymer is cured with heat generally around  $80^{\circ}\text{C}$  so that the polymer will become solid. After curing the PDMS, the solidified PDMS is gently peeled off from the mold, and is cut with proper size by a cutter blade before bonding to glass slide with oxygen plasma treatment for creating the microchannel.

In this study, we have fabricated a mold by using a CNC-processed acrylic substrate. The method gives us more convenient than the conventional method because we can cut down the number of steps in chemical preparation, which deals with an expensive cost or a non-uniform mold resulting from setting the substrate unsuitably while spinning. As a result, we can use an acrylic as a mold which has minimum resolution giving us a channel larger than  $100 \mu\text{m}$  in height and  $500 \mu\text{m}$  in

width, which is still acceptable in the study. The detail of fabrication process reviewed and adapted from Jeongnum et al (2013) is indicated that they mixed liquid PDMS with curing agent at ratio 10:1 by weight and let the bubble while mixing off by using a vacuum chamber. Then, they cured PDMS at  $80^{\circ}\text{C}$  for an hour and bonded it with cleaned glass slide to treat with oxygen plasma machine at 250W, 80 mTorr for 50 seconds. After oxygen treatment, the PDMS was soaked in absolute ethanol solution in order to be capable of aligning the PDMS channel on glass slide arbitrary. They continued treating the PDMS in oven at  $80^{\circ}\text{C}$  for 90 minutes for irreversible bonding before they connected the tube, inlets and outlets, with epoxy glue.

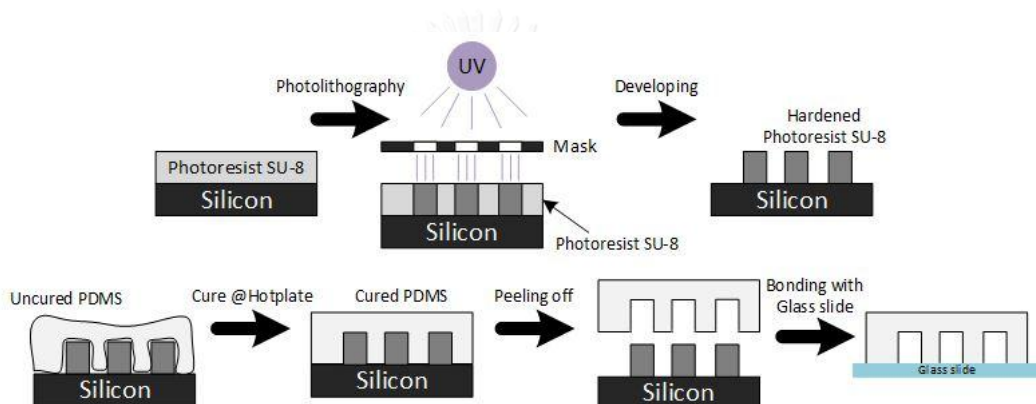


Figure 3.1 Process flow of Soft lithography process

This study applies and adjusts the fabrication procedure which is already reviewed from many studies because some of the instruments used in our study have different specifications leading to several issues in fabrication. For instance, we use the oven to cure PDMS at  $80^{\circ}\text{C}$  for 1 hour similar to the study of Jeongnum et al (2013), but it is not well-cured and causes difficulty in cutting PDMS device as it is still sticky. Therefore, in the process of curing PDMS, curing time needs to be increased up to 2-3 hours and The PDMS structure will be already hardened enough to cut.

### 3.2 Equipment and fabrication process

#### 3.2.1 List of equipment

All instruments and materials used in the study are listed below

##### *3.2.1.1. Instruments*

- Vacuum oven, Jeio Tech, model OV-11
- Optical microscope, Seek Inter Co., Ltd., model SK-XJM series
- Cutter, Horses
- Belt Puncher, Sunkey
- Plasma Cleaner, Harrick Plasma, model PDC-32G, cooperating with Prof. Orawan Chailapakul, Department of Chemistry, Faculty of Science, Chulalongkorn University

##### *3.2.1.2. Materials and reagents*

- Acrylic plate size 12x12x1 cm, purchased from Quality product manufacturing and trading (Thailand) Co., LTD.
- Isopropyl Alcohol (IPA)
- Deionized water (DI water), Millipore, Model Direct-Q
- PDMS (Polydimethylsiloxane), Sylgard 184 silicone elastomer base
- PDMS curing agent, Sylgard 184 silicone elastomer curing agent
- 96% Sulfuric acid, Carlo Erba Reagents, batch number 3A0573131A
- Hydrogen peroxide ( $H_2O_2$ ) solution 40% m/v in water, Carlo Erba Reagents, Code no. 307701
- Glass slide, Sail brand, 25.4x76.2 mm 1mm-1.2mm thick, Cat. No. 7107
- $N_2$  tank, Thai Special Gas Co., Ltd.
- Tube, Cole Palmer RF#06422-00, with inner diameter 0.5 millimeters and outer diameter 2.1 millimeters.

### 3.2.2 Fabrication process

#### 3.2.2.1. Preparation of acrylic mold

- Design the pattern drawn with Microsoft Visio and cut with CNC process
- Inspect the CNC-processed acrylic mold, clean with IPA and DI water
- Use acrylic thin piece to create a wall of the mold and attach them with acrylic glue

#### 3.2.2.2. PDMS casting

- Mix PDMS liquid form 60 g with PDMS curing agent 6 g and stir thoroughly. The more bubbles they happen, the better they are well mixed

- Pour onto prepared acrylic mold and let it spread till it is uniform on the mold
- Put it in vacuum chamber to remove bubbles out from the mold for 5-10 minutes at 55°C.

Note: During setting the temperature, In order to avoid the fluctuation of temperature, the oven should be set before using around two hours.

- Cure it at 80°C for 1 hour
- Peel the PDMS off from the mold. In this stage, after curing just 1 hour is to peel easily and to make sure that we do not damage the channel.
- Continue heating it in the oven for 2 hours to get well-cured PDMS

#### 3.2.2.3. Glass preparation

- Clean glass slide with Piranha treatment, mixing H<sub>2</sub>SO<sub>4</sub> 50 mL with H<sub>2</sub>O<sub>2</sub> 5 mL, for 30 minutes

Note: Be careful the heat originating from the reaction.

- Wash the Piranha solution out with DI water before using IPA to further clean the surface of the glass
- Dry the glass slide with blowing N<sub>2</sub>

Note: Do not let it dry itself because the solution may leave the stain onto the glass, leading to have unclear visibility during observing under a microscope or make it difficult to bond with PDMS.

#### *3.2.2.4. Bonding PDMS with glass slide*

- After cutting PDMS with proper size to glass slide, punch inlets and outlets with the belt puncher size 2 millimeter in diameter
- Also, cut the PDMS at the area beside to the channel for laying a magnet array similar to figure 2.13
- Put them into the plasma treatment chamber by setting the side which we want to articulate together

Note: During the process, use disposable glove not to make the surface of each element contaminated with dust or fingerprint.

- Plasma treatment; vacuum the chamber, turn on the power, adjust the inlet air flow into the chamber to get violet color resulting from plasma ignition, leave it for 3 minutes
- After plasma treatment, we put them attach with each other and cure it again in the oven at 80°C for irreversible bonding for 2 hours

#### *3.2.2.5. Connect inlet and outlet tubes and inspection*

- Cut a tube with proper length.
- Connect prepared segmented tubes to inlets and outlets

- In order to prevent the flow to leak out of the system, we have to seal inlets and outlets with only liquid PDMS, around 2 g
- Cure them in the oven at 80°C and lay the chip upside down not to make it clogged because of permeation of PDMS liquid into the channel.
- After the device is well-cured, inject the DI water into the device to make sure that the device does not have leakage and also there is no clog inside the device.

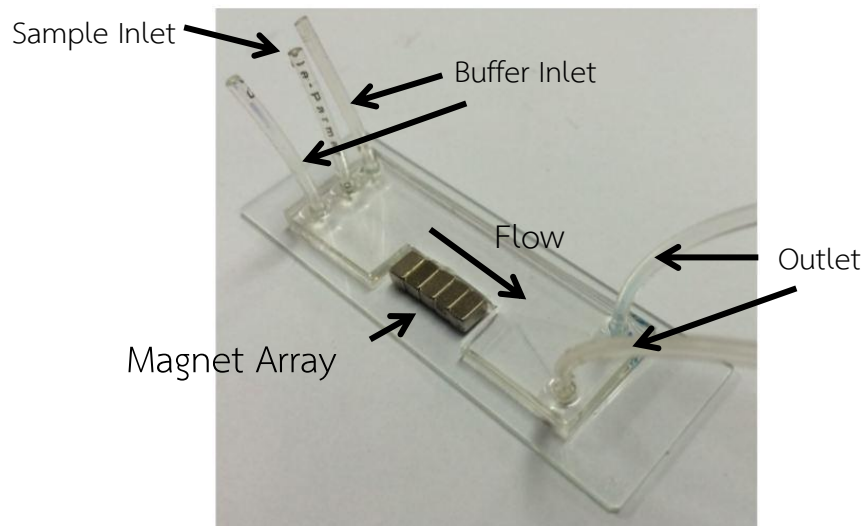


Figure 3.2 A microfluidic device used in the study

CHULALONGKORN UNIVERSITY

### 3.3 Summary

The overall procedure to fabricate a microfluidic device is already proposed. Besides, the reader could see a list of equipment and materials as well as necessary reagents to conduct the experiment. In the next chapter, there is a discussion on the magnetic bead experiment, which the computational model will be comparing to the experimental result. After that, the total uncertainty is investigated and included the suggestion to edit our model or the experimental procedure for improving the quality of our separation device in the next experiment with actual blood sample further.

## Chapter 4

### Magnetic bead experiment

This chapter discusses the magnetic bead experiment in the all aspects including the mathematical model, a set of governing equations, experimentation and model validation in order to illustrate the method to predict the trajectory of the magnetic beads.

#### 4.1 Trajectory of magnetic beads by influence of an array of magnets

The study has given the same coordinate as the study in Appendix C.2 shown in Figure 4.1a. The force diagram is also represented in Figure 4.1b. In this model, we have used magnetic beads as a model of infected erythrocytes. A form of equations is also similar to the previous model as describes.

$$F_{m,x} + 6\pi\mu_f a(v_f - v_{p,x}) = \rho_p A \frac{d^2x}{dt^2} \quad (4.1)$$

$$F_{m,z} - 6\pi\mu_f a v_{p,z} = \rho_p A \frac{d^2z}{dt^2} \quad (4.2)$$

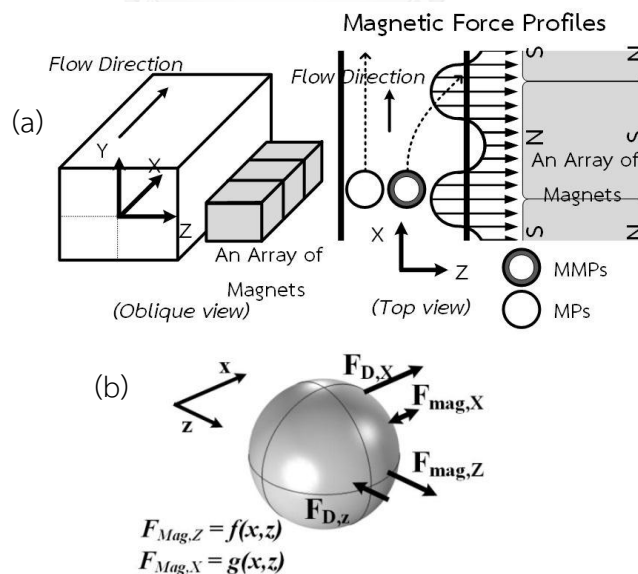


Figure 4.1 (a) Schematic diagram of study domain (b) Force diagram acting on two types of particles in the experiment under exposed to non-uniform magnetic force.

Similarly, the method that fits magnetic force equations is the same as previous model shown all details in Appendix C.2.

$$F_{m,x,5,\mu m,z=1.7mm} = (8.293 \times 10^{-15} + 1.516 \times 10^{-14} \cos(2112x) + 1.388 \times 10^{-12} \sin(2112x)) \cdot (-6.914 \times 10^6 z^2 + 5.332 \times 10^4 z - 101) \quad (4.3)$$

$$F_{m,z,5,\mu m,z=1.7mm} = (6.438 \times 10^{-12} + 9.609 \times 10^{-13} \cos(2094x) + 9.917 \times 10^{-14} \sin(2094x)) \cdot (1.712 \times 10^4 e^{-2323}) \quad (4.4)$$

$$F_{m,x,10,\mu m,z=1.7mm} = (6.634 \times 10^{-14} + 1.213 \times 10^{-13} \cos(2112x) + 1.111 \times 10^{-11} \sin(2112x)) \cdot (-8.936 \times 10^{-14} e^{6871z} + 380.5 e^{-1358z}) \quad (4.5)$$

$$F_{m,z,10,\mu m,z=1.7mm} = (5.151 \times 10^{-11} + 7.687 \times 10^{-12} \cos(2094x) + 7.933 \times 10^{-13} \sin(2094x)) \cdot (1.712 \times 10^4 e^{-2323z}) \quad (4.6)$$

Equations (4.3) – (4.4) are for 5  $\mu\text{m}$  of magnetic beads and Equations (4.5) – (4.6) are for 10  $\mu\text{m}$  of magnetic beads at the distance of 1.7 mm from the magnet. Calculating the trajectory is described in Appendix C.2 In this case, we define time step to be 0.1  $\mu\text{s}$ . The MATLAB code are in detail in Appendix A.3 and also the detail about computational data and equations are shown in Appendix B.3 – B.6.

The defined conditions used in the study are no interaction between cells, neglecting all secondary flow effects such as pressure gradient, basset effect etc. defining y-coordinate at the floor of the channel from the previous model and the object will move on the floor plane.

## 4.2 Preparation of magnetic bead experiment

### 4.2.1 List of equipment

All instruments and materials used in the study are listed below

#### *4.2.1.1. Instruments*

- Syringe pump, Cole-Parmer Model 100
- Syringe pump, Multi-Phaser model NE-1600/NE-1800
- Optical microscope, Seek Inter Co., Ltd., model SK-XJM series
- Camera, Digital Camera Viscam, Seek Inter Co., Ltd., model SK-X.M
- Vortex, Biosan, model Vortex V-1 plus

#### *4.2.1.2. Materials and reagents*

- Neodymium permanent magnets, MISUMI MGLN3-3-5
- A microfluidic device
- Syringe 10 ml 3 ea, Nipro Disposable Syringe, Lot#15G09T
- Deionized water (DI water) from Millipore, Model Direct-Q
- PBS solution, Sigma Aldrich
- Tween20, Sigma Aldrich, Product no. P1379
- 5  $\mu\text{m}$  magnetic beads stock, Sigma Aldrich, Product no. 39689, Lot#1459204  
with  $1.462 \times 10^9$  beads/mL
- 10  $\mu\text{m}$  magnetic beads stock, Sigma Aldrich, Product no. 49664,  
Lot#1379936 with  $7.639 \times 10^8$  beads/mL

#### 4.2.2 Sample preparation

1. Mix DI water or PBS with Tween20, surfactant playing a role in preventing agglomeration of beads, 10:1 V/V.
2. Add artificial food color to distinguish the buffer and the sample solution by using green for the sample and blue for the buffer
3. Dilute the magnetic beads from the stock with the ratio 1:1000
4. Use the vortex for mixing uniformly

5. Use a syringe to take up the solution
6. Install syringes into both pumps
7. In order to avoid bubbles in the device and during feeding the syringe by pumps, we need to submerge the device under DI water and be under vacuum condition for 1 hour
8. Connect the tip of the needle connected to syringes under the water in order to avoid letting bubbles into the device.

Note: Before the experiment, all syringes have to fill in all spaces with solution. The system requires no because if bubbles happen in the device, the bubbles will block the flow and all assumptions defined in the mathematical model will be inappropriate for predicting trajectories.

#### 4.2.3 Experiment condition and installation

After all connectors are in position, the magnet array lies on the space which is cut in the fabrication. The flow rate will be defined as the parameter in Figure 2.10. All conditions used in the experiment are shown in Table 4.1 including the medium mixed for the experiment. After flowing since steady state, the video is recorded, by the camera, having 15 fps, which is attached into the optical microscope with V.I.S. ver3.00, Seek Inter Operation Limited. Then, the video is converted into a single picture. After that, the distance in x- and z- axis is measured for plotting the trajectories. All experiments are performed three times. The schematic diagram of the experiment is shown in Figure 4.2.

To approximate the computational error, the position of simulated data every 200,000 time steps is gathered in order to plot the trajectory of the experimental result. Then, the percent error of the model is computed by comparing the final distance as proposed in Figure 4.3.

The number of samples of 5- $\mu\text{m}$  and 10- $\mu\text{m}$  magnetic beads is 30 data sets and 10 data sets, respectively. All experiments will be repeated three times.

Table 4.1 conditions in the magnetic bead experiment

Medium	Bead size ( $\mu\text{m}$ )	$Q_1$ ( $\mu\text{l/min}$ )	$Q_2$ ( $\mu\text{l/min}$ )	$Q_3$ ( $\mu\text{l/min}$ )	Total flow rate ( $\mu\text{l/min}$ )
DI Water	5	0.1	0.95	0.95	2
	10	2	9	9	20
PBS		0.1	0.95	0.95	2
	5	1	4.5	4.5	10
	10	2	9	9	20

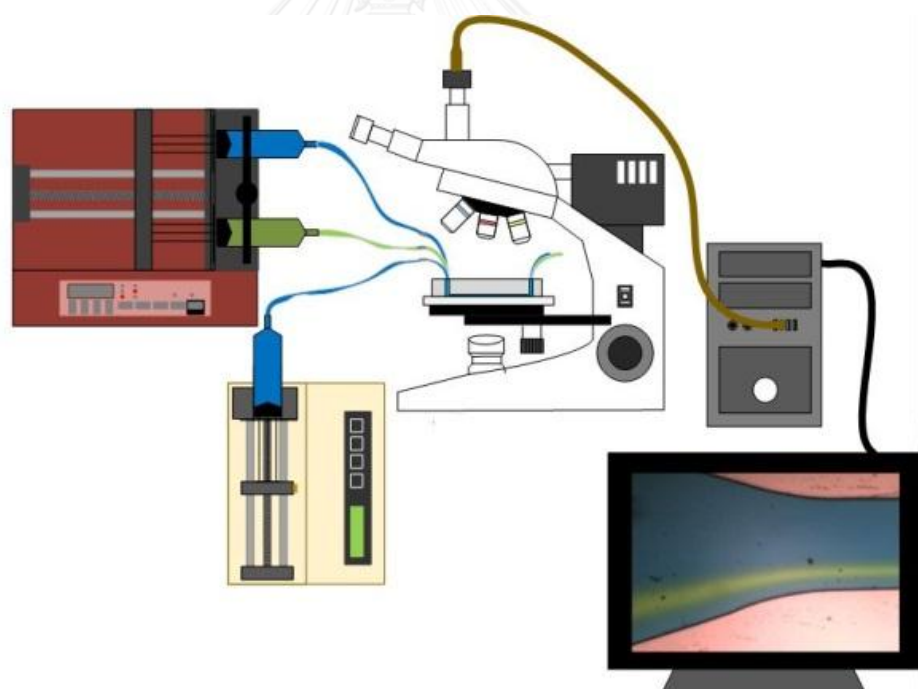


Figure 4.2 Schematic diagram of the experiment for both sizes of magnetic beads

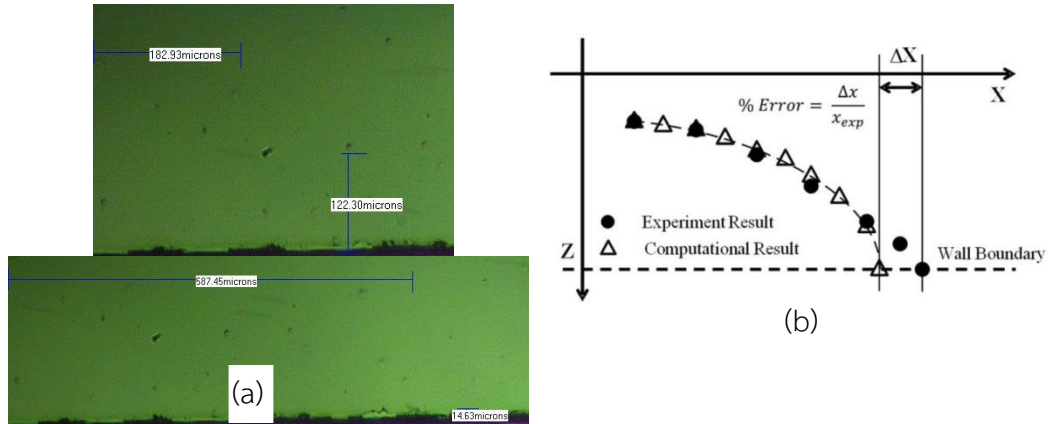


Figure 4.3 Calculation of uncertainty between the model and experiment (a) taken by a microscope (b) the conceptual principle of calculating error compared to experimental result

### 4.3 Experiment result of magnetic beads

#### 4.3.1 Magnetic beads in DI water medium

After converting the recorded video into a series of single images, we measure the distance in x- and z- axis in order to gather position data of each observed particle. The position of each particle is plotted comparing to the simulated trajectories as shown in Figure 4.5 and Figure 4.6 for 5 and 10  $\mu\text{m}$  respectively. In addition, the computational model can be validated by the means proposed as Figure 4.4 and the percent error is average 18.61% and 17.61% as shown in Figure 4.7 and 4.8 for 5- and 10- $\mu\text{m}$  magnetic beads respectively.

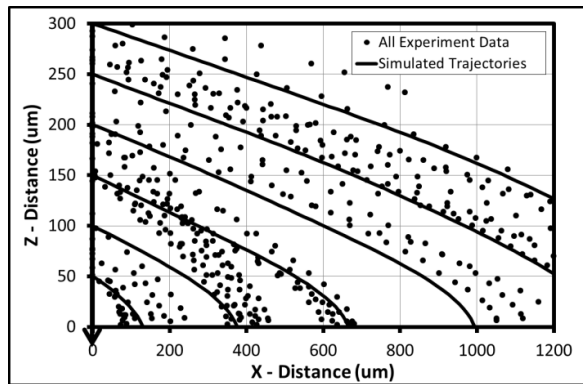


Figure 4.4 Example of experiment result of 5- $\mu\text{m}$  diameter magnetic beads in DI water medium plotted for comparing to the calculated result

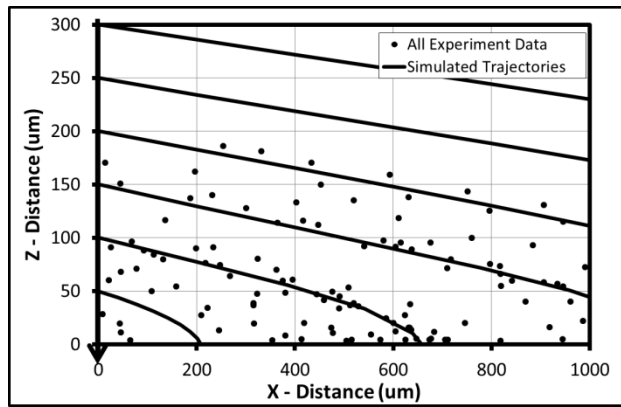


Figure 4.5 Example of experiment result of 10- $\mu\text{m}$  diameter magnetic beads in DI water medium plotted for comparing to the calculated result

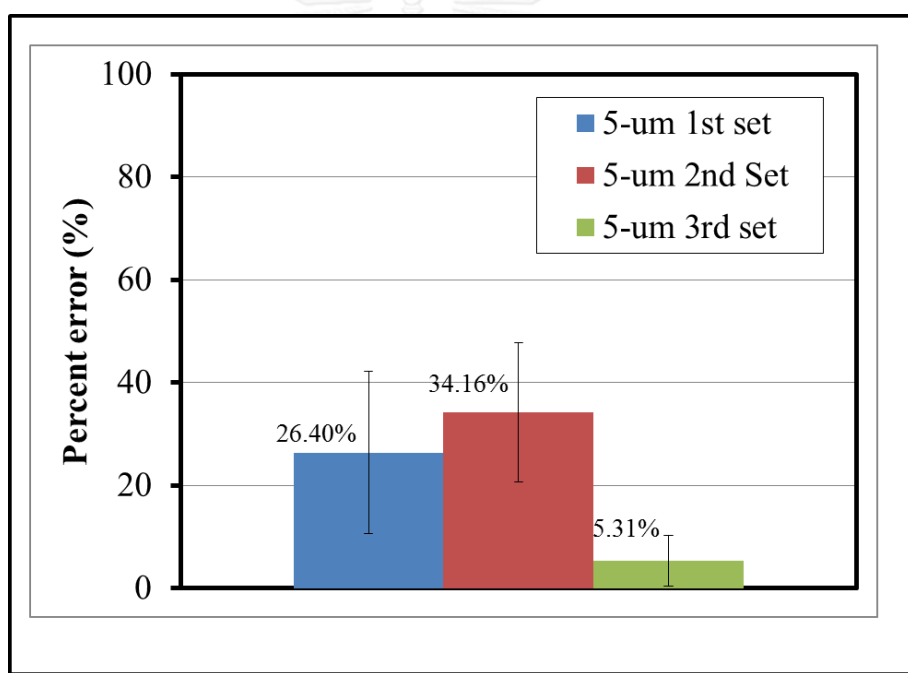


Figure 4.6 Average deviation including the error bar from 5.31% to 34.16% for 5- $\mu\text{m}$  diameter magnetic beads (three replicates) at 2  $\mu\text{L}/\text{min}$ .

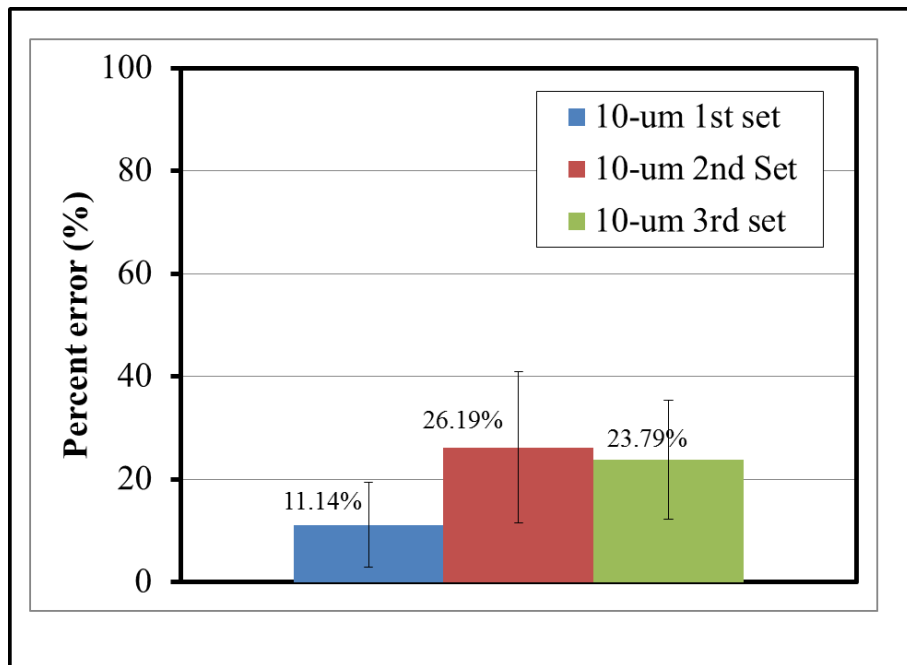


Figure 4.7 Average deviation including the error bar from 11.14% to 26.19% for 10- $\mu\text{m}$  diameter magnetic beads (three replicates) at 20  $\mu\text{L}/\text{min}$ .

Note: the example of the raw data from both experimental and computational result is shown in Appendix C and the raw data of percent error calculation is also shown in Appendix D.

#### 4.3.2 Magnetic beads in PBS medium

In this experiment, it is similar to the previous experiment with DI water medium. This study also performs the experiment with PBS medium and different flow rates. Similarly, the percent error of computational model can be validated by the approach of Figure 4.4 and shown in Figure 4.9.

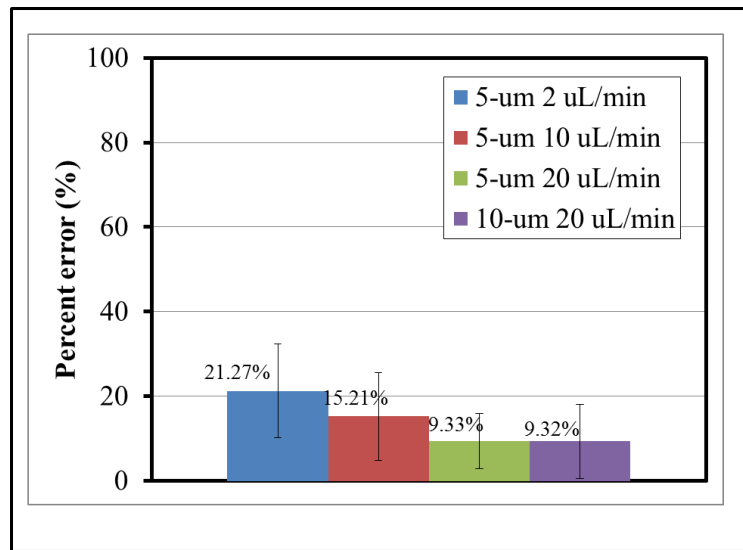


Figure 4.8 Average deviation including the error bar from 5.31% to 34.16% for 5- $\mu\text{m}$  diameter magnetic beads (three flow rates) at 2, 10 and 20  $\mu\text{L}/\text{min}$  and for 10- $\mu\text{m}$  diameter magnetic beads (one flow rate) at 20  $\mu\text{L}/\text{min}$ .

#### 4.4 Discussion

From both experiments, DI water and PBS medium, the deviation is around 5.31% to 34.16% and 9.32% to 21.27% respectively as exhibited in Figure 4.7 – 4.9. The major uncertainty results from non-uniform wall thickness during cutting process displayed in Figure 4.10. This leads to the fluctuation of magnetic force along the channel because the magnetic force equation is the function of position. It is thought that the deviation of trajectory between two studies should significantly come from this reason. From the approximation, the deviation of the measured distance is 6.13% and 9.01% in average for 5- $\mu\text{m}$  and 10- $\mu\text{m}$  magnetic bead devices respectively. This error can be analyzed and calculated that the magnitude of the magnetic force varies  $\pm 5\%$ .

Another uncertainty is the measuring error by an optical microscope resulting from the focus length of the microscope. The photo taken by the recorder may be captured the observed particle from different layer of focused plane. In the

computational condition, we assume that particles will move on the floor of the channel. Therefore, y-coordinate as well as magnitude of magnetic force defined in calculation programming is on the floor. However, if we compute at the center plane of the channel, the percent error significantly decreases as shown in Figure 4.11. Lastly, the constant values used for computation as shown in Tables 2.2 – 2.4 have their heterogeneity in nature, which brings about the uncertainty in magnitude of magnetic force.

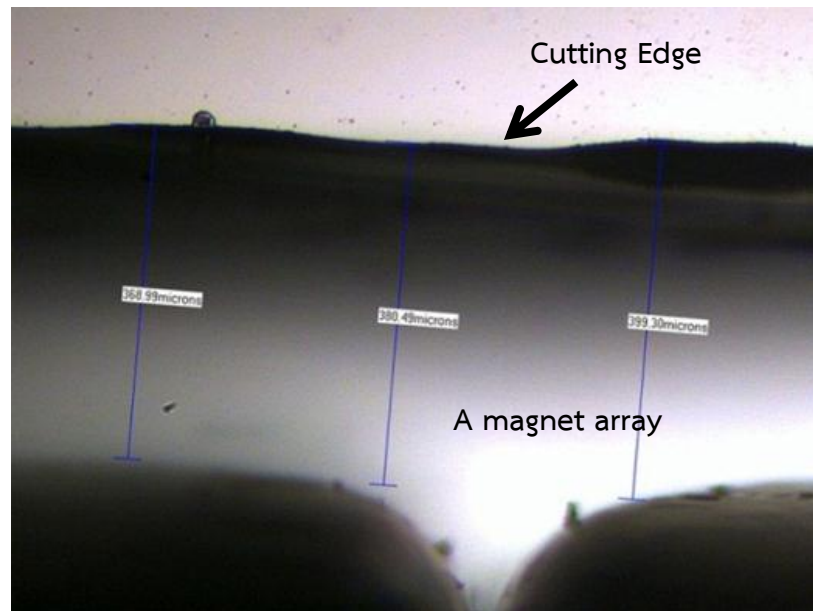


Figure 4.9 Non-uniform thickness of wall channel

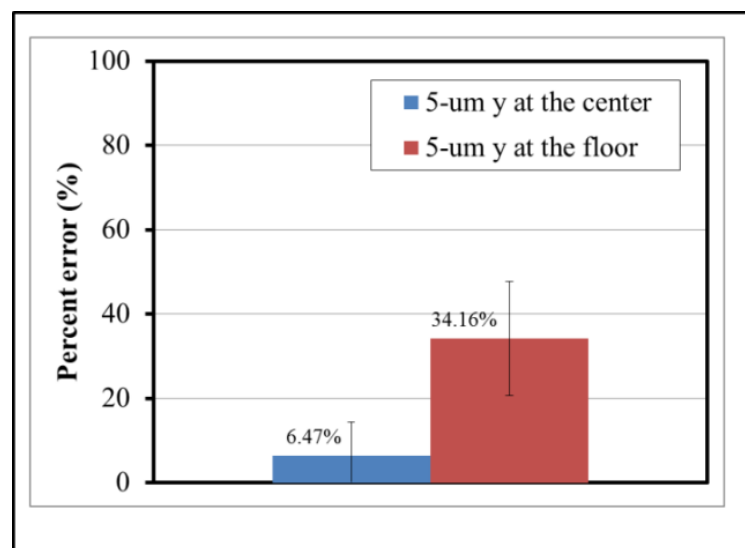


Figure 4.10 Percentage of error of different y-coordinate calculation

#### 4.5 Summary

In this chapter, the magnetic bead experiment is performed and validates the computational result. The experiment includes two sizes of magnetic beads, three flow rates and two medium. The overall deviation from all cases is from 5.31% to 34.16%. From our observation, the error originates from mostly the non-uniform thickness of channel wall, difference plane between experiment and calculation, and the variation of constant parameters in the nature used in the computation can influence the magnitude of magnetic force as well. The next chapter discusses mouse blood experiment including sample preparation, a list of reagents and instruments used in the experiment.



## Chapter 5

### Mouse blood experiment

After validating and developing the mathematical model by using two sizes of magnetic beads as the model of malaria-infected erythrocytes, this chapter goes into detail of mouse blood experiment such as sample preparation and cell culture, shows as well as discusses the result of the experiment.

#### **5.1 Mice blood experiment**

##### **5.1.1 List of equipment**

All instruments and materials used in the study are listed below

###### *5.1.1.1. Instruments*

- Syringe pump, Cole-Parmer Model 100
- Syringe pump, Multi-Phaser model NE-1600/NE-1800
- Optical microscope, Seek Inter Co., Ltd., model SK-XJM series
- Camera, Digital Camera Viscam, Seek Inter Co., Ltd., model SK-X.M
- Vortex, Biosan, model Vortex V-1 plus
- Centrifuger, Biosan Microspin 12
- Optical Microscope, Olympus DP21

###### *5.1.1.2. Materials and reagents*

- Neodymium permanent magnets, MISUMI MGLN3-3-5
- A microfluidic device
- Syringe 1 ml 3 ea, Nipro Disposable Syringe, Lot#14E19
- Deionized water (DI water) from Millipore, Model Direct-Q

- 1 X Phosphate Buffer Saline (PBS), Sigma Aldrich
- Tris/HCL, Bio Basic Canada INC.
- Calcium disodium EDTA (CaNa<sub>2</sub>.EDTA), Sigma Aldrich
- Potassium Chloride (KCl), Suksapan Panit
- Nycodenz powder, Axis-Shield
- Giemsa staining solution
- Absolute methanol
- Immersion oil for high magnification lens

### 5.1.2 Sample preparation

#### 5.1.2.1. Culture infected erythrocytes

Many study proposed that mice blood cells could be employed because its physical and biological characteristics are similar to human blood cells [31]. In this study, *P.Berghei*, malaria species in mice is preferred, because it contains more hemozoin when they become mature. The mouse used in this study for parasite culture is coming from National Laboratory Animal Center, Mahidol University (NALC MU). In the culture method, the infected erythrocytes from freezing at -20°C are thawed. Then we inject the blood sample into a mouse intraperitoneally, and after that, investigate the percent parasimia by using Giemsa staining technique.

Giemsa staining technique is the method that we can perceive each component of blood sample and also can investigate whether the sample contains parasite or not. The color of Giemsa will attach to the parasite inside the infected erythrocytes. First of all, the tip of the mouse's tail is cut and the blood is dropped onto the glass slide. Then, the cover slip is used to make thin film of blood. Before treating blood cells, the sample needs to be already dry. After that, the blood cells are fixed with methanol 2-3 minutes. Then, Giemsa solution diluted from stock 1:10 is covered all areas over the glass slide. After staining for 45 minutes, the sample

needs to be cleaned for removing the staining solution with cleaned water. Before observing under the microscope, it needs to be dry as well. In order to clarify whether the blood cells have parasite or not, the high magnification of lens, in this case 100x is used along with the immersion oil. Percent parasimia can be calculated from the ratio of infected erythrocytes to total erythrocytes. Then, we count and distinguish the type of blood cells under the microscope and calculate by the ratio mentioned above.

In this procedure, we cannot predict that how long it should be taken to wait for getting the percent parasimia to reach to approximately 40-50% because it is based on mouse's health and the activation of infected sample coming from hibernation at -20°C. The more frequently we check the percent parasimia, the better we can keep the sample before it is dead. Commonly, it takes time approximately five days to let the parasite become mature enough. Figure 5.1 illustrates the number of infected erythrocytes which significantly increase after cultured in mouse 2<sup>nd</sup> day and 5<sup>th</sup> day.

#### *5.1.2.2. Nycodenz preparation*

Nycondenz solution is used to separate the infected erythrocytes in the stage of schizont, containing more hemozoin than other stages, by using the principles of density gradient of concentration. From the study of Janse C. J. et al (2006), Nycodenz solution is prepared by adding the 2.76 g of Nycodenz powder into 10 mL of buffered medium solution, comprising 5mM Tris/HCl, 3mM KCl and 0.3 mM CaNa<sub>2</sub>EDTA [32]. The detail about mixing buffered medium protocol is indicated in Appendix F. After that, Nycodenz stock solution is diluted with PBS in the ratio of 1:1 by volume. In separation process, 50  $\mu$ L of Nycodenz-PBS solution is underplayed before putting in 150  $\mu$ L of blood sample. Then, the sample is centrifuged at 460g for five minutes. The layer of the schizont stage is distinguished between serum and agglomeration of other types of blood cells. The principle of Nycodenz gradient centrifugation is displayed in Figure 5.2.

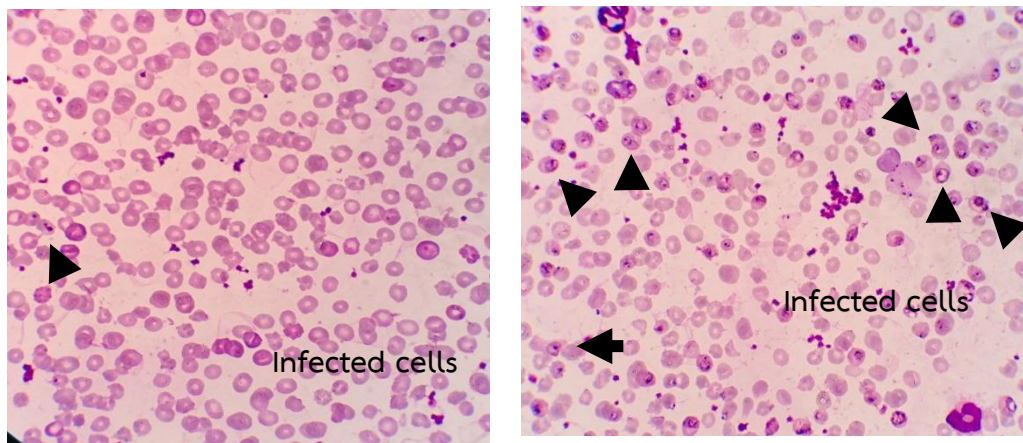


Figure 5.1 Giemsa staining of the infected mouse **left 2<sup>nd</sup> day right 5<sup>th</sup> day**

The final sample is checked whether we can filter to get just only the Schizont stages or not as shown in Figure 5.3 by Giemsa staining. The result is that the low amount of white blood cells and healthy erythrocytes comparing to the sample without being passed Nycodenz gradient method is clearly seen shown in Figure 5.1. There are a lot of white blood cells, platelets and normal red blood cells if not treated. However, this method may not filter the schizont stage out 100%, but we can get the sample more concentrated with infected erythrocytes.

Then a micro pipette is used to keep just only the sample in that layer and put into culture medium for sustaining the quality of blood cells. Then the solution is kept and can reassure that the sample is ready. A Syringe takes the sample and PBS is used as a buffer solution in this case. We will install all instruments involved similar to the magnetic bead experiment as shown in Figure 4.3.

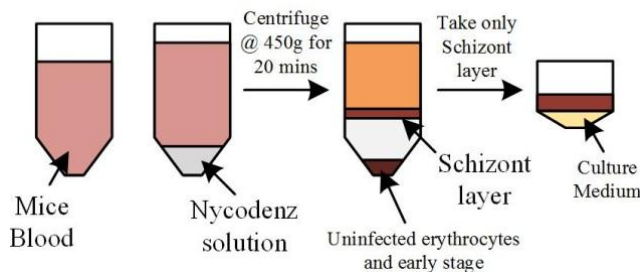


Figure 5.2 Schematic procedure of separation with Nycodenz gradient

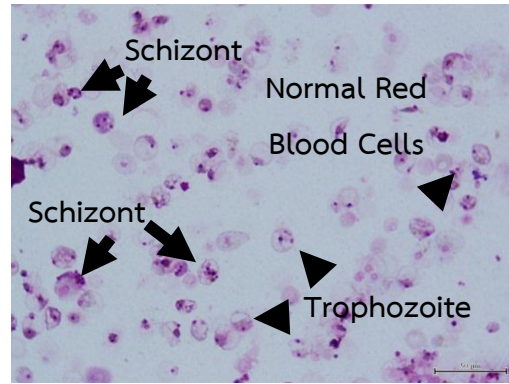


Figure 5.3 Giemsa staining after passing Nycodenz gradient centrifugation

### 5.1.3 Experiment condition and setup

#### 5.1.3.1 Flowing fluid

After all connectors are in position, the magnet array lies on the space which is cut in fabrcation. The flow rate will be defined as the parameter in Figure 4.2. All conditions used in the experiment are shown in Table 5.1. After flowing since steady state, the video is recording the phenomena by the camera attached with the optical microscope. Then, the video is extracted into a single image. After that, the distance is measured between the streamline supposed to be infected erythrocytes from the preparation, and the wall boundary in z-axis two areas, first at the initial part of the channel called area I and the other at the final part of the channel called area II as shown in Figure 5.4. Measurement data of all cases is shown in Table 5.2 and illustrated in Figure 5.6. As the blood sample is too concentrated, during the sample preparation, the sample will be diluted 1:25 in 1xPBS.

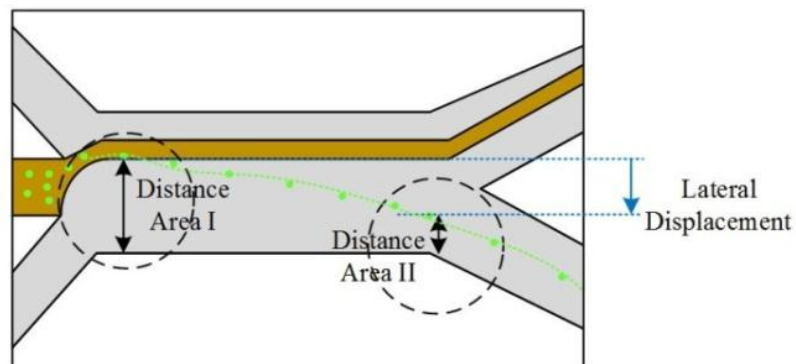
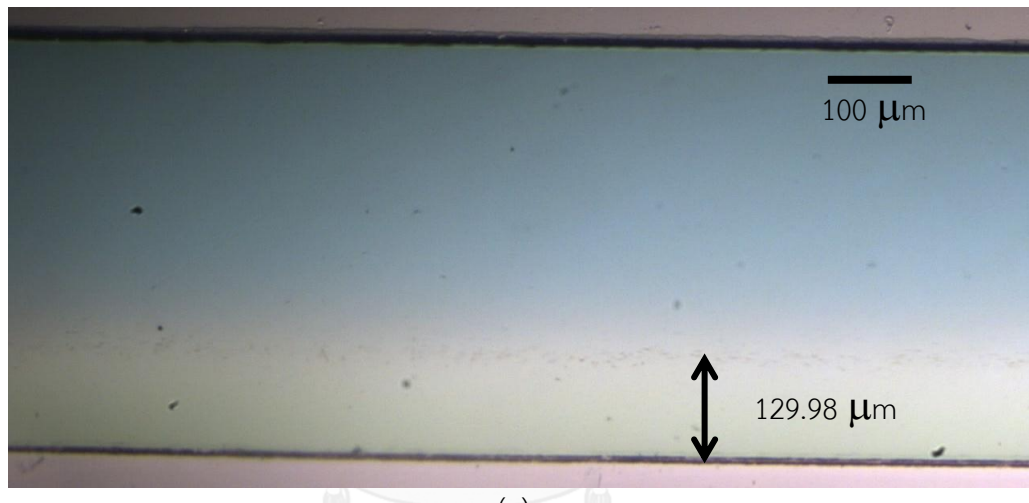


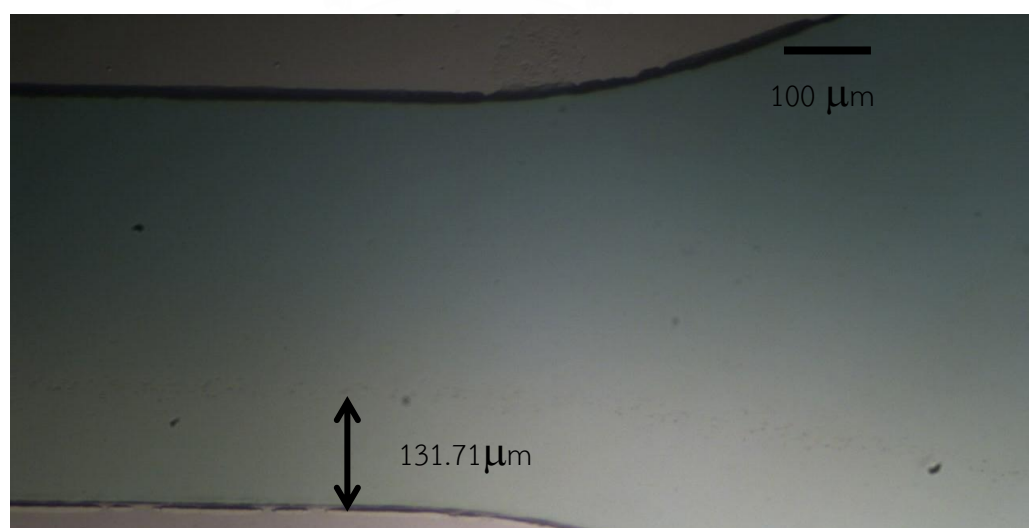
Figure 5.4 Investigation window for examining the lateral displacement

Table 5.1 Conditions in the mouse blood experiment

$Q_1$ ( $\mu\text{l}/\text{min}$ )	$Q_2$ ( $\mu\text{l}/\text{min}$ )	$Q_3$ ( $\mu\text{l}/\text{min}$ )	Total flow rate ( $\mu\text{l}/\text{min}$ )
0.05	0.05	0.1	0.2
0.1	0.1	0.1	0.3
0.15	0.15	0.1	0.4
0.2	0.2	0.1	0.5



(a)



(b)

Figure 5.5 Example of the distance measurement in the (a) area I (b) area II under total flow rate 0.5  $\mu\text{l}/\text{min}$

Table 5.2 Distance measured at the area I and the area II

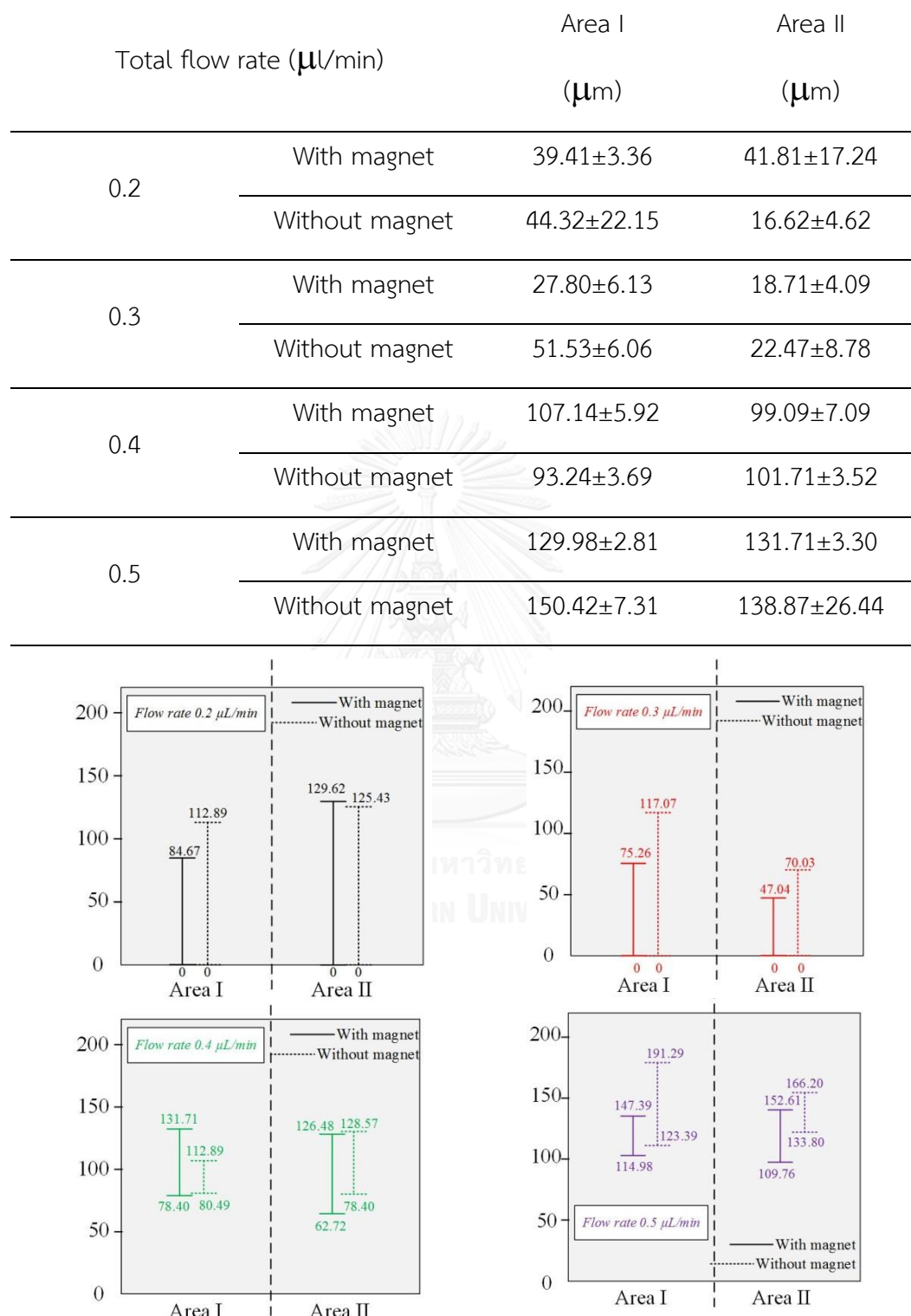


Figure 5.6 Plotted data from the Table 5.2 to illustrate the result under various flow rates

### 5.1.3.2 Stagnant fluid

After we flow samples, laying a magnet array on the space we cut. We stop all flow in order to get fluid to be stagnant and then record the video for 5 minutes. Then, we converted the video into a single picture. After that, we observe the behavior of infected erythrocytes under the presence and absence of a magnet array.

## 5.2 Experiment result of mouse blood cells and discussion

It is quite difficult to observe the motion of infected blood cells by using an optical microscope even if the experiment is performed in the case of *flowing fluid* and *stagnation fluid*. The lateral displacement may happen supported by the computational result.

In the *flowing fluid* experiment, the result extracted from the recorded video shown in Table 5.2. From Figure 5.6, the line in each graph shows the range of the position of blood cells flowing in the channel in both areas, area I and area II. The nearest and farthest distances are measured and compared the results between two areas. Obviously, in all cases, the streamline of blood and expected lateral displacement are difficult to observe coming from the effect of diffusion and low magnitude of magnetic force as well as the limited view taken by the microscope.

The diffusion of the particles moving in flowing fluid could happen particularly operating under low flow rates. Therefore, the result indicated that the range of the blood stream is wider in the area II than the area I under flow rate of 0.2  $\mu\text{L}/\text{min}$ .

The possibility of low magnitude of magnetic force is the limitation of the fabrication process because the longer distance between the magnet array and the position of infected cells is, the lower magnetic force acting on the infected cells will be. The magnetic force is in the order merely  $10^{-15}$  Newton at the distance which is wider than 500  $\mu\text{m}$  as shown in force distribution in Figure 5.7.

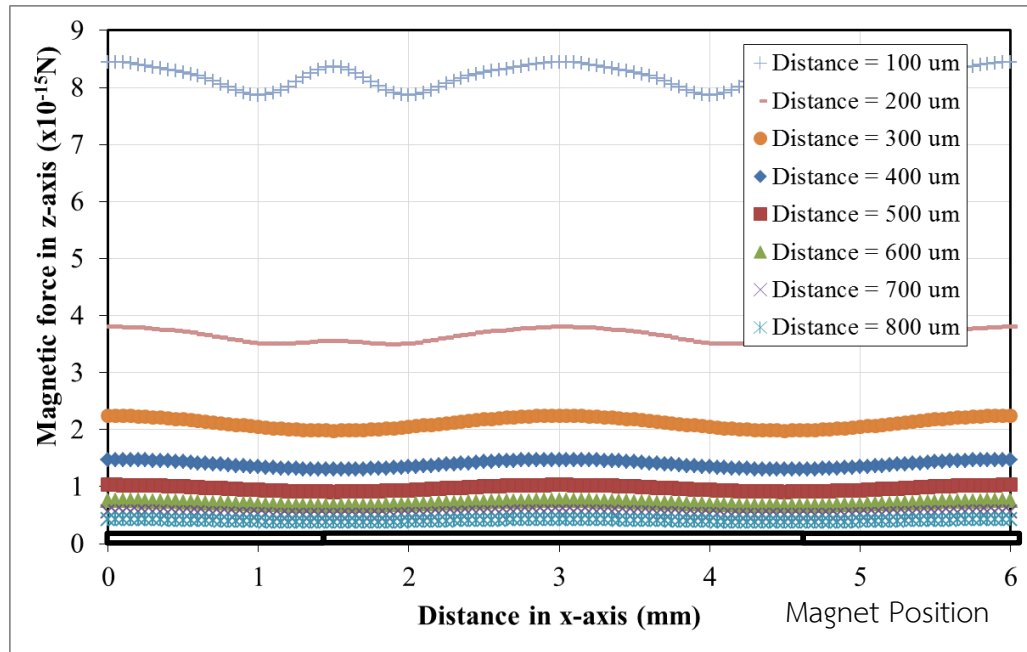


Figure 5.7 Example of force distribution in various distance from the streamline to the surface of a magnet array

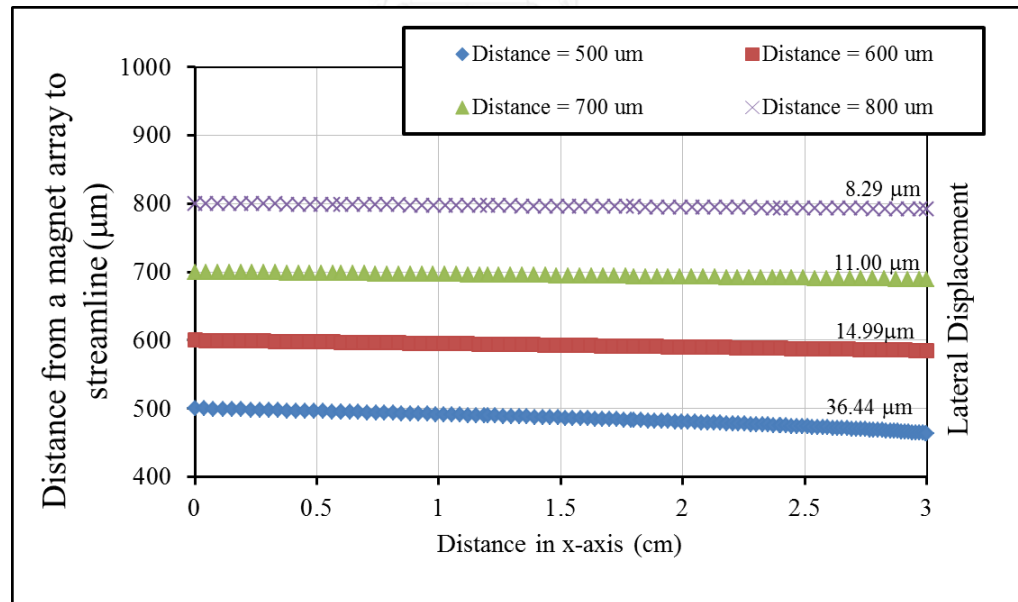


Figure 5.8 Computational trajectory of infected cells under various distances from the surface of a magnet array at flow rate 0.2  $\mu\text{L}/\text{min}$

The computational also supports this possibility that the example of trajectory under flow rate from 0.2  $\mu\text{L}/\text{min}$  illustrated in Figure 5.8 indicates that they have the highest lateral displacement approximately 36.44  $\mu\text{m}$  and 8.29  $\mu\text{m}$  in the case of the distance 500  $\mu\text{m}$  and 800  $\mu\text{m}$  respectively.

Moreover, the computational result suggests that the distance between the streamline of infected cells and the surface of a magnet array should not be longer than 300  $\mu\text{m}$  as exhibited in Figures 2.16 – 2.17 and the operating flow rate should lower than 0.28  $\mu\text{L}/\text{min}$  because at this distance the order of magnetic force can attract infected cells out around at least 50  $\mu\text{m}$  in lateral direction.

### 5.3 Summary

In this chapter, this study attempts to perform the experiment with an actual blood sample. The chapter includes cell culture, sample preparation and the conditions in the experiment. The experiment determines that our setup cannot observe the motion of malarial-infected erythrocytes clearly due to the limitation of fabrication process. The longer distance between the magnet array and streamline of the infected cells it is, the lower magnitude of magnetic force will be. Besides, the lateral displacement of infected cells is difficult to observe because the effect of diffusion occurs when the device operates with low flow rates and the extent of lateral distance is too small supported by the computational result. Therefore, the recently experimental setup may not appropriate for observing the phenomena.

## Chapter 6

### Conclusion

This thesis has illustrated the overall picture of the Malaria disease in terms of the health issue, diagnosis method and the scope of the study. The spreading of Malaria becomes more severe due to the delay of separating infected patient out from the community in low-resource settings. The drawbacks of conventional method are time-consuming process and need an expert to diagnose. Besides, another method can reduce trouble is rapid diagnostic tests (RDTs). Nevertheless, RDTs face a degradable problem and need appropriate conditions to store the test. Thus, magnetophoresis is one of the alternative diagnostic methods to clarify whether the sample contains the parasite or not. In accordance with some studies, they account for the parasite invades the erythrocytes and generates magnetic product called Hemozoin which is sensitive to the magnetic field. This study aims to propose a novel method to separate the Malaria-infected erythrocytes by using a microfluidic device and the principle of magnetophoresis.

The fundamental of magnetism particularly the magnetophoresis principle is already summarized. The important factors having an impact on the magnitude of magnetic force are its magnetic properties of the targeted object, size of its object and the size of gradient magnetic field. One of these parameters is the gradient magnetic field for which the system must be designed or fabricated the system to achieve the highest magnitude of magnetic force as much as possible. We have used COMSOL Multiphysics to simulate magnetic field distribution for the complex model, in this case a magnet array. Then, the mathematical model is developed in order to predict the trajectory of magnetic beads and also infected erythrocytes by using the law of motion. Actually, forces exerting on the objects moving into the fluid are including drag force, pressure gradient force and external force as well as the effect of added mass and Basset force, which can happen when the object and the fluid are accelerated or decelerated in high order. Nonetheless, these effects can be neglected as previously mentioned in the literatures. In case of pressure gradient

force, some studies argued that the force is already added into a fluid inertial term; hence, this term can also be neglected. As a consequence, this study consider the force acting on both models is only drag force and magnetic force. Finally, The experimental is performed to validate the model we proposed. After that, the study has already proposed the procedure to fabricate a microfluidic device by using soft lithography. Conditions used in the study as well as the list of equipment and necessary reagents are provided.

The magnetic bead experiment has been performed with two sizes of magnetic beads, different flow rates and two medium, DI water and PBS. The average deviation of 5- $\mu\text{m}$  and 10- $\mu\text{m}$  magnetic beads is 18.61% and 17.61% respectively. From our observation, the major error stems from mostly the non-uniform distance between the magnet array and the streamline of the particles flowed into channel. This cause is already investigated by calculating the variation of the distances which cause the change in magnetic force around 6.13 – 9.01%. In addition, the photo taken by the optical microscope may be coming from another focal plane because the model assumes that the objects move on the floor plane. The other problem is the variation of constant values used in the computation influences the magnitude of the magnetic force.

After that, the model is predicted the trajectory for the blood sample. The experiment with an actual blood sample coming from the mouse is also done to compare the results. We have cultured *P.Berghei*, Malaria species in the mouse, into a mouse. The experiment suggests that the optical microscope used for observing the phenomena cannot clearly distinguish the motion of malarial-infected mouse blood cells. Firstly, the fabrication limitations that cannot get the wall thickness less than 300  $\mu\text{m}$  in the cutting step. This point leads to low magnitude of magnetic force acting on infected cells. The shorter distance between the magnet and the streamline it is, the larger magnitude of magnetic force it will be. Secondly, the diffusion at low flow rates can affect the motion of infected cells, and it makes a difficulty to observe the motion too. Therefore, it is better to find a more appropriate method to reduce the gap between the magnet array and the streamline of the

blood flowing in the channel. Besides, the observing method is needed to be improved. For example, the sample may be tagged with some signals such as fluorescence dye so that the phenomena can be easily seen.



## REFERENCES

- [1] ศ. ช. สยามพร ศิรินาวิน, แนวทางเวชปฏิบัติโรคติดเชื้อ เล่มที่ 1 : โรคติดต่อ / คณะกรรมการจัดทำแนวทางเวชปฏิบัติโรคติดเชื้อเครื่องข่ายแนวทางเวชปฏิบัติ ร่วมกับ กรมควบคุมโรคติดต่อ กระทรวงสาธารณสุข: โภลทองมาสเตอร์พรีน์จำกัด, 2002.
- [2] J. B. S. Kasetsirikul, W. Srituravanich, M. Kaewthamasorn, A. Pimpin, "The development of malaria diagnostic techniques: a review of the approaches with focus on dielectrophoretic and magnetophoretic methods," *Malaria Journal*, vol. 15, 2016.
- [3] M. D. E.A. Ashley, R.M. Fairhurst, C. Amaratunga, P.Lim,, "Spread of Artemisinin Resistance in Plasmodium falciparum Malaria," *The New England Journal of Medicine*, vol. 371, pp. 411-423, 2014.
- [4] C. f. D. C. a. Prevention. (2016). *Malaria*. Available: <http://www.cdc.gov/malaria/about/biology/>
- [5] ยุทธนา หมันดี, "บทบาทuhnวิชาการ: มาลาเรีย," วารสารเทคนิคการแพทย์เชียงใหม่ vol. 41, pp. 156-166, 3 กันยายน 2551 2551.
- [6] H. B. A. S. Bhagat, H. W. Hou, S. J. Tan, J. Han, C. T. Lim, "Microfluidics for cell separation," *Med Biol Eng Comput*, vol. 48, pp. 999-1014, 2010.
- [7] M. J. G. e. al., "Genome Sequence of the human malaria parasite Plasmodium falciparum," *Nature*, vol. 3, pp. 498-511, 2002.
- [8] ศ. ก. กระทรวงสาธารณสุข, คู่มือการตรวจวินิจฉัยโรคติดต่อนำโดยแมลง โดยใช้ชุดน้ำยาตรวจอย่างรวดเร็ว, 2552.
- [9] J. S. P. Gascoyne, M. Ruchirawat,, "Microfluidic approaches to malaria detection," *Acta Tropica*, vol. 89, pp. 357-369, 2004.
- [10] V. L. C.D.Chi, S. K.Sia, , "Commercialization of microfluidic point-of-care diagnostic devices," *Lab on a Chip*, vol. 12, pp. 2118-2134, 2012.
- [11] H. K. C. C.Stemple, J. Yoon,, "Rapid and Sensitive Detection of Malaria Antigen in Human Blood with Lab-on-a-Chip," *IEEE Sensor journal*, vol. 12, pp. 2735-2736, 2012.

- [12] A. A. S. B. H. W. Hou, Alvin Guo Lin Chong, Pan Mao, Kevin Shyong Wei Tan, Jongyoon Han, Chwee Teck Lim,, "Deformability based cell margination – A simple microfluidic design for malaria-infected erythrocyte separation," *Lab on a chip*, vol. 10, pp. 2605-2613, 2010.
- [13] D. T. C. S. Handayani, E. Tjitra, J. S. Kuo, D. Lampah, E. Kenangalem, L. Renia, G. Snounou, R. N. Price, N. M. Anstey, B. Russell,, "High Deformability of Plasmodium vivax–Infected Red Blood Cells under Microfluidic Conditions," *The journal of infectious diseases*, vol. 199, pp. 445-450, 2009.
- [14] C. J. F. N. S. Juul, R. Labouriau, A. Roy, C. Tesauro, P. W. Jensen, C. Harmsen, E. L. Kristoffersen, Y. Chiu, R. Fröhlich, P. Fiorani, J. Cox-Singh, D. Tordrup, J. Koch, A. Bienvenu, A. Desideri, S. Picot, E. Petersen, K. W. Leong, Y. Ho, M. Stougaard, and B. R. Knudsen, , "Droplet Microfluidics Platform for Highly Sensitive and Quantitative Detection of Malaria-Causing Plasmodium Parasites Based on Enzyme Activity Measurement," *ACS Nano*, vol. 6, pp. 10676-10683, 2012.
- [15] P. L. Y. Hsu, J. L. Coleman, W. C. Tang,, "A microfluidic platform to isolate avian erythrocytes infected with Plasmodium gallinaceum malaria parasites based on surface morphological changes," *Biomed Microdevices* 2011.
- [16] T. J. Egan, "Haemozooin formation," *Molecular & Biochemical Parasitology* vol. 157, pp. 127-136, 2008.
- [17] S. R. F. Paul, D. Melville, D.C. Warhurst, J. O. S. Osisanya, "Separation of malaria-infected erythrocytes from whole blood: use of a selective high-gradient magnetic separation technique," *The Lancet*, 1981.
- [18] T. P. Zimmerman, J., Fujioka, H., Collins, W., and Zborowski, M.,, "Diagnosis of malaria by magnet deposition microscopy," *Am. J. Trop. Med. Hyg.*, vol. 74, pp. 568-572, 2006.
- [19] A. O. S. C. Bhakdi, S. Somsri, P. Sratongno, P. Pannadaporn, P. Chimma, P. Malasit, K. Pattanapanyasat, H. Neumann, "Optimized high gradient magnetic separation for isolation of Plasmodium-infected red blood cells," *Malaria Journal* vol. 9, 2010.

- [20] M. M. J. Kim, J. F. Antaki, A. Gandini,, "Removal of malaria-infected red blood cell using magnetic cell separators: A computational study," *Appl Math Comput*, vol. 218, pp. 6841-6850, 2012.
- [21] H. H. J. Nam, H. Lim, C. Lim, S. Shin,, "Magnetic Separation of Malaria-Infected Red Blood Cells in Various Developmental Stages," *Analytical chemistry*, vol. 85, pp. 7316-7323, 2013.
- [22] W. Y. T. Kong, W. K. Peng, H. W. Hou, Marcos, P. Preiser, N. Nguyen, J. Han, "Enhancing malaria diagnosis through microfluidic cell enrichment and magnetic resonance relaxometry detection," 2015.
- [23] B. J. Kirby, *Micro- and Nanoscale Fluid Mechanics: Transport In Microfluidic devices*: Cambridge University Press, 2010.
- [24] P. J. Pritchard, *Introduction to Fluid Mechanics*, 8th ed.: John Wiley & Sons, Inc., 2011.
- [25] S. Aldrich, "The magnetic susceptibility of micro magnetic particles," ed, 2015.
- [26] I. M. M. B. Angelov, "On the geometry of red blood cell," Institute of Biophysics, Bulgarian Academy of Sciences2000.
- [27] M. D. M. Diez-Silva, J. Han, C. Lim, S. Suresh, "Shape and Biomechanical Characteristics of Human Red Blood Cells in Health and Disease," *MRS Bull.*, vol. 35, pp. 382-388, 2010.
- [28] I. Udroiu, "Estimation of erythrocyte surface area in mammals," U. d. S. R. T. Dipartimento di Scienze, Ed., ed, 2014.
- [29] S. Y. A. Zhanov, "Microfluidics blood separations through Optical sorting and deterministic lateral displacement," in *ICQNM 2011*, 2011, pp. 103-108.
- [30] D. R. K. M. Takayasu, J. V. Minervini, "Continuous Magnetic Separation of Blood Components from Whole Blood," *IEEE Transaction*, vol. 10, pp. 927-930, 1999.
- [31] T. C. T. Hanscheid, M.P. Grobusch, "Hemozoin Detection for Human Malaria Diagnosis Investigated in Rodent Models: How Similar Is Similar?," *Trends in Parasitology*, vol. 32, pp. 94-96, 2016.
- [32] J. R. C. J. Janse, A. P. Waters, "High-efficiency transfection and drug selection of genetically transformed blood stages of the rodent malaria parasite *Plasmodium berghei*," *Nature Protocols*, vol. 1, pp. 346-356, 2006.

- [33] S. L. Soo, "Equation of motion of a solid particle suspended in a fluid," *Physics of fluids*, vol. 18, p. 263, 1975.
- [34] S. L. Soo, "Net effect of pressure gradient on a sphere," *Physics of fluids*, vol. 19, p. 757, 1976.
- [35] A. B. F. K. Han, "Continuous magnetophoretic separation of blood cells in microdevice format," *Journal of Applied Physics*, vol. 96, 2004.
- [36] A. B. F. K. Han, "Paramagnetic capture mode magnetophoretic microseparator for high efficiency blood cell separations," *Lab on a Chip*, vol. 6, pp. 265-273, 2006.
- [37] A. B. F. K. Han, "Paramagnetic capture mode magnetophoretic microseparator for blood cells," *IEE Proc.-Nanobiotechnol.*, vol. 153, pp. 67-73, 2006.





## APPENDIX

จุฬาลงกรณ์มหาวิทยาลัย  
CHULALONGKORN UNIVERSITY

## Appendix A. Numerical calculation and Code MATLAB

In this study, we realize that we are unable to solve the motion equation analytically. Therefore, we have proposed the numerical method which may not give the exact solution but it is acceptable to use that result in order to design the system and understand the system. The numerical method used in this study is involved with 4<sup>th</sup> order Runge-kutta and finite difference method. Besides, the mathematical model included programming code in MATLAB will be discussed in this part in more detail.

#### A.1 Numerical solution – fourth-order Runge-Kutta method

Runge-Kutta solving method is one of the most popular methods used to solve ordinary differential equation numerically. General equations used for programming are defining

$$y_{i+1} = y_i + \left[ \frac{1}{6}(k_1 + 2k_2 + 2k_3 + k_4) \right] h$$

By

$$k_1 = f(x_i, y_i)$$

$$k_2 = f(x_i + 0.5h, y_i + 0.5hk_1)$$

$$k_3 = f($$

$$k_4 = f(x_i + h, y_i + hk_3)$$

We need to adapt the idea for using to solve second-order ordinary differential equation that rearrange and change the form of the equation to first-order then using this method will be coded with MATLAB shows below

```

%% CODE PROFILE
%NAME: 4thOrder RungeKutta.m
%LAST EDITED: 3 AUGUST 2014
%%%%%%%%%%%%%
%
%-----DEFINE FUNCTION-----
%%
func1=inline('zx','t','x','zx');
func2=inline('-2*zx + 4*t','t','x','zx');
%Change second-order ODE into first order ODE
%%
%
%-----PARAMETER INPUT-----
%%
t=input('\nEnter Value of t: ');

```

```

x=input ('\nEnter Value of X: ');
z=input ('\nEnter Value of Z: ');
zx=input ('\nEnter Value of Zx: ');
n=input ('\nEnter Value of n: ');
h=input ('\nEnter Value of h: ');
fprintf ('\nSOLUTION WITH STEP SIZE = %10.4e IS:',h);
fprintf ('\n      t          z          X');
fprintf ('\n%16.6e%16.6e%16.6e',t,z,x);
%-----%
%-----PROGRAMMING-----
%-----%
for i = 1:n
    ak1y1=func1x(t,x,zx);
    ak1z1=func2x(t,x,zx);
    tt1=t + h/2.;
    xx=x + h*ak1y1/2.;
    zxx=zx + h*ak1z1/2.;
    ak2y1=func1x(tt1,xx,zxx);
    ak2z1=func2x(tt1,xx,zxx);
    xx=x + h*ak2y1/2.;
    zxx=zx + h*ak2z1/2.;
    ak3y1=func1x(tt1,xx,zxx);
    ak3z1=func2x(tt1,xx,zxx);
    tt1=t + h;
    xx=x + h*ak3y1/2.;
    zxx=zx + h*ak3z1/2.;
    ak4y1=func1x(tt1,xx,zxx);
    ak4z1=func2x(tt1,xx,zxx);
    z=z +(ak1y1 +2.*ak2y1 + 2.*ak3y1 + ak4y1)*h/6.;
    zx=zx +(ak1z1 +2.*ak2z1 + 2.*ak3z1 + ak4z1)*h/6.;
    t = t + h;
    fprintf ('\n%16.6e%16.6e%16.6e',t,z,x);
end

```

### A.2 Model Constant force, fourth-order Runge-kutta sovling method

From Equations 18 and 19, the motion equations are in the form of differential equation. One of the possible methods to solve numerically is Runge-kutta solving method. The motion in y-axis proposed in Chapter 2 will be influenced predominantly by gravitational force after being replaced with given value following

$$\begin{aligned}
 -\frac{6\pi\mu_f a}{\rho_{cell} \forall} \frac{dy}{dt} - \frac{1}{2} \frac{C_L A_s}{\forall} \left( \frac{dy}{dt} \right)^2 - \left( \frac{\rho_f g}{\rho_{cell}} - g \right) &= \frac{d^2 y}{dt^2} \\
 319880.597 \frac{dy}{dt} + 750000 \left( \frac{dy}{dt} \right)^2 - 0.078 &= \frac{d^2 y}{dt^2}
 \end{aligned}$$

MATLAB code used to create the trajectory of the object is shown below



```

%
%
%
a1=8.1179*10^12;
% Coefficient in the equation
a2=409633.0275;
% Coefficient in the equation
fmz=0.01*10^-12;
% Magnetic force in z-axis (constant value)
fmx=0;
% Magnetic force in x-axis is disregarded in this model
%
%
%
%%%%%%%%% Display function
%%%%%%%%% %%%%%%%%
%
%
%
fprintf ('\nSOLUTION WITH STEP SIZE = %10.4e IS:',h);
fprintf ('\n          t           z           x');
fprintf ('\n%16.6e%16.6e%16.6e',t,z,x);
%
%
%
%%%%%%%%% Iteration function
%%%%%%%%% %%%%%%%%
%
%
%
for i = 1:n
    vf=funcvf(z);
    ak1y1=func1x(t,x,zx);
    ak1z1=func2x(t,x,zx,fmx,vf,a1,a2);
    ak1y2=func1z(t,z,zd);
    ak1z2=func2z(t,z,zd,fmz,a1,a2);
    tt1=t + h/2.;
    xx=x + h*ak1y1/2.;
    zxx=zx + h*ak1z1/2.;
    tt2=t + h/2.;
    zz=z + h*ak1y1/2.;
    zdd=zd + h*ak1z1/2.;
    ak2y1=func1x(tt1,xx,zxx);
    ak2z1=func2x(tt1,xx,zxx,fmx,vf,a1,a2);
    ak2y2=func1z(tt2,zz,zdd);
    ak2z2=func2z(tt2,zz,zdd,fmz,a1,a2);
    xx=x + h*ak2y1/2.;
    zxx=zx + h*ak2z1/2.;
    zz=z + h*ak2y1/2.;
    zdd=zd + h*ak2z1/2.;
    ak3y1=func1x(tt1,xx,zxx);
    ak3z1=func2x(tt1,xx,zxx,fmx,vf,a1,a2);

```

```

ak3y2=func1z(tt2,zz,zdd);
ak3z2=func2z(tt2,zz,zdd,fmz,a1,a2);
tt1=t + h;
xx=x + h*ak3y1/2.;
zxx=zx + h*ak3z1/2.;
tt2=t + h;
zz=z + h*ak3y1/2.;
zdd=zd + h*ak3z1/2.;
ak4y1=func1x(tt1,xx,zxx);
ak4z1=func2x(tt1,xx,zxx,fmx,vf,a1,a2);
ak4y2=func1z(tt2,zz,zdd);
ak4z2=func2z(tt2,zz,zdd,fmz,a1,a2);
x=x +(ak1y1 +2.*ak2y1 + 2.*ak3y1 + ak4y1)*h/6.;
zx=zx +(ak1z1 +2.*ak2z1 + 2.*ak3z1 + ak4z1)*h/6.;
z=z +(ak1y2 +2.*ak2y2 + 2.*ak3y2 + ak4y2)*h/6.;
zd=zd +(ak1z2 +2.*ak2z2 + 2.*ak3z2 + ak4z2)*h/6.;
t = t + h;
%%%%% Display condition
%%%%%%%%%%%%%%%
% Because in each iteration is calculated too quickly and a lot of
% information will not be used in every single point, we decide to
store
% the data every 400000 iterations.
%
%
%
if i/400000 == floor(i/400000)
fprintf('\n%16.6e%16.6e%16.6e',t,z,x);
end
%
%
%
end

```

จุฬาลงกรณ์มหาวิทยาลัย  
CHULALONGKORN UNIVERSITY

In each case shown in figure 2.18 and 2.19, we need to change  $a_1$  and  $a_2$ , which are the coefficient depending on size and mass of targeted object as well as magnetic value. This section shows a part of data because it has too much data iRBC, hRBC and WBC motion equation are described as follows

For iRBCs at size 5  $\mu\text{m}$  with magnetic force 1 pN and velocity equation

$$\frac{d^2z}{dt^2} + 639708.118 \frac{dz}{dt} - 15.202 = 0$$

$$v(z) = 0.00299z^3 + 0.112z^2 + 1.982z + 198.5$$

For iRBCs at size 5  $\mu\text{m}$  with magnetic force 0.1 pN and velocity equation

$$\frac{d^2z}{dt^2} + 639708.118 \frac{dz}{dt} - 1.520 = 0$$

$$v(z) = 0.00299z^3 + 0.112z^2 + 1.982z + 198.5$$

For iRBCs at size 5  $\mu\text{m}$  with magnetic force 0.01 pN and velocity equation

$$\frac{d^2z}{dt^2} + 639708.118 \frac{dz}{dt} - 0.152 = 0$$

$$v(z) = 0.00299z^3 + 0.112z^2 + 1.982z + 198.5$$

For hRBCs at size 5  $\mu\text{m}$  with magnetic force 0.00556 pN and velocity equation

$$\frac{d^2z}{dt^2} + 639708.118 \frac{dz}{dt} - 0.0106 = 0$$

$$v(z) = 0.00299z^3 + 0.112z^2 + 1.982z + 198.5$$

For hRBCs at size 5  $\mu\text{m}$  with magnetic force 0.000556 pN and velocity equation

$$\frac{d^2z}{dt^2} + 639708.118 \frac{dz}{dt} - 0.00106 = 0$$

$$v(z) = 0.00299z^3 + 0.112z^2 + 1.982z + 198.5$$

For hRBCs at size 5  $\mu\text{m}$  with magnetic force 0.0000556 pN and velocity equation

$$\frac{d^2z}{dt^2} + 639708.118 \frac{dz}{dt} - 0.000106 = 0$$

$$v(z) = 0.00299z^3 + 0.112z^2 + 1.982z + 198.5$$

For WBCs at size 5  $\mu\text{m}$  with magnetic force 1.44 pN and velocity equation

$$\frac{d^2z}{dt^2} + 639708.118 \frac{dz}{dt} - 21.952 = 0$$

$$v(z) = 0.00299z^3 + 0.112z^2 + 1.982z + 198.5$$

For WBCs at size 5  $\mu\text{m}$  with magnetic force 0.144 pN and velocity equation

$$\frac{d^2z}{dt^2} + 639708.118 \frac{dz}{dt} - 2.1952 = 0$$

$$v(z) = 0.00299z^3 + 0.112z^2 + 1.982z + 198.5$$

For WBCs at size 5  $\mu\text{m}$  with magnetic force 0.0144 pN and velocity equation

$$\frac{d^2z}{dt^2} + 639708.118 \frac{dz}{dt} - 0.21952 = 0$$

$$v(z) = 0.00299z^3 + 0.112z^2 + 1.982z + 198.5$$

### A.3 Model Magnetic beads, linear discrete calculation

In this previous model, we used the fourth-order Runge-Kutta solving method to solve a motion equation, in the form of ordinary differential equation. However, the Runge-Kutta takes too much computation time. Therefore, in the next model, we take advantage of calculating small period of trajectory, which can be considered as linear motion, from one point to another point or so called Finite difference method, which is more flexible and deals with more complex form of equation. The flowchart of the program is shown in figure 2.22 and coded with MATLAB as follows.

For 5- $\mu\text{m}$  magnetic beads

```

%%%% CODE PROFILE
%%%%%%%%%%%%%%%
%NAME: 5-um Magnetic bead calculation.m
%LAST EDITED: 5 MAY 2016
%%%%%%%%%%%%%%%
%%%%% DEFINITION OF FUNCTION
%%%%%%%%%%%%%%%
%
%
%
%%%% Magnetic force equation
funcafmz=inline('(1.712e4*exp(-2323.*z))*((6.438e-12)+(9.609e-
13*cos(2094.*x))+(9.917e-14*sin(2094.*x)))','z','x');
%Magnetic force equation z-axis
funcafmx=inline('(-6.914e6*z^2+5.332e4*z-101)*((8.293e-15)+(1.516e-
14*cos(2112.*x))+(1.388e-12*sin(2112.*x)))','z','x');
%Magnetic force equation x-axis
%
%%%% Dragforce
funcdz=inline('6*pi*8.1e-04*0.0000025*vfz','vfz');
%Drag force equation z-axis
funcdx=inline('6*pi*8.1e-04*0.0000025*(vfx-vpx)','vfx','vpx');
%Drag force equation x-axis
%
funcvf=inline('umax.*sumupk./sumdownk','y','z','umax','wc','hc','sumu
pk','sumdownk');
%Velocity Equation
%
%
%%%% INPUT PARAMETER AND CONSTANT
VALUE%%%%%%%%%%%%%%%
%
%
%
t=input('\nEnter Value of t: ');
%t = time
%
xm=input('\nEnter Value of X mm : ');
x = xm*10^-3;
% initial position of x
y=input('\nEnter Value of Y: ');
% initial position of y
zm=input('\nEnter Value of Z (Range 4.516 - 3.978) mm: ');
z = zm*10^-3;
% initial position of z
zmf=input('\nEnter Value of Z final (Range 4.516 - 3.978) mm: ');
zf = zmf*10^-3;
% initial position of z
n=input('\nEnter Value of n: ');
% a number of solving iterations
h=input('\nEnter Value of h: ');

```

```

% time step
%
wc= 538.25;
% width of channel
hc= 100;
% height of channel
flowrate=input('\nEnter Value of total flow rate (uL/min): ');
uavg = flowrate/wc/hc/60*1000000000;
umax = 1.4175*uavg;
%maximum velocity of fluid
%
vfz = 0;
vpx = 0;
%
mass = 1.0014e-13;
% mass of magnetic beads 5 um
%
%
%%%%% Display function
%%%%%
%
%
fprintf('\nSOLUTION WITH STEP SIZE = %10.4e IS:',h);
fprintf('\n      t      z      x');
fprintf('\n%16.6e%16.6e%16.6e',t,z,x);
%
%
%
%%%%% Iteration function
%%%%%
%
%
for i = 1:n
%%%%% Magnetic force calculation
%%%%%
% input position for getting magnetic force at individual position
%
fmz = funcafmx(z,x);
fmx = funcafmx(z,x);

%%%%% Velocity calculation
%%%%%
% input position for getting magnetic force at individual position
%
zv = z*10^6;
vcy=y-(hc/2);
vcz=zv-(3978+(wc/2));

```

```

upk1=(1)*(1-
((cosh(pi*vcy/wc))/(cosh(pi*hc/2/wc)))* (cos(pi*vcz/wc));
upk3=(-1/27)*(1-
((cosh(3*pi*vcy/wc))/(cosh(3*pi*hc/2/wc)))* (cos(3*pi*vcz/wc));
upk5=(1/125)*(1-
((cosh(5*pi*vcy/wc))/(cosh(5*pi*hc/2/wc)))* (cos(5*pi*vcz/wc));
upk7=(-1/343)*(1-
((cosh(7*pi*vcy/wc))/(cosh(7*pi*hc/2/wc)))* (cos(7*pi*vcz/wc));
sumupk=upk1+upk3+upk5+upk7;
downk1=(1)*(1-(1/(cosh(pi*hc/2/wc))));
downk3=(-1/27)*(1-(1/(cosh(3*pi*hc/2/wc))));
downk5=(1/125)*(1-(1/(cosh(5*pi*hc/2/wc))));
downk7=(-1/343)*(1-(1/(cosh(7*pi*hc/2/wc))));
sumdownk=downk1+downk3+downk5+downk7;
vfxu = funcvf(y,z,umax,wc,hc,sumupk,sumdownk);
vfx = vfxu*10^-6;
%%%%% Drag force calculation
%%%%%%%%%%%%%%%
% input velocity of fluid and particle for getting magnetic force at
% individual position
%
fdz = funcdz(vfz);
fdx = funcdx(vfx,vpx);

%%%%% Acceleration calculation
%%%%%%%%%%%%%%%
az = (fmz - fdz)/mass;
ax = (fmx + fdx)/mass;

%%%%% Displacement calculation
%%%%%%%%%%%%%%%
dz = (vfz*h) + (0.5*az*h^2);
z = z-dz;

dx = (vpx*h) + (0.5*ax*h^2);
x = x+dx;
Chulalongkorn University

%%%%% Time increment
%%%%%%%%%%%%%%%
t = t+h;

%%%%% Final velocity calculation
%%%%%%%%%%%%%%%
vfz = vfz + (az*h);
vpx = vpx + (ax*h);

%%%%% Break Condition
%%%%%%%%%%%%%%%
% Sometimes particles go out of the range we define. This condition
will
% terminate the program.
%
%
if z <= zf
    fprintf('\n BREAK !! because particles have already collided
with channel wall ');
    fprintf('\n%16.6e%16.6e%16.6e',t,z,x);

```

```

        break
    end
%
%
%
%%%%% Display Condition
%%%%% Because in each iteration is calculated too quickly and a lot of
% information will not be used in every single point, we decide to
store
% the data every 200000 iterations.
%
%
%
if i/200000 == floor(i/200000)
fprintf('\n%16.6e%16.6e%16.6e%16.6e',t,z,x);
end
%
%
%
end

```

For 10- $\mu\text{m}$  magnetic beads

```

%%%% CODE PROFILE
%%%%%% NAME: 10-um Magnetic bead calculation.m
%%%%%% LAST EDITED: 5 MAY 2016
%%%%%% DEFINITION OF FUNCTION
%%%%%% Magnetic force equation
funcafmz=inline('(1.712e4*exp(-2323.*z))*((5.151e-11)+(7.687e-
12*cos(2094.*x))+(7.933e-13*sin(2094.*x)))','z','x');
%Magnetic force equation z-axis
funcafmx=inline('(-8.936e-14*exp(6871.*z)+(380.5*exp(
-1358.*z))*((6.634e-14)+(1.213e-13*cos(2112.*x))+(1.111e-
11*sin(2112.*x))))','z','x');
%Magnetic force equation x-axis
%
%%%%% Dragforce
funcdz=inline('6*pi*8.1e-04*0.000005*vfz','vfz');
%Drag force equation z-axis
funcdx=inline('6*pi*8.1e-04*0.000005*(vfx-vpx)','vfx','vpx');
%Drag force equation x-axis
%
funcvf=inline('umax.*sumupk./sumdownk','y','z','umax','wc','hc','sumu
pk','sumdownk');
%Velocity Equation

```

```

%%%%% INPUT PARAMETER AND CONSTANT
VALUE%%%%%
%
%
%
t=input('\nEnter Value of t: ');
% t = time
%
xm=input('\nEnter Value of X mm : ');
x = xm*10^-3;
% initial position of x
y=input('\nEnter Value of Y: ');
% initial position of y
zm=input('\nEnter Value of Z (Range 4.428976 - 3.879760) mm: ');
z = zm*10^-3;
% initial position of z

zmf=input('\nEnter Value of Z final (Range 4.428976 - 3.879760) mm:');
zf = zmf*10^-3;
% initial position of z
n=input('\nEnter Value of n: ');
% a number of solving iterations
h=input('\nEnter Value of h: ');
% time step
%
wc= 529.96;
% width of channel
hc= 100;
% height of channel
flowrate=input('\nEnter Value of total flow rate (uL/min): ');
uavg = flowrate/wc/hc/60*1000000000;
umax = 1.4175*uavg;
%maxmimum velocity of fluid
%
vfz = 0;
vpx = 0;
%
mass = 8.9535e-13;
% mass of magnetic beads 10 um
%
%
%%%%% Display function
%%%%%
%
```

```

fprintf('\nSOLUTION WITH STEP SIZE = %10.4e IS:',h);
fprintf('\n      t          z           x');
fprintf('\n%16.6e%16.6e%16.6e',t,z,x);
%
%
%
%%%%%%%%%%%%%% Iteration function
%%%%%%%%%%%%%%%
%
%
%
for i = 1:n
%%%%%%%%% Magnetic force calculation
%%%%%%%%%%%%%%%
% input position for getting magnetic force at individual position
%
fmz = funcfmz(z,x);
fmx = funcfmz(z,x);

%%%%%%%%% Velocity calculation
%%%%%%%%%%%%%%%
% input position for getting magnetic force at individual position
%
zv = z*10^6;
vcy=y-(hc/2);
vcz=zv-(3879.760+(wc/2));
upk1=(1)*(1-
((cosh(pi*vcy/wc))/(cosh(pi*hc/2/wc)))*(cos(pi*vcz/wc));
upk3=(-1/27)*(1-
((cosh(3*pi*vcy/wc))/(cosh(3*pi*hc/2/wc)))*(cos(3*pi*vcz/wc));
upk5=(1/125)*(1-
((cosh(5*pi*vcy/wc))/(cosh(5*pi*hc/2/wc)))*(cos(5*pi*vcz/wc));
upk7=(-1/343)*(1-
((cosh(7*pi*vcy/wc))/(cosh(7*pi*hc/2/wc)))*(cos(7*pi*vcz/wc));
sumupk=upk1+upk3+upk5+upk7;
downk1=(1)*(1-(1/(cosh(pi*hc/2/wc))));
downk3=(-1/27)*(1-(1/(cosh(3*pi*hc/2/wc))));
downk5=(1/125)*(1-(1/(cosh(5*pi*hc/2/wc))));
downk7=(-1/343)*(1-(1/(cosh(7*pi*hc/2/wc))));
sumdownk=downk1+downk3+downk5+downk7;
vfxu = funcvf(y,z,umax,wc,hc,sumupk,sumdownk);
vfx = vfxu*10^-6;

%%%%%%%%% Drag force calculation
%%%%%%%%%%%%%%%
% input velocity of fluid and particle for getting magnetic force at
% individual position
%
fdz = funcdz(vfz);
fdx = funcdx(vfx,vpx);

%%%%%%%%% Acceleration calculation
%%%%%%%%%%%%%%%
az = (fmz - fdz)/mass;

```

```

ax = (fmx + fdx)/mass;

%%%%% Displacement calculation
%%%%%
dz = (vfvz*h) + (0.5*az*h^2);
z = z-dz;

dx = (vpx*h) + (0.5*ax*h^2);
x = x+dx;

%%%%% Time increment
%%%%%
t = t+h;

%%%%% Final velocity calculation
%%%%%
vfvz = vfvz + (az*h);
vpx = vpx + (ax*h);

%%%%% Break Condition
%%%%%
% Sometimes particles go out of the range we define. This condition
will
% terminate the program.
%
%
if z <= zf
    fprintf('\n BREAK !! because particles have reached the
defined z-coordinate ');
    fprintf('\n%16.6e%16.6e%16.6e',t,z,x);
    break
end
%
%
%
%%%%% Display Condition
%%%%%
% Because in each iteration is calculated too quickly and a lot of
% information will not be used in every single point, we decide to
store
% the data every 200000 iterations.
%
%
%
if i/200000 == floor(i/200000)
fprintf('\n%16.6e%16.6e%16.6e%16.6e',t,z,x);
end
%
%
%
End

```

#### A.4 Model Actual Blood cell; Finite difference of trajectories

In this model, we try to fabricate the device that has the narrowest distance between a magnet array and the channel as much as possible. The value of magnetic field from the simulation of magnetic field distribution where is very close to the magnet is quite sensitive. Therefore, in this model, we separate the calculation into 3 distances, 100  $\mu\text{m}$ , 200  $\mu\text{m}$  and 300  $\mu\text{m}$  away from the a magnet array. A set of magnetic force equations acting on red blood cells is different in each case will be coded with MATLAB for trajectory as follows

Case 100  $\mu\text{m}$  away from an array of magnets

```
%%%%
%CODE PROFILE
%NAME: 100 um away actual iRBCs calculation.m
%LAST EDITED: 5 MAY 2016
%%%%%
%%%%% DEFINITION OF FUNCTION
%%%%%
%
%
%
%%%%% Magnetic force equation
funcafmz=inline('((4.723e17*exp(-1.52e4.*z))+(1.593e04*exp(-
3344.*z)))*(1.383e-15 + 2.734e-17*cos(2094*x) - 1.17e-20*sin(2094*x)
+ 2.913e-17*cos(2*2094*x) + 1.933e-19*sin(2*2094*x) - 2.014e-
17*cos(3*2094*x) + 2.212e-19*sin(3*2094*x) + 9.52e-18*cos(4*2094*x) -
6.058e-20*sin(4*2094*x))','z','x');
% Neglect x-axis force equation because from the data, it showed very
small
% Magnetic force equation z-axis
%
%%%%% Dragforce
funcdz=inline('12*3*vfz*17*10^-12/0.0396','vfz');
%Drag force equation z-axis
funcdx=inline('12*3*(vfx-vpx)*17*10^-12/0.0396','vfx','vpx');
%Drag force equation x-axis
%
funcvf=inline('umax.*sumupk./sumdownk','y','z','umax','wc','hc','sumu
pk','sumdownk');
%Velocity Equation
%
%
%
%%%%% INPUT PARAMETER AND CONSTANT
VALUE%%%%%
```



```

%%%% Iteration function
%%%%%
%
%
%
for i = 1:n
%%%% Magnetic force calculation
%%%%%
% input position for getting magnetic force at individual position
%
fmx = 0;
fmz = funcafmx(z,x);

%%%% Velocity calculation
%%%%%
% input position for getting magnetic force at individual position
%
zv = z*10^6;
vcy=y-50;
vcz=zv-(2600+(wc/2));
upk1=(1)*(1-
((cosh(pi*vcy/wc))/(cosh(pi*hc/2/wc)))*(cos(pi*vcz/wc));
upk3=(-1/27)*(1-
((cosh(3*pi*vcy/wc))/(cosh(3*pi*hc/2/wc)))*(cos(3*pi*vcz/wc));
upk5=(1/125)*(1-
((cosh(5*pi*vcy/wc))/(cosh(5*pi*hc/2/wc)))*(cos(5*pi*vcz/wc));
upk7=(-1/343)*(1-
((cosh(7*pi*vcy/wc))/(cosh(7*pi*hc/2/wc)))*(cos(7*pi*vcz/wc));
sumupk=upk1+upk3+upk5+upk7;
downk1=(1)*(1-(1/(cosh(pi*hc/2/wc))));
downk3=(-1/27)*(1-(1/(cosh(3*pi*hc/2/wc))));
downk5=(1/125)*(1-(1/(cosh(5*pi*hc/2/wc))));
downk7=(-1/343)*(1-(1/(cosh(7*pi*hc/2/wc))));
sumdownk=downk1+downk3+downk5+downk7;
vfxu = funcvf(y,z,umax,wc,hc,sumupk,sumdownk);
vfx = vfxu*10^-6;

%%%% Drag force calculation
%%%%%
% input velocity of fluid and particle for getting magnetic force at
% individual position
%
fdz = funcdz(vfz);
fdx = funcdx(vfx,vpx);

%%%% Acceleration calculation
%%%%%
az = (fmz - fdz)/mass;
ax = fdx/mass;

%%%% Displacement calculation
%%%%%
dz = (vfz*h) + (0.5*az*h^2);
z = z-dz;

dx = (vpx*h) + (0.5*ax*h^2);

```

```

x = x+dx;

%%%% Time increment
t = t+h;

%%%% Final velocity calculation
vfz = vfz + (az*h);
vpx = vpx + (ax*h);

%%%% Break Condition
% Sometimes particles go out of the range we define. This condition
will
% terminate the program.
%
%
if z <= zi-dzfm
    fprintf('\n BREAK !! because it reaches the defined lateral
distance');
    fprintf('\n%16.6e%16.6e%16.6e',t,z,x);
    break
end
%
if x >= 0.006
    fprintf('\n BREAK !! because it reaches the maximum domain of
x-axis');
    fprintf('\n%16.6e%16.6e%16.6e',t,z,x);
    break
end
%
%
%
%
%%%% Display Condition
% Because in each iteration is calculated too quickly and a lot of
% information will not be used in every single point, we decide to
store
% the data every 1000000 iterations.
%
%
%
if i/1000000 == floor(i/1000000)
    fprintf('\n%16.6e%16.6e%16.6e%16.6e',t,z,x);
end
%
%
%
end
fprintf('\n Finish!! What a long calculation!');
fprintf('\n          t           x           z');

```

```
fprintf('\n%16.6e%16.6e%16.6e',t,z,x);
```

Case 200  $\mu\text{m}$  away from an array of magnets

```
%%%%% CODE PROFILE
%%%%% NAME: 200 um away actual iRBCs calculation.m
%%%%% LAST EDITED: 5 MAY 2016
%%%%% %%%%%% %%%%%% %%%%%% %%%%%% %%%%%% %%%%%% %%%%%% %%%%%% %%%%%% %%%%%% %%%%%%
%%%%% %%%%%% %%%%%% %%%%%% %%%%%% %%%%%% %%%%%% %%%%%% %%%%%% %%%%%% %%%%%% %%%%%% %%%%%%
%%%%% %%%%%% DEFINITION OF FUNCTION
%%%%% %%%%%% %%%%%% %%%%%% %%%%%% %%%%%% %%%%%% %%%%%% %%%%%% %%%%%% %%%%%% %%%%%%
%%%%% %
%%%%% %
%%%%% %
%%%%% %%%%%% Magnetic force equation
funcafmz=inline('((7.274e11*exp(-9906.*z))+(2369*exp(-
2623.*z)))*(9.688e-16 + 3.976e-17*cos(2094*x) + 1.999e-
19*sin(2094*x) + 8.639e-18*cos(2*2094*x) - 1.056e-19*sin(2*2094*x) -
6.43e-18*cos(3*2094*x) + 5.17e-19*sin(3*2094*x) + 2.925e-
18*cos(4*2094*x) - 1.534e-19*sin(4*2094*x))','z','x');
% Neglect x-axis force equation because from the data, it showed very
small
% Magnetic force equation z-axis
%
%%%%% Dragforce
funcdz=inline('12*3*vfz*17*10^-12/0.0396','vfz');
%Drag force equation z-axis
funcdx=inline('12*3*(vfx-vpx)*17*10^-12/0.0396','vfx','vpx');
%Drag force equation x-axis
%
funcvf=inline('umax.*sumupk./sumdownk','y','z','umax','wc','hc','sumu
pk','sumdownk');
%Velocity Equation
%
%
%%%%% INPUT PARAMETER AND CONSTANT
VALUE%%%%% %%%%%% %%%%%% %%%%%% %%%%%% %%%%%% %%%%%% %%%%%% %%%%%% %%%%%% %%%%%%
%
%
%
t=input('\nEnter Value of t: ');
% t = time
%
xm=input('\nEnter Value of X mm: ');
x = xm*10^-3;
% initial position of x
y=input('\nEnter Value of Y: ');
% initial position of y
zm=input('\nEnter Value of Z mm (Range 2.6 - 3.1 ): ');
z = zm*10^-3;
```

```

zi = zm*10^-3;
% initial position of z
%
dzf=input('\nEnter Value of lateral distance um: ');
dzfm = dzf*10^-6;
%
n=input('\nEnter Value of n: ');
% a number of solving iterations
%
h=input('\nEnter Value of h: ');
% time step
%
wc= 500;
% width of channel
hc= 100;
% height of channel
flowrate=input('\nEnter Value of total flow rate (uL/min): ');
uavg = flowrate/wc/hc/60*1000000000;
umax = 1.4175*uavg;
% maximum velocity of fluid
%
vfz = 0;
vpx = 0;
%
mass = 1125*88.68*10^-15;
% mass of blood cels
%
%
%%%%% Display function
%%%%% %%%%%% %%%%%% %%%%%% %%%%%% %%%%%% %%%%%% %%%%%% %%%%%% %%%%%% %
%
fprintf('\nSOLUTION WITH STEP SIZE = %10.4e IS:',h);
fprintf('\n          t           z           x');
fprintf('\n%16.6e%16.6e%16.6e',t,zm,x);
%
%
%%%%% Iteration function
%%%%% %%%%%% %%%%%% %%%%%% %%%%%% %%%%%% %%%%%% %%%%%% %%%%%% %%%%%% %
%
%
%
for i = 1:n
%%%%% Magnetic force calculation
%%%%% %%%%%% %%%%%% %%%%%% %%%%%% %%%%%% %%%%%% %%%%%% %%%%%% %%%%%% %
% input position for getting magnetic force at individual position
%
fmx = 0;
fmz = funcafmz(z,x);

```

```

%%%%% Velocity calculation
%%%%%%%%%%%%%%%
% input position for getting magnetic force at individual position
%
zv = z*10^6;
vcy=y-50;
vcz=zv-(2600+(wc/2));
upk1=(1)*(1-
((cosh(pi*vcy/wc))/(cosh(pi*hc/2/wc)))*(cos(pi*vcz/wc));
upk3=(-1/27)*(1-
((cosh(3*pi*vcy/wc))/(cosh(3*pi*hc/2/wc)))*(cos(3*pi*vcz/wc));
upk5=(1/125)*(1-
((cosh(5*pi*vcy/wc))/(cosh(5*pi*hc/2/wc)))*(cos(5*pi*vcz/wc));
upk7=(-1/343)*(1-
((cosh(7*pi*vcy/wc))/(cosh(7*pi*hc/2/wc)))*(cos(7*pi*vcz/wc));
sumupk=upk1+upk3+upk5+upk7;
downk1=(1)*(1-(1/(cosh(pi*hc/2/wc))));
downk3=(-1/27)*(1-(1/(cosh(3*pi*hc/2/wc))));
downk5=(1/125)*(1-(1/(cosh(5*pi*hc/2/wc))));
downk7=(-1/343)*(1-(1/(cosh(7*pi*hc/2/wc))));
sumdownk=downk1+downk3+downk5+downk7;
vfxu = funcvf(y,z,umax,wc,hc,sumupk,sumdownk);
vfx = vfxu*10^-6;

%%%%% Drag force calculation
%%%%%%%%%%%%%%%
% input velocity of fluid and particle for getting magnetic force at
% individual position
%
fdz = funcdz(vfz);
fdx = funcdx(vfx,vpx);

%%%%% Acceleration calculation
%%%%%%%%%%%%%%%
az = (fmz - fdz)/mass;
ax = fdx/mass;

%%%%% Displacement calculation
%%%%%%%%%%%%%%%
dz = (vfz*h) + (0.5*az*h^2);
z = z-dz;

dx = (vpx*h) + (0.5*ax*h^2);
x = x+dx;

%%%%% Time increment
%%%%%%%%%%%%%%%
t = t+h;

%%%%% Final velocity calculation
%%%%%%%%%%%%%%%
vfz = vfz + (az*h);
vpx = vpx + (ax*h);

```

```

%%%%% Break Condition
%%%%%%%%%%%%%%%
% Sometimes particles go out of the range we define. This condition
will
% terminate the program.
%
%
if z <= zi-dzfm
    fprintf('\n BREAK !! because it reaches the defined lateral
distance');
    fprintf('\n%16.6e%16.6e%16.6e',t,z,x);
    break
end
%
if x >= 0.006
    fprintf('\n BREAK !! because it reaches the maximum domain of
x-axis');
    fprintf('\n%16.6e%16.6e%16.6e',t,z,x);
    break
end
%
%
%
%
%%%%% Display Condition
%%%%%%%%%%%%%%%
% Because in each iteration is calculated too quickly and a lot of
% information will not be used in every single point, we decide to
store
% the data every 1000000 iterations.
%
%
%
if i/1000000 == floor(i/1000000)
fprintf('\n%16.6e%16.6e%16.6e%16.6e',t,z,x);
end
%
%
%
fprintf('\n Finish!! What a long calculation!');
fprintf('\n      t           x           z');
fprintf('\n%16.6e%16.6e%16.6e',t,z,x);

```

Case 300  $\mu\text{m}$  away from an array of magnets

```

%%%%% CODE PROFILE
%%%%%%%%%%%%%%%
%NAME: 300 um away actual iRBCs calculation.m
%LAST EDITED: 5 MAY 2016
%%%%%%%%%%%%%%%

```

```

%%%%% DEFINITION OF FUNCTION
%%%%% %%%%%% %%%%%% %%%%%% %%%%%% %%%%%% %%%%%% %%%%%% %%%%%% %%%%%%
%
%
%
%%%%% Magnetic force equation
funcafmz=inline('((1.487e10*exp(-8350.*z))+(2265*exp(-
2521.*z)))*(7.063*e-16 + 4.373e-17*cos(2094*x) + 1.357e-
19*sin(2094*x))','z','x');
% Neglect x-axis force equation because from the data, it showed very
small
% Magnetic force equation z-axis
%
%%%%% Dragforce
funcdz=inline('12*3*vfz*17*10^-12/0.0396','vfz');
%D drag force equation z-axis
funcdx=inline('12*3*(vfx-vpx)*17*10^-12/0.0396','vfx','vpx');
%D drag force equation x-axis
%
funcvf=inline('umax.*sumupk./sumdownk','y','z','umax','wc','hc','sumu
pk','sumdownk');
%Velocity Equation
%
%
%
%%%%% INPUT PARAMETER AND CONSTANT
VALUE%%%%% %%%%%% %%%%%% %%%%%% %%%%%% %%%%%% %%%%%% %%%%%% %%%%%% %%%%%%
%
%
%
t=input('\nEnter Value of t: ');
% t = time
%
xm=input('\nEnter Value of X mm: ');
x = xm*10^-3;
% initial position of x
y=input('\nEnter Value of Y: ');
% initial position of y
zm=input('\nEnter Value of Z mm (Range 2.6 - 3.1 ): ');
z = zm*10^-3;
zi = zm*10^-3;
% initial position of z
%
dzf=input('\nEnter Value of lateral distance um: ');
dzfm = dzf*10^-6;
%
n=input('\nEnter Value of n: ');
% a number of solving iterations
%
h=input('\nEnter Value of h: ');
% time step
%
wc= 500;
% width of channel
hc= 100;

```

```

% height of channel
flowrate=input('\nEnter Value of total flow rate (uL/min): ');
uavg = flowrate/wc/hc/60*1000000000;
umax = 1.4175*uavg;
% maximum velocity of fluid
%
vfxz = 0;
vpzx = 0;
%
mass = 1125*88.68*10^-15;
% mass of blood cels
%
%
%
%%%%% Display function
%%%%% SOLUTION WITH STEP SIZE = %10.4e IS: ,h);
fprintf('nSOLUTION WITH STEP SIZE = %10.4e IS:',h);
fprintf('n t z x');
fprintf('n%16.6e%16.6e%16.6e',t,zm,x);
%
%
%
%%%%% Iteration function
%%%%% for i = 1:n
%%%%% Magnetic force calculation
%%%%% input position for getting magnetic force at individual position
%
fmx = 0;
fmz = funcafmz(z,x);

%%%%% Velocity calculation
%%%%% input position for getting magnetic force at individual position
%
zv = z*10^6;
vcy=y-50;
vcz=zv-(2600+(wc/2));
upk1=(1)*(1-
((cosh(pi*vcy/wc))/(cosh(pi*hc/2/wc)))*(cos(pi*vcz/wc));
upk3=(-1/27)*(1-
((cosh(3*pi*vcy/wc))/(cosh(3*pi*hc/2/wc)))*(cos(3*pi*vcz/wc));
upk5=(1/125)*(1-
((cosh(5*pi*vcy/wc))/(cosh(5*pi*hc/2/wc)))*(cos(5*pi*vcz/wc));

```

```

upk7=(-1/343)*(1-
((cosh(7*pi*vcy/wc))/(cosh(7*pi*hc/2/wc))))*(cos(7*pi*vcz/wc));
sumupk=upk1+upk3+upk5+upk7;
downk1=(1)*(1-(1/(cosh(pi*hc/2/wc)))); 
downk3=(-1/27)*(1-(1/(cosh(3*pi*hc/2/wc)))); 
downk5=(1/125)*(1-(1/(cosh(5*pi*hc/2/wc)))); 
downk7=(-1/343)*(1-(1/(cosh(7*pi*hc/2/wc)))); 
sumdownk=downk1+downk3+downk5+downk7;
vfxu = funcvf(y,z,umax,wc,hc,sumupk,sumdownk);
vfx = vfxu*10^-6;

%%%%% Drag force calculation
%%%%%%%%%%%%%
% input velocity of fluid and particle for getting magnetic force at
% individual position
%
fdz = funcdz(vfz);
fdx = funcdx(vfx,vpx);

%%%%% Acceleration calculation
%%%%%%%%%%%%%
az = (fmz - fdz)/mass;
ax = fdx/mass;

%%%%% Displacement calculation
%%%%%%%%%%%%%
dz = (vfz*h) + (0.5*az*h^2);
z = z-dz;

dx = (vpx*h) + (0.5*ax*h^2);
x = x+dx;

%%%%% Time increment
%%%%%%%%%%%%%
t = t+h;

%%%%% Final velocity calculation
%%%%%%%%%%%%%
vfz = vfz + (az*h);
vpx = vpx + (ax*h);

%%%%% Break Condition
%%%%%%%%%%%%%
% Sometimes particles go out of the range we define. This condition
will
% terminate the program.
%
%
if z <= zi-dzfm
    fprintf('\n BREAK !! because it reaches the defined lateral
distance');
    fprintf('\n%16.6e%16.6e%16.6e',t,z,x);
    break
end
%
if x >= 0.006
    fprintf('\n BREAK !! because it reaches the maximum domain of
x-axis');
    fprintf('\n%16.6e%16.6e%16.6e',t,z,x);
    break

```

```

    end
%
%
%
%
%%%%% Display Condition
%%%%% Because in each iteration is calculated too quickly and a lot of
% information will not be used in every single point, we decide to
store
% the data every 1000000 iterations.
%
%
%
if i/1000000 == floor(i/1000000)
fprintf('\n%16.6e%16.6e%16.6e%16.6e',t,z,x);
end
%
%
%
%%%%% Finish!! What a long calculation!;
fprintf('\n      t          x          z');
fprintf('\n%16.6e%16.6e%16.6e',t,z,x);

```

## Appendix B. COMSOL Multiphysics

COMSOL Multiphysics is used in this study because of its friendly interface and ease to use. In this section, we are going to introduce how to use the program and also show the detail of the model and domain used in this study.

### B.1 Introduction to COMSOL

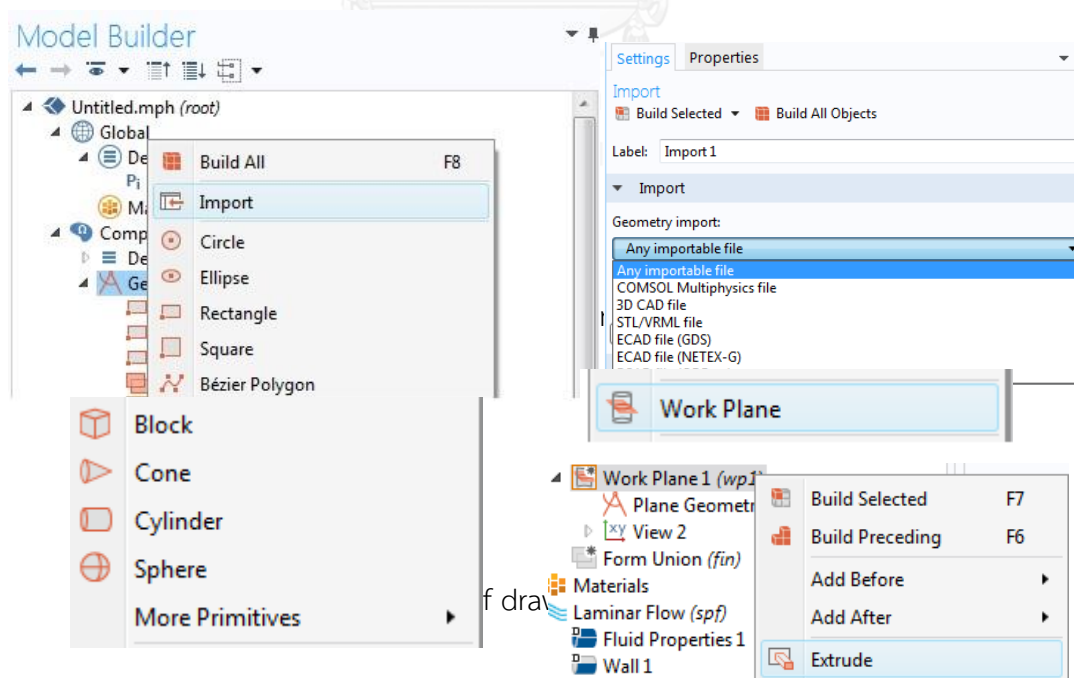
The procedure we like to simulate a case with COMSOL can be described by following

1. Building a model

Drawing a model can be built in mainly two ways

1.1 Import the model already drawn by AUTOCAD, SolidWork, or even COMSOL itself with a few working filetype such as .mphbin, .dwg, .sldprt etc. The figure is shown in fig. B1.

1.2 Draw with COMSOL. It depends on our model whether it is 2D or 3D. in case 3D, we has two choices that first, we can use ready-made shape such as sphere, cube or cone etc., or second, we choose work plane to draw in 2D then extrude for 3D model. The figure is shown in fig. B2.



## 2. Material selection

In each study, we know that the properties used for calculation need to be filled. In license file, we found that problem that we need to purchase these data additionally. Therefore, sometimes we need to add the properties from journal papers instead which may be better than the provided data by the program because it may be in the same condition and more appropriate.

## 3. Boundary condition definition

It is based on what physics you choose to study. The example shown in fig B.3 is used in fluid laminar flow study.

## 4. Meshing

One of the advantages of COMSOL Multiphysics is auto meshing by the program that we can increase or decrease the size of meshes by ourselves for improving the accuracy of the calculation or use ready-made command by the program. The meshing step is shown in fig B.4.

## 5. Study and Result

After meshing, we will let it compute and show the result after that. It relies on what you want to see the result. We can set them to show the color range or even export the data for further analysis.

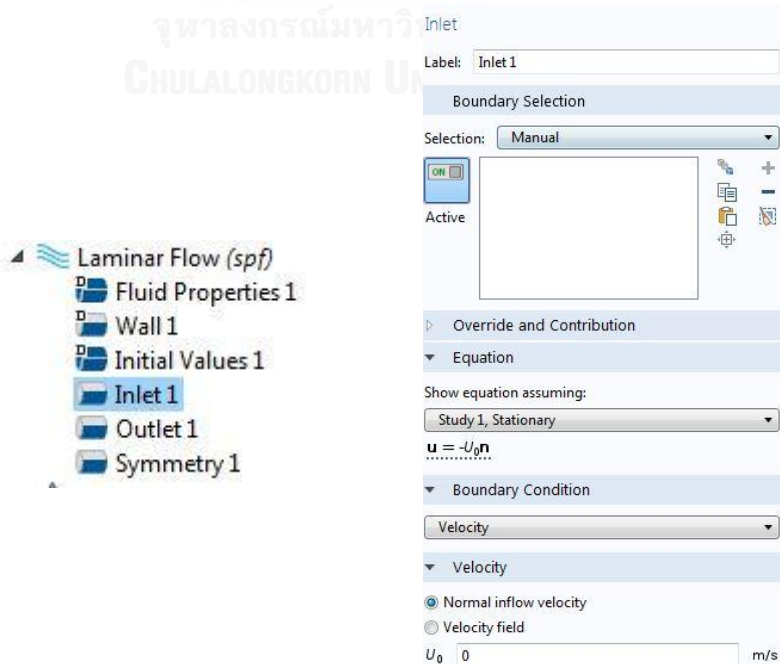


Figure B.3 the illustration of defining conditions to the study

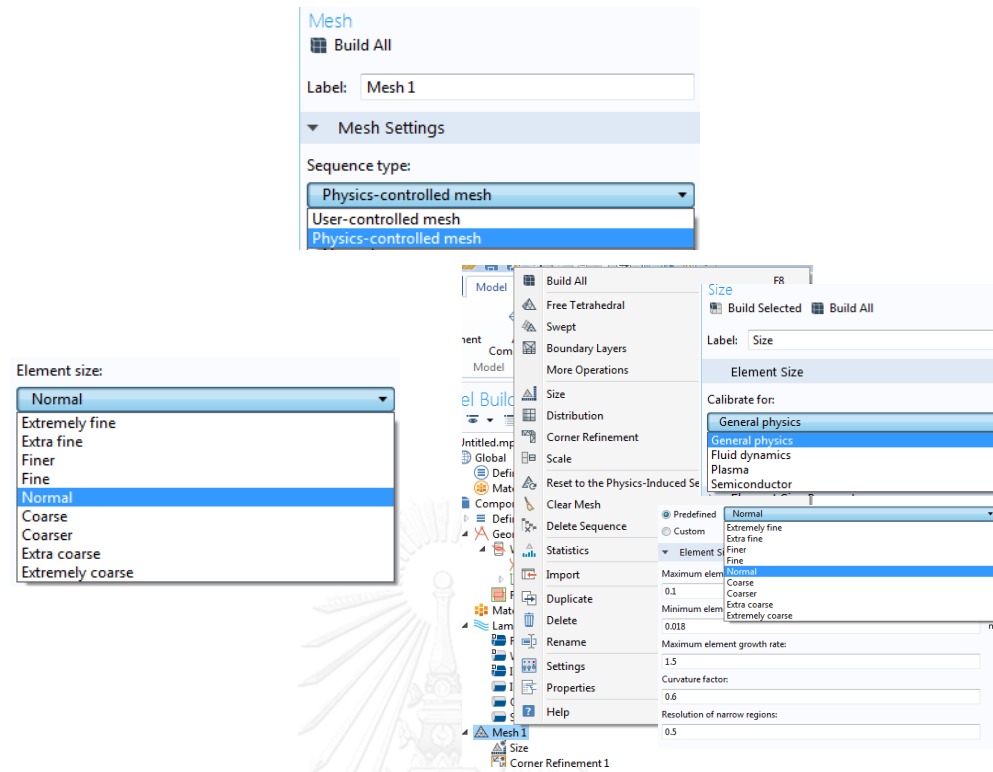


Figure B.4 meshing steps

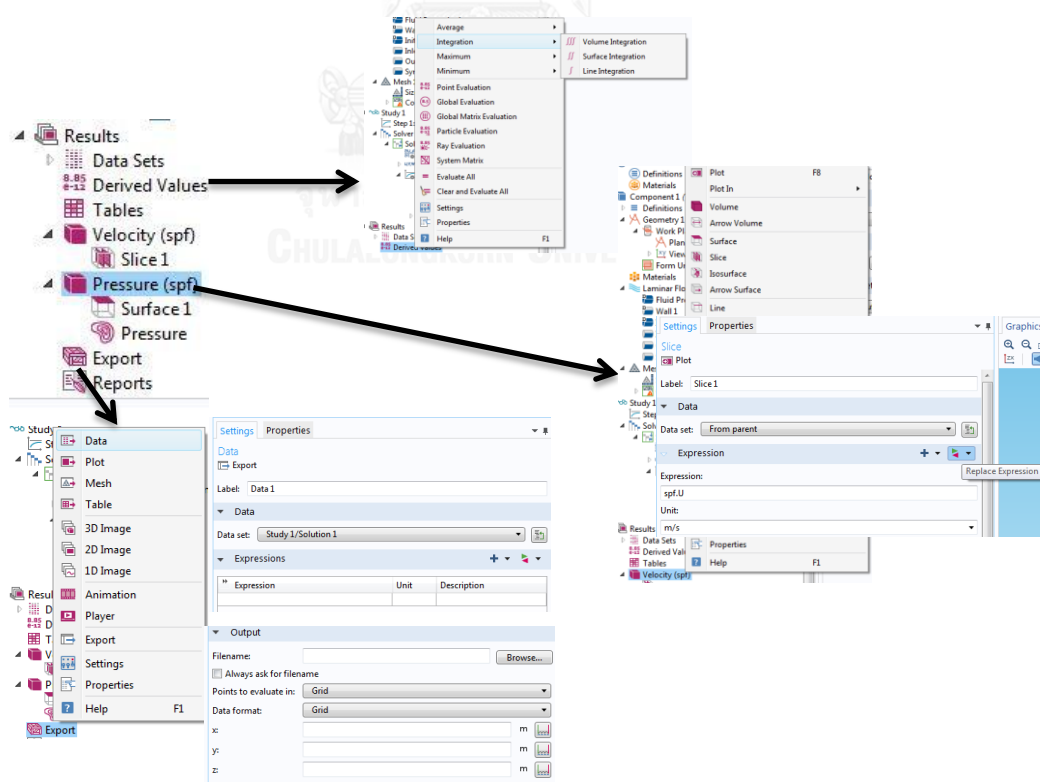


Figure B.5 the illustration of many functions in Results tab after computation

## B.2 Validation COMSOL Multiphysics with analytical solution

According to G.Xiao-fan et al. (2004), they proposed the analytical solving equations shown from Equations (2.5) to (2.16). This section shows how to define the conditions in COMSOL Multiphysics so that we can adapt it into more difficult model.

We define the domain to be in the shape of sphere and other elements are shown in Fig. B6 and the conditions similar to the condition of analytical solution are also displayed in Fig. B7.

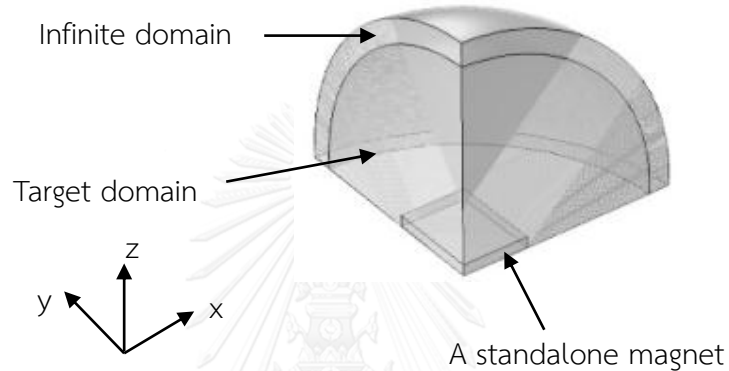


Figure B.6 the domain and details of each element modeled by COMSOL Multiphysics

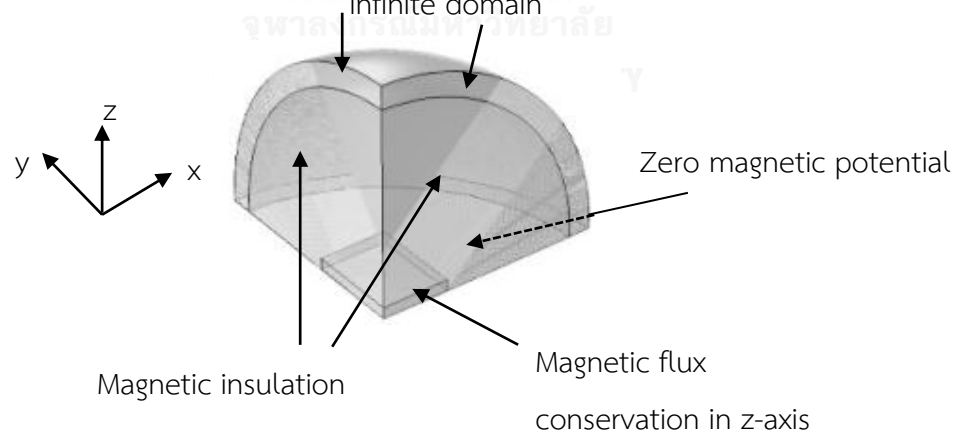


Figure B.7 the conditions given to the software

### B.3 Extraction of Data from COMSOL

Data shown in Table B.1 is extracted by COMSOL Multiphysics in the form of the excel file.

Table B.1 the magnetic field at arbitrary point

	0	0.05	0.1	0.15	0.2	0.25	0.3	0.35	0.4	0.45	0.5	0.55	0.6	0.65	0.7	0.75	0.8	0.85	0.9	0.95
2.5	223617.85	223469.43	224916.71	224104.96	223599.56	224045.16	223841.18	222437.01	222499.47	222499.78	222499.36	226453.26	222499.378	220287.48	220961.62	220674.26	219712.08	218961.01	217433.14	217761.76
2.55	184247.13	184971.29	184055.29	183848.13	184502.74	184088.49	182813.63	183437.54	18165.62	182457.95	182045.80	182380.13	181573.28	180683.74	180194.83	17930.39	178822.68	178020.40	17703.90	176986.35
2.6	155222.24	155224.51	155058.85	154975.25	154880.27	154782.29	154549.87	154282.01	153987.49	155286.53	153058.77	152780.83	152182.23	151899.40	151335.82	150753.34	150362.48	149571.44	149120.65	148531.22
2.65	136234.63	135889.73	135837.48	135739.06	135602.47	135432.00	135294.50	135011.76	134757.34	134442.18	134045.82	133715.64	133133.65	132779.43	132342.99	131813.61	131257.96	130817.43	130368.39	129879.42
2.7	12181.43	121854.95	12170.45	121690.74	121588.25	121254.15	120996.78	120700.53	120442.21	120119.60	11975.12	11957.07	118927.60	118488.82	118011.20	117600.51	116691.89	116318.48		
2.75	110883.52	110847.04	110820.74	110724.21	110620.39	110462.51	110225.68	110018.59	109803.61	109500.52	109236.78	108833.40	108507.02	108052.76	107677.59	107251.14	106827.27	106400.96	106020.90	105618.01
2.8	101808.37	101846.62	101772.95	101697.13	101574.94	101396.57	101255.54	100993.72	100793.91	100522.78	100247.18	99882.70	99255.41	99180.69	98781.21	98386.23	97979.03	97553.92	97176.30	96755.86
2.85	94177.75	94164.48	94028.71	94010.48	93983.66	93759.64	93605.30	93399.64	93148.63	92893.74	92607.12	92272.18	91944.47	91583.94	91210.22	90845.28	90428.28	89624.89	89252.15	
2.9	87492.18	87482.63	87442.03	87354.05	87246.04	87177.34	86944.45	86757.44	86510.59	86258.84	85963.39	85657.26	85319.55	84968.17	84590.50	84255.60	83820.04	83427.88	83050.50	82661.98
2.95	81583.00	81591.22	81543.08	81461.60	81341.41	81215.04	80849.88	80105.56	80036.17	80089.74	79772.12	79456.94	79102.21	78723.78	78362.36	77967.83	77582.72	77190.94	76812.99	
3	76305.01	76292.19	76240.02	76166.58	75928.43	75752.76	75566.22	75325.52	75086.35	74809.11	74512.11	74184.59	73839.74	73475.22	73100.50	72730.10	71924.73	71553.44		
3.05	71522.24	71487.26	71437.24	71373.24	71253.38	7125.90	70948.62	70764.38	70549.57	70295.14	7020.81	69776.38	69406.24	69065.23	68708.46	68320.78	67952.92	67570.11	66784.75	
3.1	67111.90	67090.03	67049.41	66975.14	66862.73	66733.30	66577.13	66383.70	66165.54	65918.52	65643.80	65340.78	65035.53	64699.53	64347.44	63982.92	63604.96	63217.27	62823.99	62440.10
3.15	63068.93	63051.01	63011.06	62936.91	62833.58	62701.70	62544.04	62254.17	62131.14	61893.71	61626.30	61336.82	61024.50	60682.13	60344.94	59983.75	59607.70	59222.45	58842.37	58460.80
3.2	59327.47	59325.92	59282.07	59209.49	58973.81	58628.76	58413.35	58157.45	57862.76	57591.35	57214.38	56919.49	56521.45	56219.29	55914.54	55521.45	55177.54	551407.79		
3.25	55876.16	55863.67	55812.41	55743.29	55644.45	55509.58	55356.52	55177.22	54966.58	54724.83	54469.36	54191.09	53882.77	53523.59	52847.96	52518.76	52147.93	51777.54	51407.79	
3.3	52643.79	52638.50	52599.01	52525.05	52423.56	52302.18	52142.14	51965.41	51758.41	51520.24	51273.31	50997.39	50697.38	50383.79	50053.31	49708.23	49348.01	48995.18	48634.02	48272.34
3.35	49647.50	49632.57	49519.78	49422.69	49422.69	494147.92	494147.92	48976.17	48767.17	48592.74	4819.22	47730.47	47330.47	46958.79	46465.72	46411.07	45710.35	45354.20		
3.4	46830.88	46821.04	46793.74	46767.97	46705.99	46614.07	46493.30	46343.12	46176.53	45977.99	45750.34	45505.62	45242.92	44958.79	44657.79	44342.54	44010.51	43673.47	43330.65	42644.66
3.45	44203.58	44192.52	44149.12	44082.21	43987.27	43868.33	43724.83	43455.36	43359.39	43138.69	42901.70	42644.77	42365.65	42072.02	41766.12	41455.44	41017.33			
3.5	41728.11	41721.03	41683.12	41616.64	41527.41	41405.16	41268.31	41099.01	40911.25	40701.62	40464.33	40211.00	39842.93	39654.83	39354.24	39095.41	38727.03	38401.04	38078.80	37755.37
3.55	39494.36	39406.89	39304.96	39210.61	38962.97	39101.58	38719.97	38467.81	38179.37	37890.90	37597.95	35271.42	35231.50	35231.50	35231.50	35231.50	35231.50	35231.50		
3.6	37241.98	37232.22	37196.63	37132.89	37048.57	36801.10	36640.67	36461.15	36259.82	36039.21	35798.95	35543.59	35271.42	34687.86	34687.86	34391.00	34083.50	33780.80	33478.92	
3.65	35200.77	35189.05	35153.87	35093.24	35007.94	34899.04	34770.15	34616.30	34438.63	34243.95	34027.80	33796.36	33544.58	33280.55	33003.18	3275.44	32421.83	32125.67	31831.25	31537.04
3.7	3382.05	3322.51	3177.12	3139.73	30987.53	32860.67	32170.81	31349.81	31074.81	30813.71	30540.97	30290.16	29906.31	29656.02	29389.71	29121.53	28842.79	28562.66	28014.23	
3.75	31476.23	31464.72	31428.05	31374.02	31294.42	31193.31	30921.01	30754.98	30568.22	30364.77	30143.50	29806.16	29566.02	29210.50	28906.11	28659.54	28397.23	28034.97	27694.95	
3.8	29764.30	29730.03	29677.00	29606.60	29501.34	2942.15	29077.46	28898.05	28697.35	28482.75	28249.52	28006.34	27750.00	27485.57	27212.94	26937.55	26665.06	26394.76		
3.85	28179.01	28132.06	28081.88	27928.74	27658.57	27412.34	27026.20	26939.55	26786.22	26512.78	26290.94	26069.43	25845.50	25680.54	25414.95	25143.95	24879.02			
3.9	26663.34	26633.34	26581.08	26510.20	26306.28	26172.50	26018.51	25850.66	25645.95	25324.59	25001.03	24745.30	24501.66	24237.50	23974.63	23713.35	23451.64			
3.95	25256.04	25246.86	25215.82	25169.31	25099.84	25012.74	24903.99	24747.37	24627.17	24461.84	24275.76	24078.76	23861.76	23631.61	23439.30	23193.37	22883.64	22622.85	22363.11	22106.42
4	23922.04	23911.62	23884.34	23840.43	23775.07	23691.35	23586.81	23462.17	23319.33	23158.56	22980.00	22784.80	22572.58	22348.06	22108.58	21864.04	21608.22	21351.25	21093.67	20838.40
4.05	2265.71	22655.54	22581.01	22549.22	22527.61	22449.22	22309.32	22195.86	21976.15	21751.19	21364.94	21141.60	20906.11	20750.54	20515.70	20315.54	20151.70	19869.23	19640.95	
4.1	21476.76	21468.48	21410.50	21355.62	21279.22	21187.95	20935.75	20787.61	20619.00	20430.52	20285.95	20010.74	19777.5	19533.85	19280.52	19024.34	18768.01	18513.27		
4.15	20354.15	20349.43	20330.23	20300.39	20254.59	20185.71	20097.41	19987.44	19856.45	19710.19	19547.45	19367.29	19167.99	18950.50	18718.90	18422.85	18218.99	17964.11	17705.97	17451.26
4.2	19291.32	19288.47	19277.12	19254.10	19217.47	19077.88	18971.02	18843.80	18698.70	18542.49	18370.34	18178.38	17953.38	17726.38	17499.37	17203.69	16971.58	16699.22	16448.80	
4.25	18272.93	18282.58	18279.51	18254.11	18202.43	18129.58	18022.43	17889.15	17752.45	17602.98	17442.37	17259.41	16934.66	16812.63	16495.78	16204.19	15897.24	15744.09	15495.56	
4.3	16395.77	16417.14	16512.23	16523.16	16592.82	16408.44	16436.44	16408.44	16308.77	16129.81	15979.05	15886.66	15755.34	15528.81	15341.89	14916.40	14765.43	14551.63	13874.79	
4.35	15348.54	15462.73	15607.13	15621.38	15613.78	15533.03	15505.48	15411.61	15346.41	15204.22	14798.54	14586.29	14379.23	14160.45	13940.11	13709.93	13364.70	13025.19		
4.4	14304.10	14424.90	14907.17	14939.36	14984.37	15048.31	15086.29	15101.38	14142.64	14236.74	14130.39	14077.66	14033.87	13921.07	13680.23	13453.65	13271.72	13157.93	12763.48	12040.09
4.45	13263.10	13999.73	14019.93	14045.85	14101.38															

Table B.1 (Continued)

	1	1.05	1.1	1.15	1.2	1.25	1.3	1.35	1.4	1.45	1.5	1.55	1.6	1.65	1.7	1.75	1.8	1.85	1.9	1.95
217845.90	217099.00	215699.61	216857.91	216465.26	221673.31	221230.43	226202.65	239099.00	273798.75	480723.30	274790.37	238966.09	226150.21	219920.42	217884.52	216233.52	216707.76	216281.91	217524.82	
17671.54	175582.85	175192.89	17549.34	175240.68	176200.83	182004.63	190344.62	206294.64	227159.14	270965.96	182232.74	177924.29	175247.68	175013.53	175247.68	175247.68	175247.68	175247.68	175247.68	
147852.25	147164.90	147222.66	147107.52	147476.14	148255.33	150047.31	153157.75	157850.02	163930.03	167613.62	163916.93	157871.96	152003.93	150114.36	148446.66	147521.20	147499.29	147244.41	147606.40	
129454.19	129162.65	129009.59	128910.50	129367.39	130023.70	131376.31	133308.19	135823.55	138352.18	139447.96	138434.04	136025.12	133345.57	131388.23	129949.41	129243.35	128927.97	129048.37	129141.64	
115891.30	115653.31	115507.77	115512.06	115677.36	116295.62	117139.55	118315.82	119669.71	120388.77	121223.03	120734.41	119696.60	118304.99	117155.08	116265.33	115743.27	115528.93	115502.12	115694.10	
102626.34	105023.87	104836.32	104809.41	104918.87	105201.15	105734.94	106398.01	107133.59	107582.59	107853.94	107637.71	107081.54	106355.82	105680.52	105266.72	104942.98	104834.18	104862.66	105047.91	
96450.18	96180.26	95979.61	95897.86	95867.55	96019.23	96243.32	96595.23	96911.00	97217.53	97221.93	97128.56	96591.74	96277.57	96050.99	95883.73	95904.80	96028.88	96213.82		
88920.95	88601.33	88338.52	88195.89	88117.81	88130.22	88178.89	88299.35	88442.97	88553.30	88610.24	88586.34	88458.12	883350.66	88181.70	88121.67	88130.33	88223.67	88391.06	88651.22	
82308.66	82001.85	81734.28	81499.20	81363.33	81228.67	81181.05	81190.26	81219.39	81236.27	81249.07	81220.66	81224.32	82207.36	81201.52	81241.79	81351.89	81508.83	81745.30	82013.34	
76449.40	76123.29	75789.66	75540.49	75157.10	75046.23	74942.35	74903.00	74914.96	74942.35	74903.00	74943.06	74984.73	74984.73	75058.36	75182.35	75182.35	75182.35	75182.35	75182.35	
71183.78	70829.95	70519.34	70215.22	69897.83	69768.88	69602.46	69488.70	69397.36	69349.91	69347.04	69359.46	69409.57	69490.57	69490.57	69618.09	69768.39	69988.30	70226.28	70534.55	
66416.80	66060.64	65717.76	65134.15	64902.44	64712.68	64567.80	64465.39	64379.55	64379.55	64404.24	64466.74	64575.49	64730.30	64914.94	65157.14	65433.54	65742.54	66084.22		
62064.67	61694.86	61360.56	61048.98	60770.06	60519.93	60310.74	60153.70	60037.57	59959.38	59955.31	59975.98	60049.26	60158.46	60325.20	60526.50	60794.89	61069.67	61387.46	61377.75	
58085.76	57722.14	57383.64	57064.39	56311.22	56215.12	56029.81	55954.58	55921.39	55954.58	56029.01	56151.27	56293.16	56329.16	56787.29	57395.81	57474.60	57534.89	57584.89		
54424.76	54064.84	53726.06	53407.06	53119.58	52872.04	52482.84	52360.83	52287.61	52286.97	52288.24	52378.45	52500.56	52680.80	52894.43	53149.93	53439.19	53755.78	54100.82		
51041.15	50692.38	50360.52	50048.62	49763.40	49511.66	49296.19	49131.09	49023.06	48938.63	48910.58	48949.70	49031.43	49153.96	49328.68	49547.30	49797.34	50081.91	50395.35	50728.96	
47915.84	47571.42	47237.35	46940.53	46666.83	46425.02	46211.97	46047.81	45927.99	45866.02	45844.37	45873.32	45949.48	46073.28	46240.81	46454.41	46703.15	46982.55	47282.36	47615.26	
45007.20	44599.81	44359.44	44062.93	43799.01	43559.37	43197.16	43088.92	43086.86	43086.86	43086.86	43086.86	43106.54	43226.55	43326.55	43397.36	43835.75	43908.00	44100.83		
42308.77	41988.53	41682.58	41393.74	41135.24	40908.44	40559.53	40451.14	40384.26	40362.59	40362.59	40450.81	40468.31	40496.81	40496.81	40590.48	40749.44	40947.44	41139.14	41276.66	
39791.40	39476.18	39182.81	38809.30	38656.09	38436.49	38250.39	38102.52	37999.40	37955.63	37919.79	37950.48	38020.61	38134.46	38291.46	38482.06	38708.44	38958.92	39235.51	39532.35	
37438.55	37139.48	36852.11	36583.87	36345.28	36134.48	35815.43	35713.12	35655.88	35713.12	35642.05	35667.92	35738.72	35849.07	36005.97	36164.47	36313.44	36646.47	36913.44		
35242.03	34949.07	34672.41	34415.15	34183.60	33984.64	33811.62	33678.71	33587.39	33528.11	33515.42	33544.11	33611.90	33714.47	33865.91	34044.12	34250.94	34489.52	34749.35	35020.15	
33182.55	32899.89	32634.75	32386.56	32163.46	31968.53	31807.77	31678.93	31587.00	31524.33	31523.73	31555.04	31622.10	31726.32	31864.21	32037.63	32241.20	32469.25	32715.80	32980.67	
31254.23	30979.94	30719.35	30481.80	30267.88	30082.11	29925.83	29803.85	29717.02	29668.74	29660.97	29689.10	29757.71	29857.01	29995.87	30162.54	30356.08	30574.81	30812.39	31070.30	
29437.53	29175.38	28923.53	28692.81	28385.04	28070.34	28158.62	27958.61	27638.77	27638.77	27626.24	27626.24	27626.24	27640.85	27640.85	27640.85	27640.85	27640.85	27640.85		
27734.03	27475.49	27234.79	27010.27	26813.26	26638.11	26426.77	26296.48	26264.61	26264.61	26264.61	26264.61	26264.61	26264.61	26264.61	26264.61	26264.61	26264.61	26264.61		
26133.29	25880.28	25646.08	25427.81	25232.14	25065.78	24926.58	24822.26	24748.53	24748.53	24711.68	24711.68	24743.32	24811.59	24910.34	25041.48	25194.87	25257.13	25297.17	26202.74	
24621.36	24376.11	24146.13	23934.61	23744.22	23584.80	23450.62	23347.30	23278.55	23244.65	23246.74	23282.81	23352.60	23451.05	23557.49	23732.58	23910.84	2410.77	24317.37	24541.44	
23205.47	22956.71	22729.78	22518.89	22300.80	22091.62	21851.78	21676.63	21507.00	21504.44	21504.44	21504.44	21504.44	21504.44	21504.44	21504.44	21504.44	21504.44	21504.44		
20590.94	20352.19	20130.29	19928.38	19747.25	19593.95	19469.66	19378.21	19312.90	19312.90	19312.90	19312.90	19312.90	19312.90	19312.90	19312.90	19312.90	19312.90	19312.90		
19394.93	19159.90	18935.79	18730.91	18550.37	18397.12	18274.97	18185.87	18133.14	18114.76	18134.15	18188.21	18272.89	18390.28	18530.60	18692.67	18875.15	19067.49	19267.20	19471.95	
18267.18	17802.46	17597.20	17409.93	17257.95	17135.66	17048.02	16997.28	16986.37	16986.37	17010.57	17164.24	17287.86	17439.64	17691.49	17870.74	17997.30	1820.19	1840.25		
17202.09	16961.17	16729.94	16517.39	16329.20	16170.12	16046.71	15959.47	15913.40	15906.69	15939.14	16006.04	16109.46	16243.75	16406.42	16591.93	16791.49	16987.49	17207.74	17405.59	
16207.85	15957.25	15710.85	15487.92	15296.71	15132.60	15002.75	14915.99	14873.44	14873.44	14873.44	14873.44	14873.44	14873.44	14873.44	14873.44	14873.44	14873.44	14873.44		
15281.81	14973.65	14748.79	14480.78	14135.72	13944.35	13694.12	13413.38	13273.38	13087.80	13087.80	13087.80	13087.80	13087.80	13087.80	13087.80	13087.80	13087.80	13087.80		
14359.13	14132.26	13914.27	13567.38	13464.43	13175.42	12989.03	12931.05	12895.88	12895.88	12895.88	12895.88	12895.88	12895.88	12895.88	12895.88	12895.88	12895.88	12895.88		
13547.16	13301.28	13027.45	12759.05	12414.52	12176.14	12042.68	11979.50	11953.66	11930.82	12071.90	12151.04	12279.79	12478.76	12727.32	13054.56	13246.39	13425.62	14506.01		
12733.61	12493.00	12328.07	11932.61	11558.27	11235.61	11092.07	10956.82	11001.89	11147.74	11198.92	11268.42	11409.92	11603.72	11870.31	12026.54	12631.20	1313.15	13711.29	14159.06	
11897.08	11990.00	11547.67	11143.62	10782.14	10467.64	10201.79	10119.05	10056.38	10265.49	10344.04	10389.45	10525.65	10744.08	11042.21	11413.05	11866.29	12313.56	13673.47	13767.19	
11722.35	11229.65	10772.16	10354.53	9981.78	9659.11	9391.67	9184.30	88446.50	9558.55	9510.50	9484.67	9627.07	9882.74	10243.22	10697.92	11235.39	11849.23	13063.76		

Table B.1 (Continued)

	2	2.05	2.1	2.15	2.2	2.25	2.3	2.35	2.4	2.45	2.5	2.55	2.6	2.65	2.7	2.75	2.8	2.85	2.9	2.95
217298.97	217101.96	218134.53	218319.17	220811.60	219137.42	224444.44	221292.69	220632.43	221062.45	222431.00	223406.74	222964.32	223676.08	223394.81	224520.97	223350.10	224865.51	225587.24	224813.63	
165565.55	177064.62	177526.08	178313.27	178790.14	179274.74	180279.51	180905.01	181045.83	181802.05	182034.45	182893.04	182930.78	183118.83	183809.21	183933.41	184394.73	184079.11	184149.31	184208.51	
148466.31	149017.44	149742.15	150432.86	150856.83	151709.36	152215.77	153036.56	153275.19	153454.38	153894.09	154021.32	154502.01	154804.24	154932.85	154786.63	155046.51	155167.36			
129529.39	129593.41	130291.40	131280.72	131846.58	132279.62	132778.60	132550.88	133641.92	133979.59	134368.20	134633.10	135160.63	135339.89	135686.33	135737.84	135922.19	135895.99			
115952.50	116302.24	116732.68	117184.04	117617.83	118020.63	118530.18	118913.06	119364.28	119763.80	120126.45	120409.41	120730.61	120993.68	121284.31	121475.68	121579.46	121640.49	121806.44	121902.02	
105342.96	105680.96	106019.61	106440.05	106853.21	107263.63	107692.85	108094.40	108476.63	108821.14	109202.82	109507.98	109789.34	110026.45	110266.67	110452.88	110732.28	111025.28	111082.74	111085.52	
96433.56	96820.45	97177.71	97592.51	98325.59	98793.57	99182.86	99562.39	99833.07	100225.18	100508.83	100792.65	101001.82	101247.98	101430.21	101555.86	101694.94	101773.05	101834.41		
88953.58	89272.72	89656.05	90041.83	90427.79	91951.92	92894.02	92601.92	92895.79	93151.81	93366.80	93582.89	93764.94	93917.22	94023.47	94144.34	94159.46				
82346.14	82687.36	83038.34	83444.46	83848.85	84220.27	84612.41	84881.47	85339.31	85673.58	85956.11	86255.90	86507.89	86873.85	87098.99	87257.94	87342.04	87430.73	87489.07		
76468.92	76826.89	77211.75	77584.98	77984.73	78363.92	78758.64	79110.42	79454.30	79781.65	80090.00	80359.49	80620.01	80860.06	81041.63	81212.43	81346.44	81437.58	81523.31	81570.42	
66334.59	66813.27	67194.38	67570.58	67960.48	70342.91	74185.18	74509.60	74796.80	75072.04	75326.60	75523.04	75744.96	76144.93	76269.86						
62083.60	62454.77	62849.53	63228.56	63620.95	63979.27	64354.65	64694.93	65035.49	65350.83	65641.01	65912.01	66151.95	66367.53	66552.13	66710.35	66842.82	66946.30	67022.27	67060.17	
58121.92	58477.94	58866.57	59247.96	59611.97	59994.00	60352.72	60702.36	61018.67	61328.75	61618.09	61884.10	62119.01	62333.47	62511.41	62670.83	62794.41	62907.22	62983.68	63024.85	
54457.47	54821.91	55195.25	55573.28	55942.15	56298.13	56661.24	57320.17	57619.12	57904.91	58162.01	58460.83	58789.40	58978.52	59070.23	59167.67	59243.08	59284.71			
51076.58	51433.37	51797.11	52169.92	52555.05	52889.87	53237.95	53571.29	53878.73	54181.92	54461.00	54713.12	54941.51	55147.57	55338.82	5569.46	55813.80				
47950.49	48298.96	48660.04	49015.41	49378.19	49725.90	50060.82	50387.24	50697.23	50985.75	51256.51	51509.32	51732.86	51932.36	52109.32	52260.31	52380.91	52476.76	52545.79	52582.60	
40504.27	45393.10	45742.18	46089.29	46434.85	46770.20	47104.34	47422.71	47724.48	48010.29	48271.41	48513.45	48737.68	48930.41	49105.25	49252.04	49372.87	49468.63	49533.57	49573.34	
45336.45	46687.55	47031.55	47402.75	47751.17	48154.58	49505.58	50255.58	51025.58	51618.09	52118.09	52651.41	53233.47	53511.41	53670.83	53794.41	54023.22	54144.87	54264.44	54384.73	
398841.17	40166.09	40490.69	41159.92	41545.76	41772.80	42072.84	42354.58	42625.08	42877.09	43108.72	43318.93	43503.72	43669.40	43811.04	43924.24	44015.63	44118.24			
37498.70	37808.37	38125.11	38440.54	38757.04	39062.15	39361.14	39653.47	39929.07	40190.67	40434.25	40657.53	40859.77	41047.68	41202.04	41341.80	41453.84	41537.70	41605.29	41636.06	
326307.59	356044.78	35909.57	36215.84	36518.91	37104.00	37328.29	37654.64	37907.70	38142.83	38358.09	38562.08	38725.47	38890.06	39025.83	39135.34	39217.04	39281.84	39316.08		
33258.13	33547.43	33836.39	34132.37	34241.60	34511.28	34900.02	35211.89	35518.89	35765.12	36001.74	36204.89	36450.52	36705.54	36715.33	36848.12	36955.39	37094.18	37131.81		
31338.09	31613.30	31893.66	32178.58	32456.21	32737.79	33006.93	33268.21	33514.46	33751.69	33974.30	34178.16	34363.38	34532.77	34678.06	34805.96	34987.35	35047.05	35076.41		
29537.00	29803.39	30071.46	30342.63	30615.16	30881.46	31143.19	31393.07	31636.36	31858.75	32074.04	32272.03	32452.70	32614.90	32755.55	32878.41	32977.17	33056.67	33107.12	33145.16	
27849.28	28103.62	28362.92	28627.33	28886.01	29142.53	29391.33	29631.90	29865.21	30084.55	30288.95	30479.69	30651.88	30807.96	30947.94	31066.48	31240.03	31325.73			
19676.61	19880.13	20082.94	20280.69	20476.24	20666.55	20853.99	21034.65	21207.92	21447.87	22279.12	22494.22	22894.06	23020.21	23235.15	23456.85	23547.10	23617.02	23668.63	23699.39	
18599.84	18796.04	18988.40	19173.77	19358.74	19537.11	19706.54	19875.38	20036.29	20189.20	20340.89	20485.56	20622.81	20750.74	20869.86	20976.76	21069.46	21143.99	21199.74	21233.30	
17597.01	17783.26	17963.11	18138.01	18308.25	18474.33	18633.29	18782.91	18926.61	19067.84	19207.90	19345.93	19478.54	19605.11	19725.29	19834.41	19931.20	20009.86	20068.17	20106.34	
16664.29	16838.47	17008.31	17166.17	17317.66	17476.10	17623.36	17751.25	17875.49	18001.07	18128.90	18298.76	18403.94	18533.04	18633.82	18746.97	18852.49	18938.20	19003.56	19046.17	
15814.18	15919.39	16084.67	16253.01	16447.66	16647.75	16875.62	16979.52	17093.91	17216.37	17342.53	17468.98	17597.05	17709.51	17834.61	17929.44	17991.23	18056.72			
15209.29	15218.31	15269.90	15421.49	15578.50	15657.47	15792.28	15840.72	15909.65	15998.21	16099.11	16210.74	16324.42	16467.53	16599.16	16711.03	16858.54	16977.93	17052.08	17124.64	
14714.63	14868.36	14659.88	14778.28	14823.23	14932.97	14918.52	14982.31	15058.59	15169.41	15265.72	15366.05	15504.07	15609.10	15788.62	15916.87	16069.74	16249.11	16355.34		
14215.40	14410.29	14515.32	14645.70	14745.70	14845.70	14945.70	15045.70	15145.70	15245.70	15345.70	15445.70	15545.70	15645.70	15745.70	15845.70	15945.70	16045.70	16145.70	16245.70	
13640.62	13658.63	13632.40	13628.13	13645.86	13685.48	13638.54	13685.86	13746.82	13720.59	13710.98	13713.78	13729.43	13336.04	13483.81	13564.67	13676.35	13818.11	13898.03	14188.06	
12992.50	12945.52	12923.09	12952.33	13003.67	13079.31	13178.76	13301.48	12087.37	12298.32	12353.80	12446.89	12576.77	12742.31	12942.13	13174.68	13438.27	13731.10	14051.34		

Table B.1 (Continued)

3	3.05	3.1	3.15	3.2	3.25	3.3	3.35	3.4	3.45	3.5	3.55	3.6	3.65	3.7	3.75	3.8	3.85	3.9	3.95	
225673.92	22339.45	224736.43	223742.43	223750.58	223841.86	222642.77	222078.37	222941.27	222892.23	221302.06	222005.05	221787.56	220248.89	221129.79	220036.29	221154.54	218867.66	217746.53	217663.08	
18451.79	18409.24	184478.20	184430.85	184236.29	183610.80	183620.88	183248.19	182859.97	182431.72	182010.73	182051.62	181054.64	180544.70	179876.48	179367.25	178826.44	178243.45	177587.95	176981.05	
155391.76	155118.06	155262.44	155109.70	155109.89	154622.45	154321.39	153848.46	153579.46	153509.19	135215.56	135023.35	134576.19	134417.42	134032.22	133658.73	133247.52	132739.78	132244.99	131829.09	131421.34
155398.39	135907.48	135927.01	135927.01	135929.93	135599.33	135599.19	135215.56	135023.35	134576.19	134417.42	134032.22	132010.52	132010.52	119727.81	119218.70	118923.82	118531.47	117539.58	117113.11	
121773.59	121817.22	121813.67	121764.55	121551.93	121461.18	121190.10	120950.93	120721.30	120423.33	120105.22	119727.81	109759.91	109473.03	109212.68	108851.77	108482.79	108099.19	107676.47	10725.65	
110866.84	110839.38	110804.56	110799.71	110584.53	110449.78	110231.22	110036.91	109759.91	109473.03	109212.68	108851.77	108482.79	108099.19	107676.47	106806.38	106405.71	106023.65	105609.47	104966.47	
104183.85	101804.81	101841.72	101787.97	101684.41	101420.66	101246.05	101043.24	100745.87	100527.89	100206.29	99896.80	99546.73	99139.70	98764.95	98369.59	97948.59	97552.15	97163.12	96815.99	
94450.05	94152.48	94100.46	94023.88	93913.50	93781.42	93594.00	93372.18	93146.76	92890.76	92589.58	92268.69	91931.15	91569.74	91186.21	90811.29	90414.63	90013.72	89637.45	89250.90	
87484.87	87499.16	87436.26	87332.30	87079.02	86926.33	86723.30	86262.33	86492.50	8628.47	85966.50	85639.58	85303.92	84954.80	84593.64	84199.74	83820.31	83428.32	83056.80	82667.11	
81595.22	81574.93	81524.63	81453.82	81334.17	81183.67	81030.15	80832.57	80597.04	80349.37	80071.76	7973.60	79443.55	79100.95	78719.48	78347.39	77976.02	77574.81	77190.30	76821.73	
76289.66	76222.49	76131.58	76031.57	75906.30	75730.36	75549.31	75318.07	75066.83	74785.53	74494.13	74162.31	73824.73	73467.20	73091.59	72707.95	72326.18	71940.04	71559.82	71559.82	
71470.36	71451.49	71420.71	71338.72	71227.03	71085.78	70935.44	70737.58	70529.80	70278.64	700041.07	69708.75	69393.75	69050.49	68695.63	68334.18	67948.18	67562.05	67175.53	66789.81	
67078.49	6702.13	67017.58	66944.82	66839.99	66706.04	66542.16	66356.36	66140.73	65896.25	65626.54	65331.45	65020.92	64688.84	64340.56	63975.50	63595.29	63204.64	6289.31	62446.19	
63034.36	63022.34	62968.44	62899.35	62800.38	62666.87	62505.44	62316.58	62102.69	61872.58	61598.81	61314.73	61004.03	60676.67	60334.09	59966.98	59602.56	59222.36	58840.75	58463.68	
59320.69	59266.50	59243.43	59159.48	59064.73	58938.04	58774.50	58592.40	58382.60	58144.82	57885.22	57598.42	57297.64	56939.86	56635.97	56279.64	55921.65	55546.02	55169.55	54799.69	
55831.05	55807.32	55768.23	55702.33	55598.03	55466.76	55317.05	55135.76	54926.40	54695.29	54442.93	54159.51	53864.85	53548.08	53212.16	52867.07	52513.78	52138.77	51775.93	51412.69	
52601.40	52581.67	52539.59	52469.42	52373.15	52244.34	52095.50	51946.71	51711.03	51485.64	51235.20	50962.09	50670.33	50360.16	50041.85	49668.83	49347.04	48992.20	48633.10	48272.39	
49587.64	49574.75	49525.02	49454.46	49362.30	49239.27	49089.93	48915.08	48716.57	48489.03	48247.66	47977.57	47696.03	47393.46	47078.24	46741.23	46404.29	46060.68	45709.92	45359.42	
46765.80	46751.69	46716.59	46650.71	46548.17	46428.03	46216.93	46011.74	45896.97	45689.19	45453.94	45196.64	44916.34	44621.35	44313.77	43658.44	43329.44	42986.98	42653.70	42339.44	
44127.06	44115.15	44071.91	44004.95	43908.03	43790.31	43562.01	43479.83	43291.83	43080.12	42847.17	42592.98	42322.37	41936.47	41736.70	41423.70	41013.28	40445.87	40130.50	39735.44	
41651.04	41635.78	41592.56	41531.14	41439.37	41323.34	41184.33	41020.68	40831.06	40624.18	40397.52	40153.71	39890.38	39613.56	39318.58	39020.43	38708.33	38397.65	38081.91	37767.40	
37295.09	37308.62	37271.31	37204.89	37117.24	37006.19	38686.16	38279.65	38252.78	38102.64	37866.17	37581.75	37343.34	37060.38	36764.20	36471.17	36170.48	35861.55	35560.33	35493.05	
37141.14	3715.68	37086.82	37025.15	36936.61	36825.65	36536.41	36362.92	36166.45	35915.75	35727.52	35472.77	35211.61	34934.99	34656.91	34369.83	34074.95	33783.42	33493.05	33152.40	
35086.74	35072.26	35034.39	34979.25	34886.99	34648.52	34496.99	34326.31	34136.55	33997.26	33703.74	33463.65	33209.93	32948.87	32677.58	32397.04	32116.00	31834.11	31552.40	31237.52	
33152.82	33119.08	33101.80	33042.30	32953.71	32849.90	32275.04	32141.14	32026.58	32023.05	31804.63	31572.78	31327.52	31074.33	30812.08	30546.33	30270.29	30001.27	29735.44	29401.44	
32134.26	32138.68	32128.85	32113.47	32103.54	32037.26	30913.18	30769.66	30604.25	30474.45	30203.81	29793.97	29560.16	29313.83	29060.67	28784.81	28545.03	28280.75	28025.92	27805.77	
29620.01	29607.08	29569.28	29511.51	29430.53	2930.04	29206.62	29066.38	28899.13	28731.79	28541.32	28338.31	28121.77	27856.24	27413.55	27165.55	26862.99	26419.08	26190.44	25892.22	
2807.61	27990.70	27957.02	27897.69	27818.91	27711.97	27598.04	27462.37	27308.26	27137.46	26963.39	26753.04	26542.75	26323.49	26095.82	25860.71	25620.30	25380.39	25140.04	24902.22	
26488.20	26474.04	26437.93	26378.39	26299.06	26202.51	26082.89	25948.32	25797.16	25629.32	25448.35	25257.06	25054.22	24839.55	24620.80	24394.10	24164.80	23933.68	23701.92	23475.84	
2507.03	25043.20	24947.25	24868.92	24771.02	24593.69	24371.37	24176.67	24029.54	23844.03	23512.78	23229.31	23011.72	22789.11	22491.44	2218.44	21913.16	21704.62	21491.44	21278.69	
23706.74	23664.32	23657.52	23599.92	23519.51	23419.09	23304.49	23169.13	23022.62	22860.48	22689.06	22507.58	22314.54	22131.16	21913.16	21704.62	21491.44	21278.69	21056.47	20856.27	
22437.46	22423.16	22386.40	22328.18	22146.85	22028.78	21893.40	21747.25	21588.39	21418.19	21241.81	21055.71	20865.72	20668.44	20466.83	20262.68	20058.62	19851.66	19652.90	19451.66	
21243.66	21229.79	21131.20	21047.88	20943.84	20824.01	20688.31	20537.61	20379.45	20212.25	20039.54	19860.69	19676.72	19487.62	19293.88	19097.44	18899.68	18705.45	18511.73	17428.21	
20117.95	20107.66	20068.79	20003.95	19918.17	19809.46	19682.13	19542.32	19389.18	19250.14	19063.39	18894.63	18723.50	18546.07	18365.10	18179.23	17991.51	17803.44	17615.66	17428.21	
19064.03	19052.91	19015.36	18945.70	18854.33	18740.45	18607.18	18495.05	18295.90	18132.01	17964.54	17801.04	17637.40	17477.40	17297.33	17118.80	16939.53	16795.66	16590.70	16395.70	
18080.77	18059.18	18024.54	17951.67	17855.96	17735.39	17587.99	17427.26	17251.95	17075.58	16904.40	16746.43	16593.78	16443.81	16284.11	16109.80	15895.65	15749.55	15630.47	15295.67	
17142.51	17166.35	17098.32	16962.44	16942.48	16806.43	16650.35	16467.42	16249.32	16042.29	15869.62	15721.81	15595.83	15459.83	15330.89	15128.36	15001.70	14801.67	14651.90	14418.12	
16454.68	16415.62	16300.50	16167.74	16043.38	15979.53	15805.32	15622.75	15422.86	15222.86	15022.86	14849.54	14652.03	14452.64	14208.37	14069.71	13823.12	13695.23	13553.33	13495.23	
15760.92	15718.62	15463.34	15367.31	15235.39	15139.56	15015.36	14844.44	14643.79	14438.80	14213.16	13830.69	13688.71	13550.07	13356.29	13149.43	13030.76	12890.61	12749.58	12615.27	
14454.30	14673.93	14295.37	13934.46	13592.61	13271.28	12972.02	12696.36	124												

Table B.1 (Continued)

	4	4.05	4.1	4.15	4.2	4.25	4.3	4.35	4.4	4.45	4.5	4.55	4.6	4.65	4.7	4.75	4.8	4.85	4.9	4.95
27119.33	218154.71	216444.62	220330.55	219686.90	220535.72	226935.85	23889.37	274367.43	466177.94	272519.98	238771.51	226367.15	221518.49	218580.88	217373.80	216726.47	215778.00	218422.29	218422.29	
176250.99	175625.61	174823.59	174685.92	174997.43	175084.31	175190.77	182118.51	191152.96	163837.13	167203.75	164186.26	190552.66	182187.90	17955.72	176137.63	175223.88	174826.63	175002.26	175496.35	
148163.45	147640.30	147280.68	147211.64	147429.81	153190.77	158045.95	163837.13	167203.75	161419.26	158097.10	15317.52	150019.70	15248.99	148391.52	147443.73	14728.25	147392.68	147392.68	147392.68	
129360.31	129192.97	128937.73	128936.42	129288.25	130034.03	131323.84	133322.22	135820.65	138398.13	139485.05	138322.13	135741.96	133255.54	131503.20	130058.69	129215.57	128921.60	128936.58	129185.12	
115898.61	115657.38	115510.85	115549.99	115738.02	116272.14	117184.99	118325.34	119617.69	120794.72	121261.73	12067.98	119693.74	118321.68	117171.16	116401.13	115767.77	115566.68	115500.85	115642.70	
105279.57	104988.52	104837.20	104793.43	104899.15	105230.88	105761.48	106366.92	107103.46	107645.08	107869.41	107630.73	107101.35	106387.99	105716.24	105201.08	104948.13	104811.76	104828.86	104972.95	
96450.13	96191.85	95992.13	95869.37	95910.78	96037.96	96304.24	96590.03	969412.00	97138.62	97270.14	97160.52	96602.88	96009.80	95861.75	95653.76	95482.93	953863.83	95286.93	95178.55	
88930.15	88610.49	88369.73	88208.30	88113.59	88128.58	88203.99	88314.94	88452.12	88535.89	88600.92	88554.26	88447.06	88311.55	88164.80	88104.11	88077.63	88136.70	88324.03	88620.49	
82293.17	82001.72	81734.67	81504.44	81341.60	81233.87	81176.86	81180.44	81180.75	81232.29	81235.69	81219.71	81184.57	81193.41	81187.39	81262.79	81326.83	81490.32	81711.90	81989.65	
76447.59	76117.30	75810.39	75551.36	75329.62	75170.88	75061.92	74958.78	74923.01	74906.23	74867.20	74907.63	74928.42	74936.09	75012.02	75160.58	75344.88	75353.09	75793.53	76071.64	
71188.33	70833.23	70509.36	70229.99	69777.95	69613.01	69591.79	69382.59	69350.79	69293.52	69345.52	69345.52	69345.52	69345.52	69345.52	69345.52	69751.38	70208.87	70501.68	70821.70	
66420.45	66063.20	65734.53	65416.35	65136.18	64908.58	64714.83	64554.51	64452.77	64390.48	64377.73	64389.11	64448.20	64573.99	64715.81	64900.37	65133.23	65406.05	65712.04	66050.06	
62072.28	61712.70	61372.18	61051.75	60766.42	60522.25	60315.75	60149.46	60011.54	59952.28	59925.53	59948.80	60029.06	60139.47	60304.12	60515.36	60752.07	61051.76	61350.05	61692.19	
59090.30	57719.50	57383.75	56307.78	56785.59	56244.39	56307.87	56141.82	56019.03	56939.86	56912.42	56940.35	56231.06	56303.65	56519.21	56738.09	57061.13	57383.09	57720.01	57720.01	
54431.52	54075.68	53740.82	53423.74	53133.80	52980.78	52662.60	52499.45	52329.50	52285.04	52285.04	52283.67	52283.67	52283.67	52283.67	52654.94	52859.81	53115.89	53401.01	53723.27	54059.28
51054.62	50732.54	50372.54	50064.51	49730.46	49313.98	49142.20	49017.62	48940.86	48914.24	48936.47	49014.18	49132.84	49297.98	49761.59	50043.15	50355.64	50685.80	51043.15	51043.15	
47922.97	47589.67	47263.54	46680.56	46460.56	46228.88	46053.93	45936.84	45860.22	45841.51	45858.07	45928.53	46050.62	46216.20	46420.98	46664.49	46933.41	47233.90	47562.26	47562.26	
45231.65	42003.53	44663.53	44381.26	44086.12	43781.23	43378.01	43215.69	43097.56	43205.04	42999.87	43017.37	43087.84	43200.55	43357.84	43562.49	43794.12	44056.29	44438.39	44670.84	
39804.74	39498.15	39218.58	38935.87	38687.50	38466.50	38280.57	38125.55	38017.57	37950.59	37944.09	38061.12	38110.00	38252.85	38440.03	38657.14	38904.32	39173.85	39468.85	39468.85	
37460.65	37164.61	36879.90	36619.89	36382.62	36168.40	35996.88	35848.17	35741.09	35674.94	35647.54	35665.22	35726.95	35824.31	35963.53	36138.12	36348.70	36582.71	36846.21	37124.24	
33211.02	32955.82	32677.50	32436.08	32218.38	32024.59	31857.47	31724.41	31622.47	31564.91	31541.70	31557.53	31607.53	31697.89	31823.33	31980.47	32167.31	32387.66	32566.93	32886.08	
31283.94	31021.52	30773.02	30329.47	30143.77	29985.59	29859.40	29764.09	29705.95	29682.91	29695.74	29742.03	29830.62	29948.76	30096.48	30279.19	30480.47	30713.77	30963.78	30963.78	
29473.24	29222.14	28987.71	28762.39	28559.89	28384.32	28231.92	28107.15	28019.31	27961.40	27935.52	27948.26	28077.76	28186.37	28331.90	28504.89	28699.51	28921.11	29157.74	29157.74	
27474.87	27524.92	27303.13	27057.72	26900.99	26729.85	26585.42	26468.09	26379.17	26324.18	26324.18	26324.18	26324.18	26423.34	26533.82	26833.22	27018.44	27231.71	27459.40	27459.40	
26174.51	25944.68	25755.33	25533.74	25175.30	25034.12	24922.11	24838.28	24784.72	24761.54	24770.73	24879.77	24979.75	25016.89	25262.11	25441.60	25642.17	25861.08	26043.22	26243.22	
24672.44	24448.89	24236.11	24043.51	23865.70	23708.41	23576.15	23468.94	23389.21	23335.75	23312.74	23317.70	23352.68	23417.92	23514.80	23636.01	23782.57	23951.55	24143.42	24354.22	
23251.38	23040.35	22839.66	22649.61	22483.23	22333.07	22204.93	22098.97	22021.43	21972.85	21950.16	21985.38	22046.88	22133.86	22246.69	22366.06	22547.91	22729.88	22931.00	22931.00	
21914.66	21709.38	21539.42	21334.15	21177.49	20930.19	20760.48	20533.69	20465.41	20333.70	20231.29	20149.52	20064.42	20064.42	20281.29	20293.70	20480.49	20689.50	20821.29	21221.66	21394.84
20651.44	20456.51	20271.46	20099.75	19944.38	19806.44	19688.31	19593.81	19521.61	19472.98	19449.53	19449.53	19452.77	19452.77	19452.77	19452.77	19621.40	19702.60	19823.38	19967.09	20133.61
1945.98	19269.17	19091.09	18928.17	18780.29	18649.40	18537.42	18446.61	18375.66	18328.90	18328.90	18328.90	18328.90	18328.90	18328.90	18328.90	18369.85	18440.44	18520.69	18645.34	
18226.05	18147.30	17980.11	17823.42	17682.94	17557.17	17450.77	17362.78	17298.67	17252.89	17225.66	17222.98	17241.70	17282.07	17342.38	17423.84	17530.12	17658.76	17805.78	17971.42	
17250.66	17081.48	16923.77	16779.04	16644.73	16525.60	16426.54	16346.03	16281.87	16226.77	16209.86	16206.07	16221.26	16251.75	16302.29	16376.45	16471.59	16593.29	16688.96	16688.96	
16221.95	16071.86	15910.92	15794.32	15656.71	15553.03	15461.35	15394.12	15275.33	15246.13	15246.13	15246.13	15246.13	15246.13	15246.13	15246.13	15376.43	15461.04	15461.04	15672.04	
15180.94	15087.05	14985.56	14896.39	14783.37	14599.24	14548.13	14475.28	14431.63	14431.63	14431.63	14431.63	14431.63	14431.63	14431.63	14431.63	14431.63	14431.63	14431.63	14431.63	
14338.25	14218.44	14118.83	14001.55	13926.67	13633.52	13583.58	13520.44	13533.81	13533.81	13533.81	13533.81	13533.81	13533.81	13533.81	13533.81	13495.84	13501.13	13540.13	13487.28	
13465.63	13226.65	13085.80	12938.30	12851.63	12708.11	12616.64	12516.33	12424.79	12343.79	12276.32	12228.79	12121.70	12082.60	12121.52	12228.79	12343.79	12424.79	12516.33	12616.33	
12581.42	12589.74	12341.98	12240.74	12246.44	12243.79	12156.63	12108.79	12079.50	12082.60	12121.52	12121.52	12121.52	12121.52	12121.52	12121.52	12121.52	12121.52	12121.52	12121.52	
11684.81	11624.39	11626.21	11626.21	11626.21	11626.21	11626.21	11626.21	11626.21	11626.21	11626.21	11626.21	11626.21	11626.21	11626.21	11626.21	11626.21	11626.21	11626.21	11626.21	
10859.50	10836.10	11180.12	11090.37	10969.33	10850.59	10771.22	10732.71	10755.50	10779.56	10864.38	10989.03	11152.15	10102.05	10142.89	10219.28	10330.40	10475.17	10652.21	10859.94	

Table B.1 (Continued)

5	5.05	5.1	5.15	5.2	5.3	5.35	5.4	5.45	5.5	5.55	5.6	5.65	5.7	5.75	5.8	5.85	5.9	5.95	
12	216666.14	216944.11	218697.40	218741.90	220096.98	220997.92	221163.55	221243.70	221707.53	221761.55	222413.50	223111.02	223955.52	225998.32	227995.97	228522.97	229552.97	232532.98	
13	217167222.20	2176899.31	217746.39	217915.00	217997.97	218100.41	218137.59	218170.49	218218.88	218256.88	218296.58	218339.60	218372.39	218331.42	218423.37	218394.35	218463.38	218439.39	218495.98
14	147950.10	149002.53	149343.22	149602.53	149856.99	150288.95	152364.08	153167.02	152729.04	153606.93	153807.44	154181.31	154615.51	154580.77	154952.14	155149.33	155156.58	155323.51	155169.49
15	129695.13	130181.53	131013.73	131317.00	132276.11	133220.88	133273.13	134227.69	134227.69	134227.69	134247.17	134250.07	134253.88	134253.97	134253.97	134253.97	134253.97	134253.97	
16	116766.74	117121.75	117169.80	118048.72	118496.72	118949.73	119345.73	119758.58	120104.44	120104.44	120930.85	121245.70	121428.39	121428.39	121428.39	121428.39	121428.39	121428.39	
17	105352.34	105580.01	105894.18	106385.90	106827.25	107247.13	107682.40	108090.03	108493.09	108852.71	109194.10	109512.83	109787.44	110203.51	110266.56	110405.95	110608.92	110867.16	
18	96800.05	96811.95	96871.95	97052.72	97957.23	98379.48	98627.89	99158.93	99535.30	99882.01	100221.69	100493.97	100771.90	101035.84	101258.33	101452.31	101567.53	101694.24	
19	98614.53	99003.92	99429.49	99814.53	99815.95	99815.95	99815.95	99815.95	99815.95	99815.95	99815.95	99815.95	99815.95	99815.95	99815.95	99815.95	99815.95	99815.95	
20	82310.63	82672.87	83023.65	83427.58	83818.25	84214.08	84574.13	84962.82	85311.88	85635.16	85963.64	86241.92	86506.47	86731.30	86927.59	87115.38	87250.95	87347.32	
21	76444.18	76809.82	77187.70	77574.74	77961.56	78233.23	79099.39	79448.82	79777.70	80085.10	80610.81	80835.38	81038.02	81358.02	81455.70	81543.24	81585.26	81575.13	
22	71540.14	72194.17	73082.73	73622.73	74175.19	74893.71	74982.86	75065.34	75236.03	75501.73	75741.12	76025.03	76155.11	76292.69	76320.05	76427.23	76478.23	76520.57	
23	66404.11	66787.00	67167.50	67522.55	68041.55	68394.40	68717.40	69145.74	69708.26	70285.38	70753.70	71059.80	71079.65	71111.85	71158.22	71247.23	71474.55	71749.77	
24	62605.83	62432.83	62816.39	63208.30	63591.47	63695.77	64062.83	64161.52	64689.77	65095.13	65633.08	66371.25	66652.16	66775.65	66845.22	66954.50	67037.72	67076.65	
25	54414.07	54784.73	55151.98	55538.90	56031.48	56563.44	57089.85	58163.93	58634.20	59119.51	59567.72	60120.25	60212.73	60244.94	60284.83	60300.65	60357.19	60416.66	
26	51031.13	51384.96	51767.40	52134.25	52507.69	52863.52	53203.36	53547.58	53870.98	54166.28	54450.03	54711.62	54949.52	55153.10	55330.55	55497.12	55629.92	55728.64	
27	48615.38	48899.30	49265.36	49635.36	49863.44	50236.00	50530.80	50830.80	51050.80	51500.09	51508.00	51739.08	51742.73	51780.56	52045.12	52576.00	52618.56	52662.87	
28	44997.06	45434.71	45863.91	46043.23	46387.37	46702.48	47328.81	47705.54	47992.52	48371.48	48743.87	48947.29	49121.74	49270.36	49389.61	49495.53	49602.97	49624.51	
29	42297.32	42629.73	43311.28	43650.61	43986.43	44312.48	44623.94	44929.04	45212.02	45474.67	45720.68	45944.62	46139.73	46320.40	46465.12	46586.25	46685.56	46755.01	
30	39777.55	40098.55	40430.43	40799.23	41049.52	41412.81	42334.28	42865.22	43016.54	43232.88	43326.81	43432.66	43873.93	44053.09	44118.23	44161.04	44168.74	44216.74	
31	37423.25	37735.13	38052.69	38373.54	39170.45	39412.81	39610.38	39897.19	40175.09	40466.00	40724.36	41061.51	41322.92	41373.68	41493.14	41583.16	41653.05	41697.56	
32	35221.68	35830.13	36137.09	36449.08	36905.39	37058.53	37349.14	37683.69	38073.91	38363.91	38757.08	38759.13	38922.93	39177.68	39268.87	39333.75	39384.97	39438.84	
33	33164.14	33450.69	33744.66	34045.28	34344.83	34642.42	34933.03	35217.93	35487.29	35867.32	36107.83	36407.83	36703.41	37003.81	37297.83	37505.12	37704.76	37913.27	
34	23146.86	23379.95	23616.93	23863.70	24112.36	24364.58	24614.44	24857.68	25093.94	25319.05	25530.02	25778.55	25906.51	26069.67	26221.16	26333.36	26432.92	26511.01	
35	21795.10	22015.20	22392.51	22744.31	23051.25	23293.99	23511.65	23799.54	24072.48	24362.33	24744.99	25122.31	25417.65	25804.28	26051.93	26295.65	26514.88	26711.18	
36	20516.44	20799.30	21201.32	21671.90	22023.11	22311.55	22611.95	22909.75	23109.26	23283.23	23468.84	23702.21	23926.22	24117.52	24308.27	24580.55	24822.76	25022.76	
37	19303.86	19509.41	19728.05	19956.55	20192.60	20431.81	20671.66	20904.17	21131.12	21351.21	21556.17	21746.52	21923.55	22079.06	22217.38	22333.28	22426.69	22500.55	
38	18215.84	18415.19	18624.77	18816.29	19015.22	19214.48	19416.24	19615.00	19814.76	20014.50	20210.93	20412.71	20602.51	20794.17	20935.51	21126.93	21317.44	21507.17	
39	17050.86	17244.22	17450.52	17677.50	17883.33	20363.33	20637.94	20964.20	21209.31	21451.36	21709.82	21940.71	22120.96	22304.76	22493.00	22616.90	22717.27	22814.26	
40	16016.66	16183.92	16369.99	16565.93	16855.01	17102.39	17339.12	17576.24	17808.13	18019.26	18221.79	18416.27	18598.87	18763.68	18901.97	19012.46	19097.74	19228.35	
41	15040.21	15192.47	15437.04	15711.02	15979.45	16248.08	16518.00	16788.00	17058.00	17329.92	17671.98	17961.89	18217.89	18471.82	18718.82	18919.57	18921.12	18929.37	
42	14071.59	14198.21	14387.61	14604.55	14858.51	15139.04	15414.00	15784.00	15984.16	16207.28	16481.53	16760.93	17061.93	17362.50	17627.50	17923.50	18223.50	18523.50	
43	13089.75	13209.43	13422.91	13674.66	13922.33	14181.30	14430.31	14784.30	15139.25	15416.08	14157.84	14454.88	14683.77	14947.71	15201.16	15401.40	15730.12	15321.24	
44	12098.79	12200.86	12439.39	12743.22	13017.22	13270.53	13521.22	13768.00	13994.66	14281.73	14597.55	14821.71	15108.92	14425.74	14708.92	14905.53	15118.52	15309.53	
45	11096.63	11215.23	11447.95	11682.33	11922.33	12170.45	12429.00	12677.62	12927.90	13176.62	13421.62	13674.53	13924.53	14190.68	14409.91	14606.52	14801.68	15016.33	
46	10138.74	10282.08	10482.08	10682.08	10882.08	11121.55	11363.00	11616.60	11866.60	12142.99	12411.62	12678.62	12937.90	13204.30	13481.20	13764.50	14027.34	13293.33	

#### B.4 Calculation force on magnetic beads

Force calculation is computed with equation (3) by all data shown in Table B.1. Besides, all parameters used for calculation are already shown in Table 3.

Table B.2 the example of data about the magnetic force acting on 5- $\mu\text{m}$  magnetic beads in x-axis at arbitrary point (all in pN)

	0	0.05	0.1	0.15	0.2	0.25	0.3	0.35	0.4	0.45	0.5	0.55	0.6	0.65	0.7	0.75	0.8	0.85	0.9	0.95
2.5	12.72	-124.14	70.16	43.38	-38.19	34.47	6.34	97.16	-342.48	302.88	39.68	96.20	91.96	-56.90	24.34	81.39	63.25	128.23	-27.39	-7.02
2.55	-51.14	64.94	14.61	-46.13	29.30	89.95	-43.72	19.11	49.70	28.82	-23.33	56.40	61.91	33.86	59.71	34.90	54.99	48.89	22.80	20.13
2.6	-0.14	9.86	4.97	5.64	5.82	13.79	15.87	17.42	23.67	31.07	16.31	35.05	16.50	32.81	33.79	22.59	45.59	25.84	33.69	38.65
2.65	18.01	2.72	5.12	7.11	8.86	7.14	14.66	13.17	16.28	20.43	16.96	29.83	18.08	22.21	26.85	28.07	22.16	22.52	24.43	21.17
2.7	1.24	3.95	3.72	4.78	7.78	7.77	11.97	13.74	11.95	14.89	16.78	17.63	20.29	20.00	21.69	18.58	20.13	16.70	19.05	
2.75	1.55	1.12	4.10	4.41	6.69	10.03	8.75	9.07	12.76	11.07	16.89	13.61	18.89	15.54	17.60	17.42	17.46	15.50	16.37	14.12
2.8	-1.49	2.88	2.96	4.76	6.94	5.48	10.16	7.73	10.47	10.62	14.00	13.68	13.15	15.19	15.64	14.67	15.96	14.12	14.17	12.83
2.85	0.48	2.27	2.63	4.15	5.54	5.55	7.38	8.99	9.10	10.21	11.89	11.59	12.71	13.12	14.82	12.97	12.80	11.33		
2.9	0.32	1.36	2.95	4.30	5.77	6.23	8.22	8.34	9.77	10.09	11.09	11.49	12.31	12.15	12.77	12.60	12.07	12.37	11.19	
2.95	-0.26	1.51	2.55	3.75	3.94	5.12	6.23	7.26	7.68	8.55	9.75	9.64	10.80	11.47	10.91	11.85	11.51	11.65	11.18	10.70
3	0.37	1.53	2.15	3.19	3.76	5.11	5.42	6.97	6.91	7.98	8.52	9.35	9.81	10.32	10.55	10.71	10.82	11.24	10.24	10.14
3.05	0.96	1.37	1.75	2.38	3.48	4.83	5.01	5.83	6.88	7.39	7.90	8.56	9.44	10.21	9.63	9.97	10.20	10.08	9.42	
3.1	0.56	1.04	1.91	2.89	3.32	3.99	4.95	5.54	6.26	6.94	7.62	7.65	8.38	8.73	8.99	9.27	9.45	9.53	9.24	8.99
3.15	0.43	0.97	1.79	2.49	3.18	3.79	4.55	5.33	5.65	6.34	6.84	7.34	8.01	7.84	8.35	8.65	8.80	8.63	8.61	8.40
3.2	0.04	1.00	2.95	3.62	4.30	5.77	6.23	8.22	8.34	9.77	10.09	11.09	11.49	12.31	12.15	12.77	12.60	12.07		
3.25	0.27	1.10	1.48	2.11	2.88	3.26	3.80	4.45	5.09	5.36	5.81	6.41	6.70	7.26	7.38	7.82	7.93	7.96	8.13	7.64
3.3	0.11	0.80	1.49	2.04	2.44	3.21	3.53	4.12	4.73	4.88	5.42	5.86	6.09	6.38	6.62	6.86	6.67	6.78	6.74	6.60
3.35	0.28	0.75	1.39	1.84	2.51	2.69	3.35	3.81	4.20	4.65	5.06	5.31	5.62	6.00	5.95	6.32	6.14	6.28	6.24	6.03
3.4	0.18	0.79	1.27	1.65	2.16	2.68	3.60	3.92	4.29	4.58	4.93	5.20	5.39	5.64	5.69	5.74	5.68	5.67	5.49	
3.45	0.19	0.74	1.13	1.60	2.01	2.41	2.87	3.25	3.67	3.92	4.23	4.56	4.77	4.93	5.13	5.18	5.29	5.21	5.16	5.01
3.5	0.11	0.61	1.06	1.46	1.91	2.17	2.68	2.96	3.29	3.70	3.93	4.13	4.41	4.57	4.66	4.76	4.84	4.74	4.72	4.58
3.55	0.19	0.58	1.34	1.72	2.08	2.40	2.77	3.08	3.36	3.56	3.81	4.40	4.68	4.81	4.97	5.28	5.45	5.66	5.72	5.72
3.6	0.14	0.51	0.91	1.20	1.63	1.87	2.26	2.52	2.81	3.07	3.32	3.50	3.71	3.86	4.00	3.95	4.05	3.95	3.91	3.80
3.65	0.16	0.47	0.82	1.15	1.46	1.72	2.05	2.36	2.57	2.84	3.02	3.26	3.39	3.54	3.64	3.68	3.68	3.63	3.59	3.42
3.7	0.12	0.45	0.77	1.06	1.34	1.60	2.13	2.39	2.59	2.83	3.01	3.09	3.24	3.33	3.37	3.35	3.40	3.27	3.16	
3.75	0.14	0.44	0.65	0.96	1.21	1.52	1.73	1.97	2.20	2.38	2.58	2.74	2.87	3.03	3.11	3.10	3.06	3.02	2.90	
3.8	0.13	0.39	0.60	0.87	1.13	1.35	1.57	1.85	2.00	2.22	2.36	2.55	2.63	2.75	2.81	2.87	2.87	2.81	2.76	2.65
3.85	0.11	0.40	0.54	0.80	1.26	1.45	1.67	1.84	2.03	2.02	2.26	2.43	2.54	2.61	2.63	2.65	2.61	2.55	2.46	
3.9	0.11	0.31	0.53	0.72	0.93	1.14	1.35	1.54	1.68	1.88	2.02	2.15	2.26	2.36	2.40	2.47	2.45	2.40	2.38	2.26
3.95	0.09	0.30	0.45	0.67	0.84	1.04	1.24	1.40	1.56	1.75	1.83	2.00	2.10	2.19	2.25	2.29	2.25	2.25	2.20	2.11
4	0.10	0.25	0.40	0.60	0.76	0.95	1.13	1.28	1.44	1.59	1.72	1.85	1.94	2.05	2.07	2.14	2.13	2.11	2.06	1.98
4.05	0.07	0.21	0.36	0.53	0.68	0.87	1.01	1.18	1.32	1.47	1.59	1.71	1.83	1.91	1.98	2.02	1.97	1.95	1.85	
4.1	0.07	0.17	0.30	0.45	0.63	0.74	0.94	1.07	1.22	1.34	1.49	1.58	1.69	1.79	1.85	1.90	1.89	1.87	1.83	1.75
4.15	0.04	0.15	0.23	0.36	0.53	0.68	0.85	1.00	1.11	1.23	1.35	1.49	1.59	1.68	1.77	1.80	1.78	1.78	1.67	
4.2	0.02	0.08	0.17	0.27	0.42	0.61	0.78	0.93	1.05	1.12	1.22	1.39	1.53	1.56	1.75	1.78	1.53	1.53	1.60	1.52
4.25	-0.07	0.02	0.03	0.17	0.33	0.51	0.74	0.92	0.94	1.02	1.08	1.22	1.25	1.29	1.24	1.25	1.21	1.21	1.22	
4.3	0.05	-0.05	-0.07	-0.03	0.30	0.25	0.78	1.14	0.88	0.87	0.92	1.04	1.16	1.22	1.32	1.32	1.32	1.32	1.32	1.29
4.35	-0.13	-0.60	-0.07	-0.44	0.17	0.83	0.80	1.12	0.93	0.75	0.62	1.37	1.11	1.09	1.43	1.34	1.34	1.34	1.34	
4.4	-0.67	-0.86	-1.32	-0.06	0.15	1.39	0.48	1.35	1.11	0.30	0.23	1.30	1.16	1.21	1.20	1.23	1.21	1.21	1.24	
4.45	-0.66	-2.67	-0.18	-0.36	-0.23	-0.13	-0.02	2.51	0.64	1.22	1.67	1.25	1.08	1.14	1.02	1.65	1.71	1.52	1.40	
4.5	-3.74	-0.11	-0.18	-0.26	-0.33	-0.40	0.58	0.29	0.24	0.61	1.29	1.19	1.83	1.66	1.50	1.34	1.34	1.34	1.34	

Table B.2 (Continued)

	1	1.05	1.1	1.15	1.2	1.25	1.3	1.35	1.4	1.45	1.5	1.55	1.6	1.65	1.7	1.75	1.8	1.85	1.9	1.95
62.37	116.45	95.76	32.64	-432.11	37.63	-421.63	-1118.15	-3180.09	-21715.93	37945.13	3773.24	1173.87	540.01	171.62	137.88	-38.73	34.79	-103.04	18.83	
73.72	26.24	32.47	-35.54	-64.99	-122.92	-271.66	-581.53	-1163.69	-1282.90	1413.85	1197.98	623.95	300.56	164.43	33.99	-15.71	2.64	-42.59	-48.73	
13.45	22.19	6.50	-18.53	-50.25	-97.90	-178.89	-215.46	-231.45	-282.65	379.80	181.25	95.96	52.66	12.4	9.89	-15.92	-29.02			
14.47	7.58	4.90	-22.38	-32.54	-67.41	-97.28	-128.53	-131.64	-58.11	54.19	127.82	139.71	100.04	72.46	35.17	15.62	-5.95	-4.61	-19.19	
10.57	6.45	-0.19	7.32	-27.41	-37.62	-52.81	-61.40	-53.62	-20.11	25.04	48.03	63.85	52.14	39.95	23.27	9.51	1.19	-8.50	-11.46	
9.90	7.55	1.08	4.40	-11.31	-21.56	-26.87	-30.00	-18.44	-11.19	8.94	22.95	29.79	27.53	16.76	13.06	4.38	-1.14	-7.45	-11.88	
9.98	9.48	7.40	3.01	1.11	-5.57	-8.25	-12.98	-11.69	-11.39	-2.03	3.48	9.14	12.68	11.63	8.36	6.16	-6.81	-8.84		
10.59	7.77	6.29	2.64	-0.42	-1.64	-4.07	-4.86	-3.74	-1.93	-0.81	4.35	3.64	5.72	2.03	-0.29	-3.15	-5.66	8.81	-10.27	
9.68	8.41	7.36	4.24	4.20	1.48	-0.29	-0.91	-0.53	-0.40	0.88	-0.11	0.53	0.18	-3.43	-4.89	-7.39	-8.40	-10.46		
9.56	9.73	7.24	6.12	4.96	3.19	2.39	0.59	0.79	0.03	0.31	-1.15	-1.20	-2.12	-3.57	-4.71	-6.53	-7.62	-9.06	-9.40	
9.65	8.43	8.22	6.52	5.47	4.45	3.03	2.43	1.26	0.08	-0.33	-1.33	-2.14	-3.41	-4.01	-5.88	-8.30	-8.66	-9.38		
9.07	8.68	7.03	5.78	4.72	3.59	2.53	1.49	0.61	-1.59	-0.61	-1.59	-2.64	-3.83	-4.58	-6.03	-6.90	-7.75	8.61	-8.87	
8.80	7.91	7.33	6.53	5.83	4.85	3.63	2.68	1.80	0.55	-0.93	-1.68	-2.51	-3.84	-4.66	-6.22	-6.40	-7.44	-8.24	-8.18	
8.10	7.49	7.02	6.36	5.53	4.52	3.80	2.37	1.70	0.52	-0.71	-1.59	-2.63	-3.83	-4.52	-5.67	-6.25	-6.75	-7.76	-8.26	
7.51	7.02	6.56	5.90	5.04	4.51	3.37	2.45	1.48	0.40	-0.40	-0.88	-1.61	-2.45	-3.62	-4.32	-5.18	-5.89	-6.48	-7.11	
6.82	6.45	6.02	5.47	4.80	4.09	3.12	2.03	1.59	0.53	-0.73	-1.53	-2.30	-3.29	-4.13	-4.75	-5.43	-6.02	-6.44	-6.76	
6.33	6.09	5.37	4.92	4.33	3.79	2.91	2.11	1.09	0.38	-0.51	-1.34	-2.18	-2.96	-3.79	-4.43	-5.00	-5.40	-6.03	-6.12	
5.65	5.49	5.04	4.46	4.02	3.30	2.74	1.79	1.16	0.31	-0.37	-1.43	-1.95	-2.82	-3.33	-3.98	-4.45	-5.12	-5.46	-5.65	
5.19	4.92	4.62	4.10	3.58	3.03	2.43	1.69	1.04	0.34	-0.53	-1.11	-1.89	-2.47	-3.09	-3.59	-4.16	-4.57	-4.89	-5.20	
4.81	4.44	4.11	3.78	3.25	2.74	2.17	1.51	0.93	0.23	-0.45	-1.02	-1.66	-2.29	-2.80	-3.34	-3.72	-4.13	-4.46	-4.68	
4.29	4.09	3.79	3.35	2.94	2.46	1.95	1.40	0.78	0.19	-0.35	-0.97	-1.51	-2.16	-2.55	-2.94	-3.40	-3.75	-4.07	-4.24	
3.97	3.71	3.42	3.05	2.61	2.25	1.72	1.18	0.76	0.16	-0.37	-0.87	-1.32	-1.96	-2.31	-2.70	-3.13	-3.43	-3.61	-3.86	
3.60	3.34	3.10	2.77	2.40	1.97	1.57	1.12	0.64	0.13	-0.38	-0.81	-1.26	-1.68	-2.12	-2.50	-2.82	-3.07	-3.32	-3.51	
3.30	3.08	2.80	2.50	2.16	1.80	1.40	0.99	0.55	0.09	-0.32	-0.78	-1.13	-1.59	-1.92	-2.24	-2.55	-2.78	-3.05	-3.19	
2.96	2.82	2.28	1.94	1.61	1.25	0.90	0.45	0.08	-0.34	-0.69	-1.10	-1.44	-1.73	-2.09	-2.28	-2.56	-2.74	-2.89		
2.75	2.53	2.34	2.04	1.80	1.43	1.17	0.77	0.42	0.02	-0.32	-0.66	-1.02	-1.33	-1.62	-1.89	-2.09	-2.33	-2.45	-2.70	
2.53	2.32	2.15	1.91	1.61	1.34	1.00	0.70	0.35	0.00	-0.30	-0.65	-0.94	-1.25	-1.47	-1.75	-1.95	-2.11	-2.27	-2.41	
2.31	2.15	1.96	1.75	1.45	1.21	0.93	0.62	0.30	0.02	-0.32	-0.62	-0.88	-1.14	-1.40	-1.62	-1.80	-1.95	-2.09	-2.18	
2.17	2.00	1.80	1.60	1.35	1.11	0.83	0.53	0.25	-0.04	-0.33	-0.58	-0.85	-1.12	-1.31	-1.50	-1.65	-1.81	-1.89	-2.02	
2.00	1.85	1.28	1.16	0.93	0.68	0.41	0.16	0.09	-0.35	-0.59	-0.82	-1.06	-1.25	-1.41	-1.55	-1.68	-1.76	-1.81		
1.88	1.73	1.56	1.38	1.16	0.93	0.68	0.41	0.16	-0.09	-0.35	-0.59	-0.82	-1.06	-1.25	-1.41	-1.54	-1.65	-1.64		
1.75	1.65	1.49	1.30	1.09	0.86	0.62	0.37	0.13	-0.13	-0.38	-0.59	-0.82	-0.99	-1.15	-1.31	-1.39	-1.46	-1.51	-1.53	
1.67	1.57	1.39	1.26	1.01	0.81	0.58	0.33	0.07	-0.16	-0.39	-0.61	-0.81	-1.01	-1.16	-1.27	-1.34	-1.40	-1.44		
1.59	1.50	1.36	1.19	1.00	0.76	0.54	0.28	0.04	-0.20	-0.41	-0.63	-0.83	-1.01	-1.17	-1.27	-1.33	-1.37	-1.30	-1.28	
1.56	1.51	1.34	1.14	0.96	0.75	0.50	0.21	0.07	-0.34	-0.59	-0.85	-1.03	-1.22	-1.35	-1.41	-1.55	-1.68	-1.76		
1.49	1.49	1.35	1.29	1.07	0.87	0.62	0.37	0.12	-0.11	-0.35	-0.59	-0.71	-0.85	-1.07	-1.22	-1.32	-1.43	-1.48		
1.39	1.34	1.20	1.04	0.89	0.64	0.40	0.16	0.03	-0.03	-0.22	-0.47	-0.67	-0.87	-1.07	-1.22	-1.32	-1.40	-1.41		
1.28	1.28	1.18	1.04	0.89	0.64	0.40	0.16	0.03	-0.03	-0.22	-0.47	-0.67	-0.87	-1.07	-1.22	-1.32	-1.40	-1.41		
1.17	0.97	1.87	1.71	1.43	1.02	0.78	0.43	0.18	-0.18	-0.33	-0.59	-0.79	-0.99	-1.19	-1.39	-1.59	-1.66	-1.71		
0.42	2.03	1.79	1.54	1.30	1.07	0.52	0.24	-0.81	-0.31	-0.18	-0.54	-0.88	-1.23	-1.57	-1.98	-2.03	-2.42	-2.92		
2.21	1.97	1.72	1.48	1.23	0.99	0.75	0.26	0.18	0.09	-0.52	-0.94	-1.37	-1.79	-2.20	-2.62	-2.62	-2.62	-2.62		

Table B.2 (Continued)

	2.05	2.1	2.15	2.2	2.25	2.3	2.35	2.4	2.45	2.5	2.55	2.6	2.65	2.7	2.75	2.8	2.85	2.9	2.95	
2	16.41	55.92	-15.44	-208.57	141.70	-445.76	271.14	56.00	-36.37	-115.96	-83.19	37.88	-60.83	24.11	-96.43	100.76	-129.73	-62.21	66.89	-74.13
	-31.32	-53.56	-32.59	-33.21	-69.04	-43.22	-9.76	-52.48	-16.19	-59.91	-2.64	-13.19	-48.46	-8.75	-32.52	22.31	-4.95	4.48	-3.06	
	-33.78	-31.36	-41.39	-39.64	-24.45	-48.84	-5.45	-24.46	-45.96	-10.53	-25.86	-18.12	-17.77	-18.14	-7.39	8.68	-15.42	-7.18	-13.35	
	-20.31	-17.58	-23.11	-26.39	-28.47	-21.88	-25.30	-24.04	-19.97	-17.30	-19.96	-19.10	-19.10	-1.41	-9.30	-17.97	-2.68	-9.59	-0.13	
	-15.54	-19.19	-20.20	-19.48	-18.16	-23.05	-17.39	-20.57	-18.28	-13.03	-14.82	-12.17	-13.48	-8.90	-4.83	-2.84	-7.74	-4.46	6.00	
	-13.65	-17.09	-17.09	-16.86	-16.81	-17.65	-16.58	-15.84	-16.44	-13.80	-12.77	-11.81	-9.98	-8.12	-5.10	-6.87	-3.71	-4.22	-0.65	
	-13.56	-13.26	-15.45	-14.99	-15.00	-15.12	-14.74	-13.06	-13.10	-10.90	-10.93	-8.08	-9.53	-7.08	-4.88	-5.41	-3.04	-2.39	-0.17	
	-10.88	-13.12	-13.26	-13.32	-13.52	-13.57	-13.64	-12.43	-11.71	-11.21	-10.46	-9.12	-8.39	-7.02	-6.53	-5.47	-3.27	-1.63	0.34	
	-10.77	-11.12	-12.93	-12.93	-11.94	-12.66	-11.97	-11.66	-10.93	-9.28	-9.88	-8.33	-7.62	-6.84	-5.18	-5.31	-2.81	-2.97	0.14	
	-10.49	-11.33	-11.05	-11.89	-11.33	-11.86	-10.62	-10.43	-9.97	-9.43	-8.27	-8.02	-7.42	-5.63	-5.31	-4.17	-2.84	-2.68	-0.78	
	-10.04	-10.62	-10.67	-10.87	-10.55	-10.37	-9.77	-10.11	-9.22	-8.20	-7.89	-7.32	-6.54	-5.56	-4.51	-4.06	-3.07	-2.02	-1.63	
	-9.64	-9.76	-9.69	-10.10	-9.96	-9.81	-9.57	-8.61	-8.29	-7.65	-7.72	-6.48	-5.97	-5.15	-4.45	-3.57	-2.96	-1.74	-1.44	
	-8.83	-9.45	-9.13	-9.51	-8.74	-9.21	-8.39	-8.45	-7.86	-7.27	-6.82	-6.06	-5.47	-4.70	-4.04	-3.39	-2.65	-1.95	-0.47	
	-7.93	-8.71	-8.61	-8.27	-8.73	-8.25	-8.09	-7.36	-7.25	-6.80	-6.28	-5.57	-5.11	-4.25	-3.82	-2.97	-1.84	-0.99	-0.23	
	-7.61	-7.84	-8.00	-7.86	-7.63	-7.84	-7.26	-7.10	-6.57	-6.31	-5.71	-5.23	-4.67	-4.14	-3.48	-2.91	-2.16	-1.71	-0.95	
	-6.99	-7.17	-7.40	-7.30	-7.14	-7.06	-6.80	-6.30	-6.27	-5.80	-5.26	-4.79	-4.34	-3.83	-3.30	-2.65	-1.98	-1.44	-0.95	
	-6.40	-6.68	-6.63	-6.82	-6.58	-6.38	-6.26	-5.99	-5.61	-5.29	-4.97	-4.41	-3.96	-3.52	-3.02	-2.42	-1.92	-1.39	-0.38	
	-5.80	-6.13	-6.09	-6.10	-5.97	-5.99	-5.75	-5.49	-5.23	-4.81	-4.48	-4.17	-3.60	-3.28	-2.76	-2.28	-1.81	-1.23	-0.76	
	-5.40	-5.47	-5.52	-5.66	-5.54	-5.46	-5.19	-4.76	-4.76	-4.13	-3.83	-3.35	-3.07	-2.96	-2.59	-2.07	-1.19	-0.71	-0.13	
	-4.96	-5.00	-5.08	-5.03	-4.96	-5.06	-4.80	-4.54	-4.39	-4.12	-3.81	-3.47	-3.07	-2.76	-2.38	-1.90	-1.54	-1.06	-0.67	
	-4.45	-4.59	-4.61	-4.59	-4.61	-4.48	-4.41	-4.19	-4.00	-3.75	-3.46	-3.15	-2.94	-2.43	-2.21	-1.78	-1.33	-1.08	-0.49	
	-4.02	-4.16	-4.22	-4.21	-4.16	-4.07	-4.01	-3.85	-3.65	-3.42	-3.15	-3.00	-2.56	-2.30	-2.02	-1.64	-1.23	-0.97	-0.52	
	-3.69	-3.72	-3.84	-3.78	-3.82	-3.71	-3.65	-3.47	-3.38	-3.08	-2.94	-2.65	-2.44	-2.09	-1.81	-1.52	-1.17	-0.80	-0.54	
	-3.31	-3.40	-3.48	-3.42	-3.50	-3.38	-3.31	-3.14	-3.05	-2.88	-2.65	-2.43	-2.23	-1.92	-1.66	-1.37	-1.09	-0.80	-0.39	
	-3.02	-3.06	-3.13	-3.17	-3.13	-3.10	-2.98	-2.93	-2.70	-2.63	-2.43	-2.23	-2.02	-1.76	-1.54	-1.24	-1.00	-0.64	-0.48	
	-2.71	-2.79	-2.87	-2.84	-2.84	-2.78	-2.71	-2.65	-2.51	-2.36	-2.21	-2.01	-1.83	-1.65	-1.41	-1.17	-0.90	-0.65	-0.38	
	-2.45	-2.55	-2.59	-2.56	-2.59	-2.52	-2.46	-2.38	-2.29	-2.13	-2.04	-1.85	-1.66	-1.54	-1.27	-1.07	-0.81	-0.60	-0.38	
	-2.24	-2.30	-2.34	-2.31	-2.28	-2.22	-2.18	-2.06	-1.96	-1.84	-1.68	-1.54	-1.36	-1.22	-0.99	-0.76	-0.54	-0.35	-0.08	
	-2.05	-2.09	-2.07	-2.15	-2.09	-2.05	-2.00	-1.93	-1.88	-1.80	-1.66	-1.53	-1.42	-1.28	-1.10	-0.91	-0.71	-0.51	-0.31	
	-1.86	-1.89	-1.90	-1.92	-1.88	-1.85	-1.82	-1.74	-1.68	-1.61	-1.51	-1.43	-1.29	-1.16	-1.00	-0.87	-0.68	-0.49	-0.27	
	-1.70	-1.71	-1.70	-1.69	-1.66	-1.62	-1.57	-1.50	-1.46	-1.38	-1.27	-1.21	-1.09	-0.94	-0.81	-0.63	-0.47	-0.28	-0.07	
	-1.53	-1.52	-1.52	-1.50	-1.48	-1.44	-1.39	-1.35	-1.30	-1.24	-1.19	-1.10	-0.98	-0.92	-0.74	-0.64	-0.46	-0.25	-0.08	
	-1.40	-1.39	-1.36	-1.32	-1.27	-1.23	-1.17	-1.12	-1.13	-1.08	-1.01	-0.95	-0.86	-0.75	-0.60	-0.45	-0.27	-0.08	-0.08	
	-1.26	-1.23	-1.20	-1.18	-1.17	-1.13	-1.07	-1.03	-1.02	-1.02	-0.98	-0.94	-0.90	-0.82	-0.74	-0.60	-0.45	-0.29	-0.09	
	-1.11	-1.10	-1.03	-1.00	-1.05	-0.99	-0.96	-0.86	-0.86	-0.88	-0.90	-0.86	-0.81	-0.76	-0.62	-0.47	-0.31	-0.13	-0.09	
	-0.64	-1.01	-1.04	-1.34	-1.14	-0.23	-0.59	-0.64	-0.67	-0.74	-0.80	-0.83	-0.86	-0.76	-0.65	-0.42	-0.45	-0.17	-0.13	
	-0.05	-0.30	-0.89	-0.93	-0.47	-0.81	-0.29	-0.42	-0.54	-0.62	-0.69	-0.71	-0.83	-0.71	-0.94	-0.77	-0.48	-0.47	-0.12	
	0.15	0.16	-0.67	-0.08	-0.54	-0.08	-0.20	-0.60	-0.64	-0.66	-0.62	-0.61	-0.59	-0.81	-0.62	-1.08	-0.93	-0.66	-0.62	
	0.41	0.05	0.03	-0.23	0.04	-0.12	1.14	-0.61	-0.63	-0.38	-0.40	-1.12	-0.61	-0.77	-0.90	-1.00	-0.96	-1.16	-1.40	
	-0.09	0.14	0.02	-0.09	-0.21	-0.32	0.14	3.21	-0.11	-0.80	-0.22	-0.76	-0.42	-0.58	-0.74	-0.91	-1.49	-1.59	-1.09	
	0.23	0.11	-0.01	-0.13	-0.26	-0.38	-0.50	-0.62	6.19	-0.98	-0.26	-0.44	-0.62	-0.80	-0.98	-1.15	-1.33	-1.51	-1.69	

Table B.2 (Continued)

	3	3.05	3.1	3.15	3.2	3.25	3.3	3.35	3.4	3.45	3.5	3.55	3.6	3.65	3.7	3.75	3.8	3.85	3.9
199.34	-117.04	85.62	-0.71	-7.82	102.88	-207.85	184.37	7.61	132.41	-59.63	18.51	130.80	-74.37	92.68	-94.31	193.85	94.05	6.96	
11.34	-27.30	3.35	13.75	44.17	-0.71	26.23	27.27	30.02	29.44	-2.85	69.57	35.39	46.24	35.11	37.18	39.96	44.78	41.31	
16.30	-8.57	9.08	5.34	17.16	6.44	17.84	27.97	16.11	18.02	27.44	27.97	28.39	32.17	33.19	32.02	26.00	35.04	33.14	
-0.47	-1.02	6.67	10.39	4.68	15.25	9.96	13.83	17.50	19.85	19.19	21.07	25.93	21.08	20.60	29.71	25.32	19.34		
-2.04	0.17	2.29	9.92	4.23	12.62	11.11	10.65	13.79	14.68	17.37	23.36	13.48	17.88	21.19	23.78	19.21	19.86	18.21	
1.17	1.48	4.03	5.31	5.71	9.25	8.21	11.68	12.07	10.92	15.11	15.39	15.95	17.52	16.54	19.30	16.40	15.58	16.83	
1.36	0.63	4.04	3.49	6.78	6.79	7.87	11.52	8.42	12.39	11.89	13.40	15.53	14.24	14.96	15.88	14.88	14.55	12.94	
-0.09	1.88	2.76	3.98	4.75	6.74	7.96	8.07	9.13	10.73	11.39	11.94	12.73	13.46	13.10	13.89	12.98			
0.53	1.10	3.48	3.31	4.56	5.70	6.86	7.57	8.42	8.99	10.77	11.02	11.42	11.76	12.77	12.23	12.23	12.05		
0.63	1.57	2.21	3.74	4.69	4.78	6.14	7.30	7.65	8.55	9.15	10.09	10.43	11.57	11.23	11.43	11.43	10.90		
0.35	0.98	1.91	2.15	2.87	3.69	4.10	4.71	5.32	5.79	6.34	6.64	7.22	7.29	7.74	7.72	8.05	8.02	7.82	
0.51	0.84	1.41	2.23	2.80	3.18	3.86	4.41	4.87	5.30	5.90	6.12	6.54	6.89	7.04	7.19	7.52	7.25	7.21	
0.40	0.85	1.41	1.94	2.59	2.98	3.57	4.09	4.47	4.94	5.36	5.70	6.02	6.14	6.77	6.51	6.71	6.74	6.72	
0.25	0.94	1.34	1.75	2.33	2.82	3.29	3.72	4.25	4.74	6.20	6.81	7.42	7.78	8.28	8.64	9.00	9.52	9.09	
0.25	0.63	1.19	1.82	2.16	2.60	3.03	3.59	3.67	5.11	5.48	6.49	6.71	7.30	7.65	7.97	8.38	8.66	8.50	
0.20	0.73	1.13	1.63	1.98	2.32	2.88	3.13	3.51	4.10	4.71	5.32	5.79	6.34	6.64	7.22	7.72	8.05	8.02	
0.24	0.69	0.98	1.46	1.84	2.20	2.58	2.98	3.24	3.53	4.41	4.87	5.30	5.90	6.12	6.54	6.89	7.04	7.25	
0.25	0.56	1.00	1.32	1.67	2.05	2.38	2.68	2.97	3.30	3.57	4.09	4.47	4.94	5.36	5.70	6.02	6.14	6.72	
0.22	0.55	0.88	1.26	1.57	1.86	2.21	2.43	2.74	3.29	4.49	4.99	5.18	5.53	5.73	6.08	6.04	6.11	6.14	
0.19	0.51	0.83	1.14	1.43	1.75	2.01	2.26	2.50	3.03	3.67	4.28	4.48	4.85	5.08	5.26	5.45	5.64	5.48	
0.17	0.47	0.76	1.12	1.31	1.57	1.85	2.08	2.29	2.51	3.85	4.17	4.42	4.65	4.81	5.01	5.09	5.11	5.20	
0.19	0.43	0.71	0.98	1.24	1.48	1.70	1.95	2.07	2.29	2.44	2.60	2.67	2.79	2.84	2.87	2.89	2.76	2.71	
0.15	0.43	0.65	0.92	1.13	1.36	1.59	1.75	1.97	2.10	2.22	2.44	2.60	2.79	2.91	3.05	4.21	4.13	4.28	
0.18	0.36	0.64	1.06	1.29	1.44	1.62	1.79	1.92	2.07	2.15	2.34	2.43	2.54	2.73	2.72	3.81	3.81		
0.14	0.37	0.60	0.80	0.97	1.20	1.35	1.50	1.66	1.78	1.87	1.96	2.06	2.08	2.14	2.14	2.13	2.05		
0.13	0.37	0.55	0.75	0.93	1.11	1.27	1.39	1.54	1.64	1.71	1.80	1.86	1.91	1.94	1.96	1.94	1.94	1.87	
0.11	0.33	0.52	0.73	0.91	1.03	1.21	1.30	1.43	1.50	1.58	1.67	1.68	1.74	1.75	1.77	1.74	1.74	1.68	
0.12	0.32	0.50	0.68	0.87	1.00	1.14	1.23	1.32	1.41	1.45	1.52	1.53	1.58	1.60	1.60	1.58	1.59	1.52	
0.11	0.30	0.50	0.67	0.84	0.96	1.08	1.20	1.25	1.31	1.34	1.37	1.40	1.43	1.45	1.45	1.45	1.41	1.39	
0.08	0.30	0.50	0.66	0.83	0.97	1.05	1.15	1.18	1.23	1.23	1.24	1.27	1.29	1.31	1.31	1.30	1.28		
0.08	0.27	0.51	0.66	0.82	0.96	1.07	1.14	1.15	1.16	1.16	1.17	1.18	1.18	1.18	1.17	1.15	1.18		
0.08	0.31	0.50	0.66	0.83	1.00	1.08	1.17	1.17	1.17	1.17	1.17	1.17	1.17	1.17	1.17	1.17	1.17	2.01	
-0.16	0.45	0.89	0.13	0.88	1.01	1.17	1.38	1.38	1.39	1.39	1.39	1.40	1.40	1.40	1.40	1.40	1.36	0.80	
0.25	0.72	0.83	0.77	0.39	1.38	1.77	1.39	1.18	1.00	0.85	0.75	0.65	0.61	0.74	0.76	1.33	0.68	0.74	
0.26	1.54	0.57	0.25	1.47	1.34	1.21	1.08	2.36	0.98	0.75	0.73	-0.03	0.71	0.58	0.68	0.93	1.20	0.66	
0.07	-0.43	1.68	1.55	1.42	1.30	1.17	1.04	0.91	2.64	0.61	-0.46	-0.13	1.16	1.00	0.83	0.67	0.51		
-1.22	2.13	1.98	1.83	1.67	1.52	1.37	1.22	1.07	0.92	1.62	1.62	1.62	1.62	1.62	1.62	1.62	0.74	0.58	

Table B.2 (Continued)

3.95	4	4.05	4.1	4.15	4.2	4.25	4.3	4.35	4.4	4.45	4.5	4.55	4.6	4.65	4.7	4.75	4.8	4.85	4.9	4.95
45.37	-86.17	142.99	-322.39	317.20	-273.47	-56.20	-541.01	-1034.54	-3253.24	-2071.58	34603.67	3525.23	1135.25	420.70	249.42	101.13	53.93	28.79	-218.70	147.03
49.52	42.25	53.99	9.23	-20.86	-66.20	-132.26	-284.66	-630.65	-1166.98	-1034.07	1153.05	1257.24	610.95	295.54	124.01	61.69	26.68	-11.77	-33.14	-48.83
20.10	26.64	23.41	3.90	-12.31	-48.72	-114.26	-166.41	-285.08	-350.82	-211.42	193.52	298.13	185.75	93.93	7.32	16.14	-0.75	-12.28	-15.89	-28.95
28.84	8.30	12.64	0.06	-17.39	-36.96	-64.29	-100.59	-127.67	-134.18	-57.66	62.17	136.80	129.37	89.50	72.81	42.03	14.56	-0.46	-12.28	-15.89
16.26	10.72	6.50	-1.73	-8.33	-23.69	-40.68	-51.22	-58.61	-53.97	-21.62	27.46	45.20	62.95	52.18	34.58	28.26	8.92	2.92	-6.28	-12.96
13.35	11.34	6.49	1.76	-4.25	-13.34	-21.40	-24.54	-30.03	-22.23	-9.26	9.87	21.84	29.28	27.39	20.87	10.20	5.49	-0.69	-5.79	-14.10
13.56	9.55	7.36	4.52	-1.52	-4.68	-9.80	-10.55	-11.92	-8.42	-4.90	4.09	9.64	11.10	13.13	8.80	5.37	-0.70	-2.97	-7.90	-10.78
10.97	10.90	8.18	5.47	3.20	-0.51	-2.55	-3.75	-3.73	-3.75	-2.21	1.58	3.64	4.59	4.97	2.05	0.89	-4.02	-6.33	-8.01	-10.04
11.85	9.19	8.39	7.21	5.09	3.36	1.77	-0.11	-0.01	-1.60	-0.11	0.50	1.09	-0.28	0.19	-2.35	-1.99	-5.10	-6.92	-8.70	-10.09
11.02	9.68	8.95	7.53	6.42	4.58	3.14	2.97	1.03	0.48	1.12	-1.16	-0.60	-1.00	-1.98	-3.70	-5.31	5.49	-7.48	-8.08	-10.86
10.19	9.69	8.79	7.55	6.78	5.82	4.53	3.17	2.41	0.85	1.53	-1.39	-0.64	-2.28	-3.29	-4.59	-5.67	-6.58	-7.88	-8.65	-9.61
9.46	9.10	8.32	8.02	7.03	5.68	4.82	3.98	2.52	1.54	0.31	-0.28	-1.46	-3.11	-3.51	-4.58	-5.79	-6.81	-7.67	-8.51	-8.96
8.95	8.56	8.05	7.54	6.68	5.69	4.79	3.18	1.36	0.61	-0.53	-1.84	-2.54	-3.80	-4.88	-5.49	-6.98	-8.05	-8.68	-9.66	-10.04
8.37	8.26	7.21	7.10	6.24	5.69	4.69	3.58	2.64	1.70	0.59	-0.60	-1.56	-2.36	-3.82	-4.77	-5.59	-6.18	-7.04	-7.41	-7.99
7.73	7.42	6.94	6.53	5.94	5.15	4.42	3.29	2.55	1.76	0.37	-0.35	-1.56	-2.45	-3.43	-4.14	-4.19	-4.59	-5.80	-6.60	-6.92
7.06	6.62	6.68	5.95	5.48	4.74	4.11	3.25	1.44	0.50	-0.42	-1.46	-2.23	-3.11	-3.91	-4.37	-5.37	-5.99	-6.31	-6.71	-7.35
6.47	6.12	5.95	5.49	5.03	4.33	3.76	3.07	2.07	1.35	0.33	-0.29	-1.24	-2.15	-2.92	-3.63	-4.33	-4.81	-5.41	-5.94	-6.14
5.84	5.70	5.35	5.02	4.58	3.91	3.41	2.70	1.96	1.20	0.42	-0.29	-1.16	-1.86	-2.60	-3.39	-3.88	-4.40	-4.93	-5.48	-5.59
5.43	5.16	4.90	4.45	4.12	3.61	3.10	2.38	1.84	1.16	0.35	-0.26	-1.02	-1.77	-2.31	-2.94	-3.59	-4.06	-4.56	-4.84	-5.14
5.01	4.68	4.28	4.20	3.71	3.28	2.74	2.27	1.58	0.98	0.33	-0.23	-1.50	-2.09	-2.74	-3.20	-3.66	-4.02	-4.69	-4.93	-5.35
4.44	4.25	4.06	3.68	3.33	2.99	2.38	2.05	1.47	0.91	0.37	-0.24	-0.84	-1.33	-1.91	-2.41	-2.92	-3.26	-3.69	-3.93	-4.25
4.01	3.86	3.63	3.35	2.96	2.68	2.31	1.79	1.29	0.85	0.30	-0.19	-0.73	-1.17	-1.77	-2.18	-2.50	-3.00	-3.33	-3.60	-3.80
3.62	3.50	3.26	3.02	2.71	2.39	2.05	1.53	1.24	0.70	0.28	-0.19	-0.61	-1.09	-1.52	-2.19	-2.29	-2.72	-3.24	-3.50	-3.70
3.25	3.15	2.95	2.73	2.48	2.16	1.83	1.45	1.09	0.66	0.26	-0.15	-0.53	-1.01	-1.35	-1.70	-2.11	-2.34	-2.73	-2.94	-3.10
2.98	2.84	2.63	2.50	2.23	1.92	1.66	1.35	0.95	0.62	0.28	-0.14	-0.52	-0.87	-1.17	-1.57	-1.88	-2.13	-2.44	-2.62	-2.86
2.70	2.55	2.17	2.07	1.76	1.48	1.20	0.90	0.56	0.24	-0.12	-0.40	-0.70	-1.12	-1.38	-1.67	-1.91	-2.21	-2.58	-2.88	-3.22
2.48	2.31	2.18	1.81	1.57	1.36	1.07	0.80	0.51	0.22	-0.09	-0.37	-0.66	-1.22	-1.49	-1.74	-2.14	-2.46	-2.80	-3.13	-3.45
2.19	2.11	1.99	1.79	1.64	1.44	1.20	0.97	0.72	0.48	0.21	-0.04	-0.31	-0.58	-0.87	-1.09	-1.33	-1.54	-1.76	-1.95	-2.10
2.02	1.88	1.77	1.66	1.44	1.29	1.10	0.90	0.66	0.41	0.22	-0.03	-0.30	-0.52	-0.74	-0.96	-1.19	-1.57	-1.75	-1.90	-2.05
1.80	1.72	1.59	1.47	1.32	1.16	1.01	0.81	0.59	0.38	0.20	-0.04	-0.22	-0.44	-0.66	-0.86	-1.04	-1.23	-1.41	-1.58	-1.72
1.64	1.54	1.45	1.33	1.20	1.05	0.90	0.71	0.54	0.36	0.18	-0.01	-0.18	-0.40	-0.56	-0.76	-0.91	-1.09	-1.27	-1.40	-1.57
1.48	1.39	1.32	1.19	1.07	0.94	0.80	0.65	0.50	0.33	0.19	0.00	-0.15	-0.32	-0.50	-0.64	-0.81	-0.97	-1.10	-1.30	-1.39
1.32	1.26	1.16	1.08	0.96	0.85	0.72	0.59	0.43	0.30	0.18	0.02	-0.12	-0.27	-0.40	-0.54	-0.71	-0.86	-1.00	-1.13	-1.25
1.19	1.12	1.03	0.94	0.86	0.76	0.63	0.51	0.40	0.28	0.17	0.02	-0.09	-0.19	-0.31	-0.46	-0.60	-0.77	-0.89	-0.99	-1.10
1.09	0.93	0.99	0.71	0.83	0.62	0.55	0.40	0.35	0.25	0.17	0.02	-0.11	-0.22	-0.33	-0.50	-0.74	-0.82	-0.90	-0.98	-1.08
0.67	0.55	0.59	0.51	0.65	1.04	0.29	0.24	0.14	0.04	-0.06	-0.14	-0.03	-0.02	-0.02	-0.07	-0.07	-1.29	-0.58	-0.64	-0.64
0.44	0.66	0.54	0.63	0.40	0.71	0.26	0.33	0.07	-0.33	0.11	0.37	0.06	-0.09	-0.14	-0.27	-1.21	-0.78	-0.54	-0.44	-0.44
0.46	0.14	1.09	0.33	0.38	0.74	0.42	0.38	0.20	-0.32	-0.28	0.41	0.71	0.06	-0.17	0.69	-0.97	-0.80	-0.96	-0.70	0.62
0.16	-0.04	1.20	0.48	-0.03	0.01	0.41	0.22	0.14	-0.01	-0.18	-0.50	0.99	-0.22	-0.22	-0.74	-0.51	-1.05	-1.19	-2.27	-1.10
0.58	0.13	0.14	0.26	-0.51	0.57	0.39	0.20	0.01	-0.17	-0.13	-0.01	2.67	0.66	-0.68	-0.42	-0.43	-0.66	-0.85	-0.97	-1.10
0.26	0.10	-1.43	1.19	-0.28	0.50	0.33	0.16	-0.01	-0.18	-0.35	-0.52	-0.69	4.49	-0.16	-0.30	-0.44	-0.57	-0.71	-0.85	-0.99

Table B.2 (Continued)

	5	5.05	5.1	5.15	5.2	5.25	5.3	5.35	5.4	5.45	5.5	5.55	5.6	5.65	5.7	5.75	5.8	5.85	5.9	5.95
-23.08	-138.51	-8.76	-112.56	31.04	-102.64	-21.66	7.31	-15.59	-14.77	-61.78	-131.77	-148.59	-44.18	55.34	200.18	-80.04	-74.26	-74.27	184.17	
-45.73	-51.19	-6.28	-93.94	-38.05	-20.42	-77.57	-19.08	-22.89	-33.38	-69.22	-14.50	-29.67	-23.67	-63.65	27.96	-20.75	-48.99	17.04	-14.24	
-30.00	-32.33	-33.38	-36.81	-35.55	-31.23	-30.12	-26.70	-21.31	-25.64	-25.83	-11.81	-22.04	-25.68	2.08	-22.00	-11.71	-0.43	-9.93	9.17	
-12.96	-31.44	-25.35	-19.43	-31.17	-20.55	-27.80	-18.85	-22.26	-16.94	-16.09	-13.61	-15.75	-7.16	-13.99	-6.03	-2.84	-1.94	-18.18	-0.07	
-14.74	-17.63	-20.54	-22.36	-19.34	-20.27	-19.79	-18.84	-18.89	-15.88	-15.30	-12.52	-10.32	-14.57	-8.98	-5.33	-1.90	-5.87	-0.74	-0.30	
-10.39	-16.35	-16.30	-17.99	-17.19	-17.89	-16.82	-16.70	-14.95	-14.24	-13.34	-11.50	-10.30	-9.74	-6.06	-9.01	-3.31	-4.57	-2.74	-0.30	
-12.17	-14.54	-15.13	-15.85	-14.46	-14.99	-14.31	-13.23	-13.00	-10.46	-10.71	-10.19	-8.62	-6.48	-5.53	-4.94	-3.02	-3.10	1.75		
-11.37	-12.48	-13.38	-13.91	-13.88	-13.36	-13.46	-12.27	-12.13	-11.81	-10.33	-9.40	-8.71	-6.90	-6.14	-5.01	-4.76	-2.79	-1.62	-0.38	
-11.43	-11.12	-12.85	-12.49	-12.72	-11.62	-12.60	-11.37	-10.60	-10.75	-9.17	-8.74	-7.42	-6.94	-6.26	-5.53	-3.22	-2.56	-1.92	-0.11	
-10.71	-11.13	-11.45	-11.50	-11.56	-11.25	-11.35	-10.59	-10.02	-9.40	-8.74	-8.83	-7.73	-7.41	-6.40	-5.60	-5.07	-3.77	-2.73	0.32	
-9.94	-10.53	-10.85	-10.90	-10.47	-10.63	-10.04	-9.97	-8.94	-8.83	-7.79	-7.45	-6.70	-6.08	-5.09	-4.47	-3.86	-2.87	-3.32	-0.37	
-9.62	-9.87	-9.91	-10.09	-9.75	-9.18	-9.34	-8.58	-8.58	-7.79	-6.79	-6.17	-5.63	-4.60	-4.43	-3.06	-2.80	-2.14	-1.00	-0.47	
-8.91	-9.18	-9.44	-9.28	-9.12	-8.9	-8.71	-8.33	-7.93	-7.29	-6.79	-6.17	-5.63	-4.30	-3.06	-2.44	-1.83	-1.02	-0.34		
-8.19	-8.66	-8.53	-8.49	-8.63	-8.42	-8.12	-7.66	-7.66	-6.89	-6.19	-5.76	-5.10	-4.62	-4.53	-3.05	-2.73	-1.31	-0.32		
-7.73	-7.71	-8.18	-7.98	-7.81	-7.68	-7.35	-7.05	-6.83	-6.45	-5.88	-5.30	-4.70	-4.24	-3.58	-2.95	-2.30	-1.66	-0.89	-0.56	
-6.92	-7.53	-7.28	-7.46	-7.16	-6.89	-7.02	-6.64	-6.10	-5.89	-5.46	-4.99	-4.29	-3.96	-3.32	-2.82	-2.10	-1.48	-0.90	-0.40	
-6.54	-6.66	-6.67	-6.84	-6.65	-6.51	-6.33	-6.02	-5.85	-5.39	-5.08	-4.55	-4.04	-3.57	-3.13	-2.54	-2.01	-1.43	-0.86	-0.17	
-5.98	-6.09	-6.12	-6.25	-6.07	-5.98	-5.98	-5.58	-5.26	-5.00	-4.65	-4.23	-3.80	-3.27	-2.80	-2.42	-1.84	-1.32	-0.81	-0.32	
-5.39	-5.57	-5.61	-5.63	-5.62	-5.29	-5.22	-4.87	-4.55	-4.29	-3.92	-3.44	-3.20	-2.57	-2.16	-1.77	-1.24	-0.69	-0.28		
-4.88	-5.10	-5.10	-5.24	-5.01	-5.05	-4.96	-4.73	-4.51	-4.13	-3.95	-3.66	-3.22	-2.89	-2.42	-2.00	-1.62	-1.10	-0.72	0.13	
-4.47	-4.59	-4.68	-4.71	-4.61	-4.74	-4.36	-4.35	-4.25	-3.87	-3.63	-3.31	-2.95	-2.70	-2.22	-1.89	-1.43	-1.11	-0.60	-0.11	
-4.04	-4.21	-4.22	-4.32	-4.23	-4.13	-3.92	-3.84	-3.59	-3.32	-3.06	-2.77	-2.42	-2.10	-1.72	-1.37	-0.98	-0.60	-0.17		
-3.64	-3.77	-3.89	-3.91	-3.92	-3.86	-3.84	-3.62	-3.47	-3.36	-3.06	-2.75	-2.60	-2.25	-1.94	-1.58	-1.26	-0.92	-0.52	-0.16	
-3.36	-3.46	-3.52	-3.55	-3.54	-3.55	-3.51	-3.34	-3.24	-3.03	-2.81	-2.56	-2.33	-2.05	-1.76	-1.46	-1.14	-0.86	-0.49	-0.16	
-3.00	-3.13	-3.21	-3.29	-3.21	-3.17	-3.08	-2.97	-2.75	-2.70	-2.37	-2.16	-1.93	-1.65	-1.35	-1.10	-0.77	-0.45	-0.18		
-2.72	-2.84	-2.96	-2.91	-3.03	-3.00	-2.91	-2.75	-2.60	-2.41	-2.21	-2.04	-1.75	-1.49	-1.33	-0.98	-0.73	-0.44	-0.14		
-2.48	-2.58	-2.65	-2.73	-2.74	-2.75	-2.69	-2.61	-2.53	-2.40	-2.19	-2.09	-1.84	-1.66	-1.41	-1.19	-0.93	-0.63	-0.41	-0.13	
-2.24	-2.34	-2.46	-2.51	-2.53	-2.49	-2.40	-2.31	-2.23	-2.07	-1.91	-1.73	-1.53	-1.33	-1.08	-0.85	-0.61	-0.37	-0.13		
-2.07	-2.12	-2.23	-2.33	-2.33	-2.29	-2.27	-2.17	-2.05	-1.94	-1.76	-1.42	-1.22	-1.00	-0.79	-0.57	-0.35	-0.11			
-1.84	-1.97	-2.06	-2.10	-2.13	-2.16	-2.13	-2.09	-2.01	-1.90	-1.81	-1.65	-1.51	-1.33	-1.12	-0.95	-0.74	-0.53	-0.31	-0.10	
-1.68	-1.79	-1.88	-1.95	-1.99	-2.01	-1.99	-1.94	-1.88	-1.79	-1.69	-1.55	-1.41	-1.23	-1.05	-0.86	-0.70	-0.49	-0.29	-0.09	
-1.52	-1.63	-1.73	-1.81	-1.85	-1.84	-1.82	-1.78	-1.68	-1.57	-1.48	-1.31	-1.17	-0.99	-0.80	-0.63	-0.45	-0.26	-0.09		
-1.37	-1.49	-1.61	-1.69	-1.73	-1.75	-1.75	-1.72	-1.66	-1.58	-1.50	-1.38	-1.26	-1.09	-0.92	-0.74	-0.57	-0.41	-0.23	-0.09	
-1.21	-1.36	-1.52	-1.60	-1.64	-1.65	-1.63	-1.63	-1.56	-1.50	-1.41	-1.33	-1.20	-1.03	-0.86	-0.70	-0.51	-0.36	-0.19	-0.08	
-1.03	-1.15	-1.80	-1.33	-1.53	-1.55	-1.51	-1.63	-1.44	-1.40	-1.36	-1.29	-1.17	-0.99	-0.80	-0.62	-0.45	-0.29	-0.13		
-0.88	-0.80	-0.87	-2.45	-1.48	-1.45	-1.49	-1.20	-1.25	-1.34	-1.38	-1.23	-1.05	-0.86	-0.66	-0.63	-0.45	-0.21	0.02		
-0.68	-1.03	-1.16	-1.21	-1.54	-2.05	-1.19	-1.49	-1.12	-1.28	-1.25	-1.30	-1.17	-0.99	-0.80	-0.63	-0.45	-0.25	0.00		
-0.58	-1.10	-1.29	-1.45	-1.72	-1.78	-0.91	-1.32	-1.42	-0.70	-1.23	-1.21	-1.51	-1.19	-1.33	-0.70	-0.58	-0.43	-0.23		
-0.50	-1.09	-1.65	-2.02	-1.23	-1.93	-1.84	0.02	-1.19	-0.70	-0.99	-1.47	-1.46	-1.17	-0.29	-0.42	-0.95	0.81	0.67		
3.50	-1.28	-1.69	-1.91	-2.12	-1.34	-2.05	-1.93	0.05	0.29	-0.94	-4.99	-0.52	-0.26	0.13	-0.09	-0.14	-0.19	3.36	0.67	
4.07	-1.36	-1.58	-1.80	-2.01	-2.23	-2.45	-0.44	-1.62	-1.73	-0.65	-0.47	-1.73	0.02	-0.03	-0.08	-0.13	-0.18	-0.23	4.98	

## B.5 Calculation force on blood cells

Force calculation is computed with equation (3) by all data shown in Table B.1. Besides, all parameters used for

Table B.3 the example of data about the magnetic force acting on infected erythrocytes in x-axis at arbitrary point (all in pN)

Table B.3 (Continued)

	1	1.05	1.1	1.15	1.2	1.25	1.3	1.35	1.4	1.45	1.5	1.55	1.6	1.65	1.7	1.75	1.8	1.85	1.9	1.95
8.67E-04	1.62E-03	-1.33E-03	4.54E-04	-6.01E-03	5.23E-04	-5.86E-03	-1.55E-02	-4.42E-02	-3.02E-01	5.28E-01	5.25E-02	1.63E-02	7.51E-03	2.39E-03	1.92E-03	-5.38E-04	4.84E-04	-1.43E-03	2.62E-04	
1.03E-03	3.65E-04	4.51E-04	4.94E-04	-9.04E-04	-1.71E-03	-3.78E-03	-8.09E-03	-1.62E-02	-1.78E-02	1.97E-02	1.67E-02	8.68E-03	4.18E-03	2.29E-03	4.73E-04	-2.18E-04	3.67E-05	-5.92E-04	-6.78E-04	
1.87E-04	3.09E-04	9.03E-05	-2.58E-04	-6.99E-04	-1.36E-03	-2.49E-03	-3.83E-03	-5.11E-03	-3.22E-03	3.30E-03	5.28E-03	3.93E-03	2.52E-03	1.33E-03	7.32E-04	1.72E-05	1.37E-04	-2.21E-04	4.04E-04	
2.01E-04	1.05E-04	6.81E-05	-3.14E-04	-4.53E-04	-9.37E-04	-1.35E-03	-1.79E-03	-1.83E-03	-8.08E-04	-7.54E-04	1.78E-03	1.94E-03	1.39E-03	1.01E-03	4.89E-04	2.17E-04	-8.27E-05	-6.41E-05	-2.67E-04	
1.47E-04	8.97E-05	-2.64E-05	-5.23E-04	-7.34E-04	-8.54E-04	-7.46E-04	-8.54E-04	-2.80E-04	-3.48E-04	6.68E-04	8.88E-04	7.25E-04	5.56E-04	3.23E-04	1.32E-04	6.65E-05	-1.18E-04	-1.59E-04	-1.65E-04	
1.38E-04	1.05E-04	1.50E-05	-6.11E-04	-1.57E-04	-3.00E-04	-1.57E-04	-3.00E-04	-4.17E-04	-2.56E-04	-1.56E-04	1.24E-04	3.19E-04	4.14E-04	3.63E-04	2.33E-04	1.82E-04	6.09E-05	-1.59E-05	-1.04E-04	-1.65E-04
1.39E-04	1.03E-04	4.18E-05	1.55E-05	-7.75E-05	-1.15E-04	-1.81E-04	-1.63E-04	-1.58E-04	-1.58E-04	-2.82E-05	4.84E-05	1.27E-04	1.76E-04	1.62E-04	1.16E-04	8.56E-05	-1.08E-05	-6.34E-05	-9.47E-05	-1.23E-04
1.47E-04	1.08E-04	8.74E-05	3.67E-05	-5.83E-06	-2.29E-05	-5.66E-05	-6.76E-05	-5.20E-05	-2.69E-05	1.13E-05	6.05E-05	5.07E-05	7.96E-05	2.82E-05	4.07E-06	4.38E-05	-7.87E-05	-1.23E-04	-1.43E-04	
1.35E-04	1.17E-04	1.02E-04	5.90E-05	5.84E-05	2.06E-05	-3.98E-06	-1.26E-05	-7.31E-06	-5.54E-06	1.23E-05	-1.58E-06	7.34E-06	-2.53E-06	-1.74E-05	-4.77E-05	-6.80E-05	-1.03E-04	-1.17E-04	-1.45E-04	
1.33E-04	1.35E-04	1.01E-04	8.51E-05	6.90E-05	4.44E-05	3.33E-05	8.25E-06	4.62E-07	4.29E-06	-1.60E-05	-1.66E-05	-2.94E-05	-5.66E-05	-2.94E-05	-4.74E-05	-5.58E-05	8.18E-05	-8.88E-05	-1.06E-04	
1.34E-04	1.17E-04	1.14E-04	9.07E-05	7.61E-05	6.19E-05	4.22E-05	3.38E-05	1.75E-05	1.06E-06	4.59E-06	-1.85E-05	-2.98E-05	4.74E-05	-2.98E-05	-4.74E-05	-5.75E-05	-7.20E-05	-1.20E-04	-1.30E-04	
1.26E-04	1.21E-04	1.06E-04	9.78E-05	8.04E-05	5.65E-05	4.99E-05	3.51E-05	2.08E-05	8.87E-06	-8.47E-06	-2.21E-05	-3.67E-05	-5.33E-05	-6.37E-05	-8.38E-05	-9.60E-05	-1.08E-04	-1.20E-04	-1.23E-04	
1.22E-04	1.10E-04	1.02E-04	9.08E-05	8.10E-05	6.75E-05	5.05E-05	3.72E-05	2.50E-05	7.69E-06	-1.30E-05	-2.34E-05	-3.49E-05	-5.35E-05	-6.48E-05	-8.65E-05	-8.90E-05	-8.90E-05	-1.03E-04	-1.14E-04	
1.13E-04	1.04E-04	9.76E-05	8.84E-05	7.68E-05	6.28E-05	5.29E-05	3.30E-05	2.37E-05	7.21E-06	9.92E-06	-2.22E-05	-3.65E-05	-5.32E-05	-6.29E-05	-7.89E-05	-8.69E-05	-9.39E-05	-1.08E-04	-1.15E-04	
1.04E-04	9.76E-05	9.12E-05	8.20E-05	7.01E-05	6.26E-05	4.68E-05	3.41E-05	2.06E-05	5.63E-06	-8.71E-06	-2.24E-05	-3.41E-05	-5.03E-05	-6.01E-05	-7.20E-05	-8.19E-05	-9.02E-05	-9.89E-05	-1.03E-04	
9.49E-05	8.92E-05	8.37E-05	7.61E-05	6.68E-05	5.69E-05	4.34E-05	2.83E-05	2.21E-05	7.32E-06	-1.02E-05	-2.13E-05	-3.20E-05	-4.58E-05	-5.75E-05	-6.60E-05	-7.55E-05	-8.37E-05	-9.40E-05	-9.40E-05	
8.80E-05	8.47E-05	7.47E-05	6.85E-05	6.01E-05	5.27E-05	4.04E-05	2.94E-05	1.52E-05	5.29E-06	-7.07E-06	-1.86E-05	-3.03E-05	-4.11E-05	-5.26E-05	-6.16E-05	-6.95E-05	-7.51E-05	-8.39E-05	-8.51E-05	
7.85E-05	7.63E-05	7.01E-05	6.20E-05	5.59E-05	4.59E-05	3.81E-05	2.94E-05	2.37E-05	5.72E-06	-7.37E-06	-1.54E-05	-2.63E-05	-3.63E-05	-4.29E-05	-5.17E-05	-5.74E-05	-6.21E-05	-6.51E-05	-7.23E-05	
7.22E-05	6.85E-05	6.42E-05	5.70E-05	4.97E-05	4.21E-05	3.38E-05	2.41E-05	1.44E-05	4.66E-06	-7.37E-06	-1.54E-05	-2.63E-05	-3.63E-05	-4.29E-05	-5.17E-05	-5.74E-05	-6.21E-05	-6.51E-05	-7.23E-05	
6.68E-05	6.17E-05	5.71E-05	5.25E-05	4.52E-05	3.81E-05	3.01E-05	2.09E-05	1.29E-05	3.20E-06	-6.20E-06	-1.42E-05	-2.31E-05	-3.19E-05	-3.85E-05	-4.64E-05	-5.17E-05	-5.74E-05	-6.21E-05	-6.51E-05	
5.97E-05	5.69E-05	5.22E-05	4.65E-05	4.25E-05	3.62E-05	2.40E-05	1.64E-05	1.06E-05	2.27E-06	-5.12E-06	-1.21E-05	-1.84E-05	-2.72E-05	-3.22E-05	-3.75E-05	-4.78E-05	-5.42E-05	-5.66E-05	-5.90E-05	
5.52E-05	5.15E-05	4.75E-05	4.25E-05	3.62E-05	3.13E-05	2.40E-05	1.71E-05	1.05E-05	2.27E-06	-5.12E-06	-1.21E-05	-1.84E-05	-2.72E-05	-3.22E-05	-3.75E-05	-4.78E-05	-5.42E-05	-5.66E-05	-5.90E-05	
5.00E-05	4.65E-05	4.32E-05	3.85E-05	3.34E-05	2.74E-05	2.18E-05	1.55E-05	8.87E-06	1.78E-06	-5.26E-06	-1.13E-05	-1.76E-05	-2.33E-05	-2.94E-05	-3.48E-05	-4.25E-05	-4.99E-05	-5.60E-05	-6.35E-05	
4.59E-05	4.29E-05	3.89E-05	3.48E-05	3.00E-05	2.51E-05	1.95E-05	1.38E-05	7.65E-06	1.23E-06	-4.45E-06	-1.09E-05	-1.57E-05	-2.21E-05	-2.66E-05	-3.11E-05	-3.54E-05	-4.24E-05	-4.43E-05	-4.43E-05	
4.11E-05	3.92E-05	3.56E-05	3.18E-05	2.70E-05	2.24E-05	1.74E-05	1.25E-05	6.19E-06	1.15E-06	-4.69E-06	-9.63E-06	-1.53E-05	-2.00E-05	-2.41E-05	-2.91E-05	-3.16E-05	-3.56E-05	-3.80E-05	-4.02E-05	
3.82E-05	3.52E-05	3.26E-05	2.84E-05	2.50E-05	1.99E-05	1.63E-05	1.07E-05	5.87E-06	3.32E-07	-4.43E-06	-9.17E-06	-1.42E-05	-1.84E-05	-2.25E-05	-2.63E-05	-2.90E-05	-3.24E-05	-3.40E-05	-3.75E-05	
3.52E-05	3.23E-05	2.98E-05	2.65E-05	2.24E-05	1.86E-05	1.39E-05	8.68E-06	5.21E-06	4.86E-06	5.21E-06	-8.21E-06	-1.31E-05	-1.84E-05	-2.44E-05	-2.72E-05	-3.23E-05	-3.66E-05	-3.95E-05		
3.22E-05	2.99E-05	2.72E-05	2.43E-05	2.02E-05	1.69E-05	1.29E-05	8.55E-06	4.21E-06	5.58E-07	4.47E-06	-8.66E-06	-1.23E-05	-1.58E-05	-2.03E-05	-2.31E-05	-2.71E-05	-3.03E-05	-3.30E-05		
3.01E-05	2.78E-05	2.50E-05	2.22E-05	1.87E-05	1.54E-05	1.16E-05	7.43E-06	3.47E-06	5.46E-07	4.56E-06	-8.09E-06	-1.19E-05	-1.55E-05	-1.83E-05	-2.08E-05	-2.25E-05	-2.51E-05	-2.80E-05		
2.78E-05	2.58E-05	2.33E-05	2.07E-05	1.74E-05	1.39E-05	1.05E-05	6.68E-06	2.92E-06	1.60E-07	3.08E-06	-6.11E-06	-9.19E-06	-1.14E-05	-1.47E-05	-1.74E-05	-2.15E-05	-2.33E-05	-2.44E-05	-2.51E-05	
2.62E-05	2.41E-05	2.17E-05	1.92E-05	1.61E-05	1.30E-05	9.49E-06	2.25E-06	1.20E-06	4.91E-06	-8.25E-06	-1.14E-05	-1.40E-05	-1.64E-05	-1.89E-05	-2.05E-05	-2.13E-05	-2.29E-05	-2.29E-05		
2.43E-05	2.29E-05	2.07E-05	1.80E-05	1.52E-05	1.20E-05	8.68E-06	5.11E-06	1.78E-06	-1.87E-06	-5.22E-06	-8.21E-06	-1.21E-05	-1.38E-05	-1.60E-05	-1.82E-05	-2.03E-05	-2.10E-05	-2.12E-05		
2.32E-05	2.18E-05	1.94E-05	1.76E-05	1.41E-05	1.12E-05	8.00E-06	4.61E-06	9.89E-07	-2.19E-06	-5.48E-06	-8.48E-06	-1.13E-05	-1.40E-05	-1.61E-05	-1.77E-05	-1.87E-05	-1.94E-05	-1.96E-05		
2.21E-05	2.09E-05	1.90E-05	1.66E-05	1.38E-05	1.06E-05	7.46E-06	3.92E-06	5.69E-07	-2.75E-06	-5.68E-06	-8.82E-06	-1.15E-05	-1.41E-05	-1.62E-05	-1.76E-05	-1.84E-05	-1.90E-05	-1.78E-05		
2.16E-05	2.10E-05	1.87E-05	1.58E-05	1.27E-05	9.2E-05	6.94E-06	3.38E-06	1.60E-07	-3.08E-06	-6.11E-06	-9.19E-06	-1.19E-05	-1.44E-05	-1.70E-05	-1.83E-05	-1.87E-05	-1.87E-05	-1.55E-05		
2.51E-05	1.79E-05	2.11E-05	1.27E-05	1.35E-05	1.09E-05	6.40E-06	2.59E-06	3.49E-07	-3.05E-06	-6.49E-06	-9.91E-06	-1.19E-05	-1.49E-05	-1.84E-05	-1.94E-05	-1.95E-05	-1.96E-05	-1.21E-05		
2.43E-05	2.57E-05	2.74E-06	2.07E-05	1.31E-05	1.01E-06	4.01E-06	1.73E-06	1.40E-05	-1.43E-06	-1.43E-06	-9.39E-06	-1.27E-05	-1.62E-05	-1.96E-05	-2.09E-05	-2.31E-05	-2.37E-05	-1.28E-05		
2.32E-05	2.18E-05	1.94E-05	1.76E-05	1.41E-05	1.12E-05	8.00E-06	4.00E-06	5.09E-07	-2.63E-06	-5.09E-06	-8.34E-06	-1.30E-05	-1.65E-05	-1.94E-05	-2.22E-05	-2.59E-05	-2.86E-05	-8.46E-06		
2.21E-05	2.09E-05	1.90E-05	1.66E-05	1.38E-05	1.06E-05	7.46E-06	3.92E-06	5.69E-07	-2.75E-06	-5.68E-06	-8.82E-06	-1.15E-05	-1.41E-05	-1.62E-05	-1.76E-05	-1.84E-05	-1.90E-05	-1.78E-05		
2.16E-05	2.10E-05	1.87E-05	1.58E-05	1.27E-05	9.2E-05	6.94E-06	3.38E-06	1.60E-07	-3.08E-06	-6.11E-06	-9.19E-06	-1.19E-05	-1.44E-05	-1.70E-05	-1.83E-05	-1.87E-05	-1.87E-05	-1.55E-05		
2.51E-05	1.79E-05	2.11E-05	1.27E-05	1.35E-05	1.09E-05	6.40E-06	2.59E-06	3.49E-07</												

Table B.3 (Continued)

Table B.3 (Continued)

Table B.3 (Continued)

	4	4.05	4.1	4.15	4.2	4.25	4.3	4.35	4.4	4.45	4.5	4.55	4.6	4.65	4.7	4.75	4.8	4.85	4.9	4.95
-1.20E-03	1.99E-03	-4.48E-03	4.41E-03	-3.80E-03	-7.81E-03	-7.52E-03	-1.44E-02	-4.52E-02	-2.80E-01	4.81E-01	4.90E-01	1.58E-02	5.85E-03	3.44E-03	1.41E-03	7.50E-04	1.10E-03	-3.04E-03	2.04E-03	
5.87E-04	7.51E-04	1.28E-04	-2.90E-04	-9.20E-04	-1.84E-03	-3.96E-03	-8.77E-03	-1.62E-02	-1.44E-02	1.60E-02	1.75E-02	8.49E-03	4.11E-03	1.72E-03	8.58E-04	3.71E-04	-1.64E-04	-4.61E-04	-6.79E-04	
3.70E-04	3.26E-04	5.42E-05	-1.71E-04	-6.77E-04	-1.59E-03	-2.31E-03	-3.96E-03	-4.88E-03	-2.94E-03	2.69E-03	5.33E-03	4.15E-03	2.58E-03	1.30E-03	7.50E-04	1.02E-04	2.24E-04	-2.86E-04	-4.03E-04	
1.15E-04	1.76E-04	9.02E-07	2.42E-04	5.14E-04	-8.94E-04	-1.40E-03	-1.78E-03	-1.87E-03	-8.02E-04	8.65E-04	1.90E-03	1.80E-03	1.24E-03	1.01E-03	5.84E-04	2.02E-04	-1.04E-05	-1.71E-04	-2.21E-04	
1.49E-04	9.03E-05	-2.41E-05	-1.16E-04	-3.29E-04	-5.66E-04	-7.12E-04	-8.15E-04	-7.50E-04	-3.01E-04	3.82E-04	6.28E-04	8.75E-04	7.26E-04	4.81E-04	4.05E-05	8.73E-05	-1.80E-04			
1.58E-04	9.03E-05	2.45E-05	-1.85E-05	-2.98E-04	-5.90E-04	-1.18E-04	-3.41E-04	-1.18E-04	-1.29E-04	1.37E-04	3.04E-04	4.07E-04	3.81E-04	2.90E-04	1.42E-04	7.63E-05	-9.55E-06	-8.05E-05	-1.96E-04	
1.33E-04	1.02E-04	6.28E-05	-2.12E-05	-6.50E-05	-1.36E-04	-1.47E-04	-1.66E-04	-1.17E-04	-6.81E-05	5.68E-05	1.34E-04	1.54E-04	1.82E-04	1.22E-04	1.22E-04	4.74E-05	-9.76E-05	-4.13E-05	-1.10E-04	-1.50E-04
1.52E-04	1.14E-04	7.60E-05	4.45E-05	-7.04E-06	-3.54E-05	-5.22E-05	-5.19E-05	-5.22E-05	-3.07E-05	2.20E-05	5.06E-05	6.39E-05	6.91E-05	2.85E-05	1.24E-05	5.59E-05	-8.81E-05	-1.11E-04	-1.40E-04	
1.28E-04	1.17E-04	1.00E-04	7.07E-05	4.67E-05	2.47E-05	-1.55E-06	-1.32E-07	-2.23E-05	-1.47E-06	6.92E-06	1.52E-05	-3.82E-06	2.60E-06	-3.26E-05	-2.77E-05	-7.09E-05	-9.62E-05	-1.21E-04	-1.40E-04	
1.35E-04	1.25E-04	1.05E-04	8.93E-05	6.37E-05	4.37E-05	4.13E-05	4.13E-05	6.70E-06	1.56E-05	-1.61E-05	8.30E-06	-1.38E-05	-2.75E-05	-5.14E-05	-7.38E-05	-7.64E-05	-1.04E-04	-1.12E-04	-1.51E-04	
1.35E-04	1.22E-04	1.05E-04	9.43E-05	8.09E-05	4.41E-05	3.35E-05	1.18E-05	2.13E-05	1.18E-05	-1.93E-05	8.91E-06	-3.18E-05	4.58E-05	-6.38E-05	-7.88E-05	-9.15E-05	-1.10E-04	-1.20E-04	-1.34E-04	
1.26E-04	1.16E-04	1.11E-04	9.77E-05	7.90E-05	5.53E-05	3.50E-05	2.14E-05	4.37E-06	-3.91E-06	-2.03E-05	4.32E-05	-4.98E-05	6.37E-05	-8.05E-05	-8.05E-05	-6.37E-05	-6.37E-05	-1.25E-04		
1.19E-04	1.12E-04	1.05E-04	9.28E-05	7.91E-05	6.66E-05	5.35E-05	4.42E-05	1.90E-05	8.55E-06	-7.43E-06	-2.56E-05	-3.53E-05	5.28E-05	6.79E-05	-7.63E-05	-7.63E-05	-9.70E-05	-9.70E-05	-1.20E-04	
1.15E-04	1.00E-04	9.88E-05	8.67E-05	7.91E-05	6.52E-05	4.98E-05	3.67E-05	2.36E-05	8.18E-06	-8.32E-06	-2.18E-05	-3.28E-05	5.31E-05	-6.56E-05	-7.77E-05	-8.59E-05	-9.79E-05	-1.03E-04	-1.11E-04	
1.03E-04	9.65E-05	9.08E-05	8.26E-05	7.17E-05	6.15E-05	4.58E-05	3.54E-05	2.45E-05	5.12E-06	-4.80E-06	-2.17E-05	-3.41E-05	4.78E-05	-5.75E-05	-7.21E-05	-8.07E-05	-9.17E-05	-9.62E-05	-1.02E-04	
9.21E-05	9.29E-05	8.27E-05	7.62E-05	6.59E-05	5.71E-05	4.51E-05	3.26E-05	2.01E-05	6.94E-06	-5.79E-06	-2.03E-05	-3.10E-05	4.32E-05	-5.44E-05	-6.77E-05	-7.47E-05	-8.33E-05	-8.86E-05	-9.33E-05	
8.1E-05	8.28E-05	7.63E-05	7.00E-05	5.35E-05	3.50E-05	2.50E-05	1.72E-05	1.88E-05	1.72E-05	4.72E-05	-2.99E-05	4.06E-05	-5.04E-05	-6.02E-05	-6.02E-05	-6.02E-05	-6.69E-05	-7.52E-05	-8.34E-05	
7.92E-05	7.44E-05	6.36E-05	5.44E-05	4.74E-05	3.75E-05	2.72E-05	1.67E-05	5.77E-06	4.01E-06	-1.62E-05	-2.59E-05	3.62E-05	-4.72E-05	5.39E-05	6.12E-05	6.86E-05	7.62E-05	7.77E-05		
7.17E-05	6.81E-05	5.73E-05	5.02E-05	4.30E-05	3.31E-05	2.56E-05	1.61E-05	4.87E-06	-3.62E-06	-1.42E-05	-2.47E-05	-3.21E-05	-4.09E-05	-4.99E-05	-5.64E-05	-6.33E-05	-6.73E-05	-7.15E-05		
6.50E-05	5.96E-05	5.15E-05	4.56E-05	3.81E-05	3.16E-05	2.19E-05	1.36E-05	4.58E-06	-3.26E-06	-1.27E-05	-2.08E-05	-2.90E-05	-3.82E-05	-4.45E-05	-5.09E-05	-5.59E-05	-6.16E-05	-6.51E-05		
5.91E-05	5.64E-05	5.11E-05	4.63E-05	4.15E-05	3.31E-05	2.85E-05	2.05E-05	1.26E-05	5.21E-06	-3.36E-06	-1.17E-05	-1.85E-05	-2.66E-05	-3.35E-05	-4.06E-05	-4.53E-05	-5.14E-05	-5.46E-05	-5.92E-05	
5.36E-05	5.05E-05	4.66E-05	4.11E-05	3.72E-05	2.81E-05	2.48E-05	1.80E-05	1.18E-05	9.87E-06	-5.15E-06	-2.64E-06	-4.15E-06	-5.04E-06	-5.40E-05	-6.02E-05	-6.02E-05	-6.69E-05	-7.52E-05	-8.34E-05	
4.87E-05	4.55E-05	4.20E-05	3.76E-05	3.33E-05	2.85E-05	2.26E-05	1.72E-05	1.22E-05	9.70E-06	-3.63E-06	-8.44E-06	-1.52E-05	-2.47E-05	-3.21E-05	-4.09E-05	-4.99E-05	-5.64E-05	-6.33E-05	-7.15E-05	
4.38E-05	4.11E-05	3.80E-05	3.45E-05	3.00E-05	2.54E-05	2.02E-05	1.52E-05	9.22E-05	6.65E-06	-2.03E-06	-7.33E-06	-1.40E-05	-2.18E-05	-2.98E-05	-3.82E-05	-4.45E-05	-5.09E-05	-5.59E-05	-6.16E-05	
3.94E-05	3.65E-05	3.48E-05	3.10E-05	2.67E-05	2.31E-05	1.88E-05	1.32E-05	8.65E-06	3.86E-06	-1.90E-06	-7.23E-06	-1.21E-05	-1.63E-05	-2.19E-05	-2.61E-05	-3.23E-05	-3.96E-05	-4.59E-05		
3.55E-05	3.40E-05	3.02E-05	2.81E-05	2.45E-05	2.06E-05	1.66E-05	1.25E-05	7.73E-06	3.38E-06	-1.71E-06	-5.62E-06	-9.97E-06	-1.56E-05	-1.92E-05	-2.32E-05	-2.65E-05	-3.07E-05	-3.58E-05		
3.21E-05	3.03E-05	2.78E-05	2.52E-05	2.18E-05	1.90E-05	1.49E-05	1.11E-05	7.09E-06	3.06E-06	-1.21E-06	-5.15E-06	-9.22E-06	-1.33E-05	-1.62E-05	-2.08E-05	-2.42E-05	-2.73E-05	-3.23E-05		
2.94E-05	2.77E-05	2.49E-05	2.28E-05	2.00E-05	1.67E-05	1.35E-05	9.97E-06	6.66E-06	-6.16E-07	-4.35E-06	-8.12E-06	-1.21E-05	-1.85E-05	-2.45E-05	-2.71E-05	-3.09E-05	-3.49E-05			
2.62E-05	2.46E-05	2.31E-05	2.01E-05	1.80E-05	1.53E-05	1.25E-05	9.13E-05	5.70E-06	3.07E-06	-4.09E-07	-4.12E-06	-8.21E-06	-1.02E-05	-1.35E-05	-1.65E-05	-1.93E-05	-2.19E-05	-2.44E-05		
2.40E-05	2.21E-05	2.05E-05	1.84E-05	1.62E-05	1.40E-05	1.13E-05	8.18E-06	5.34E-06	2.82E-06	-5.06E-07	-3.06E-06	-6.14E-06	-9.23E-06	-1.20E-05	-1.45E-05	-1.72E-05	-1.96E-05	-2.20E-05		
2.15E-05	2.02E-05	1.86E-05	1.66E-05	1.47E-05	1.25E-05	9.92E-06	7.54E-06	5.06E-06	2.54E-06	-1.06E-07	-2.47E-06	-5.59E-06	-7.72E-06	-1.06E-05	-1.27E-05	-1.52E-05	-1.77E-05	-1.95E-05		
1.94E-05	1.83E-05	1.66E-05	1.49E-05	1.31E-05	1.11E-05	8.97E-06	4.58E-06	2.59E-06	2.15E-06	-2.15E-06	-4.40E-06	-6.91E-06	-8.87E-06	-1.13E-05	-1.35E-05	-1.54E-05	-1.81E-05	-1.94E-05		
1.75E-05	1.62E-05	1.50E-05	1.33E-05	1.19E-05	9.96E-06	8.18E-06	5.93E-06	4.22E-06	2.50E-06	-2.46E-07	-2.12E-06	-3.71E-06	-5.75E-06	-7.55E-06	-9.87E-06	-1.13E-05	-1.34E-05	-1.57E-05		
1.56E-05	1.44E-05	1.31E-05	1.20E-05	1.06E-05	8.72E-06	7.05E-06	5.59E-06	3.91E-06	2.33E-06	-2.38E-07	-1.31E-06	-2.64E-06	-4.38E-06	-6.44E-06	-8.30E-06	-1.07E-05	-1.24E-05	-1.38E-05		
1.30E-05	1.38E-05	9.89E-06	8.65E-06	8.65E-06	7.60E-06	5.54E-06	4.93E-06	4.80E-06	2.38E-06	-2.40E-07	-1.51E-06	-1.12E-06	-3.11E-06	-4.64E-06	-6.93E-06	-1.03E-05	-1.13E-05	-1.25E-05		
7.60E-06	8.16E-06	7.12E-06	6.97E-06	6.97E-06	5.98E-06	5.65E-06	3.37E-06	1.26E-05	8.88E-06	-8.32E-07	-2.01E-06	-3.83E-07	-2.49E-07	-3.71E-06	-1.02E-06	-1.79E-05	-2.11E-06	-2.25E-05		
9.16E-06	7.55E-06	8.82E-06	5.59E-06	1.18E-05	9.81E-06	3.63E-06	4.57E-06	9.63E-07	4.65E-06	5.10E-06	8.14E-07	-1.24E-06	-1.95E-06	-2.42E-06	-3.81E-06	-1.68E-05	-1.08E-05	-8.89E-06		
1.98E-06	1.51E-05	4.65E-06	5.25E-06	1.03E-05	1.03E-05	5.86E-06	5.28E-06	2.75E-06	-4.44E-06	-3.95E-06	5.76E-06	9.84E-06	8.79E-07	-2.47E-05	-9.66E-06	-1.35E-05	-1.11E-05	-9.75E-06		
-5.58E-07	1.66E-05	6.66E-06	-3.72E-07	1.73E-07	5.69E-06	3.10E-06	1.89E-06	-2.00E-07	2.51E-06	-6.93E-06	6.43E-06	-1.46E-05	-1.46E-05	-1.46E-05	-1.46E-05	-1.46E-05	-1.46E-05	-1.53E-05		
1.78E-06	1.98E-06	3.59E-06	7.9E-06	2.78E-06	7.96E-06	5.37E-06	2.37E-06	1.99E-07	-2.37E-06	-1.80E-06	-9.97E-08	3.71E-05	9.11E-06	-9.46E-06	-5.82E-06	-6.03E-06	-9.21E-06	-1.18E-05		
1.35E-06	1.95E-05	1.65E-05	3.87E-06	6.98E-06	4.59E-06	2.21E-06	-1.60E-07	2.52E-06	-4.87E-06	-7.22E-06	-9.55E-06	6.24E-05	-2.20E-06	-2.13E-06	-6.05E-06	-7.97E-06	-9.88E-06	-1		

Table B.3 (Continued)

5	5.05	5.1	5.15	5.2	5.25	5.3	5.35	5.4	5.45	5.5	5.55	5.6	5.65	5.7	5.75	5.8	5.85	5.9	5.95
-3.321E-04	-1.93E-03	-1.22E-04	-1.57E-03	4.33E-04	-1.43E-03	-3.01E-04	1.02E-04	-2.17E-04	-2.05E-04	-8.59E-04	-1.83E-03	-2.07E-03	-6.14E-04	7.69E-04	-1.11E-03	-1.03E-03	-1.03E-03	2.56E-03	
-6.413E-04	-3.73E-05	-5.29E-04	-8.73E-05	-1.31E-03	-5.29E-04	-1.08E-03	-2.65E-04	-3.18E-04	-4.64E-04	-9.62E-04	-2.02E-04	-4.13E-04	-3.29E-04	-3.89E-04	-8.85E-04	-2.88E-04	-1.98E-04	-1.98E-04	
-4.50E-04	-4.64E-04	-5.12E-04	-4.9E-04	-4.34E-04	-4.19E-04	-3.71E-04	-2.96E-04	-3.57E-04	-3.57E-04	-1.64E-04	-2.24E-04	-1.42E-04	-1.89E-04	-1.30E-04	-3.06E-04	-1.63E-04	-5.99E-06	-1.38E-04	
-2.118E-04	-1.80E-04	-2.86E-04	-3.37E-04	-2.45E-04	-2.86E-04	-3.11E-04	-2.68E-04	-3.09E-04	-2.35E-04	-2.24E-04	-1.43E-04	-1.43E-04	-1.21E-04	-1.89E-04	-1.95E-04	-9.96E-05	-2.70E-05	-5.23E-04	
-2.86E-04	-3.11E-04	-2.62E-04	-2.75E-04	-3.87E-04	-2.63E-04	-2.62E-04	-2.62E-04	-2.21E-04	-2.13E-04	-1.74E-04	-1.43E-04	-1.43E-04	-1.25E-04	-1.12E-04	-1.25E-04	-7.41E-05	-8.16E-05	-9.11E-07	
-2.27E-04	-2.50E-04	-2.39E-04	-2.49E-04	-2.10E-04	-2.01E-04	-2.01E-04	-2.08E-04	-2.08E-04	-1.98E-04	-1.81E-04	-1.45E-04	-1.49E-04	-1.60E-04	-1.42E-04	-1.42E-04	-1.20E-05	-4.20E-05	-4.31E-05	
-1.69E-04	-2.02E-04	-1.87E-04	-2.10E-04	-1.93E-04	-1.86E-04	-1.78E-04	-1.99E-04	-1.84E-04	-1.84E-04	-1.61E-04	-1.44E-04	-1.31E-04	-1.21E-04	-1.21E-04	-1.21E-04	-9.01E-05	-9.16E-05	-2.44E-05	
-1.58E-04	-1.74E-04	-1.86E-04	-1.74E-04	-1.58E-04	-1.77E-04	-1.75E-04	-1.58E-04	-1.77E-04	-1.77E-04	-1.62E-04	-1.22E-04	-1.22E-04	-1.22E-04	-1.22E-04	-1.22E-04	-9.01E-05	-8.70E-05	-5.26E-06	
-1.59E-04	-1.74E-04	-1.60E-04	-1.59E-04	-1.55E-04	-1.51E-04	-1.56E-04	-1.58E-04	-1.47E-04	-1.47E-04	-1.61E-04	-1.22E-04	-1.22E-04	-1.22E-04	-1.22E-04	-1.22E-04	-9.63E-05	-8.46E-05	-4.41E-06	
-1.38E-04	-1.51E-04	-1.52E-04	-1.46E-04	-1.46E-04	-1.40E-04	-1.39E-04	-1.24E-04	-1.24E-04	-1.23E-04	-1.07E-04	-1.03E-04	-1.03E-04	-1.03E-04	-1.03E-04	-1.03E-04	-8.90E-05	-7.79E-05	-5.12E-06	
-1.34E-04	-1.37E-04	-1.38E-04	-1.40E-04	-1.36E-04	-1.37E-04	-1.37E-04	-1.28E-04	-1.30E-04	-1.19E-04	-1.08E-04	-1.04E-04	-1.04E-04	-1.04E-04	-1.04E-04	-1.04E-04	-8.46E-05	-7.08E-05	-1.39E-06	
-1.24E-04	-1.28E-04	-1.31E-04	-1.29E-04	-1.27E-04	-1.29E-04	-1.29E-04	-1.27E-04	-1.27E-04	-1.27E-04	-1.21E-04	-1.16E-04	-1.16E-04	-1.16E-04	-1.16E-04	-1.16E-04	-7.82E-05	-6.40E-05	-6.53E-06	
-1.14E-04	-1.14E-04	-1.20E-04	-1.18E-04	-1.17E-04	-1.17E-04	-1.17E-04	-1.17E-04	-1.17E-04	-1.17E-04	-1.01E-04	-9.44E-05	-8.58E-05	-7.82E-05	-7.82E-05	-7.82E-05	-6.15E-05	-4.25E-05	-3.89E-05	
-1.07E-04	-1.07E-04	-1.07E-04	-1.07E-04	-1.07E-04	-1.07E-04	-1.07E-04	-1.07E-04	-1.07E-04	-1.07E-04	-1.01E-04	-9.58E-05	-8.01E-05	-6.42E-05	-6.42E-05	-6.42E-05	-5.75E-05	-3.93E-05	-2.94E-05	
-9.62E-05	-1.05E-04	-1.01E-04	-9.58E-05	-8.96E-05	-6.42E-05	-6.42E-05	-6.42E-05	-5.75E-05	-3.94E-05	-2.95E-05									
-8.90E-05	-9.23E-05	-8.95E-05																	
-8.38E-05	-8.38E-05	-8.38E-05	-8.38E-05	-8.38E-05	-8.38E-05	-8.38E-05	-8.38E-05	-8.38E-05	-8.38E-05	-8.14E-05	-7.49E-05	-7.06E-05	-6.33E-05	-6.33E-05	-6.33E-05	-5.62E-05	-4.35E-05	-3.53E-05	
-7.84E-05	-7.84E-05	-7.84E-05	-7.84E-05	-7.84E-05	-7.84E-05	-7.84E-05	-7.84E-05	-7.84E-05	-7.84E-05	-7.31E-05	-6.96E-05	-6.47E-05	-5.88E-05	-5.88E-05	-5.88E-05	-5.28E-05	-3.89E-05	-3.37E-05	
-7.31E-05	-7.31E-05	-7.31E-05	-7.31E-05	-7.31E-05	-7.31E-05	-7.31E-05	-7.31E-05	-7.31E-05	-7.31E-05	-6.71E-05	-6.32E-05	-5.64E-05	-5.15E-05	-5.15E-05	-5.15E-05	-4.78E-05	-3.74E-05	-3.24E-05	
-6.86E-05	-6.86E-05	-6.86E-05	-6.86E-05	-6.86E-05	-6.86E-05	-6.86E-05	-6.86E-05	-6.86E-05	-6.86E-05	-6.32E-05	-5.96E-05	-5.46E-05	-4.94E-05	-4.94E-05	-4.94E-05	-4.45E-05	-3.57E-05	-3.00E-05	
-6.40E-05	-6.40E-05	-6.40E-05	-6.40E-05	-6.40E-05	-6.40E-05	-6.40E-05	-6.40E-05	-6.40E-05	-6.40E-05	-5.96E-05	-5.51E-05	-5.15E-05	-4.62E-05	-4.62E-05	-4.62E-05	-4.23E-05	-3.24E-05	-2.74E-05	
-5.95E-05	-5.95E-05	-5.95E-05	-5.95E-05	-5.95E-05	-5.95E-05	-5.95E-05	-5.95E-05	-5.95E-05	-5.95E-05	-5.51E-05	-5.15E-05	-4.73E-05	-4.32E-05	-4.32E-05	-4.32E-05	-3.93E-05	-3.57E-05	-3.14E-05	
-5.56E-05	-5.56E-05	-5.56E-05	-5.56E-05	-5.56E-05	-5.56E-05	-5.56E-05	-5.56E-05	-5.56E-05	-5.56E-05	-5.15E-05	-4.73E-05	-4.32E-05	-3.93E-05	-3.93E-05	-3.93E-05	-3.53E-05	-3.14E-05	-2.74E-05	
-5.17E-05	-5.17E-05	-5.17E-05	-5.17E-05	-5.17E-05	-5.17E-05	-5.17E-05	-5.17E-05	-5.17E-05	-5.17E-05	-4.73E-05	-4.32E-05	-3.93E-05	-3.53E-05	-3.53E-05	-3.53E-05	-3.14E-05	-2.74E-05	-2.34E-05	
-4.81E-05	-4.81E-05	-4.81E-05	-4.81E-05	-4.81E-05	-4.81E-05	-4.81E-05	-4.81E-05	-4.81E-05	-4.81E-05	-4.42E-05	-4.21E-05	-3.91E-05	-3.56E-05	-3.56E-05	-3.56E-05	-3.12E-05	-2.69E-05	-2.23E-05	
-4.46E-05	-4.46E-05	-4.46E-05	-4.46E-05	-4.46E-05	-4.46E-05	-4.46E-05	-4.46E-05	-4.46E-05	-4.46E-05	-4.11E-05	-3.89E-05	-3.57E-05	-3.28E-05	-3.28E-05	-3.28E-05	-2.82E-05	-2.43E-05	-2.03E-05	
-4.17E-05	-4.17E-05	-4.17E-05	-4.17E-05	-4.17E-05	-4.17E-05	-4.17E-05	-4.17E-05	-4.17E-05	-4.17E-05	-3.89E-05	-3.57E-05	-3.28E-05	-2.93E-05	-2.93E-05	-2.93E-05	-2.52E-05	-2.13E-05	-1.74E-05	
-3.82E-05	-3.82E-05	-3.82E-05	-3.82E-05	-3.82E-05	-3.82E-05	-3.82E-05	-3.82E-05	-3.82E-05	-3.82E-05	-3.51E-05	-3.21E-05	-2.93E-05	-2.65E-05	-2.65E-05	-2.65E-05	-2.28E-05	-1.88E-05	-1.49E-05	
-3.45E-05	-3.45E-05	-3.45E-05	-3.45E-05	-3.45E-05	-3.45E-05	-3.45E-05	-3.45E-05	-3.45E-05	-3.45E-05	-3.14E-05	-2.84E-05	-2.54E-05	-2.25E-05	-2.25E-05	-2.25E-05	-1.84E-05	-1.44E-05	-1.04E-06	
-3.11E-05	-3.11E-05	-3.11E-05	-3.11E-05	-3.11E-05	-3.11E-05	-3.11E-05	-3.11E-05	-3.11E-05	-3.11E-05	-2.84E-05	-2.54E-05	-2.25E-05	-1.84E-05	-1.84E-05	-1.84E-05	-1.44E-05	-1.04E-05	-6.56E-06	
-2.84E-05	-2.84E-05	-2.84E-05	-2.84E-05	-2.84E-05	-2.84E-05	-2.84E-05	-2.84E-05	-2.84E-05	-2.84E-05	-2.54E-05	-2.25E-05	-1.84E-05	-1.44E-05	-1.44E-05	-1.44E-05	-1.04E-05	-6.56E-06	-2.34E-05	
-2.55E-05	-2.55E-05	-2.55E-05	-2.55E-05	-2.55E-05	-2.55E-05	-2.55E-05	-2.55E-05	-2.55E-05	-2.55E-05	-2.25E-05	-1.94E-05	-1.54E-05	-1.14E-05	-1.14E-05	-1.14E-05	-7.98E-06	-3.74E-06	-1.33E-06	
-2.26E-05	-2.26E-05	-2.26E-05	-2.26E-05	-2.26E-05	-2.26E-05	-2.26E-05	-2.26E-05	-2.26E-05	-2.26E-05	-1.94E-05	-1.54E-05	-1.14E-05	-7.98E-06	-7.98E-06	-7.98E-06	-3.74E-06	-1.33E-06	-1.33E-06	
-1.90E-05	-1.90E-05	-1.90E-05	-1.90E-05	-1.90E-05	-1.90E-05	-1.90E-05	-1.90E-05	-1.90E-05	-1.90E-05	-1.54E-05	-1.14E-05	-7.98E-06	-7.98E-06	-7.98E-06	-7.98E-06	-3.74E-06	-1.33E-06	-1.33E-06	
-1.60E-05	-1.60E-05	-1.60E-05	-1.60E-05	-1.60E-05	-1.60E-05	-1.60E-05	-1.60E-05	-1.60E-05	-1.60E-05	-1.21E-05	-8.14E-06	-4.14E-06	-1.14E-05	-1.14E-05	-1.14E-05	-7.98E-06	-3.74E-06	-1.33E-06	
-1.31E-05	-1.31E-05	-1.31E-05	-1.31E-05	-1.31E-05	-1.31E-05	-1.31E-05	-1.31E-05	-1.31E-05	-1.31E-05	-9.79E-06	-5.79E-06	-2.79E-06	-1.31E-05	-1.31E-05	-1.31E-05	-7.98E-06	-3.74E-06	-1.33E-06	
-1.01E-05	-1.01E-05	-1.01E-05	-1.01E-05	-1.01E-05	-1.01E-05	-1.01E-05	-1.01E-05	-1.01E-05	-1.01E-05	-6.79E-06	-3.79E-06	-1.79E-06	-1.01E-05	-1.01E-05	-1.01E-05	-7.98E-06	-3.74E-06	-1.33E-06	
-7.17E-06	-7.17E-06	-7.17E-06	-7.17E-06	-7.17E-06	-7.17E-06	-7.17E-06	-7.17E-06	-7.17E-06	-7.17E-06	-3.79E-06	-1.79E-06	-1.79E-06	-1.79E-06	-1.79E-06	-1.79E-06	-7.98E-06	-3.74E-06	-1.33E-06	
-4.17E-06	-4.17E-06	-4.17E-06	-4.17E-06	-4.17E-06	-4.17E-06	-4.17E-06	-4.17E-06	-4.17E-06	-4.17E-06	-1.79E-06	-1.79E-06	-1.79E-06	-1.79E-06	-1.79E-06	-1.79E-06	-7.98E-06	-3.74E-06	-1.33E-06	
-1.14E-06	-1.14E-06	-1.14E-06	-1.14E-06	-1.14E-06	-1.14E-06	-1.14E-06	-1.14E-06	-1.14E-06	-1.14E-06	-1.14E-06	-1.14E-06	-1.14E-06	-1.14E-06	-1.14E-06	-1.14E-06	-7.98E-06	-3.74E-06	-1.33E-06	
-1.84E-05	-1.84E-05	-1.84E-05	-1.84E-05	-1.84E-05	-1.84E-05	-1.84E-05	-1.84E-05	-1.84E-05	-1.84E-05	-1.84E-05	-1.84E-05	-1.84E-05	-1.84E-05	-1.84E-05	-1.84E-05	-8.0E-06	-4.0E-06	-2.0E-06	
-1.53E-05	-1.53E-05	-1.53E-05	-1.53E-05	-1.53E-05	-1.53E-05	-1.53E-05	-1.53E-05	-1.53E-05	-1.53E-05	-1.53E-05	-1.53E-05	-1.53E-05	-1.53E-05	-1.53E-05	-1.53E-05	-8.0E-06	-4.0E-06	-2.0E-06	

## B.6 Fitting curve for magnetic force equations by *cftool* command in MATLAB

The force equation fit by this study consists of two components of function as follows

$$f_{mag}(x, z) = f_1(x) \times f_2(z)$$

$f_1(x)$  is the function depending on position in only x-axis. Besides,  $f_2(z)$  is the function depending on position in only z-axis. This study gathers data of the magnetic force at the certain distance in order to fit one variable function.

The example of fitting curve is shown in fig B.8 – B.11

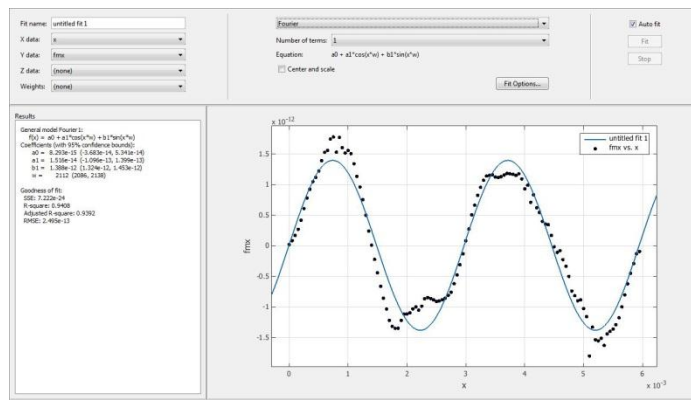


Figure B.8 fitting curve of the magnetic force in x-axis and the component of fourier series

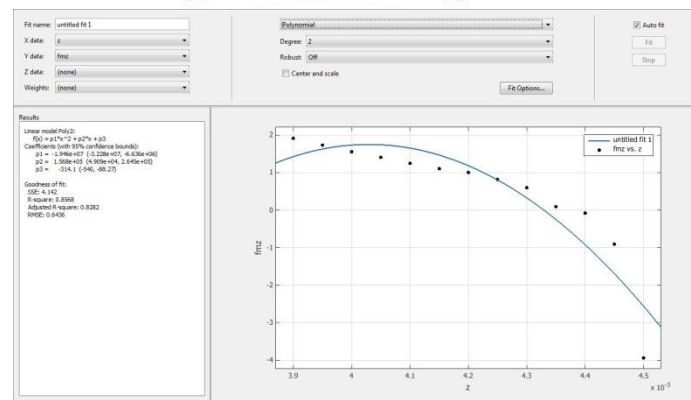


Figure B.9 fitting curve of the magnetic force in x-axis and the component of quadratic equations

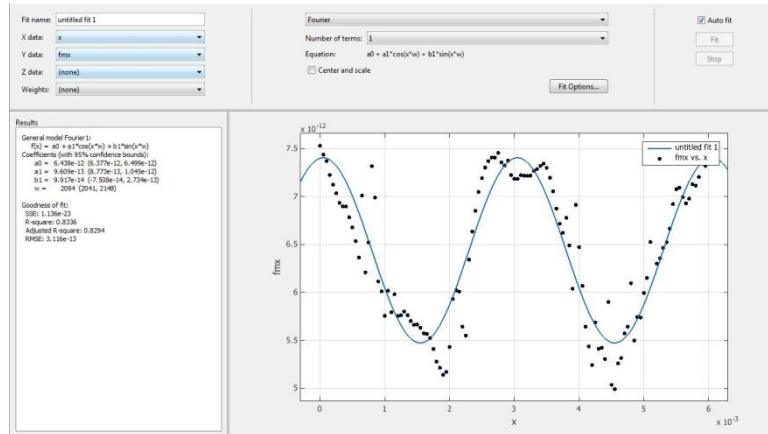


Figure B.10 fitting curve of the magnetic force in x-axis and the component of fourier series

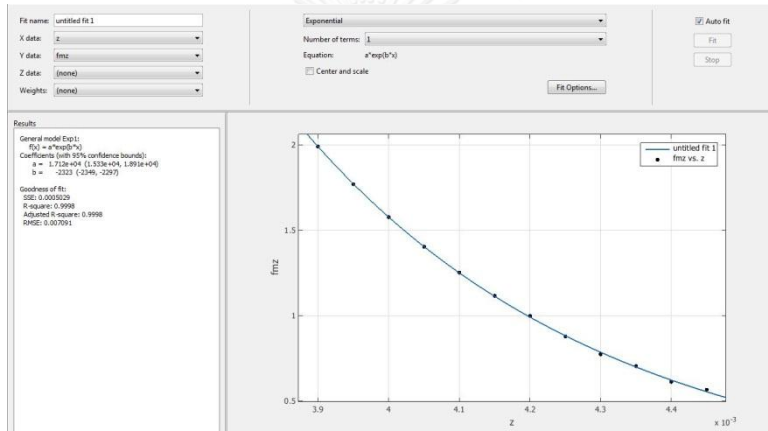


Figure B.11 fitting curve of the magnetic force in x-axis and the component of exponential equations

### 6.1 magnetic force equations for 5- $\mu\text{m}$ magnetic beads

The magnetic force equation in x-axis

$$f_1(x) = 8.293 \times 10^{-15} + 1.516 \times 10^{-14} \cos(2112x) + 1.388 \times 10^{-12} \sin(2112x)$$

$$f_2(z) = -6.914 \times 10^6 z^2 + 5.332 \times 10^4 z - 101$$

The magnetic force equation in z-axis

$$f_1(x) = 6.438 \times 10^{-12} + 9.609 \times 10^{-13} \cos(2094x) + 9.917 \times 10^{-14} \sin(2094x)$$

$$f_2(z) = 1.712 \times 10^4 e^{-2323}$$

### 6.2 magnetic force equations for 10- $\mu\text{m}$ magnetic beads

The magnetic force equation in x-axis

$$f_1(x) = 6.634 \times 10^{-14} + 1.213 \times 10^{-13} \cos(2112x) + 1.111 \times 10^{-11} \sin(2112x)$$

$$f_2(z) = -8.936 \times 10^{-14} e^{6871z} + 380.5 e^{-1358z}$$

The magnetic force equation in z-axis

$$f_1(x) = 5.151 \times 10^{-11} + 7.687 \times 10^{-12} \cos(2094x) + 7.933 \times 10^{-13} \sin(2094x)$$

$$f_2(z) = 1.712 \times 10^4 e^{-2323z}$$

### 6.3 magnetic force equations for infected erythrocytes

The magnitude of magnetic force in x-axis already calculated is too low comparing to the size of drag force. Therefore, the magnetic force equation in x-axis is neglected.

#### 6.3.1 Wall thickness 100 $\mu\text{m}$

The magnetic force equation in z-axis

$$f_1(x) = 1.383 \times 10^{-15} + 2.734 \times 10^{-17} \cos(2094x) - 1.17 \times 10^{-20} \sin(2094x)$$

$$+ 2.913 \times 10^{-17} \cos(2 \times 2094x) + 1.933 \times 10^{-19} \sin(2 \times 2094x)$$

$$- 2.014 \times 10^{-17} \cos(3 \times 2094x) + 2.212 \times 10^{-19} \sin(3 \times 2094x)$$

$$+ 9.52 \times 10^{-18} \cos(4 \times 2094x) + 6.058 \times 10^{-20} \sin(4 \times 2094x)$$

$$f_2(z) = 4.723 \times 10^{17} e^{-1.52 \times 10^4 z} + 1.593 \times 10^4 e^{-3344z}$$

#### 6.3.2 Wall thickness 200 $\mu\text{m}$

The magnetic force equation in z-axis

$$f_1(x) = 9.688 \times 10^{-16} + 3.976 \times 10^{-17} \cos(2094x) + 1.999 \times 10^{-19} \sin(2094x)$$

$$+ 8.639 \times 10^{-18} \cos(2 \times 2094x) - 1.056 \times 10^{-19} \sin(2 \times 2094x)$$

$$- 6.43 \times 10^{-18} \cos(3 \times 2094x) + 5.17 \times 10^{-19} \sin(3 \times 2094x)$$

$$+ 2.925 \times 10^{-18} \cos(4 \times 2094x) - 1.534 \times 10^{-19} \sin(4 \times 2094x)$$

$$f_2(z) = 7.274 \times 10^{11} e^{-9906z} + 2369 e^{-2623z}$$

#### 6.3.3 Wall thickness 300 $\mu\text{m}$

The magnetic force equation in z-axis

$$f_1(x) = 7.063 \times 10^{-16} + 4.373 \times 10^{-17} \cos(2094x) + 1.357 \times 10^{-19} \sin(2094x)$$

$$f_2(z) = 1.487 \times 10^{10} e^{-8350z} + 2265 e^{-2521z}$$

## Appendix C. Computational methodology

### C.1 Force Analysis

According to Basset-Bousinesq-Oseen equation (BBO), the force acting on target objects is drag force, pressure gradient force, added mass effect, basset force and summation of additional forces. This section will explain the detail of each force and give the reason why this study neglected some forces in the model.

Drag force is the total net force resulting from fluid which exerts the force in the parallel direction of flow direction. This force depends on viscosity, size of targeted objects and relative velocity between the fluid velocity and the particle velocity. In this study, drag force can both decelerate and accelerate the particles depending on the position during the observation.

Pressure gradient force is the force exerting on the particles because of pressure drop inside the channel. Some studies neglected this term from the motion equation and argued that this force is already included in fluid inertia force. Although there are some suggestions to neglect that term, this section shows the calculation of the force order by using the equation as follows [33, 34]

$$F_{\text{pressuregradient}} = \frac{\pi}{6} D^3 \nabla p \quad (\text{C.1.1})$$

$\nabla p$  is pressure gradient term which can be described by Navier-Stoke equation as

$$\nabla p = \rho_f \frac{DU}{Dt} - \mu \nabla^2 u \quad (\text{C.1.2})$$

The expansion of Equation (C.1.2) only in the x-axis is

$$\frac{\partial p}{\partial x} = \rho_f \left( \frac{\partial u}{\partial t} + u \frac{\partial u}{\partial x} + v \frac{\partial u}{\partial x} + w \frac{\partial u}{\partial x} \right) - \mu \left( \frac{\partial^2 u}{\partial x^2} + \frac{\partial^2 u}{\partial y^2} + \frac{\partial^2 u}{\partial z^2} \right) \quad (\text{C.1.3})$$

Assume that the flow will be steady and no properties vary in the x-axis and the velocity considered in the study will be the function of z-coordinate. Therefore, Equation (C.1.3) can be deducted as follows

$$\frac{\partial p}{\partial x} = -\mu \frac{\partial^2 u}{\partial z^2} \quad (\text{C.1.4})$$

Thus, the pressure gradient force is in the form as describes

$$F_{\text{pressuregradient}} = \frac{\pi}{6} D^3 (-\mu \frac{\partial^2 u}{\partial z^2}) \quad (\text{C.1.5})$$

The force acting on the targeted objects by pressure gradient effect is constant in each case. The magnitude of pressure gradient force is shown in the Table C.1

Table C.1 the magnitude of pressure gradient force acting on particles

Medium	Size of particles ( $\mu\text{m}$ )	Force (pN)
DI water	5 $\mu\text{m}$	0.00138
	10 $\mu\text{m}$	0.0110
PBS	5 $\mu\text{m}$	0.00154
	10 $\mu\text{m}$	0.0124

Added mass effect or virtual mass effect is the effect coming from the accelerating or decelerating of particles moving in the fluid. This effect may happen when the fluid takes the kinetic energy resulting from work done by the accelerating particles. The equation can be shown as follows

$$F_{\text{addedmass}} = \frac{\pi}{6} \rho_f D^3 \frac{d}{dt} (v_f - v_p) \quad (\text{C.1.6})$$

The magnitude of this force results from several parameters which are density of fluid and the acceleration of relative velocity. However, in this case, this study defined the condition of flow as steady state; therefore, the acceleration of fluid must be zero. The magnitude of this force is predominantly impacted by the acceleration of the particles. After replacing all constant values, added mass force acting on 5- and 10- $\mu\text{m}$  beads as describes

$$F_{addedmass,5} = -6.54 \times 10^{-14} \left( \frac{d}{dt} (v_p) \right) \quad (\text{C.1.7})$$

$$F_{addedmass,10} = -5.24 \times 10^{-13} \left( \frac{d}{dt} (v_p) \right) \quad (\text{C.1.8})$$

From calculating acceleration of particles, the objects will be accelerated or decelerated in the order of  $10^{-4} \sim 10^{-5}$  m/s<sup>2</sup>. Consequently, the order of added mass will reach approximately  $10^{-17} \sim 10^{-18}$  N which is quite low comparing to the order of drag force. Thus, the added mass effect can be neglected from the model.

Basset force is the effect coming from the viscous effect and delay of developing a boundary layer in the area near to the moving particles which is also accelerated or decelerated. Many studies suggest that the Basset force is hard to operate and generally neglected. However, if the particles move with high acceleration, then the model needs to consider carefully. The Basset force equation is described as

$$F_{basset} = \frac{3}{2} D^2 \sqrt{\pi \mu_f \rho_f} \int_{t_0}^t \frac{1}{\sqrt{t-\tau}} \frac{d}{dt} (v_f - v_p) d\tau \quad (\text{C.1.9})$$

After deriving Equation (C.1.9), the simplified form of Basset force equation will be as follows

$$F_{basset} = -\frac{3}{2} D^2 \sqrt{\pi \mu_f \rho_f} \cdot 2\sqrt{t} \frac{d}{dt} (v_p) \quad (\text{C.1.10})$$

Replace the constant value to Equation (C.1.10). Then, get the Basset force exerting on 5- and 10- $\mu\text{m}$  beads with two mediums, DI water and PBS, as describes

$$F_{basset,5,DI} = 1.26 \times 10^{-10} \sqrt{t} \frac{d}{dt} (v_p) \quad (\text{C.1.11})$$

$$F_{basset,10,DI} = 5.02 \times 10^{-10} \sqrt{t} \frac{d}{dt} (v_p) \quad (\text{C.1.12})$$

$$F_{basset,5,PBS} = 1.23 \times 10^{-10} \sqrt{t} \frac{d}{dt} (v_p) \quad (\text{C.1.13})$$

$$F_{basset,10,PBS} = 5.32 \times 10^{-10} \sqrt{t} \frac{d}{dt} (v_p) \quad (\text{C.1.14})$$

As mentioned above, the order of moving particles in this study is in the range of  $10^{-4} \sim 10^{-5}$  m/s<sup>2</sup>. Besides, the time step used need to be lower than  $10^{-7}$  s due to finite difference calculation. Therefore, the summation of the order by Basset effect is around the range of  $10^{-17} \sim 10^{-18}$  N, which can be clearly neglected.

In order to verify the model excluding the effect of added mass and Basset force, this study compared the computational result between adding the basset force and added mass effect into the model and the model without those effects. The result illustrated in Figure C.1.1 and Figure C.1.2 has determined that there is no difference between these two models. Therefore, the model can neglect these two effects.

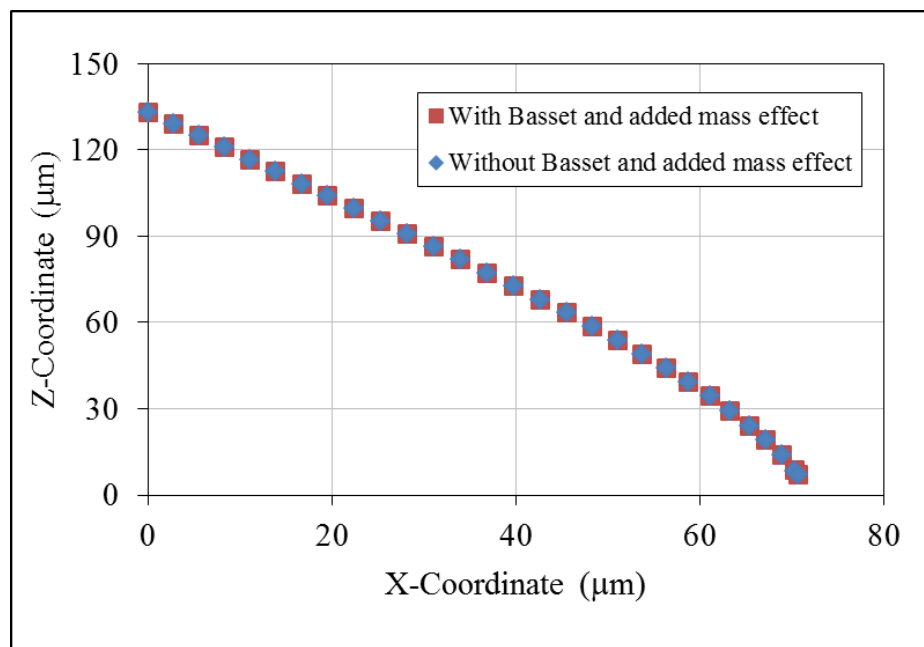


Figure C.1.1 the trajectories of 5- $\mu\text{m}$  magnetic beads in DI water under flow rate 2  $\mu\text{L}/\text{min}$  the condition between including and excluding added mass and Basset effect.

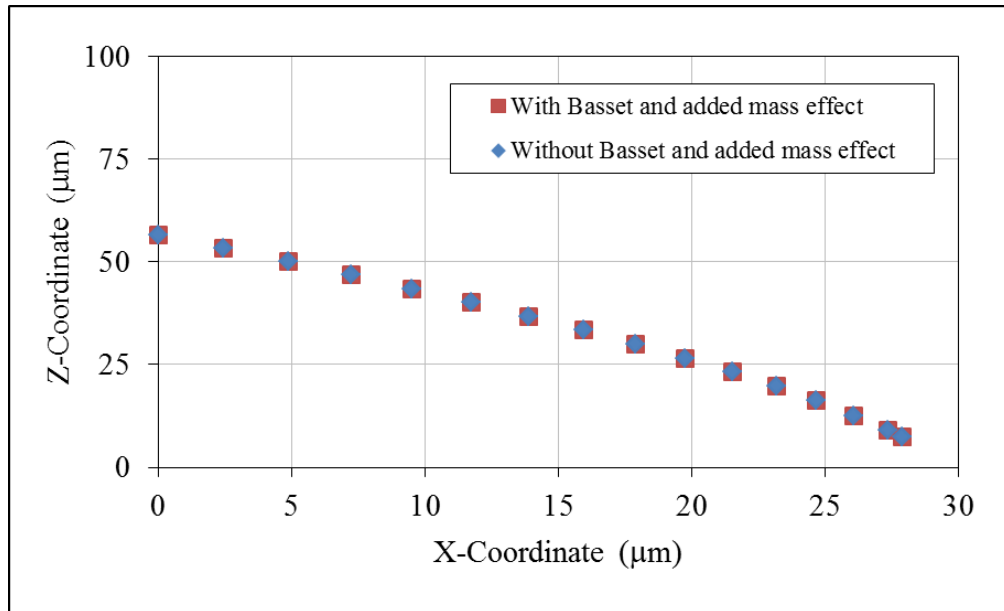


Figure C.1.2 the trajectories of 5- $\mu\text{m}$  magnetic beads in PBS under flow rate 2  $\mu\text{L}/\text{min}$  the condition between including and excluding added mass and Basset effect.

In sum, the effect of added mass and Basset force as well as pressure gradient force which is still being argued whether it should be included in the motion equation or not are totally neglected. The model in this study will propose to consider just merely two forces which are drag force and magnetic force.

## C.2 Trajectory of blood cells by the influence of defined constant magnetic force

This study has defined the coordinate shown in Figure C.2.1a by giving x-axis as flow direction, y-axis as the vertical direction comparing to the height of the channel and z-axis as the lateral direction. The force diagram is also represented in Figure C.2.1b. In this model, we have modelled the shape of red blood cells as the spherical shape. Trajectory of the model has been computed by using the Newton's motion equation. Besides, the equations used in the study are in the form of differential equations as follows

$$-\rho_{cell}V_{BC}g + 6\pi\mu_f a \frac{dy}{dt} + C_L \rho_f a^4 \left( \frac{U_{max}}{2wh/(w+h)} \right)^2 + \rho_f V_{BC}g = \rho_{cell}V_{BC} \frac{d^2y}{dt^2} \quad (C.2.1)$$

$$F_m - 6\pi\mu_f a \frac{dz}{dt} = \rho_{cell} \nabla \frac{d^2z}{dt^2} \quad (C.2.2)$$

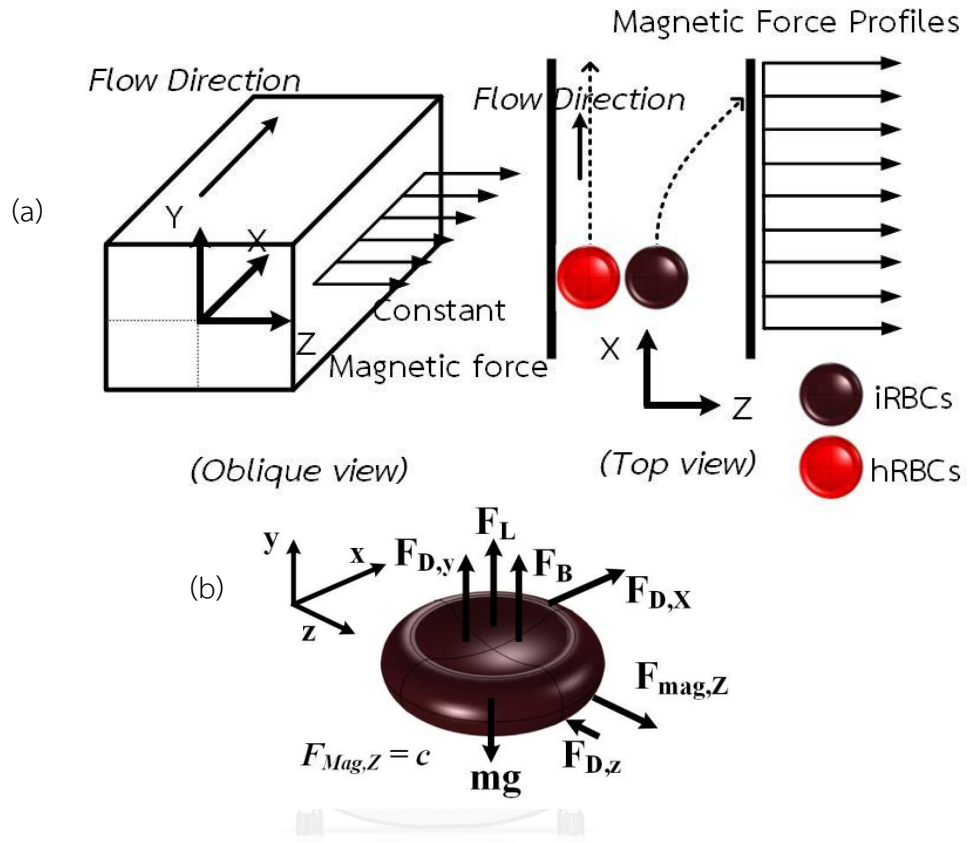


Figure C.2.1 (a) the schematic diagram of study domain (b) the force diagram acting on blood cells exposed to the given constant magnetic force.

However, the set of equations cannot be solved analytically. We therefore propose the solving method by using the 4<sup>th</sup> order Runge-Kutta coded in MATLAB. The detail of programming code is shown in Appendix A.2.

The defined conditions used in the study are following

1. The magnitude of magnetic force acting on cells is constant value represented in Tables 2.1 and 2.2
2. Consider the size of the targeted cells with 5 and 10  $\mu\text{m}$  in diameter because the size of actual red blood cells varies from 3 to 9  $\mu\text{m}$  in diameter
3. No relative motion between fluid velocity and particle velocity

#### 4. No interaction between cells and neglect all secondary flow effects

First of all, the motion equation is calculated only in y-axis so that we can know how the modeled object moves and what the trajectory is in y-coordinate. The result of calculation suggests that both sizes of targeted object have the tendency to move toward the floor of the channel thanks to the predominance of gravitational force shown in Figure C.2.2. In addition, they take the distance in x-axis around 0.5 and 2.5 millimeters for 5 and 10  $\mu\text{m}$  beads respectively. Consequently, we need to add one more assumption into the rest of the computation that is the object will move on the floor plane under flow rate 0.06 and 0.15  $\mu\text{L}/\text{min}$ .

The rest of the computation is performed. We can draw some conclusions from the result shown in Figure C.2.3. First, the sign of the relative magnetic susceptibilities results in the difference of the direction of blood cell motions. Both types of erythrocytes which have the positive value of relative magnetic susceptibilities tend to move laterally into the area which has a high gradient magnetic field, but white blood cells which have the relative magnetic susceptibilities in negative value are moving into the lower gradient magnetic field or oppositely comparing to erythrocytes. This point is related to Han K. et al (2005) and (2006) that the direction of the magnetic force acting on both white blood cells and erythrocytes is opposite comparing to each other [35-37].

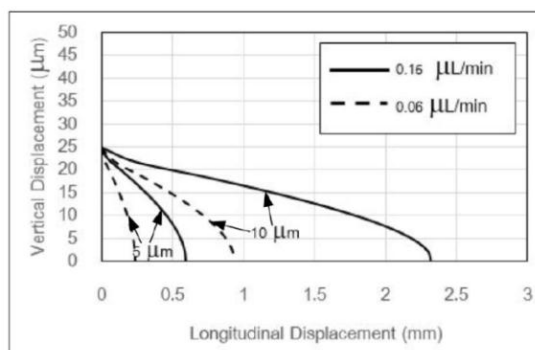


Figure C.2.2 the trajectory in the y-axis at the flow rates both 0.06 and 0.15  $\mu\text{L}/\text{min}$

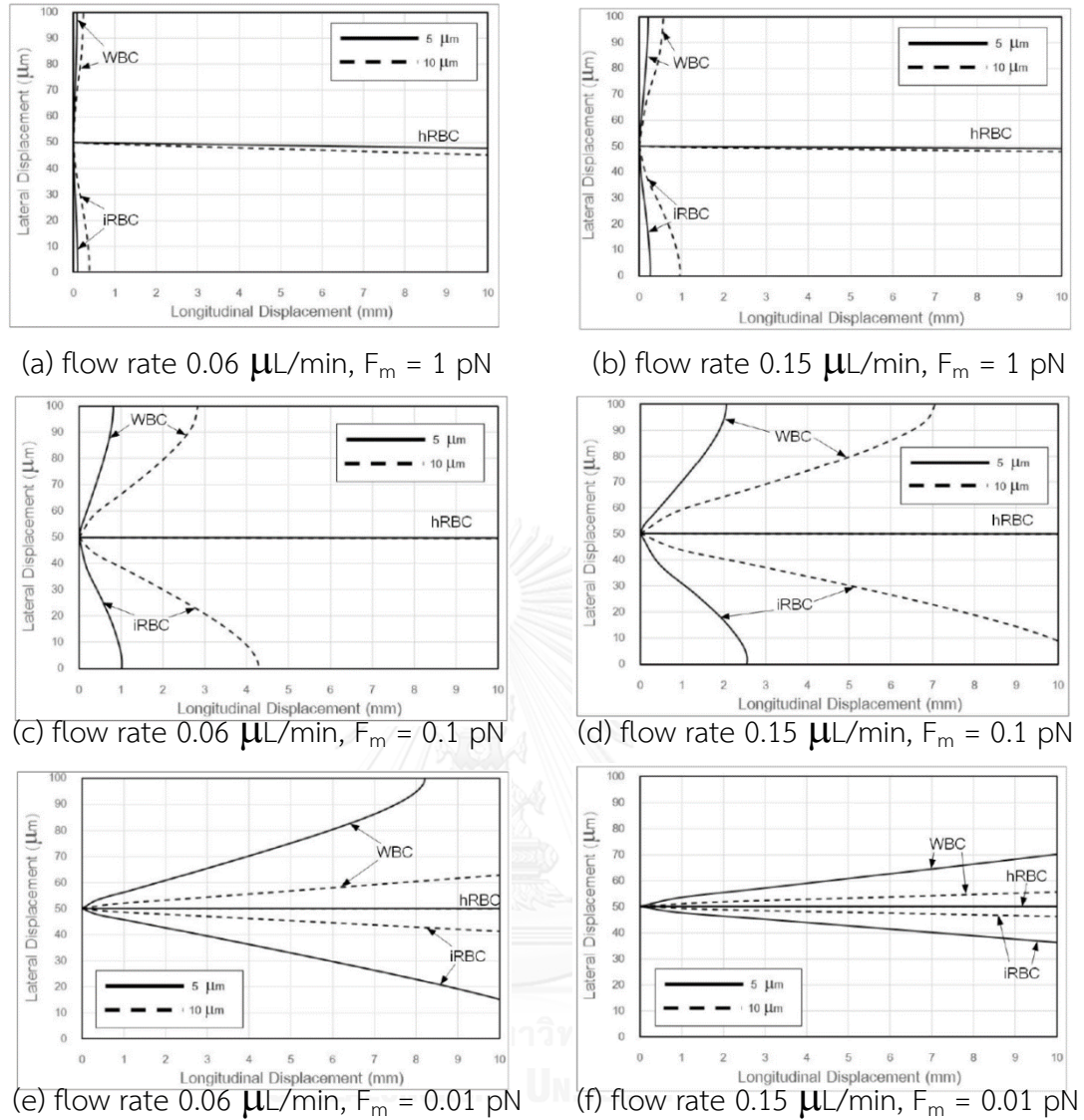


Figure C.2.3 the trajectory of blood cells at the floor of channel In various flow rate and sizes of magnetic force.

Secondly, infected erythrocytes tend to move laterally to the high gradient magnetic field more evidently than healthy erythrocytes because its relative susceptibility of infected red blood cells is much higher than that of healthy red blood cells. Therefore, the magnitude of magnetic force acting on healthy red blood cells can be neglected as the value is too low and seems not to be attracted by the magnetic force, but it does numerically

Thirdly, the size of the blood cells also plays a significant role in lateral migration. The bigger size they are, the higher drag force they will be exposed to. Therefore, the bigger size, 10  $\mu\text{m}$  in this study, needs more distance in x-axis to migrate laterally at all flow rates.

Fourthly, from Figure C.2.2. (a), (c) and (e), we demonstrate that the magnitude of magnetic force affects trajectory of the cells because if we define the higher magnetic force, they will move toward the wall faster.

Lastly, the flow rate also has an influence on drag force in x-axis. In conclusion, while we are designing the device, we have to consider two main factors, which are the size of the magnetic force acting on targeted cells that should not be lower than 0.1 pN and the flow rate used in the experiment also that should not be higher than 0.15  $\mu\text{L}/\text{min}$ , or the speed should not exceed over 500  $\mu\text{m}/\text{s}$ . In order to make sure that infected red blood cells can be filtered out with the proper distance, we will use these criteria for design, In the next model, we will get the result of magnetic field distribution from a magnet array computed by COMSOL and will do the experiment to compare and validate how accurate our model used in predicting the trajectory is.

### C.3 Trajectory of magnetic bead by influence of an array of magnets

The study used the same coordinate and governing equations as Appendix C.2. In this model, we have used magnetic beads as a model of infected erythrocytes.

$$F_{m,x} + 6\pi\mu_f a(v_f - v_{p,x}) = \rho_p \nabla \frac{d^2x}{dt^2} \quad (\text{C.3.1})$$

$$F_{m,z} - 6\pi\mu_f a v_{p,z} = \rho_p \nabla \frac{d^2z}{dt^2} \quad (\text{C.3.2})$$

The magnetic force term is fit from the result simulated by COMSOL Multiphysics, which uses the necessary constant value in Tables 2.2 – 2.3. From the magnetic force distribution, the magnetic field at each point relies on position in the

domain. Consequently, the force equation is in function of x and z coordinate as follows

$$\begin{aligned} F_{m,x,5\mu m} = & \\ (8.293 \times 10^{-15} + 1.516 \times 10^{-14} \cos(2112x) + 1.388 \times 10^{-12} \sin(2112x)) \cdot & \\ (-6.914 \times 10^6 z^2 + 5.332 \times 10^4 z - 101) & \end{aligned} \quad (C.3.3)$$

$$\begin{aligned} F_{m,z,5\mu m} = & \\ (6.438 \times 10^{-12} + 9.609 \times 10^{-13} \cos(2094x) + 9.917 \times 10^{-14} \sin(2094x)) \cdot & \\ (1.712 \times 10^4 e^{-2323}) & \end{aligned} \quad (C.3.4)$$

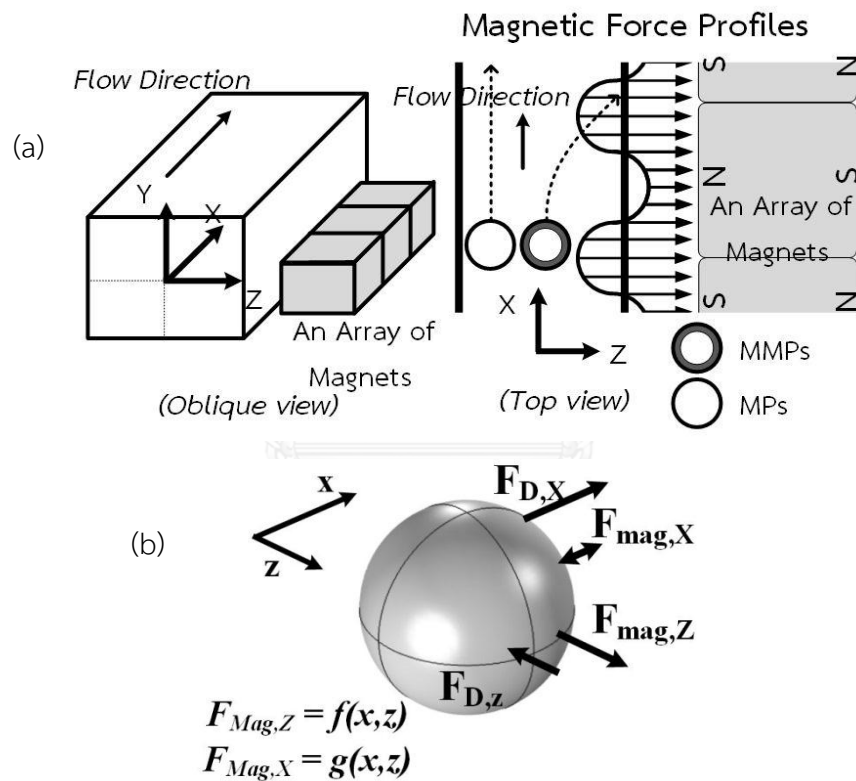


Figure C.2.1 (a) the schematic diagram of study domain (b) the force diagram acting on two types of particles in the experiment under exposed to non-uniform magnetic force.

$$\begin{aligned} F_{m,x,10\mu m} = & \\ (6.634 \times 10^{-14} + 1.213 \times 10^{-13} \cos(2112x) + 1.111 \times 10^{-11} \sin(2112x)) \cdot & \\ (-8.936 \times 10^{-14} e^{6871z} + 380.5 e^{-1358z}) & \end{aligned} \quad (C.3.5)$$

$$\begin{aligned}
 F_{m,z,10\mu m} = & \\
 & (5.151 \times 10^{-11} + 7.687 \times 10^{-12} \cos(2094x) + 7.933 \times 10^{-13} \sin(2094x)) \cdot \\
 & (1.712 \times 10^4 e^{-2323z}) \quad (C.3.6)
 \end{aligned}$$

Equations (C.3.3) – (C.3.4) are for 5  $\mu\text{m}$  of magnetic beads and Equations (C.3.5) – (C.3.6) are for 10  $\mu\text{m}$  of magnetic beads. This study cannot solve the set of equations analytically and cannot use 4<sup>th</sup> order Runge-Kutta used in the previous study because the force function is too complex to solve the problem. Besides, if this study go on with the same method, it will require small time step for calculation which brings about time-consuming computation. Therefore, we have proposed another way to calculate by still using MATLAB for programming. The concept of the calculation is shown in Figure C.3.2 and the flow chart of the program in Figure C.3.3. We will define the initial position both in x- and z- axis to the program. The whole trajectory will be separated into the very short linear motion by defining small time step, 0.1  $\mu\text{s}$  in the study. Then we have designed the program to calculate for the final position and turn it into be the next initial position as well as calculate reiterately until the program reaches the given numbers of iterations. The MATLAB code are in detail in Appendix A.3 and also the detail about computational data and equations are shown in Appendix B.3 – B.6.

The defined conditions used in the study are following

1. No interaction between cells

2. Neglect all secondary flow effects

3. Define y-coordinate at the floor of the channel from the previous model

4. The object will move on the floor plane.

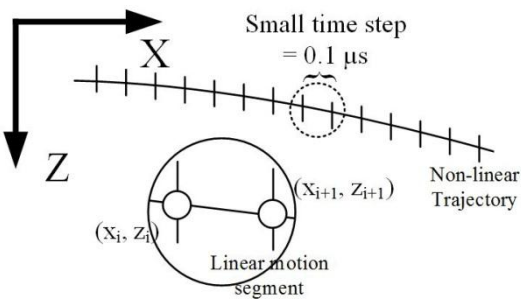


Figure C.3.2 The conceptual principle of the program used in the magnetic bead model

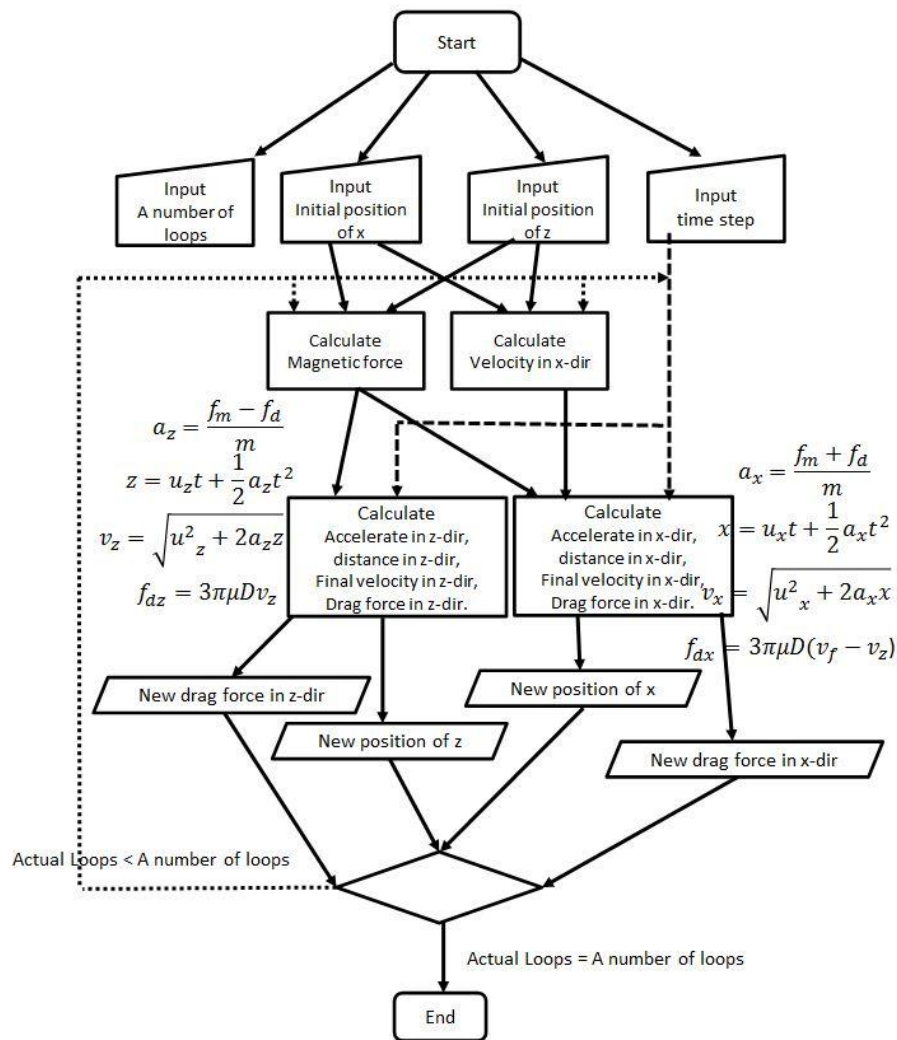


Figure C.3.3 The flowchart of the MATLAB program used in the magnetic bead model

## Appendix D. Raw data of trajectory computation

The raw data accumulated by the excel resulting from MATLAB calculation will be plotted for trajectory of each type of blood cells. This section will show a part of all raw data because it has so much data that the section can show all details.

### D.1 Model constant force

#### 1. Under flow rate 0.06 $\mu\text{L}/\text{min}$

Healthy red blood cells 5  $\mu\text{m}$

x (mm)	z(graph) (um)
0.000	50.000
0.397	49.998
1.191	49.997
1.985	49.995
2.779	49.993
3.572	49.992
4.366	49.990
5.160	49.988
5.954	49.987
6.748	49.985
7.541	49.983
8.335	49.982
9.129	49.980
9.923	49.978
10.716	49.977
11.510	49.975
12.304	49.973
13.097	49.972
13.891	49.970
14.685	49.969
15.478	49.967

x (mm)	z(graph) (um)
0.000	50.000
0.397	49.983
1.191	49.967
1.984	49.950
2.778	49.934
3.571	49.917
4.364	49.901
5.157	49.884
5.950	49.867
6.743	49.851
7.536	49.834
8.328	49.818
9.120	49.801
9.913	49.785
10.705	49.768
11.497	49.751
12.289	49.735
13.081	49.718
13.872	49.702
14.664	49.685
15.455	49.669

x (mm)	z(graph) (um)
0.000	50.000
0.396	49.834
1.188	49.669
1.979	49.503
2.768	49.337
3.557	49.171
4.344	49.006
5.130	48.840
5.914	48.674
6.698	48.509
7.480	48.343
8.262	48.177
9.042	48.012
9.821	47.846
10.600	47.680
11.377	47.514
12.153	47.349
12.929	47.183
13.703	47.017
14.476	46.852
15.249	46.686

$$F_{\text{mag}} = 0.000056 \text{ pN}$$

$$F_{\text{mag}} = 0.00056 \text{ pN}$$

$$F_{\text{mag}} = 0.0056 \text{ pN}$$

Infected red blood cells 5  $\mu\text{m}$ 

x (mm)	z(graph) um
0.000	50.000
0.389	47.624
1.160	45.248
1.920	42.872
2.673	40.496
3.418	38.120
4.158	35.744
4.892	33.367
5.619	30.991
6.336	28.615
7.041	26.239
7.729	23.863
8.395	21.487
9.033	19.111
9.637	16.735
10.197	14.359
10.706	11.983
11.153	9.607
11.528	7.231
11.818	4.854
12.011	2.478

x (mm)	z(graph) um
0.000	50.000
0.019	38.118
0.055	26.236
0.085	14.354
0.102	2.472
0.091	-9.410

x (mm)	z(graph) um
0.000	50.000
0.186	38.118
0.546	26.236
0.854	14.354
1.024	2.472
0.906	-9.410

$F_{\text{mag}} = 0.01 \text{ pN}$

$F_{\text{mag}} = 0.1 \text{ pN}$

$F_{\text{mag}} = 1 \text{ pN}$

White blood cells 5  $\mu\text{m}$ 

x(mm)	z(graph) um
0.000	50.000
0.386	53.439
1.150	56.878
1.901	60.317
2.644	63.756
3.378	67.195
4.100	70.634
4.805	74.073
5.485	77.513
6.129	80.952
6.721	84.391
7.245	87.830
7.681	91.269
8.005	94.708
8.192	98.147
8.213	101.586

x(mm)	z(graph) um
0.000	50.000
0.039	53.431
0.115	56.862
0.190	60.294
0.264	63.725
0.338	67.156
0.410	70.588
0.481	74.019
0.549	77.450
0.613	80.881
0.672	84.313
0.725	87.744
0.769	91.175
0.802	94.606
0.821	98.038
0.823	101.469

x(mm)	z(graph) um
0.000	50.000
0.004	53.432
0.011	56.863
0.019	60.295
0.026	63.726
0.034	67.158
0.041	70.589
0.048	74.021
0.055	77.452
0.061	80.884
0.067	84.316
0.073	87.747
0.077	91.179
0.080	94.610
0.082	98.042
0.082	101.473

$F_{\text{mag}} = 0.0144 \text{ pN}$

$F_{\text{mag}} = 0.144 \text{ pN}$

$F_{\text{mag}} = 1.44 \text{ pN}$

2. Under flow rate 0.15  $\mu\text{L}/\text{min}$ Healthy red blood cells 5  $\mu\text{m}$ 

x (mm)	z(graph) (um)
0.000	50.000
0.992	49.998
2.977	49.997
4.962	49.995
6.947	49.993
8.932	49.992
10.917	49.990
12.902	49.988
14.886	49.987
16.871	49.985
18.856	49.983
20.841	49.982
22.825	49.980
24.810	49.978
26.794	49.977
28.779	49.975
30.763	49.973
32.748	49.972
34.732	49.970
36.717	49.969
38.701	49.967

x (mm)	z(graph) (um)
0.000	50.000
0.992	49.983
2.977	49.967
4.961	49.950
6.945	49.934
8.928	49.917
10.912	49.901
12.894	49.884
14.877	49.867
16.859	49.851
18.841	49.834
20.823	49.818
22.804	49.801
24.785	49.785
26.766	49.768
28.746	49.751
30.726	49.735
32.706	49.718
34.685	49.702
36.664	49.685
38.643	49.669

x (mm)	z(graph) (um)
0.000	50.000
0.991	49.834
2.971	49.669
4.948	49.503
6.922	49.337
8.893	49.171
10.861	49.006
12.826	48.840
14.788	48.674
16.747	48.509
18.703	48.343
20.657	48.177
22.608	48.012
24.557	47.846
26.503	47.680
28.446	47.514
30.387	47.349
32.326	47.183
34.262	47.017
36.196	46.852
38.127	46.686

$F_{\text{mag}} = 0.000056 \text{ pN}$

$F_{\text{mag}} = 0.00056 \text{ pN}$

$F_{\text{mag}} = 0.0056 \text{ pN}$

Infected red blood cells 5  $\mu\text{m}$ 

x (mm)	z(graph) (um)
0.000	50.000
0.972	47.624
2.900	45.248
4.802	42.872
6.683	40.496
8.547	38.120
10.398	35.744
12.233	33.367
14.051	30.991
15.845	28.615
17.608	26.239
19.330	23.863
20.998	21.487
22.597	19.111
24.109	16.735
25.515	14.359
26.792	11.983
27.917	9.607
28.861	7.231
29.595	4.854
30.088	2.478

x (mm)	z(graph) (um)
0.000	50.000
0.046	38.118
0.137	26.236
0.214	14.354
0.257	2.472
0.228	-9.410

x (mm)	z(graph) (um)
0.000	50.000
0.464	38.118
1.365	26.236
2.138	14.354
2.566	2.472
2.279	-9.410

$F_{\text{mag}} = 0.01 \text{ pN}$

$F_{\text{mag}} = 0.1 \text{ pN}$

$F_{\text{mag}} = 1 \text{ pN}$

White blood cells 5  $\mu\text{m}$ 

x (mm)	z(graph) (um)	x (mm)	z(graph) (um)	x (mm)	z(graph) (um)
0.000	50.000	0.000	50.000	0.000	50.000
0.964	53.439	0.096	53.431	0.010	53.432
2.875	56.878	0.288	56.862	0.029	56.863
4.754	60.317	0.475	60.294	0.048	60.295
6.611	63.756	0.661	63.725	0.066	63.726
8.446	67.195	0.845	67.156	0.084	67.158
10.253	70.634	1.025	70.588	0.103	70.589
12.018	74.073	1.202	74.019	0.120	74.021
13.720	77.513	1.372	77.450	0.137	77.452
15.331	80.952	1.534	80.881	0.153	80.884
16.816	84.391	1.682	84.313	0.168	84.316
18.132	87.830	1.814	87.744	0.181	87.747
19.228	91.269	1.925	91.175	0.192	91.179
20.047	94.708	2.008	94.606	0.201	94.610
20.525	98.147	2.056	98.038	0.206	98.042
20.589	101.586	2.064	101.469	0.206	101.473

$F_{\text{mag}} = 0.0144 \text{ pN}$

$F_{\text{mag}} = 0.144 \text{ pN}$

$F_{\text{mag}} = 1.44 \text{ pN}$

## D.2 Model magnetic beads

## I. DI water medium

5- $\mu\text{m}$  magnetic beads under flow rate 2  $\mu\text{L}/\text{min}$ 

Experimental		Trajectory				Comp.		
z (um)	x (um)	Prog.	t	z (m)	x (m)	x (mm)	z (um)	x (um)
86.76	0		0	0.004065	0.001799	874.91	86.76	0
62.72	24.04		0.02	0.004061	0.001804	880.384	83.028	5.474
44.95	44.95		0.04	0.004058	0.001811	885.893	79.259	10.983
32.4	62.72		0.06	0.004054	0.001815	891.432	75.453	16.522
17.77	77.35		0.08	0.00405	0.001821	896.997	71.609	22.087
9.41	83.62		0.1	0.004046	0.001827	902.583	67.727	27.673
			0.12	0.004042	0.001832	908.181	63.804	33.271
			0.14	0.004038	0.001838	913.787	59.841	38.877
			0.16	0.004034	0.001843	919.39	55.837	44.48
			0.18	0.00403	0.001849	924.983	51.79	50.073
			0.2	0.004026	0.001855	930.555	47.7	55.645
			0.22	0.004022	0.00186	936.097	43.566	61.187
			0.24	0.004018	0.001866	941.599	39.386	66.689
			0.26	0.004014	0.001871	947.05	35.161	72.14
			0.28	0.004009	0.001876	952.44	30.889	77.53
			0.3	0.004005	0.001882	957.758	26.568	82.848
			0.32	0.004001	0.001887	962.995	22.199	88.085
			0.34	0.003996	0.001892	968.142	17.779	93.232
			0.36	0.003992	0.001897	973.19	13.308	98.28
			0.377252	0.003988	0.001902	977.46	9.41	102.55

10- $\mu$ m magnetic beads under flow rate 20  $\mu$ L/min

Experimental		Trajectory					
z (um)	x (um)	Prog.				Comp.	
		t	z (m)	x (m)	x (mm)	z (um)	x (um)
116.3767	0	0.00E+00	4.01E-03	9.40E-04	136.237	116.377	0
80.13667	188.1533	5.00E-03	4.01E-03	9.53E-04	149.0321	111.773	12.7951
44.94667	355.4	1.00E-02	4.00E-03	9.66E-04	161.8886	107.129	25.6516
11.84667	468.9867	1.50E-02	4.00E-03	9.79E-04	174.7947	102.452	38.5577
4.183333	489.1233	2.00E-02	4.00E-03	9.92E-04	187.7656	97.743	51.5286
		2.50E-02	3.99E-03	1.00E-03	200.814	93.001	64.577
		3.00E-02	3.99E-03	1.02E-03	213.949	88.226	77.712
		3.50E-02	3.98E-03	1.03E-03	227.177	83.416	90.94
		4.00E-02	3.98E-03	1.04E-03	240.496	78.571	104.259
		4.50E-02	3.97E-03	1.06E-03	253.899	73.691	117.662
		5.00E-02	3.97E-03	1.07E-03	267.37	68.774	131.133
		5.50E-02	3.96E-03	1.08E-03	280.887	63.819	144.65
		6.00E-02	3.96E-03	1.10E-03	294.417	58.826	158.18
		6.50E-02	3.95E-03	1.11E-03	307.918	53.794	171.681
		7.00E-02	3.95E-03	1.13E-03	321.339	48.721	185.102
		7.50E-02	3.94E-03	1.14E-03	334.619	43.606	198.382
		8.00E-02	3.94E-03	1.15E-03	347.69	38.448	211.453
		8.50E-02	3.93E-03	1.16E-03	360.476	33.244	224.239
		9.00E-02	3.93E-03	1.18E-03	372.897	27.994	236.66
		9.50E-02	3.92E-03	1.19E-03	384.866	22.696	248.629
		1.00E-01	3.92E-03	1.20E-03	396.297	17.346	260.06
		1.05E-01	3.91E-03	1.21E-03	407.103	11.943	270.866
		1.10E-01	3.90E-03	1.22E-03	417.202	6.485	280.965
		1.12E-01	3.90E-03	1.23E-03	421.201	4.183	284.964

## II. PBS medium

5- $\mu$ m magnetic beads under flow rate 2  $\mu$ L/min

Experimental		Trajectory					
z (um)	x (um)	Prog.				Comp.	
		t	z (m)	x (m)	x (mm)	z (um)	x (um)
77.35	0	0.00E+00	4.20E-03	9.98E-04	197.56	77.35	0
51.22	150.52	2.00E-02	4.20E-03	9.98E-04	201.9363	74.702	4.3763
39.72	190.24	4.00E-02	4.19E-03	1.00E-03	206.316	72.041	8.756
27.18	224.74	6.00E-02	4.19E-03	1.01E-03	210.696	69.367	13.136
15.68	247.73	8.00E-02	4.19E-03	1.01E-03	215.072	66.68	17.512
6.27	262.37	1.00E-01	4.19E-03	1.02E-03	219.442	63.979	21.882
		1.20E-01	4.18E-03	1.02E-03	223.802	61.266	26.242
		1.40E-01	4.18E-03	1.02E-03	228.147	58.538	30.587
		1.60E-01	4.18E-03	1.03E-03	232.473	55.797	34.913
		1.80E-01	4.18E-03	1.03E-03	236.776	53.042	39.216
		2.00E-01	4.17E-03	1.04E-03	241.052	50.272	43.492
		2.20E-01	4.17E-03	1.04E-03	245.296	47.488	47.736
		2.40E-01	4.17E-03	1.05E-03	249.503	44.69	51.943
		2.60E-01	4.16E-03	1.05E-03	253.667	41.876	56.107
		2.80E-01	4.16E-03	1.05E-03	257.786	39.048	60.226
		3.00E-01	4.16E-03	1.06E-03	261.853	36.204	64.293
		3.20E-01	4.16E-03	1.06E-03	265.863	33.345	68.303
		3.40E-01	4.15E-03	1.07E-03	269.813	30.47	72.253
		3.60E-01	4.15E-03	1.07E-03	273.697	27.579	76.137
		3.80E-01	4.15E-03	1.07E-03	277.511	24.672	79.951
		4.00E-01	4.14E-03	1.08E-03	281.251	21.748	83.691
		4.20E-01	4.14E-03	1.08E-03	284.913	18.807	87.353
		4.40E-01	4.14E-03	1.09E-03	288.494	15.849	90.934
		4.60E-01	4.14E-03	1.09E-03	291.99	12.874	94.43
		4.80E-01	4.13E-03	1.09E-03	295.398	9.881	97.838
		5.00E-01	4.13E-03	1.10E-03	298.717	6.87	101.157
		5.04E-01	4.13E-03	1.10E-03	299.365	6.27	101.805

5- $\mu\text{m}$  magnetic beads under flow rate 10  $\mu\text{L}/\text{min}$

Experimental		Trajectory							
z (um)	x (um)	Prog.						Comp.	
		t	z (m)	x (m)	x (mm)	z (um)	x (um)		
124.39	0	0.00E+00	4.28E-03	1.42E-03	696.16	124.39	0		
104.53	180.84	2.00E-02	4.28E-03	1.43E-03	706.493	122.381	10.333		
87.8	249.83	4.00E-02	4.27E-03	1.44E-03	716.849	120.364	20.689		
82.58	274.91	6.00E-02	4.27E-03	1.45E-03	727.231	118.34	31.071		
74.22	297.91	8.00E-02	4.27E-03	1.46E-03	737.642	116.308	41.482		
65.85	323	1.00E-01	4.27E-03	1.47E-03	748.084	114.268	51.924		
56.45	343.9	1.20E-01	4.27E-03	1.48E-03	758.558	112.219	62.398		
47.04	364.81	1.40E-01	4.26E-03	1.49E-03	769.067	110.161	72.907		
40.77	386.76	1.60E-01	4.26E-03	1.50E-03	779.613	108.095	83.453		
31.36	407.67	1.80E-01	4.26E-03	1.51E-03	790.195	106.02	94.035		
20.91	426.48	2.00E-01	4.26E-03	1.52E-03	800.815	103.935	104.655		
12.54	441.12	2.20E-01	4.26E-03	1.53E-03	811.473	101.841	115.313		
5.23	446.34	2.40E-01	4.25E-03	1.54E-03	822.169	99.736	126.009		
		2.60E-01	4.25E-03	1.55E-03	832.901	97.622	136.741		
		2.80E-01	4.25E-03	1.56E-03	843.667	95.497	147.507		
		3.00E-01	4.25E-03	1.57E-03	854.467	93.361	158.307		
		3.20E-01	4.24E-03	1.59E-03	865.296	91.214	169.136		
		3.40E-01	4.24E-03	1.60E-03	876.152	89.055	179.992		
		3.60E-01	4.24E-03	1.61E-03	887.029	86.885	190.869		
		3.80E-01	4.24E-03	1.62E-03	897.922	84.703	201.762		
		4.00E-01	4.24E-03	1.63E-03	908.826	82.509	212.666		
		4.20E-01	4.23E-03	1.64E-03	919.733	80.301	223.573		
		4.40E-01	4.23E-03	1.65E-03	930.637	78.081	234.477		
		4.60E-01	4.23E-03	1.66E-03	941.527	75.847	245.367		
		4.80E-01	4.23E-03	1.67E-03	952.395	73.6	256.235		
		5.00E-01	4.23E-03	1.68E-03	963.231	71.338	267.071		
		5.20E-01	4.22E-03	1.69E-03	974.022	69.062	277.862		
		5.40E-01	4.22E-03	1.70E-03	984.756	66.771	288.596		
		5.60E-01	4.22E-03	1.72E-03	995.421	64.465	299.261		
		5.80E-01	4.22E-03	1.73E-03	1006.003	62.144	309.843		
		6.00E-01	4.21E-03	1.74E-03	1016.486	59.806	320.326		
		6.20E-01	4.21E-03	1.75E-03	1026.854	57.453	330.694		
		6.40E-01	4.21E-03	1.76E-03	1037.091	55.083	340.931		
		6.60E-01	4.21E-03	1.77E-03	1047.181	52.696	351.021		
		6.80E-01	4.20E-03	1.78E-03	1057.104	50.292	360.944		
		7.00E-01	4.20E-03	1.79E-03	1066.842	47.87	370.682		
		7.20E-01	4.20E-03	1.80E-03	1076.376	45.431	380.216		
		7.40E-01	4.20E-03	1.81E-03	1085.687	42.974	389.527		
		7.60E-01	4.19E-03	1.81E-03	1094.755	40.498	398.595		
		7.80E-01	4.19E-03	1.82E-03	1103.56	38.004	407.4		
		8.00E-01	4.19E-03	1.83E-03	1112.081	35.491	415.921		
		8.20E-01	4.19E-03	1.84E-03	1120.298	32.959	424.138		
		8.40E-01	4.18E-03	1.85E-03	1128.192	30.407	432.032		
		8.60E-01	4.18E-03	1.86E-03	1135.742	27.837	439.582		
		8.80E-01	4.18E-03	1.86E-03	1142.93	25.246	446.77		
		9.00E-01	4.18E-03	1.87E-03	1149.737	22.637	453.577		
		9.20E-01	4.17E-03	1.88E-03	1156.144	20.007	459.984		
		9.40E-01	4.17E-03	1.88E-03	1162.136	17.358	465.976		
		9.60E-01	4.17E-03	1.89E-03	1167.696	14.688	471.536		
		9.80E-01	4.17E-03	1.89E-03	1172.81	11.999	476.65		
		1.00E+00	4.16E-03	1.90E-03	1177.465	9.289	481.305		
		1.02E+00	4.16E-03	1.90E-03	1181.65	6.56	485.49		
		1.03E+00	4.16E-03	1.90E-03	1183.506	5.23	487.346		

5- $\mu\text{m}$  magnetic beads under flow rate 20  $\mu\text{L}/\text{min}$ 

Experimental		Trajectory							
z (um)	x (um)	Prog.	t	z (m)	x (m)	x (mm)	z (um)	x (um)	
91.99	0		0.00E+00	4.21E-03	9.63E-04	166.2	91.99	0	
68.99	132.75		2.00E-02	4.21E-03	9.83E-04	186.1629	89.412	19.9629	
56.45	171.43		4.00E-02	4.21E-03	1.00E-03	206.153	86.834	39.953	
44.95	208.01		6.00E-02	4.21E-03	1.02E-03	226.153	84.257	59.953	
30.31	240.42		8.00E-02	4.20E-03	1.04E-03	246.145	81.68	79.945	
18.82	268.64		1.00E-01	4.20E-03	1.06E-03	266.109	79.102	99.909	
7.32	284.32		1.20E-01	4.20E-03	1.08E-03	286.022	76.524	119.822	
6.27	289.55		1.40E-01	4.20E-03	1.10E-03	305.861	73.945	139.661	
			1.60E-01	4.19E-03	1.12E-03	325.596	71.365	159.396	
			1.80E-01	4.19E-03	1.14E-03	345.201	68.783	179.001	
			2.00E-01	4.19E-03	1.16E-03	364.643	66.199	198.443	
			2.20E-01	4.19E-03	1.18E-03	383.89	63.612	217.69	
			2.40E-01	4.18E-03	1.20E-03	402.906	61.022	236.706	
			2.60E-01	4.18E-03	1.22E-03	421.655	58.427	255.455	
			2.80E-01	4.18E-03	1.24E-03	440.1	55.828	273.9	
			3.00E-01	4.18E-03	1.25E-03	458.2	53.224	292	
			3.20E-01	4.17E-03	1.27E-03	475.916	50.613	309.716	
			3.40E-01	4.17E-03	1.29E-03	493.205	47.995	327.005	
			3.60E-01	4.17E-03	1.31E-03	510.026	45.37	343.826	
			3.80E-01	4.17E-03	1.32E-03	526.337	42.737	360.137	
			4.00E-01	4.16E-03	1.34E-03	542.093	40.094	375.893	
			4.20E-01	4.16E-03	1.35E-03	557.252	37.442	391.052	
			4.40E-01	4.16E-03	1.37E-03	571.771	34.778	405.571	
			4.60E-01	4.15E-03	1.38E-03	585.608	32.104	419.408	
			4.80E-01	4.15E-03	1.40E-03	598.722	29.417	432.522	
			5.00E-01	4.15E-03	1.41E-03	611.072	26.717	444.872	
			5.20E-01	4.15E-03	1.42E-03	622.62	24.004	456.42	
			5.40E-01	4.14E-03	1.43E-03	633.328	21.276	467.128	
			5.60E-01	4.14E-03	1.44E-03	643.162	18.534	476.962	
			5.80E-01	4.14E-03	1.45E-03	652.088	15.777	485.888	
			6.00E-01	4.14E-03	1.46E-03	660.077	13.003	493.877	
			6.20E-01	4.13E-03	1.46E-03	667.102	10.213	500.902	
			6.40E-01	4.13E-03	1.47E-03	673.141	7.406	506.941	
			6.48E-01	4.13E-03	1.47E-03	675.29	6.27	509.09	

10- $\mu\text{m}$  magnetic beads under flow rate 20  $\mu\text{L}/\text{min}$ 

Experimental		Trajectory							
z (um)	x (um)	Prog.	t	z (m)	x (m)	x (mm)	z (um)	x (um)	
87.8	0		0.00E+00	4.06E-03	1.22E-03	345.99	87.8	0	
60.63	104.53		1.00E-02	4.06E-03	1.24E-03	361.557	80.934	15.567	
34.49	193.38		2.00E-02	4.05E-03	1.25E-03	377.177	73.974	31.187	
7.32	245.64		3.00E-02	4.04E-03	1.27E-03	392.746	66.923	46.756	
4.18	264.46		4.00E-02	4.04E-03	1.28E-03	408.15	59.777	62.16	
			5.00E-02	4.03E-03	1.30E-03	423.25	52.531	77.26	
			6.00E-02	4.02E-03	1.31E-03	437.891	45.182	91.901	
			7.00E-02	4.01E-03	1.33E-03	451.906	37.724	105.916	
			8.00E-02	4.01E-03	1.34E-03	465.122	30.151	119.132	
			9.00E-02	4.00E-03	1.35E-03	477.374	22.458	131.384	
			1.00E-01	3.99E-03	1.36E-03	488.512	14.639	142.522	
			1.10E-01	3.98E-03	1.37E-03	498.413	6.686	152.423	
			1.13E-01	3.98E-03	1.38E-03	501.232	4.18	155.242	

### D.3 Model blood cells

Flowrate ( $\mu\text{L}/\text{min}$ )	Conditions	Area I					Area II					Maximum Distance					
		1.00	2.00	3.00	4.00	5.00	Average	SD	1.00	2.00	3.00	4.00	5.00	Average	SD	Average	SD
0.2	With magnet	0.00	0.00	0.00	0.00	0.00	0.00	0.00	80.49	67.94	84.67	77.35	83.62	78.81	6.72	39.41	3.36
	Without magnet	0.00	0.00	0.00	0.00	0.00	0.00	0.00	71.08	43.90	61.67	112.89	153.66	88.64	44.31	44.32	22.15
0.3	With magnet	0.00	0.00	0.00	0.00	0.00	0.00	0.00	44.95	75.26	50.17	59.58	48.08	55.61	12.27	27.80	6.13
	Without magnet	0.00	0.00	0.00	0.00	0.00	0.00	0.00	113.94	117.07	100.35	95.12	88.85	103.07	12.11	51.53	6.06
0.4	With magnet	88.85	91.99	97.21	87.80	78.40	88.85	6.17	118.12	121.25	131.71	129.62	126.48	125.44	5.68	107.14	5.92
	Without magnet	81.53	80.49	86.76	80.49	83.62	82.58	2.38	106.62	104.53	106.62	95.12	106.62	103.90	4.99	93.24	3.69
0.5	With magnet	114.98	118.12	117.07	119.16	116.03	117.07	1.48	145.30	143.20	142.16	147.39	136.39	142.89	4.15	129.98	2.81
	Without magnet	124.39	123.34	130.66	131.71	129.62	127.94	3.41	172.47	191.29	172.47	162.02	166.20	172.89	11.20	150.42	7.31

## Appendix E. Comparison percent difference between model and experiment

### E.1 Magnetic beads experiment

#### I. DI water medium

##### 5- $\mu\text{m}$ magnetic beads

Order	20 $\mu\text{l}/\text{min}$ 10- $\mu\text{m}$				Z0 (from device measurement) X0 (from device measurement)				3.90 mm				0.80 mm				Calculation Percent Error			
	Measured initial z um	Measured initial x um	Measured final z um	Measured final x um	Prog. initial z mm	Prog. initial x mm	Prog. final z mm	Prog. final x mm	Calculation	Percent	Error	Avg	SD	Avg	SD	Avg	SD			
1.00	41.46	459.98	4.18	574.91	3.94*	1.26	3.90	1.38	1.32	3.95										
2.00	38.68	316.72	3.84	354.82	3.94*	1.12	3.90	1.16	1.18	1.48										
3.00	70.73	78.05	12.89	245.64	3.97*	0.88	3.91	1.05	0.98	6.48										
4.00	90.94	234.15	5.23	678.04	3.99*	1.04	3.90	1.48	1.19	19.75										
5.00	91.64	604.87	4.18	1198.60	3.99*	1.41	3.90	2.00	1.57	21.73										
6.00	83.97	113.24	4.18	516.37	3.98*	0.92	3.90	1.32	1.05	20.15										
7.00	58.19	907.31	4.18	1197.20	3.96*	1.71	3.90	2.00	1.80	9.88										
8.00	28.22	9.27	11.15	46.34	3.93*	0.81	3.91	0.85	0.84	1.30										
9.00	180.84	331.71	4.88	945.29	4.08*	1.14	3.90	1.75	1.48	15.51										
															11.14	8.30				
10.00	116.38	136.24	4.18	625.36	4.01*	0.94	3.90	1.43	1.14	20.22										
11.00	133.10	403.48	37.60	1308.00	4.03*	1.21	3.94	2.11	1.39	34.00										
12.00	118.12	612.19	54.01	1265.15	4.02*	1.42	3.95	2.07	1.60	22.54										
13.00	99.65	760.62	13.60	1333.79	4.00*	1.56	3.91	2.14	1.73	19.30										
14.00	19.17	44.60	3.83	65.85	3.92*	0.85	3.90	0.87	0.87	0.07										
15.00	60.28	21.95	4.53	413.93	3.96*	0.83	3.90	1.22	0.92	24.71										
16.00	170.38	14.63	90.94	1253.00	4.07*	0.82	3.99	2.06	0.97	52.63										
17.00	186.06	255.05	82.58	1307.66	4.08*	1.06	3.98	2.11	1.27	39.76										
18.00	87.80	93.03	35.54	529.96	3.99*	0.90	3.93	1.33	1.03	22.52					26.19	14.74				
19.00	116.03	417.07	4.18	1282.57	4.01*	1.22	3.90	2.09	1.43	31.63										
20.00	96.17	68.99	4.18	711.84	3.99*	0.87	3.90	1.52	1.03	31.89										
21.00	89.89	199.65	3.14	818.46	3.99*	1.00	3.90	1.62	1.15	28.81										
22.00	90.94	26.13	4.18	674.21	3.99*	0.83	3.90	1.48	0.98	33.79										
23.00	95.12	615.68	5.23	1058.88	3.99*	1.42	3.90	1.86	1.58	14.99										
24.00	150.52	44.95	4.18	1119.51	4.05*	0.85	3.90	1.92	1.23	35.94										
25.00	140.07	232.05	4.18	1118.46	4.04*	1.04	3.90	1.92	1.40	27.29										
26.00	47.04	445.29	5.23	648.00	3.94*	1.25	3.90	1.45	1.34	7.42										
27.00	27.18	624.04	4.18	706.00	3.92*	1.43	3.90	1.51	1.48	2.29										
28.00	67.94	45.99	3.14	505.92	3.97*	0.85	3.90	1.31	1.00	23.85					23.79	11.64				

##### 10- $\mu\text{m}$ magnetic beads

Order	2 $\mu\text{l}/\text{min}$ 5- $\mu\text{m}$				Z0 (from device measurement) X0 (from device measurement)				3.98 mm				0.92 mm				Calculation Percent Error			
	Measured initial z um	Measured initial x um	Measured final z um	Measured final x um	Prog. initial z mm	Prog. initial x mm	Prog. final z mm	Prog. final x mm	Calculation	Percent	Error	Avg	SD	Avg	SD	Avg	SD			
1.00	133.10	72.12	6.97	382.58	4.11	1.00	3.99	1.31	1.17	10.64										
2.00	149.48	6.13	5.93	624.04	4.13	0.93	3.98	1.55	1.13	27.25										
3.00	150.17	46.69	7.32	595.82	4.13	0.97	3.99	1.52	1.17	23.22										
4.00	180.84	12.19	6.27	457.84	4.16	0.94	3.98	1.38	1.18	14.60										
5.00	197.21	0.00	5.93	1208.01	4.18	0.92	3.98	2.13	1.19	44.00										
6.00	263.41	0.00	98.26	1337.62	4.24	0.92	4.08	2.26	1.18	47.83										
7.00	190.94	0.00	3.14	680.48	4.17	0.92	3.98	1.60	1.20	25.50										
8.00	97.56	8.36	8.71	238.68	4.08	0.93	3.99	1.16	1.05	9.74										
9.00	147.39	7.32	2.44	351.57	4.13	0.93	3.98	1.28	1.13	11.58										
10.00	153.66	6.48	7.67	361.67	4.13	0.93	3.99	1.29	1.13	12.04										
11.00	207.98	0.00	8.36	1051.56	4.19	0.92	3.99	1.98	1.22	38.47										
12.00	211.12	0.00	60.63	1336.93	4.19	0.92	4.04	2.26	1.15	49.22										
13.00	240.39	0.00	8.36	1119.51	4.22	0.92	3.99	2.04	1.26	38.25										
14.00	44.94	16.73	9.41	81.53	4.02*	0.94	3.99	1.01	0.99	1.90					AVG	SD				
15.00	264.43	0.00	2.09	1323.34	4.24*	0.92	3.98	2.25	1.31	41.78					26.40	15.84				
16.00	292.63	34.50	99.30	1288.84	4.27*	0.96	4.08	2.21	1.26	42.90										
17.00	273.83	69.00	113.94	1303.48	4.25*	0.99	4.09	2.23	1.25	44.10										
18.00	317.77	493.38	232.05	1306.61	4.30*	1.42	4.21	2.23	1.57	29.78										
19.00	111.85	314.63	2.09	741.11	4.09*	1.24	3.98	1.67	1.39	16.75										
20.00	313.59	233.10	155.75	1313.93	4.29*	1.16	4.13	2.24	1.21	45.99										
21.00	266.55	23.00	78.40	1337.97	4.25*	0.95	4.06	2.26	1.24	45.28										
22.00	260.28	44.95	57.49	1337.97	4.24*	0.97	4.04	2.26	1.28	43.43										
23.00	201.74	8.36	2.09	644.94	4.18*	0.93	3.98	1.57	1.42	9.51										
24.00	287.45	17.77	43.90	1337.97	4.27*	0.94	4.02	2.26	1.32	41.80					AVG	SD				
25.00	144.25	542.51	2.09	1211.49	4.12*	1.47	3.98	2.14	1.66	22.10					34.16	13.58				
26.00	66.90	387.80	2.09	460.97	4.05*	1.31	3.98	1.39	1.39	0.62										
27.00	77.35	373.17	8.36	482.92	4.06	1.30	3.99	1.41	1.39	1.39										
28.00	86.76	874.91	9.41	958.53	4.07*	1.80	3.99	1.88	1.90	1.01										
29.00	58.54	38.68	3.14	127.53	4.04*	0.96	3.98	1.05	1.03	2.02										
30.00	166.20	192.33	4.18	608.36	4.14*	1.12	3.98	1.53	1.34	12.38										
31.00	72.13	417.07	8.36	570.73	4.05*	1.34	3.99	1.49	1.42	4.74										
32.00	76.31	1085.01	5.23	1287.80	4.05*	2.01	3.98	2.21	2.10	5.07										
33.00	181.88	0.00	7.32	431.70	4.16*	0.92	3.99	1.36	1.17	13.84										
34.00	188.15	26.13	9.41	412.89	4.17*	0.95	3.99	1.34	1.20	10.06					AVG	SD				
35.00	51.22	177.70	6.27	256.10	4.03*	1.10	3.98	1.18	1.16	2.00					5.31	4.98				

## II. PBS medium

5- $\mu$ m magnetic beads

2uL/min		5-um		Z0 (from device measurement)			4.12 mm			0.80 mm					
Order	Measured initial z um	Measured initial x um	Measured final z um	Measured final x um	Prog. initial z mm	Prog. initial x mm	Prog. final z mm	Prog. final x mm	Calculation final x mm	Percent Error					
1.00	56.45	96.17	7.32	382.58	4.18	0.89	4.13	1.18	1.00	0.96					
3.00	97.21	85.71	3.14	810.10	4.22	0.88	4.13	1.61	3.00	1.02					
4.00	29.27	105.57	4.18	587.45	4.15	0.90	4.13	1.38	4.00	0.93					
5.00	113.94	31.36	3.14	681.53	4.24	0.83	4.13	1.48	5.00	0.99					
6.00	56.45	217.42	3.14	327.18	4.18	1.01	4.13	1.12	6.00	1.09					
7.00	78.40	403.48	3.14	752.61	4.20	1.20	4.13	1.55	7.00	1.31					
8.00	127.53	236.24	4.18	956.44	4.25	1.03	4.13	1.75	8.00	1.22					
9.00	127.53	236.24	3.14	952.26	4.25	1.03	4.13	1.75	9.00	1.22					
10.00	86.76	309.41	3.14	785.01	4.21	1.11	4.13	1.58	10.00	1.23					
11.00	71.08	217.42	3.14	739.02	4.19	1.01	4.13	1.54	11.00	1.11					
12.00	62.72	747.38	4.18	1057.83	4.19	1.54	4.13	1.85	12.00	1.63					
13.00	23.00	710.80	3.14	739.02	4.15	1.51	4.13	1.54	13.00	1.53					
14.00	68.99	313.59	4.18	965.85	4.19	1.11	4.13	1.76	14.00	1.20					
15.00	102.44	3.14	6.27	243.55	4.23	0.80	4.13	1.04	15.00	0.94					
16.00	212.19	280.14	7.32	1293.02	4.33	1.08	4.13	2.09	16.00	1.42					
17.00	77.35	197.56	6.27	459.93	4.20	0.99	4.13	1.26	17.00	1.10					
18.00	34.49	249.82	6.27	360.63	4.16	1.05	4.13	1.16	18.00	1.08					
19.00	30.31	19.86	6.27	81.53	4.15	0.82	4.13	0.88	19.00	0.85					
20.00	91.99	0.00	6.27	413.93	4.21	0.80	4.13	1.21	20.00	0.92					
21.00	129.62	88.85	15.68	472.47	4.25	0.89	4.14	1.27	21.00	1.06					
22.00	63.76	159.93	7.32	462.02	4.19	0.96	4.13	1.26	22.00	1.03					
23.00	134.84	125.43	7.32	949.12	4.26	0.92	4.13	1.75	23.00	1.12					
24.00	167.25	13.59	7.32	967.94	4.29	0.81	4.13	1.76	24.00	1.06					
25.00	96.17	478.74	4.18	1012.89	4.22	1.28	4.13	1.81	25.00	1.41					
26.00	76.31	290.59	5.23	732.75	4.20	1.09	4.13	1.53	26.00	1.19					
27.00	77.35	742.16	4.18	1100.69	4.20	1.54	4.13	1.90	27.00	1.65					
28.00	91.99	402.44	5.23	893.72	4.21	1.20	4.13	1.69	28.00	1.33					
29.00	56.45	203.83	8.36	361.67	4.18	1.00	4.13	1.16	29.00	1.07					
30.00	152.61	325.09	7.32	1036.93	4.28	1.12	4.13	1.83	30.00	1.36					
31.00	120.21	265.50	10.45	1036.93	4.24	1.06	4.13	1.83	31.00	1.23					
												Average	21.27		
												SD	11.03		

10- $\mu$ m magnetic beads

## E.2 Blood cells

Distance 200  $\mu\text{m}$  from the magnet

Flow rate	0.18 $\mu\text{L/min}$			Flow rate	0.23 $\mu\text{L/min}$		
z	x (m)	zadj ( $\mu\text{m}$ )	xadj (cm)	z	x	zadj ( $\mu\text{m}$ )	xadj (cm)
2.70E-03	4.15E-04	98.79	0.04	2.70E-03	5.30E-04	98.80	0.05
2.70E-03	8.31E-04	97.61	0.08	2.70E-03	1.06E-03	97.63	0.11
2.70E-03	1.25E-03	96.45	0.12	2.70E-03	1.59E-03	96.44	0.16
2.70E-03	1.66E-03	95.23	0.17	2.70E-03	2.12E-03	95.26	0.21
2.69E-03	2.08E-03	94.05	0.21	2.69E-03	2.64E-03	94.05	0.26
2.69E-03	2.49E-03	92.84	0.25	2.69E-03	3.19E-03	92.79	0.32
2.69E-03	2.91E-03	91.58	0.29	2.69E-03	3.72E-03	91.54	0.37
2.69E-03	3.32E-03	90.30	0.33	2.69E-03	4.25E-03	90.33	0.42
2.69E-03	3.74E-03	89.03	0.37	2.69E-03	4.78E-03	89.06	0.48
2.69E-03	4.16E-03	87.81	0.42	2.69E-03	5.31E-03	87.83	0.53
2.69E-03	4.57E-03	86.52	0.46	2.69E-03	5.84E-03	86.54	0.58
2.69E-03	4.99E-03	85.25	0.50	2.69E-03	6.00E-03	86.14	0.60
2.68E-03	5.40E-03	83.97	0.54	2.68E-03	6.53E-03	84.82	0.65
2.68E-03	5.81E-03	82.64	0.58	2.68E-03	7.06E-03	83.54	0.71
2.68E-03	6.00E-03	82.03	0.60	2.68E-03	7.59E-03	82.22	0.76
2.68E-03	6.41E-03	80.66	0.64	2.68E-03	8.12E-03	80.92	0.81
2.68E-03	6.82E-03	79.32	0.68	2.68E-03	8.64E-03	79.58	0.86
2.68E-03	7.24E-03	78.01	0.72	2.68E-03	9.17E-03	78.19	0.92
2.68E-03	7.65E-03	76.62	0.76	2.68E-03	9.69E-03	76.80	0.97
2.68E-03	8.05E-03	75.27	0.81	2.68E-03	1.02E-02	75.46	1.02
2.67E-03	8.46E-03	73.89	0.85	2.67E-03	1.07E-02	74.05	1.07
2.67E-03	8.87E-03	72.45	0.89	2.67E-03	1.13E-02	72.68	1.13
2.67E-03	9.27E-03	70.98	0.93	2.67E-03	1.18E-02	71.24	1.18
2.67E-03	9.67E-03	69.52	0.97	2.67E-03	1.20E-02	70.58	1.20
2.67E-03	1.01E-02	68.10	1.01	2.67E-03	1.25E-02	69.10	1.25
2.67E-03	1.05E-02	66.64	1.05	2.67E-03	1.30E-02	67.66	1.30
2.67E-03	1.09E-02	65.14	1.09	2.67E-03	1.35E-02	66.19	1.35
2.66E-03	1.13E-02	63.68	1.13	2.66E-03	1.40E-02	64.71	1.40
2.66E-03	1.16E-02	62.15	1.16	2.66E-03	1.45E-02	63.22	1.45
2.66E-03	1.20E-02	60.67	1.20	2.66E-03	1.50E-02	61.65	1.50
2.66E-03	1.24E-02	59.07	1.24	2.66E-03	1.55E-02	60.07	1.55
2.66E-03	1.28E-02	57.48	1.28	2.66E-03	1.60E-02	58.52	1.60
2.66E-03	1.31E-02	55.93	1.31	2.66E-03	1.65E-02	56.95	1.65
2.65E-03	1.35E-02	54.31	1.35	2.66E-03	1.69E-02	55.35	1.69
2.65E-03	1.39E-02	52.67	1.39	2.65E-03	1.74E-02	53.76	1.74
2.65E-03	1.42E-02	51.06	1.42	2.65E-03	1.79E-02	52.08	1.79
2.65E-03	1.46E-02	49.37	1.46	2.65E-03	1.80E-02	51.58	1.80
2.65E-03	1.49E-02	47.63	1.49	2.65E-03	1.84E-02	49.86	1.84
2.65E-03	1.52E-02	45.84	1.52	2.65E-03	1.89E-02	48.17	1.89
2.64E-03	1.56E-02	44.05	1.56	2.65E-03	1.93E-02	46.49	1.93
2.64E-03	1.59E-02	42.28	1.59	2.64E-03	1.97E-02	44.71	1.97
2.64E-03	1.62E-02	40.53	1.62	2.64E-03	2.01E-02	42.99	2.01
2.64E-03	1.65E-02	38.68	1.65	2.64E-03	2.05E-02	41.20	2.05
2.64E-03	1.68E-02	36.79	1.68	2.64E-03	2.09E-02	39.32	2.09
2.63E-03	1.70E-02	34.95	1.70	2.64E-03	2.13E-02	37.41	2.13
2.63E-03	1.73E-02	33.07	1.73	2.64E-03	2.17E-02	35.50	2.17
2.63E-03	1.76E-02	31.09	1.76	2.63E-03	2.20E-02	33.62	2.20
2.63E-03	1.76E-02	30.67	1.76	2.63E-03	2.23E-02	31.71	2.23
2.63E-03	1.78E-02	28.62	1.78	2.63E-03	2.24E-02	31.58	2.24
2.63E-03	1.80E-02	27.22	1.80	2.63E-03	2.27E-02	29.56	2.27
2.63E-03	1.82E-02	25.09	1.82	2.63E-03	2.30E-02	27.57	2.30
2.62E-03	1.84E-02	22.94	1.84	2.63E-03	2.32E-02	25.57	2.32
2.62E-03	1.86E-02	20.77	1.86	2.62E-03	2.35E-02	23.48	2.35
2.62E-03	1.88E-02	18.58	1.88	2.62E-03	2.37E-02	21.30	2.37
2.62E-03	1.89E-02	16.40	1.89	2.62E-03	2.39E-02	19.06	2.39
2.61E-03	1.90E-02	14.20	1.90	2.62E-03	2.40E-02	18.39	2.40
2.61E-03	1.91E-02	11.95	1.91	2.62E-03	2.42E-02	16.08	2.42
2.61E-03	1.92E-02	9.61	1.92	2.61E-03	2.43E-02	13.73	2.43
2.61E-03	1.93E-02	7.19	1.93	2.61E-03	2.45E-02	11.35	2.45
2.60E-03	1.94E-02	4.67	1.94	2.61E-03	2.46E-02	8.93	2.46
2.60E-03	1.94E-02	2.08	1.94	2.61E-03	2.47E-02	6.48	2.47
2.60E-03	1.94E-02	0.00	1.94	2.60E-03	2.47E-02	3.99	2.47
				2.60E-03	2.48E-02	1.46	2.48
				2.60E-03	2.48E-02	0.00	2.48

Distance 200  $\mu\text{m}$  from the magnet (Continued)

Flow rate	0.28	$\mu\text{L/min}$			Flow rate	0.33	$\mu\text{L/min}$	
z	x	zadj (um)	xadj (cm)		z	x	zadj (um)	xadj (cm)
2.70E-03	6.46E-04	98.80	0.06		2.70E-03	7.61E-04	98.81	0.08
2.70E-03	1.29E-03	97.64	0.13		2.70E-03	1.52E-03	97.64	0.15
2.70E-03	1.94E-03	96.45	0.19		2.70E-03	2.28E-03	96.46	0.23
2.70E-03	2.58E-03	95.26	0.26		2.70E-03	3.05E-03	95.24	0.30
2.69E-03	3.23E-03	94.02	0.32		2.69E-03	3.81E-03	94.01	0.38
2.69E-03	3.88E-03	92.79	0.39		2.69E-03	4.57E-03	92.80	0.46
2.69E-03	4.52E-03	91.57	0.45		2.69E-03	5.33E-03	91.59	0.53
2.69E-03	5.17E-03	90.35	0.52		2.69E-03	6.00E-03	90.48	0.60
2.69E-03	5.82E-03	89.08	0.58		2.69E-03	6.76E-03	89.21	0.68
2.69E-03	6.00E-03	88.72	0.60		2.69E-03	7.52E-03	87.96	0.75
2.69E-03	6.65E-03	87.42	0.66		2.69E-03	8.28E-03	86.71	0.83
2.69E-03	7.29E-03	86.17	0.73		2.69E-03	9.05E-03	85.98	0.90
2.68E-03	7.94E-03	84.88	0.79		2.68E-03	9.81E-03	84.08	0.98
2.68E-03	8.58E-03	83.59	0.86		2.68E-03	1.06E-02	82.79	1.06
2.68E-03	9.22E-03	82.24	0.92		2.68E-03	1.13E-02	81.49	1.13
2.68E-03	9.87E-03	80.91	0.99		2.68E-03	1.20E-02	80.27	1.20
2.68E-03	1.05E-02	79.58	1.05		2.68E-03	1.28E-02	78.90	1.28
2.68E-03	1.11E-02	78.25	1.11		2.68E-03	1.35E-02	77.56	1.35
2.68E-03	1.18E-02	76.88	1.18		2.68E-03	1.43E-02	76.21	1.43
2.68E-03	1.20E-02	76.40	1.20		2.67E-03	1.50E-02	74.80	1.50
2.67E-03	1.26E-02	74.99	1.26		2.67E-03	1.58E-02	73.37	1.58
2.67E-03	1.33E-02	73.62	1.33		2.67E-03	1.65E-02	71.98	1.65
2.67E-03	1.39E-02	72.20	1.39		2.67E-03	1.72E-02	70.57	1.72
2.67E-03	1.45E-02	70.80	1.45		2.67E-03	1.80E-02	69.10	1.80
2.67E-03	1.52E-02	69.31	1.52		2.67E-03	1.80E-02	69.04	1.80
2.67E-03	1.58E-02	67.84	1.58		2.67E-03	1.87E-02	67.55	1.87
2.67E-03	1.64E-02	66.39	1.64		2.67E-03	1.95E-02	66.10	1.95
2.66E-03	1.70E-02	64.91	1.70		2.66E-03	2.02E-02	64.62	2.02
2.66E-03	1.76E-02	63.41	1.76		2.66E-03	2.09E-02	63.09	2.09
2.66E-03	1.80E-02	62.39	1.80		2.66E-03	2.16E-02	61.53	2.16
2.66E-03	1.86E-02	60.82	1.86		2.66E-03	2.23E-02	60.01	2.23
2.66E-03	1.92E-02	59.30	1.92		2.66E-03	2.30E-02	58.45	2.30
2.66E-03	1.98E-02	57.71	1.98		2.66E-03	2.37E-02	56.87	2.37
2.66E-03	2.04E-02	56.15	2.04		2.66E-03	2.40E-02	56.09	2.40
2.65E-03	2.09E-02	54.58	2.09		2.65E-03	2.47E-02	54.44	2.47
2.65E-03	2.15E-02	52.83	2.15		2.65E-03	2.53E-02	52.84	2.53
2.65E-03	2.20E-02	51.19	2.20		2.65E-03	2.60E-02	51.18	2.60
2.65E-03	2.26E-02	49.51	2.26		2.65E-03	2.66E-02	49.51	2.66
2.65E-03	2.31E-02	47.84	2.31		2.65E-03	2.72E-02	47.76	2.72
2.65E-03	2.36E-02	46.11	2.36		2.65E-03	2.79E-02	46.02	2.79
2.64E-03	2.40E-02	44.81	2.40		2.64E-03	2.85E-02	44.29	2.85
2.64E-03	2.45E-02	42.99	2.45		2.64E-03	2.90E-02	42.53	2.90
2.64E-03	2.50E-02	41.22	2.50		2.64E-03	2.96E-02	40.73	2.96
2.64E-03	2.55E-02	39.41	2.55		2.64E-03	3.00E-02	39.39	3.00
2.64E-03	2.59E-02	37.55	2.59					
2.64E-03	2.63E-02	35.71	2.63					
2.63E-03	2.68E-02	33.77	2.68					
2.63E-03	2.72E-02	31.76	2.72					
2.63E-03	2.75E-02	29.74	2.75					
2.63E-03	2.79E-02	27.74	2.79					
2.63E-03	2.82E-02	25.75	2.82					
2.62E-03	2.86E-02	23.62	2.86					
2.62E-03	2.88E-02	21.49	2.88					
2.62E-03	2.91E-02	19.39	2.91					
2.62E-03	2.94E-02	17.20	2.94					
2.61E-03	2.96E-02	14.92	2.96					
2.61E-03	2.96E-02	14.81	2.96					
2.61E-03	2.98E-02	12.45	2.98					
2.61E-03	2.99E-02	10.01	2.99					
2.61E-03	3.00E-02	8.06	3.00					

Distance 300  $\mu\text{m}$  from the magnet

Flow rate	0.18 uL/min			Flow rate	0.23 uL/min		
z	x	zadj (um)	xadj (cm)	z	x	zadj (um)	xadj (cm)
2.80E-03	4.15E-04	99.29	0.04	2.80E-03	5.30E-04	99.29	0.05
2.80E-03	8.31E-04	98.59	0.08	2.80E-03	1.06E-03	98.61	0.11
2.80E-03	1.25E-03	97.93	0.12	2.80E-03	1.59E-03	97.94	0.16
2.80E-03	1.66E-03	97.25	0.17	2.80E-03	2.12E-03	97.27	0.21
2.80E-03	2.08E-03	96.58	0.21	2.80E-03	2.65E-03	96.57	0.27
2.80E-03	2.49E-03	95.88	0.25	2.80E-03	3.19E-03	95.84	0.32
2.80E-03	2.91E-03	95.16	0.29	2.80E-03	3.72E-03	95.12	0.37
2.79E-03	3.33E-03	94.43	0.33	2.79E-03	4.25E-03	94.44	0.42
2.79E-03	3.74E-03	93.71	0.37	2.79E-03	4.78E-03	93.75	0.48
2.79E-03	4.16E-03	93.02	0.42	2.79E-03	5.31E-03	93.06	0.53
2.79E-03	4.57E-03	92.33	0.46	2.79E-03	5.84E-03	92.34	0.58
2.79E-03	4.99E-03	91.64	0.50	2.79E-03	6.00E-03	92.12	0.60
2.79E-03	5.40E-03	90.93	0.54	2.79E-03	6.53E-03	91.38	0.65
2.79E-03	5.82E-03	90.20	0.58	2.79E-03	7.06E-03	90.67	0.71
2.79E-03	6.00E-03	89.87	0.60	2.79E-03	7.59E-03	89.98	0.76
2.79E-03	6.42E-03	89.12	0.64	2.79E-03	8.12E-03	89.28	0.81
2.79E-03	6.83E-03	88.40	0.68	2.79E-03	8.66E-03	88.55	0.87
2.79E-03	7.25E-03	87.69	0.72	2.79E-03	9.19E-03	87.79	0.92
2.79E-03	7.66E-03	86.98	0.77	2.79E-03	9.72E-03	87.05	0.97
2.79E-03	8.08E-03	86.28	0.81	2.79E-03	1.02E-02	86.34	1.02
2.79E-03	8.49E-03	85.54	0.85	2.79E-03	1.08E-02	85.62	1.08
2.78E-03	8.91E-03	84.78	0.89	2.78E-03	1.13E-02	84.90	1.13
2.78E-03	9.32E-03	84.01	0.93	2.78E-03	1.18E-02	84.15	1.18
2.78E-03	9.37E-03	83.26	0.94	2.78E-03	1.20E-02	83.91	1.20
2.78E-03	1.01E-02	82.53	1.01	2.78E-03	1.25E-02	83.14	1.25
2.78E-03	1.06E-02	81.80	1.06	2.78E-03	1.31E-02	82.40	1.31
2.78E-03	1.10E-02	81.08	1.10	2.78E-03	1.36E-02	81.68	1.36
2.78E-03	1.14E-02	80.33	1.14	2.78E-03	1.41E-02	80.95	1.41
2.78E-03	1.18E-02	79.56	1.18	2.78E-03	1.46E-02	80.19	1.46
2.78E-03	1.20E-02	79.17	1.20	2.78E-03	1.52E-02	79.40	1.52
2.78E-03	1.24E-02	78.38	1.24	2.78E-03	1.57E-02	78.62	1.57
2.78E-03	1.28E-02	77.61	1.28	2.78E-03	1.62E-02	77.88	1.62
2.78E-03	1.32E-02	76.87	1.32	2.78E-03	1.67E-02	77.14	1.67
2.78E-03	1.36E-02	76.12	1.36	2.78E-03	1.73E-02	76.39	1.73
2.78E-03	1.40E-02	75.37	1.40	2.78E-03	1.78E-02	75.60	1.78
2.77E-03	1.45E-02	74.60	1.45	2.78E-03	1.80E-02	75.27	1.80
2.77E-03	1.49E-02	73.80	1.49	2.77E-03	1.85E-02	74.47	1.85
2.77E-03	1.53E-02	72.98	1.53	2.77E-03	1.90E-02	73.70	1.90
2.77E-03	1.57E-02	72.18	1.57	2.77E-03	1.96E-02	72.94	1.96
2.77E-03	1.61E-02	71.41	1.61	2.77E-03	2.01E-02	72.18	2.01
2.77E-03	1.64E-02	70.64	1.64	2.77E-03	2.06E-02	71.39	2.06
2.77E-03	1.69E-02	69.87	1.69	2.77E-03	2.11E-02	70.56	2.11
2.77E-03	1.73E-02	69.09	1.73	2.77E-03	2.16E-02	69.75	2.16
2.77E-03	1.77E-02	68.28	1.77	2.77E-03	2.21E-02	68.96	2.21
2.77E-03	1.80E-02	67.61	1.80	2.77E-03	2.26E-02	68.18	2.26
2.77E-03	1.84E-02	66.77	1.84	2.77E-03	2.31E-02	67.40	2.31
2.77E-03	1.88E-02	65.95	1.88	2.77E-03	2.37E-02	66.59	2.37
2.77E-03	1.92E-02	65.16	1.92	2.77E-03	2.40E-02	66.01	2.40
2.76E-03	1.96E-02	64.37	1.96	2.77E-03	2.45E-02	65.17	2.45
2.76E-03	2.00E-02	63.57	2.00	2.76E-03	2.50E-02	64.36	2.50
2.76E-03	2.04E-02	62.76	2.04	2.76E-03	2.55E-02	63.56	2.55
2.76E-03	2.07E-02	61.91	2.07	2.76E-03	2.60E-02	62.76	2.60
2.76E-03	2.11E-02	61.05	2.11	2.76E-03	2.65E-02	61.94	2.65
2.76E-03	2.15E-02	60.18	2.15	2.76E-03	2.70E-02	61.08	2.70
2.76E-03	2.19E-02	59.34	2.19	2.76E-03	2.75E-02	60.21	2.75
2.76E-03	2.23E-02	58.53	2.23	2.76E-03	2.80E-02	59.38	2.80
2.76E-03	2.26E-02	57.70	2.26	2.76E-03	2.84E-02	58.56	2.84
2.76E-03	2.30E-02	56.88	2.30	2.76E-03	2.89E-02	57.74	2.89
2.76E-03	2.34E-02	56.04	2.34	2.76E-03	2.94E-02	56.90	2.94
2.76E-03	2.38E-02	55.16	2.38	2.76E-03	2.99E-02	56.03	2.99
2.75E-03	2.40E-02	54.55	2.40	2.76E-03	3.00E-02	55.77	3.00
2.75E-03	2.44E-02	53.65	2.44				
2.75E-03	2.47E-02	52.77	2.47				
2.75E-03	2.51E-02	51.91	2.51				
2.75E-03	2.54E-02	51.06	2.54				
2.75E-03	2.58E-02	50.21	2.58				
2.75E-03	2.61E-02	49.35	2.61				
2.75E-03	2.65E-02	48.46	2.65				
2.75E-03	2.68E-02	47.54	2.68				
2.75E-03	2.71E-02	46.60	2.71				
2.75E-03	2.75E-02	45.67	2.75				
2.74E-03	2.78E-02	44.76	2.78				
2.74E-03	2.81E-02	43.87	2.81				
2.74E-03	2.84E-02	42.98	2.84				
2.74E-03	2.88E-02	42.09	2.88				
2.74E-03	2.91E-02	41.19	2.91				
2.74E-03	2.94E-02	40.27	2.94				
2.74E-03	2.97E-02	39.32	2.97				
2.74E-03	3.00E-02	38.34	3.00				
2.74E-03	3.00E-02	38.21	3.00				

Distance 300  $\mu\text{m}$  from the magnet (Continued)

Flow rate	0.28 uL/min			Flow rate	0.33 uL/min		
z	x	zadj (um)	xadj (cm)	z	x	zadj (um)	xadj (cm)
2.80E-03	6.46E-04	99.29	0.06	2.80E-03	7.61E-04	99.30	0.08
2.80E-03	1.29E-03	98.62	0.13	2.80E-03	1.52E-03	98.63	0.15
2.80E-03	1.94E-03	97.95	0.19	2.80E-03	2.28E-03	97.96	0.23
2.80E-03	2.58E-03	97.26	0.26	2.80E-03	3.05E-03	97.24	0.30
2.80E-03	3.23E-03	96.54	0.32	2.80E-03	3.81E-03	96.53	0.38
2.80E-03	3.88E-03	95.83	0.39	2.80E-03	4.57E-03	95.85	0.46
2.80E-03	4.53E-03	95.15	0.45	2.80E-03	5.33E-03	95.17	0.53
2.79E-03	5.17E-03	94.47	0.52	2.79E-03	6.00E-03	94.54	0.60
2.79E-03	5.82E-03	93.75	0.58	2.79E-03	6.76E-03	93.81	0.68
2.79E-03	6.00E-03	93.55	0.60	2.79E-03	7.52E-03	93.13	0.75
2.79E-03	6.65E-03	92.82	0.66	2.79E-03	8.29E-03	92.44	0.83
2.79E-03	7.29E-03	92.12	0.73	2.79E-03	9.05E-03	91.70	0.90
2.79E-03	7.94E-03	91.43	0.79	2.79E-03	9.81E-03	90.97	0.98
2.79E-03	8.59E-03	90.72	0.86	2.79E-03	1.06E-02	90.28	1.06
2.79E-03	9.23E-03	89.97	0.92	2.79E-03	1.13E-02	89.57	1.13
2.79E-03	9.88E-03	89.24	0.99	2.79E-03	1.20E-02	88.93	1.20
2.79E-03	1.05E-02	88.54	1.05	2.79E-03	1.28E-02	88.18	1.28
2.79E-03	1.12E-02	87.84	1.12	2.79E-03	1.35E-02	87.48	1.35
2.79E-03	1.18E-02	87.10	1.18	2.79E-03	1.43E-02	86.77	1.43
2.79E-03	1.20E-02	86.88	1.20	2.79E-03	1.50E-02	86.02	1.50
2.79E-03	1.26E-02	86.13	1.26	2.79E-03	1.58E-02	85.26	1.58
2.79E-03	1.33E-02	85.41	1.33	2.78E-03	1.66E-02	84.55	1.66
2.78E-03	1.39E-02	84.70	1.39	2.78E-03	1.73E-02	83.83	1.73
2.78E-03	1.46E-02	83.96	1.46	2.78E-03	1.80E-02	83.14	1.80
2.78E-03	1.52E-02	83.19	1.52	2.78E-03	1.88E-02	82.38	1.88
2.78E-03	1.59E-02	82.43	1.59	2.78E-03	1.95E-02	81.65	1.95
2.78E-03	1.65E-02	81.71	1.65	2.78E-03	2.03E-02	80.92	2.03
2.78E-03	1.72E-02	80.98	1.72	2.78E-03	2.10E-02	80.15	2.10
2.78E-03	1.78E-02	80.21	1.78	2.78E-03	2.18E-02	79.37	2.18
2.78E-03	1.80E-02	79.96	1.80	2.78E-03	2.25E-02	78.63	2.25
2.78E-03	1.86E-02	79.18	1.86	2.78E-03	2.33E-02	77.89	2.33
2.78E-03	1.93E-02	78.44	1.93	2.78E-03	2.40E-02	77.15	2.40
2.78E-03	1.99E-02	77.70	1.99	2.78E-03	2.47E-02	76.36	2.47
2.78E-03	2.06E-02	76.94	2.06	2.78E-03	2.55E-02	75.61	2.55
2.78E-03	2.12E-02	76.14	2.12	2.77E-03	2.62E-02	74.86	2.62
2.78E-03	2.18E-02	75.35	2.18	2.77E-03	2.70E-02	74.06	2.70
2.77E-03	2.25E-02	74.60	2.25	2.77E-03	2.77E-02	73.26	2.77
2.77E-03	2.31E-02	73.84	2.31	2.77E-03	2.85E-02	72.49	2.85
2.77E-03	2.37E-02	73.05	2.37	2.77E-03	2.92E-02	71.73	2.92
2.77E-03	2.40E-02	72.70	2.40	2.77E-03	3.00E-02	70.92	3.00
2.77E-03	2.46E-02	71.89	2.46	2.77E-03	3.00E-02	70.88	3.00
2.77E-03	2.53E-02	71.12	2.53				
2.77E-03	2.59E-02	70.35	2.59				
2.77E-03	2.65E-02	69.56	2.65				
2.77E-03	2.71E-02	68.73	2.71				
2.77E-03	2.77E-02	67.91	2.77				
2.77E-03	2.84E-02	67.13	2.84				
2.77E-03	2.90E-02	66.34	2.90				
2.77E-03	2.96E-02	65.53	2.96				
2.76E-03	3.00E-02	64.97	3.00				

Under flow rate 0.2  $\mu\text{L}/\text{min}$

Distance	500 um						
z	x	zadj (um)	xadj (cm)	2.98E-03	1.91E-02	481.60	1.91
3.00E-03	0.00E+00	500.00	0.00	2.98E-03	1.94E-02	481.29	1.94
3.00E-03	3.85E-04	499.67	0.04	2.98E-03	1.97E-02	480.97	1.97
3.00E-03	7.68E-04	499.35	0.08	2.98E-03	2.00E-02	480.65	2.00
3.00E-03	1.15E-03	499.04	0.12	2.98E-03	2.02E-02	480.33	2.02
3.00E-03	1.53E-03	498.75	0.15	2.98E-03	2.05E-02	479.99	2.05
3.00E-03	1.91E-03	498.45	0.19	2.98E-03	2.08E-02	479.64	2.08
3.00E-03	2.29E-03	498.14	0.23	2.98E-03	2.10E-02	479.28	2.10
3.00E-03	2.67E-03	497.81	0.27	2.98E-03	2.13E-02	478.92	2.13
3.00E-03	3.04E-03	497.48	0.30	2.98E-03	2.15E-02	478.57	2.15
3.00E-03	3.41E-03	497.15	0.34	2.98E-03	2.18E-02	478.23	2.18
3.00E-03	3.78E-03	496.82	0.38	2.98E-03	2.20E-02	477.90	2.20
3.00E-03	4.16E-03	496.51	0.42	2.98E-03	2.23E-02	477.58	2.23
3.00E-03	4.52E-03	496.21	0.45	2.98E-03	2.25E-02	477.26	2.25
3.00E-03	4.89E-03	495.91	0.49	2.98E-03	2.28E-02	476.94	2.28
3.00E-03	5.26E-03	495.60	0.53	2.98E-03	2.30E-02	476.61	2.30
3.00E-03	5.62E-03	495.28	0.56	2.98E-03	2.33E-02	476.28	2.33
2.99E-03	5.98E-03	494.94	0.60	2.98E-03	2.35E-02	475.93	2.35
2.99E-03	6.00E-03	494.92	0.60	2.98E-03	2.37E-02	475.58	2.37
2.99E-03	6.36E-03	494.59	0.64	2.98E-03	2.40E-02	475.22	2.40
2.99E-03	6.72E-03	494.26	0.67	2.98E-03	2.40E-02	475.16	2.40
2.99E-03	7.08E-03	493.94	0.71	2.97E-03	2.42E-02	474.80	2.42
2.99E-03	7.43E-03	493.64	0.74	2.97E-03	2.45E-02	474.44	2.45
2.99E-03	7.78E-03	493.34	0.78	2.97E-03	2.47E-02	474.09	2.47
2.99E-03	8.14E-03	493.03	0.81	2.97E-03	2.49E-02	473.75	2.49
2.99E-03	8.49E-03	492.71	0.85	2.97E-03	2.51E-02	473.42	2.51
2.99E-03	8.83E-03	492.37	0.88	2.97E-03	2.53E-02	473.09	2.53
2.99E-03	9.18E-03	492.03	0.92	2.97E-03	2.55E-02	472.77	2.55
2.99E-03	9.53E-03	491.69	0.95	2.97E-03	2.57E-02	472.44	2.57
2.99E-03	9.87E-03	491.37	0.99	2.97E-03	2.59E-02	472.11	2.59
2.99E-03	1.02E-02	491.05	1.02	2.97E-03	2.61E-02	471.78	2.61
2.99E-03	1.05E-02	490.75	1.05	2.97E-03	2.63E-02	471.43	2.63
2.99E-03	1.09E-02	490.44	1.09	2.97E-03	2.65E-02	471.08	2.65
2.99E-03	1.12E-02	490.13	1.12	2.97E-03	2.67E-02	470.72	2.67
2.99E-03	1.16E-02	489.80	1.16	2.97E-03	2.69E-02	470.35	2.69
2.99E-03	1.19E-02	489.46	1.19	2.97E-03	2.71E-02	469.98	2.71
2.99E-03	1.20E-02	489.34	1.20	2.97E-03	2.73E-02	469.61	2.73
2.99E-03	1.23E-02	488.99	1.23	2.97E-03	2.75E-02	469.25	2.75
2.99E-03	1.27E-02	488.66	1.27	2.97E-03	2.77E-02	468.89	2.77
2.99E-03	1.30E-02	488.33	1.30	2.97E-03	2.78E-02	468.54	2.78
2.99E-03	1.33E-02	488.02	1.33	2.97E-03	2.80E-02	468.20	2.80
2.99E-03	1.36E-02	487.71	1.36	2.97E-03	2.82E-02	467.87	2.82
2.99E-03	1.39E-02	487.40	1.39	2.97E-03	2.83E-02	467.53	2.83
2.99E-03	1.43E-02	487.08	1.43	2.97E-03	2.85E-02	467.21	2.85
2.99E-03	1.46E-02	486.75	1.46	2.97E-03	2.87E-02	466.88	2.87
2.99E-03	1.49E-02	486.40	1.49	2.97E-03	2.88E-02	466.54	2.88
2.99E-03	1.52E-02	486.05	1.52	2.97E-03	2.90E-02	466.21	2.90
2.99E-03	1.55E-02	485.71	1.55	2.97E-03	2.91E-02	465.86	2.91
2.99E-03	1.58E-02	485.38	1.58	2.97E-03	2.93E-02	465.51	2.93
2.99E-03	1.61E-02	485.06	1.61	2.97E-03	2.94E-02	465.15	2.94
2.98E-03	1.64E-02	484.74	1.64	2.96E-03	2.96E-02	464.79	2.96
2.98E-03	1.67E-02	484.43	1.67	2.96E-03	2.97E-02	464.42	2.97
2.98E-03	1.70E-02	484.12	1.70	2.96E-03	2.98E-02	464.05	2.98
2.98E-03	1.73E-02	483.79	1.73	2.96E-03	3.00E-02	463.67	3.00
2.98E-03	1.76E-02	483.45	1.76	2.96E-03	3.00E-02	463.56	3.00
2.98E-03	1.79E-02	483.10	1.79				
2.98E-03	1.80E-02	482.96	1.80				
2.98E-03	1.83E-02	482.61	1.83				
2.98E-03	1.86E-02	482.26	1.86				
2.98E-03	1.89E-02	481.93	1.89				

Under flow rate 0.2  $\mu\text{L}/\text{min}$  (Continued)

Distance	600 um			Distance	700 um			Distance	800 um		
z	x	zadj (um)	xadj (cm)	z	x	zadj (um)	xadj (cm)	z	x	zadj (um)	xadj (cm)
3.10E-03	0.00E+00	600.00	0.00	3.20E-03	0.00E+00	700.00	0.00	3.30E-03	0.00E+00	800.00	0.00
3.10E-03	4.72E-04	599.76	0.05	3.20E-03	4.72E-04	699.82	0.05	3.30E-03	4.72E-04	799.86	0.05
3.10E-03	9.44E-04	599.53	0.09	3.20E-03	9.44E-04	699.65	0.09	3.30E-03	9.44E-04	799.73	0.09
3.10E-03	1.42E-03	599.31	0.14	3.20E-03	1.42E-03	699.49	0.14	3.30E-03	1.42E-03	799.61	0.14
3.10E-03	1.89E-03	599.10	0.19	3.20E-03	1.89E-03	699.32	0.19	3.30E-03	1.89E-03	799.49	0.19
3.10E-03	2.36E-03	598.87	0.24	3.20E-03	2.36E-03	699.16	0.24	3.30E-03	2.36E-03	799.36	0.24
3.10E-03	2.83E-03	598.63	0.28	3.20E-03	2.83E-03	698.98	0.28	3.30E-03	2.83E-03	799.22	0.28
3.10E-03	3.30E-03	598.39	0.33	3.20E-03	3.31E-03	698.80	0.33	3.30E-03	3.31E-03	799.09	0.33
3.10E-03	3.77E-03	598.15	0.38	3.20E-03	3.78E-03	698.62	0.38	3.30E-03	3.78E-03	798.95	0.38
3.10E-03	4.24E-03	597.93	0.42	3.20E-03	4.25E-03	698.45	0.43	3.30E-03	4.25E-03	798.83	0.43
3.10E-03	4.71E-03	597.72	0.47	3.20E-03	4.72E-03	698.29	0.47	3.30E-03	4.73E-03	798.70	0.47
3.10E-03	5.19E-03	597.49	0.52	3.20E-03	5.20E-03	698.13	0.52	3.30E-03	5.20E-03	798.58	0.52
3.10E-03	5.66E-03	597.26	0.57	3.20E-03	5.67E-03	697.95	0.57	3.30E-03	5.67E-03	798.44	0.57
3.10E-03	6.00E-03	597.08	0.60	3.20E-03	6.00E-03	697.83	0.60	3.30E-03	6.00E-03	798.35	0.60
3.10E-03	6.47E-03	596.84	0.65	3.20E-03	6.47E-03	697.64	0.65	3.30E-03	6.47E-03	798.21	0.65
3.10E-03	6.94E-03	596.61	0.69	3.20E-03	6.94E-03	697.47	0.69	3.30E-03	6.95E-03	798.08	0.69
3.10E-03	7.41E-03	596.39	0.74	3.20E-03	7.42E-03	697.31	0.74	3.30E-03	7.42E-03	797.96	0.74
3.10E-03	7.88E-03	596.17	0.79	3.20E-03	7.89E-03	697.15	0.79	3.30E-03	7.89E-03	797.83	0.79
3.10E-03	8.35E-03	595.94	0.83	3.20E-03	8.36E-03	696.98	0.84	3.30E-03	8.37E-03	797.70	0.84
3.10E-03	8.82E-03	595.70	0.88	3.20E-03	8.83E-03	696.80	0.88	3.30E-03	8.84E-03	797.57	0.88
3.10E-03	9.29E-03	595.46	0.93	3.20E-03	9.31E-03	696.61	0.93	3.30E-03	9.32E-03	797.43	0.93
3.10E-03	9.76E-03	595.22	0.98	3.20E-03	9.78E-03	696.44	0.98	3.30E-03	9.79E-03	797.30	0.98
3.09E-03	1.02E-02	594.99	1.02	3.20E-03	1.03E-02	696.27	1.03	3.30E-03	1.03E-02	797.17	1.03
3.09E-03	1.07E-02	594.77	1.07	3.20E-03	1.07E-02	696.11	1.07	3.30E-03	1.07E-02	797.05	1.07
3.09E-03	1.12E-02	594.55	1.12	3.20E-03	1.12E-02	695.94	1.12	3.30E-03	1.12E-02	796.92	1.12
3.09E-03	1.16E-02	594.31	1.16	3.20E-03	1.17E-02	695.76	1.17	3.30E-03	1.17E-02	796.79	1.17
3.09E-03	1.20E-02	594.12	1.20	3.20E-03	1.20E-02	695.64	1.20	3.30E-03	1.20E-02	796.70	1.20
3.09E-03	1.25E-02	593.88	1.25	3.20E-03	1.25E-02	695.46	1.25	3.30E-03	1.25E-02	796.56	1.25
3.09E-03	1.29E-02	593.64	1.29	3.20E-03	1.29E-02	695.28	1.29	3.30E-03	1.29E-02	796.43	1.29
3.09E-03	1.34E-02	593.42	1.34	3.20E-03	1.34E-02	695.12	1.34	3.30E-03	1.34E-02	796.30	1.34
3.09E-03	1.39E-02	593.20	1.39	3.19E-03	1.39E-02	694.95	1.39	3.30E-03	1.39E-02	796.18	1.39
3.09E-03	1.43E-02	592.97	1.43	3.19E-03	1.44E-02	694.78	1.44	3.30E-03	1.44E-02	796.05	1.44
3.09E-03	1.48E-02	592.73	1.48	3.19E-03	1.48E-02	694.60	1.48	3.30E-03	1.48E-02	795.91	1.48
3.09E-03	1.53E-02	592.48	1.53	3.19E-03	1.53E-02	694.42	1.53	3.30E-03	1.53E-02	795.77	1.53
3.09E-03	1.57E-02	592.24	1.57	3.19E-03	1.58E-02	694.24	1.58	3.30E-03	1.58E-02	795.64	1.58
3.09E-03	1.62E-02	592.02	1.62	3.19E-03	1.63E-02	694.07	1.63	3.30E-03	1.63E-02	795.51	1.63
3.09E-03	1.67E-02	591.80	1.67	3.19E-03	1.67E-02	693.91	1.67	3.30E-03	1.68E-02	795.39	1.68
3.09E-03	1.71E-02	591.57	1.71	3.19E-03	1.72E-02	693.74	1.72	3.30E-03	1.72E-02	795.26	1.72
3.09E-03	1.76E-02	591.33	1.76	3.19E-03	1.77E-02	693.56	1.77	3.30E-03	1.77E-02	795.13	1.77
3.09E-03	1.80E-02	591.13	1.80	3.19E-03	1.80E-02	693.44	1.80	3.30E-03	1.80E-02	795.04	1.80
3.09E-03	1.85E-02	590.88	1.85	3.19E-03	1.85E-02	693.25	1.85	3.29E-03	1.85E-02	794.90	1.85
3.09E-03	1.89E-02	590.64	1.89	3.19E-03	1.89E-02	693.08	1.89	3.29E-03	1.90E-02	794.77	1.90
3.09E-03	1.94E-02	590.42	1.94	3.19E-03	1.94E-02	692.91	1.94	3.29E-03	1.94E-02	794.64	1.94
3.09E-03	1.99E-02	590.20	1.99	3.19E-03	1.99E-02	692.75	1.99	3.29E-03	1.99E-02	794.52	1.99
3.09E-03	2.03E-02	589.97	2.03	3.19E-03	2.04E-02	692.58	2.04	3.29E-03	2.04E-02	794.39	2.04
3.09E-03	2.08E-02	589.72	2.08	3.19E-03	2.08E-02	692.39	2.08	3.29E-03	2.09E-02	794.25	2.09
3.09E-03	2.13E-02	589.47	2.13	3.19E-03	2.13E-02	692.21	2.13	3.29E-03	2.13E-02	794.11	2.13
3.09E-03	2.17E-02	589.23	2.17	3.19E-03	2.18E-02	692.03	2.18	3.29E-03	2.18E-02	793.98	2.18
3.09E-03	2.22E-02	589.00	2.22	3.19E-03	2.23E-02	691.86	2.23	3.29E-03	2.23E-02	793.85	2.23
3.09E-03	2.27E-02	588.78	2.27	3.19E-03	2.27E-02	691.70	2.27	3.29E-03	2.28E-02	793.72	2.28
3.09E-03	2.31E-02	588.55	2.31	3.19E-03	2.32E-02	691.53	2.32	3.29E-03	2.32E-02	793.60	2.32
3.09E-03	2.36E-02	588.31	2.36	3.19E-03	2.37E-02	691.35	2.37	3.29E-03	2.37E-02	793.46	2.37
3.09E-03	2.40E-02	588.09	2.40	3.19E-03	2.40E-02	691.22	2.40	3.29E-03	2.40E-02	793.38	2.40
3.09E-03	2.45E-02	587.84	2.45	3.19E-03	2.45E-02	691.04	2.45	3.29E-03	2.45E-02	793.24	2.45
3.09E-03	2.49E-02	587.60	2.49	3.19E-03	2.49E-02	690.86	2.49	3.29E-03	2.50E-02	793.10	2.50
3.09E-03	2.54E-02	587.38	2.54	3.19E-03	2.54E-02	690.70	2.54	3.29E-03	2.54E-02	792.98	2.54
3.09E-03	2.59E-02	587.15	2.59	3.19E-03	2.59E-02	690.53	2.59	3.29E-03	2.59E-02	792.85	2.59
3.09E-03	2.63E-02	586.92	2.63	3.19E-03	2.64E-02	690.36	2.64	3.29E-03	2.64E-02	792.72	2.64
3.09E-03	2.68E-02	586.67	2.68	3.19E-03	2.68E-02	690.18	2.68	3.29E-03	2.69E-02	792.59	2.69
3.09E-03	2.73E-02	586.42	2.73	3.19E-03	2.73E-02	689.99	2.73	3.29E-03	2.73E-02	792.44	2.73
3.09E-03	2.77E-02	586.17	2.77	3.19E-03	2.78E-02	689.81	2.78	3.29E-03	2.78E-02	792.31	2.78
3.09E-03	2.82E-02	585.94	2.82	3.19E-03	2.83E-02	689.64	2.83	3.29E-03	2.83E-02	792.18	2.83
3.09E-03	2.86E-02	585.72	2.86	3.19E-03	2.87E-02	689.47	2.87	3.29E-03	2.88E-02	792.06	2.88
3.09E-03	2.91E-02	585.49	2.91	3.19E-03	2.92E-02	689.30	2.92	3.29E-03	2.93E-02	791.93	2.93
3.09E-03	2.96E-02	585.25	2.96	3.19E-03	2.97E-02	689.12	2.97	3.29E-03	2.97E-02	791.79	2.97
3.09E-03	3.00E-02	585.01	3.00	3.19E-03	3.00E-02	689.00	3.00	3.29E-03	3.00E-02	791.71	3.00

## Appendix F. Equipment, materials and reagents

### F.1 A List of instrument



Vacuum oven, Jeio Tech, model OV-11



Cutter, Horses



Belt Puncher, Sunkey



Optical microscope, Seek Inter Co., Ltd., model SK-XJM series with video recorder



Plasma Cleaner, Harrick Plasma, model PDC-32G



Syringe pump, Multi-Phaser model NE-1600/NE-1800



Syringe pump, Cole-Parmer Model 100 & Vortex, Biosan, model Vortex V-1 plus

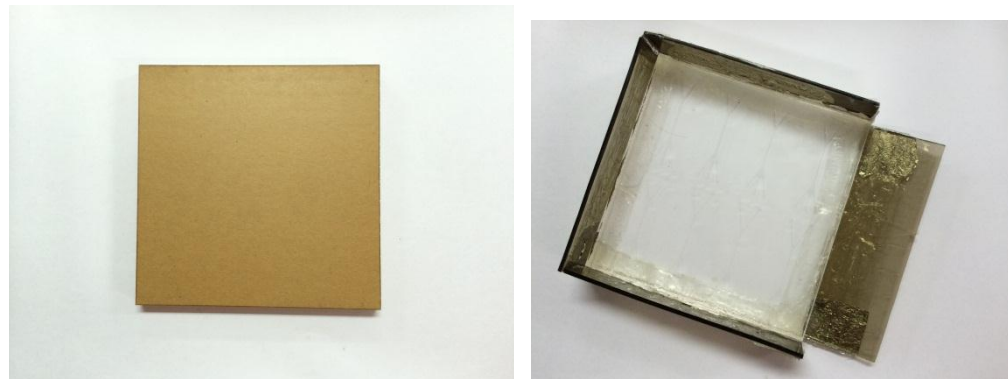


Centrifuger, Biosan Microspin 12



Optical Microscope, Olympus DP21

## F.2 Materials and reagents



Acrylic plate



Isopropyl Alcohol (IPA)

PDMS Elastomer with curing agent

96% Sulfuric acid



Hydrogen peroxide ( $H_2O_2$ ) solution 40%

Glass slide, Sail brand

$N_2$  tank



Tube, Cole Palmer Neodymium permanent magnets, MISUMI Syringe 10 ml



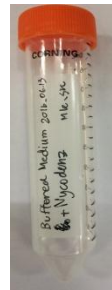
5  $\mu\text{m}$  magnetic beads stock, Sigma Aldrich      10  $\mu\text{m}$  magnetic beads stock, Sigma Aldrich



Tris/HCl, Bio Basic Canada INC.    CaNa<sub>2</sub>.EDTA, Sigma Aldrich    KCl, Suksapan Panit



Nycoden AG powder, Axis-Shield    Giemsa staining solution    Absolute methanol



Nycodenz stock solution



Mouse ICR



### Appendix G. Nycodenz stock solution preparation

The data of Janse C.J. et al. (2006) suggests that Nycodenz powder 138g add into 500 mL Buffered medium. With the same ratio of both things, this study prepares for 10 mL Buffered medium. Therefore, Nycodenz powder will be added into Buffered medium with amount of 2.76g

Concentration of buffered solution Janse C.J. et al. (2006):

5mM Tris/HCl	$5 \times 10^{-3}$ mol / 1000 mL	$\times$	10 mL	$= 5 \times 10^{-5}$ mol
3mM KCl	$3 \times 10^{-3}$ mol / 1000 mL	$\times$	10 mL	$= 3 \times 10^{-5}$ mol
0.3 mM CaNa <sub>2</sub> EDTA	$3 \times 10^{-4}$ mol / 1000 mL	$\times$	10 mL	$= 3 \times 10^{-6}$ mol

If we want final volume of buffered medium = 10 mL, each component in the final solution should be as follows

#### Preparation of medium

1. Tris/HCl (Molecular Weight = 157.64)

1st mixed: 1.576 g in 10 mL of distilled water = 1 M Tris/HCl

2nd mixed: Take 0.1 mL of 1st mixed + 9.9 mL of distilled water = 0.01 M Tris/HCl

2. KCl (Molecular Weight = 74.56)

1st mixed: 1.492 g in 20 mL of distilled water = 1 M KCl

2nd mixed: Take 0.1 mL of 1st mixed + 9.9 mL of distilled water = 0.01 M KCl

3. CaNa<sub>2</sub>EDTA (Molecular Weight = 374.27)

1st mixed: 3.7427 g in 10 mL of distilled water = 1 M CaNa<sub>2</sub>EDTA

2nd mixed: Take 0.1 mL of 1st mixed + 9.9 mL of distilled water = 0.01 M CaNa<sub>2</sub>EDTA

Then mix all together, 5 mL of 2nd mixed of Tris/HCl, 3 mL of 2nd mixed of KCl and 0.3 mL of 2nd mixed of CaNa<sub>2</sub>EDTA into 1.7 mL of distilled water

**VITA**

Surasak Kasetsirikul graduated with second class honors, Bachelor Degree of Engineering, Chulalongkorn University in academic year 2013. Then, he got admission into Master Degree of Enginnering, Chulalongkorn University in academic year 2014. His research interests are Microfluidics, MEMS and Nanotechnology and medical device applications.

